Can Soft Robots Donate Their Heart to Humans?

Emerging Technologies in Total Artificial Heart Development

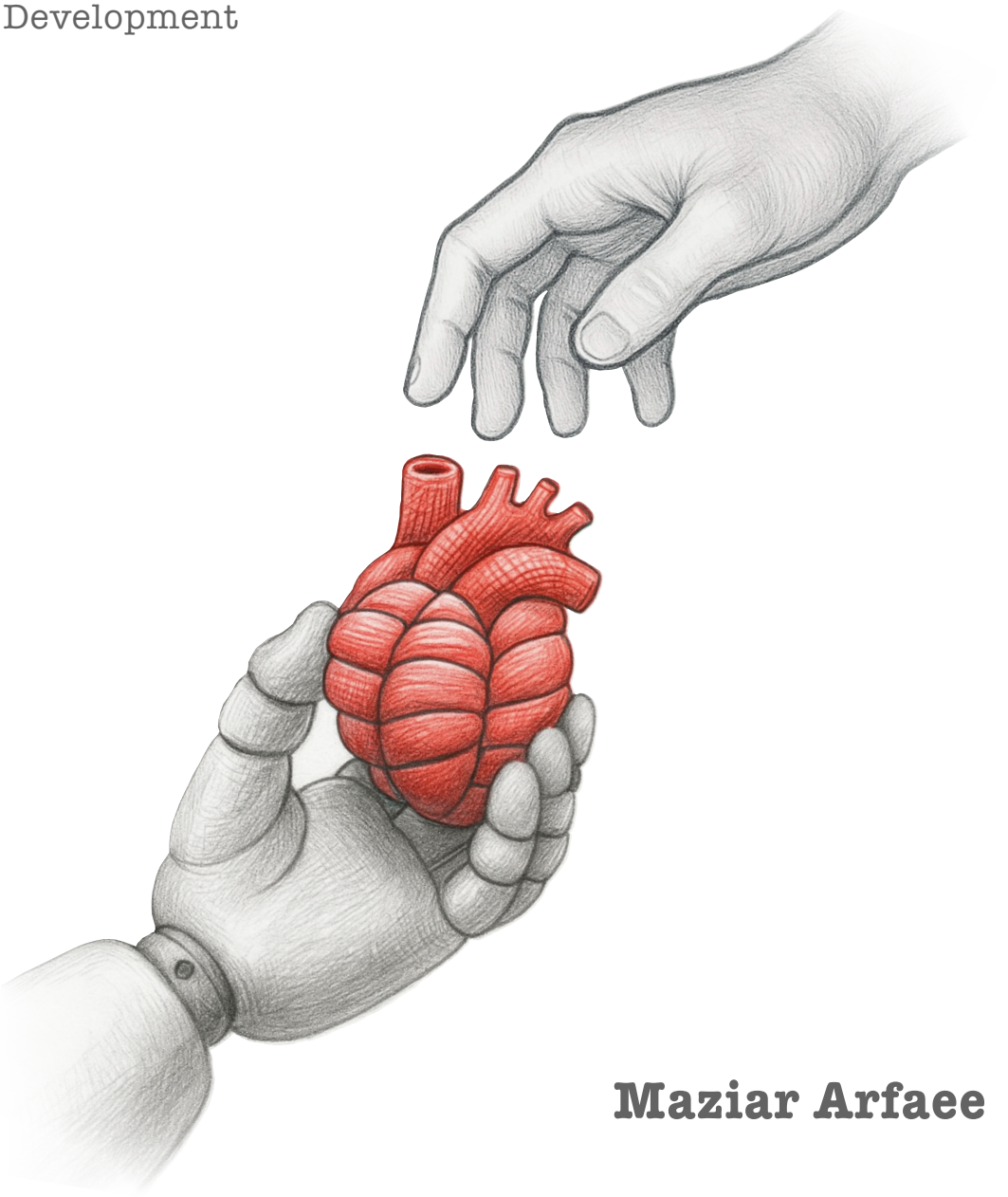

Maziar Arfaee

Can Soft Robots Donate Their Heart to Humans?

Emerging Technologies in Total Artificial Heart Development

Maziar Arfaee


Ph.D. Thesis, AmstedamUMC, December 2025

Can Soft Robots Donate Their Heart to Humans? Emerging Technologies in Total Artificial Heart Development
Maziar Arfaee

Cover design: Maziar Arfaee

ISBN: 978-94-93483-39-2
A catalogue record is available from the Amsterdam University Library.
A digital version of this thesis can be downloaded from https://amolf.nl and https://dare.uva.nl

The work described in this thesis was performed at AmsterdamUMC and AMOLF, Amsterdam, The Netherlands.

The project is initiated within the Hybrid Heart Consortium funded by the European Union Horizon 2020 research and innovation program under grant agreement no. 767195 and continued as a part of the project Holland Hybrid Heart, financed by the Hartstichting and the Dutch Research Council (NWO) with file number NWA.1518.22.049 of the research program NWA L1 - Onderzoek op Routes door Consortia 2022 - NWA-ORC 2022.

Can Soft Robots Donate Their Heart to Humans? Emerging Technologies in Total Artificial Heart Development

ACADEMISCH PROEFSCHRIFT

ter verkrijging van de graad van doctor
aan de Universiteit van Amsterdam
op gezag van de Rector Magnificus
prof. dr. ir. P.P.C.C. Verbeek
ten overstaan van een door het College voor Promoties ingestelde commissie,
in het openbaar te verdedigen in de Agnietenkapel
op maandag 8 december 2025, te 13.00 uur

door Maziar Arfaee
geboren te Shiraz

Promotiecommissie

Promotor:	prof. dr. J. Kluin	AMC-UvA
Copromotor:	dr. ir. J.T.B. Overvelde	AMOLF
Overige leden:	prof. dr. E.T. van Bavel	AMC-UvA
	prof. dr. R.J.M. Klautz	AMC-UvA
	prof. dr. M.P. Schijven	AMC-UvA
	prof. dr. D.W. Donker	Universiteit Twente
	dr. M. Schmid Daners	ETH Zurich
	dr. A. Sadeghi	Universiteit Twente

Faculteit der Geneeskunde

To my beloved parents, Esfandiar and Azar, and my dear sister, Mahsa—thank you for your endless support and love.

Summary

0.1. English Summary

This thesis investigates the transformative potential of soft robotics in the development of total artificial hearts (TAHs), a field driven by the urgent and growing burden of end-stage heart failure worldwide. Despite decades of innovation, conventional mechanical circulatory support devices, including ventricular assist devices (VADs) and current-generation TAHs, remain limited by complications such as thromboembolic events, infections, mechanical failure, and non-physiological performance. Their reliance on rigid mechanical components, driveline connections, and system complexity has constrained both durability and patient's quality of life. These challenges underline a pressing medical and engineering need: the development of artificial hearts that do not merely substitute for the native organs pumping capacity, but also emulate its dynamic, adaptive, and hemocompatible nature.

Soft robotics offers a compelling response to this challenge. By drawing inspiration from the compliant, deformable, and adaptive properties of biological tissues, soft robotic systems enable a new paradigm for cardiovascular prostheses–one that prioritizes mechanical compliance, physiological flow generation, and passive adaptability. In contrast to rigid electromechanical pumps, soft robotic designs hold the potential to replicate the hearts native contraction patterns, distribute forces more evenly, and reduce blood trauma. Moreover, the field integrates advances in material science, fluidic actuation, and biointerface engineering, creating opportunities for devices that are not only technically functional but also biologically harmonious. This thesis builds upon these principles to explore the soft robotic TAH concepts, next-generation artificial hearts that combine soft robotic actuation, fluidic transmission systems, and supramolecular coatings to address the limitations of existing devices and move toward a truly implantable, durable, and physiologically compatible TAH.

The investigation begins with a systematic review of the historical evolution of TAH development. Here, the limitations of earlier devices such as the SynCardia and Carmat systems are critically assessed, including their high complication rates, mechanical failures, limited patient mobility, and dependency on percutaneous drivelines. The review highlights both the engineering achievements and clinical shortcomings of these systems, while pointing toward new opportunities afforded by emerging soft robotics, biocompatible materials, and wireless energy transfer technologies. By mapping the trajectory of the field, this analysis clarifies why a paradigm shift is required and lays the foundation for novel approaches.

In chapter 3, the thesis introduces an analytical modeling framework for elastic pouch motors, a core actuation principle in soft robotics. These models describe the nonlinear behavior of elastomeric materials under pressurization, offering predictive insights into their deformation and force output. The analytical formulations are validated against experimental data, underscoring the importance of tuning material stretchability in design-

ing high-performance, long-lasting pumping elements. This stage provides a critical design toolkit, enabling optimization of pouch geometry and material properties for future heart prototypes.

A major contribution of the work was the introduction of the LIMO (Less In, More Out) heart, which set out to address one of the most persistent challenges in TAH development: the excessive size of pumping elements. The aim of this work was to establish a concept for minimizing device volume by leveraging an efficient soft fluidic transmission system. Instead of relying on direct displacement like membrane-based systems, the approach used thin-walled pouch actuators configured to achieve volumetric output amplification through circumferential shrinkage, thereby reducing the required volumetric input for generating physiological pressures. This principle of fluidic transmission provides a pathway to reconciling anatomical constraints with functional performance, laying the groundwork for the design of compact, energy-efficient artificial ventricles that can be scaled toward full implantability.

The thesis then introduces the Hybrid Heart concept, which represents the synthesis of another soft robotic actuation method with biomaterial innovation. By incorporating supramolecular coatings and exploring hemocompatible inner linings, this design seeks to overcome the persistent barrier of blood-material interaction. In vitro validation demonstrated improved hemocompatibility compared with uncoated materials, while acute animal studies confirmed the feasibility of pulsatile function and biocompatibility in vivo. The Hybrid Heart embodies the vision of a device that does not merely perform as a mechanical pump but integrates with the host environment, reducing the risks of thrombosis, infection, and chronic inflammation. Together, these results position the Hybrid Heart as a promising candidate for the next generation of TAHs, capable of bridging the gap between engineering innovation and clinical translation.

Taken together, the findings of this thesis highlight the transformative potential of soft robotics in cardiac replacement therapy. By merging analytical modeling, practical prototyping, and biological validation, the work outlines a pathway toward artificial hearts that are not only functional but also physiologically harmonious. Future efforts must focus on design optimization, ensuring durability, chronic evaluation in large animal models, and the development of implantable energy and control systems. With continued progress, the LIMO heart and Hybrid Heart concepts could eventually realize the long-standing vision of a durable, biocompatible, and fully implantable total artificial heart.

0.2. Nederlandse Samenvatting

Dit proefschrift onderzoekt het transformerende potentieel van zachte robotica bij de ontwikkeling van kunstharten, een onderzoeksgebied dat wordt gedreven door de sterke toename van eindstadium hartfalen wereldwijd. Ondanks decennia van innovatie blijven conventionele mechanische circulatoire ondersteuningssystemen, waaronder steunharten en de huidige generatie kunstharten, beperkt door complicaties zoals tromboemboliën, infecties, mechanisch falen en niet-fysiologische prestaties. Hun afhankelijkheid van rigide mechanische componenten, percutane verbindingen en systeemcomplexiteit beperkt zowel de duurzaamheid als de levenskwaliteit van patiënten. Deze uitdagingen geven een urgente medische en technische noodzaak weer: de ontwikkeling van kunstharten die niet enkel de pompfunctie van het lichaamseigen orgaan vervangen, maar die ook diens dynamische, adaptieve en hemocompatibele eigenschappen nabootsen.

Zachte robotica kan een antwoord bieden op deze uitdaging. Door inspiratie te putten uit de meegaande, vervormbare en adaptieve eigenschappen van biologische weefsels maken zachte robotsystemen een nieuw paradigma mogelijk voor cardiovasculaire prothesenéén dat de nadruk legt op mechanische compliantie, fysiologische flowgeneratie en passieve aanpassing. In tegenstelling tot rigide elektromechanische pompen hebben zachte robotontwerpen het potentieel om de natuurlijke samentrekkings patronen van het hart na te bootsen, krachten gelijkmatiger te verdelen en bloedtrauma te verminderen. Bovendien verenigt dit vakgebied vooruitgang in materiaalkunde, fluïdische actuatie en bio-interface-engineering, wat mogelijkheden schept voor apparaten die niet alleen technisch functioneel zijn, maar ook biologisch in harmonie met het lichaam. Dit proefschrift bouwt voort op deze principes om zachte robotische kunsthartconcepten te verkennen: kunstharten van de volgende generatie die zachte actuatie, fluïdische transmissiesystemen en supramoleculaire coatings combineren om de beperkingen van bestaande apparaten te overwinnen en de weg vrij te maken naar een echt implanteerbaar, duurzaam en fysiologisch compatibel kunsthart.

Het onderzoek begint met een systematische review van de historische evolutie van TAH-ontwikkeling. Hierin worden de beperkingen van eerdere apparaten, zoals de SynCardia en Carmat systemen, kritisch beoordeeld, waaronder hoge complicatiecijfers, mechanisch falen, beperkte mobiliteit van patiënten en afhankelijkheid van percutane verbindingen. De review belicht zowel de technische prestaties als de klinische tekortkomingen van deze systemen en wijst op nieuwe mogelijkheden die worden geboden door opkomende zachte robotica, biocompatibele materialen en draadloze energieoverdrachtstechnologieën. Door de ontwikkeling van het veld in kaart te brengen, maakt deze analyse duidelijk waarom een paradigmaverschuiving noodzakelijk is en legt zij de basis voor nieuwe benaderingen.

Vervolgens introduceert het proefschrift een analytisch modelleringskader voor elastische pouch-motoren, een kernactuatieprincipe in de zachte robotica. Deze modellen beschrijven het niet-lineaire gedrag van elastomere materialen onder druk, en bieden voorspellende inzichten in hun vervorming en krachtopbrengst. De analytische formules worden gevalideerd aan de hand van experimentele gegevens, waarmee het belang wordt onderstreept van het afstemmen van de rekbaarheid van materialen bij het ontwerpen van hoogpresterende, duurzame pompelementen. Dit hoofdstuk levert een belangrijk ontwerpinstrument op, dat de optimalisatie van geometrie en materiaaleigenschappen van pouch-actuatoren mogelijk maakt voor toekomstige hartprototypes.

In het volgende hoofdstuk wordt LIMO (Less In, More Out) hart geintroduceert, dat zich richt op een van de meest hardnekkige uitdagingen in kunsthart ontwikkeling: de buitensporige omvang van pompelementen. Het doel van dit werk was een concept te ontwikkelen voor volumeminimalisatie door gebruik te maken van een efficiënt zacht fluïdisch transmissiesysteem. In plaats van directe verplaatsing, zoals bij membraan-gebaseerde systemen, maakte deze benadering gebruik van dunwandige pouch-actuatoren die waren geconfigureerd om volumetrische outputversterking te bereiken via circumferentiële krimp, waardoor de benodigde inputvolumes voor het genereren van fysiologische drukken werden verminderd. Dit transmissieprincipe biedt een weg om anatomische beperkingen te verzoenen met functionele prestaties, en legt de basis voor het ontwerp van compacte, energie-efficiënte kunstventrikels die opgeschaald kunnen worden naar volledige implanteerbaarheid.

Daarna introduceert het proefschrift het Hybrid Heart-concept, dat de synthese beschrijft van een andere zachte actuatiemethode met biomateriaalinnovatie. Door supramoleculaire coatings en hemocompatibele binnenlagen te integreren, tracht dit ontwerp de hardnekkige barrière van bloed-materiaalinteracties te overwinnen. In vitro-validatie heeft verbeterde hemocompatibiliteit laten zien in vergelijking met ongecoate materialen, terwijl acute dierstudies de haalbaarheid van pulsatiel functioneren en biocompatibiliteit in vivo hebben bevestigd. Het Hybrid Heart belichaamt de visie van een apparaat dat niet enkel fungeert als een mechanische pomp, maar geïntegreerd is met de gastomgeving, waardoor de risicos op trombose, infectie en chronische ontsteking worden verminderd. Samen positioneren deze resultaten het Hybrid Heart als een veelbelovende kandidaat voor de volgende generatie kunstharten, die in staat zijn om de kloof tussen technische innovatie en klinische toepassing te overbruggen.

Gezamenlijk benadrukken de bevindingen van dit proefschrift het transformerende potentieel van zachte robotica in de hartvervangende therapie. Door analytische modellering, praktische prototypering en biologische validatie te combineren, schetst het werk een pad naar kunstharten die niet alleen functioneel zijn, maar ook fysiologisch in harmonie met het lichaam. Toekomstige inspanningen moeten zich richten op ontwerpoptimalisatie, het waarborgen van duurzaamheid, chronische evaluatie in grote diermodellen en de ontwikkeling van implanteerbare energie- en controlesystemen. Met voortdurende vooruitgang zouden de LIMO- en Hybrid Heart-concepten uiteindelijk de lang gekoesterde visie kunnen verwezenlijken van een duurzaam, biocompatibel en volledig implanteerbaar kunsthart.

Contents

1

Introduction

"Every leaf of the tree becomes a page of the book, once the heart is opened and it has learnt to read."

Saadi, Shiraz, 13th century

1

1.1. The Growing Burden of End-Stage heart failure

Cardiovascular diseases (CVDs) remain the leading cause of death worldwide, responsible for nearly one-third of all global fatalities [1]. Among these conditions, heart failure (HF) stands out as a particularly significant contributor to morbidity, mortality, and healthcare costs [2]. HF is not a single disease but rather a complex clinical syndrome arising from structural or functional impairment of ventricular filling or ejection of blood [3]. Despite advances in medical and device-based therapies, HF continues to impose a profound burden on patients, families, and health systems.

Globally, an estimated 64 million people live with HF , and its prevalence is steadily increasing, driven primarily by two demographic trends: the aging population and improved survival from acute cardiac [4, 5]. Advances in treatments for myocardial infarction, valvular disease, and hypertension have enabled more individuals to survive into older age, yet these same survivors often progress to chronic HF. Consequently, HF is becoming more prevalent among elderly populations, where it frequently coexists with other chronic conditions such as diabetes, renal dysfunction, and pulmonary hypertension, further complicating management [6, 7].

In European countries, Studies show a lifetime risk of developing HF of approximately 24.5% in men and 23.3% in women [8]. In the United States, projections suggest that by 2030, over 8 million adults—nearly one in every 33 people—will be living with HF, representing a 46% increase from 2012 [9]. Similar trends are observed across Europe and Asia, underscoring the global nature of this growing health crisis [10, 11].

The clinical impact of HF extends far beyond mortality. Patients frequently experience debilitating symptoms such as fatigue, dyspnea, fluid retention, and exercise intolerance, severely impairing quality of life [12]. Many individuals require repeated hospitalizations, which not only reflect disease severity but also contribute to escalating healthcare costs. In the United States alone, the total annual costs related to HF are estimated to exceed $43 billion, with nearly 80% of this figure attributed to hospitalization expenses [13, 14].

For those who progress to advanced stages—commonly referred to as end-stage HF—the prognosis remains dismal despite optimal medical therapy. Median survival for patients with end-stage HF ranges from six months to a year, depending on clinical factors such as functional status, ejection fraction, and comorbidities [15, 16]. Heart transplantation offers the best survival outcomes and quality of life for eligible patients. However, this lifesaving option is constrained by the persistent shortage of donor hearts, leaving thousands of patients on waiting lists and many more deemed unsuitable due to age, comorbidities, or other factors [17, 18].

These stark realities have catalyzed intense research into mechanical circulatory support systems, including left ventricular assist devices (LVADs) and total artificial hearts (TAHs). While LVADs have transformed the management of advanced HF for many patients, they are unsuitable for patients with severe biventricular failure or complex anatomical challenges [19]. Thus, there remains a critical unmet need for technological solutions that can fully replace the native hearts pumping function in a manner that is both durable and compatible with the human body.

As the burden of end-stage HF continues to grow, the need for innovative alternatives to heart transplantation has become increasingly urgent. Leading this effort is the development of a viable, long-term TAH—a central theme explored in depth throughout this thesis.

1.2. Mechanical Circulatory Support and Its Limitations

To address this gap, MCS devices have evolved rapidly over the past two decades. Among these, LVADs have become a mainstay of treatment for patients with advanced HF either as a bridge to transplant or as destination therapy [20–22]. These devices have extended life expectancy and improved functional capacity for many patients. However, LVADs are not a panacea. Their use is largely restricted to patients with predominantly left ventricular dysfunction. They offer limited support for patients with severe biventricular failure or those with complex anatomical or systemic conditions that preclude isolated LV support [19]. Moreover, LVADs remain associated with significant complications, including thromboembolic events, bleeding, and infections linked to percutaneous drivelines [23]. Many patients endure a diminished quality of life due to device-related limitations [24].

These challenges underscore a profound clinical need: a TAH that can function as a long-term, or destination therapy for patients with end-stage biventricular HF.

1.3. The Total Artificial Heart: Progress and Persistent Challenges

The first implantation of a TAH was done in 1969, where the Liotta-Cooley artificial heart was implanted in a patient, a landmark event that fueled decades of innovation [25]. Unlike LVADs, a TAH replaces both the left and right ventricles of the native heart, offering a complete mechanical solution for biventricular failure. To better understand the current landscape and the technological obstacles that fuel the search for new solutions, it is helpful to examine some of the leading TAH systems in more detail. Devices such as SynCardia [26], Carmat (Aeson Heart) [27], BiVACOR [28], and RealHeart [29] each embody distinct engineering philosophies and innovative features, yet they are all still constrained by important limitations: device size, biocompatibility, infection risk from percutaneous connections, mechanical complexity, and the challenge of replicating physiological heart function. These persistent hurdles drive the ongoing exploration of alternative approaches—including the integration of soft robotics, tissue engineering, and wireless energy transfer—as potential solutions to finally deliver a viable TAH suitable for long-term, destination therapy.

The following sections provide an overview of these prominent TAH designs, highlighting their current status, unique attributes, and the key limitations that still need to be addressed.

1.3.1. SynCardia TAH

The SynCardia TAH is the most established artificial heart currently in clinical use. Originally developed in the 1980s as Jarvik-7 [30, 31] and refined over subsequent decades, the SynCardia device is a pneumatically driven, pulsatile pump that replaces both ventricles and all four heart valves. It is currently the only FDA-approved device capable of completely replacing both ventricles in patients with end-stage biventricular HF, with over 2,000 implants performed worldwide to date [32]. Despite its crucial role as a bridge to transplantation, its clinical use is limited by significant challenges, including a high

incidence of complications such as thromboembolic events, bleeding, and infections—particularly those related to its percutaneous driveline system [33]. To expand its applicability, a smaller 50cc version has recently been developed, allowing implantation in patients with smaller body sizes who were previously ineligible for the standard device [34] Furthermore, while widely utilized in the United States, the SynCardia TAH remains less available internationally and is not approved as a permanent alternative to transplantation due to associated risks and limited long-term outcome data.

1.3.2. Carmat (Aeson Heart)

The Carmat TAH [27], also known as the Aeson heart, represents a newer generation of artificial hearts aimed at addressing some limitations of older devices like SynCardia. Developed in France, the Aeson heart combines mechanical components with biological materials, including bovine pericardial tissue for blood-contacting surfaces to improve biocompatibility and reduce thrombogenicity [35]. Unlike the SynCardia pneumatic mechanism, the Aeson heart uses hydraulic actuation to generate pulsatile flow, with integrated sensors to adjust flow rates dynamically in response to patient needs. The device has received conditional approval for commercial sale in Europe as a bridge to transplant and has begun early clinical trials in the United States [36]. Nevertheless, the Aeson heart remains relatively large and complex, requiring careful patient selection due to size constraints. Its reliance on an external power supply via percutaneous drivelines also poses infection risks, and long-term durability data remains limited.

1.3.3. BiVACOR TAH

BiVACOR is continuous-flow TAH based on a rotary, centrifugal pump design with a single spinning rotor suspended by magnetic levitation [37]. the BiVACOR system aims to generate both left and right ventricular flows by dynamically shifting the rotor axial position to balance systemic and pulmonary circulations [38]. This novel approach promises a smaller device footprint and reduced mechanical wear, potentially offering a fully implantable solution even for smaller patients. However, the BiVACOR heart is still in early feasibility testing stages. Despite its innovative design, the BiVACOR operates using continuous-flow technology, the long-term physiological effects of which remain unknown.

1.3.4. RealHeart TAH

The Realheart TAH is engineered to replicate the natural hearts pumping function by incorporating both atrial and ventricular chambers. Its operation relies on the movement of the atrioventricular plane, driven by electromagnetic force, which shifts blood from the atria into the ventricles and subsequently propels it into systemic circulation. Although the device shows promise [29], it remains under development, with limited experience in human implantation, and its long-term durability and clinical performance have yet to be fully established. Furthermore, its physical size may limit implantation in smaller patients, highlighting the need for ongoing design refinements to broaden its applicability.

1.4. Enter Soft Robotics: A New Frontier for TAH Development

Over the past decade, the field of soft robotics has emerged as a transformative paradigm in engineering and biomedical applications [39]. Unlike traditional rigid mechanisms, soft robots are constructed from compliant, deformable materials capable of safe and adaptable interactions with complex, dynamic environments [40, 41]. This adaptability makes soft robotics especially attractive for applications where devices must interface intimately with human tissues, such as wearable exosuits [42, 43], minimally invasive surgical tools [44], rehabilitation devices [45, 46], and more recently, implantable devices [47–49]. In recent years, soft robotics has emerged as a rapidly growing and highly promising field, generating significant excitement for its potential applications as simulators or in the treatment of CVDs, where its biomimetic motion and gentle tissue interactions offer distinct advantages over traditional mechanical systems [48–54].

In 2017, a pneumatically driven soft TAH (sTAH) was produced using 3D-printing and lost-wax casting, and tested in a hybrid mock circulation, achieving a blood flow of 2.2 l/min against a mean aortic pressure of 48 mmHg. Although the device successfully replicated physiologically shaped blood flow and pressure signals by mimicking natural heart motion, the achieved cardiac output was insufficient to sustain normal physiological afterloads. Additionally, the device operated reliably for only about half an hour, falling significantly short of the performance expected for a TAH [50]. In a later study, same group investigated the long-term performance of a pneumatically actuated soft pump (SP) designed using rubber compression technology, achieving over one million cycles and transporting more than 140,000 L of fluid in under 12 days. However, performance testing on a hybrid mock circulation showed flow rates of 1.8 l/min against 10 kPa (75 mmHg) [51]. Both devices mentioned above, were not able to provide sufficient cardiac output against physiological afterloads. In another study, a novel sTAH was developed that achieved a cardiac output exceeding 16 l/min at 60 bpm under physiological pressures in a mock circulation and maintained continuous operation for 110,000 cycles [52]. However, despite delivering sufficient cardiac output against physiological afterload, the device required relatively high input pressures of 150-200 kPa, resulting in low overall efficiency.

Soft actuators are capable of replicating the hearts natural deformation and contraction patterns, offering the potential to reduce blood damage and enhance hemodynamic performance. In a recent study, researchers developed a bioinspired soft robotic left ventricle simulator that mimics the hearts multilayered myocardial architecture using thin-filament artificial muscles, successfully reproducing ventricular motion with physiological ejection fractions [54]. However, the device requires high actuation pressures, limiting its efficiency [55], and also its operational speed to a maximum of 30 bpm, which falls below physiological heart rates and restricts its utility for simulating the ventricles dynamic behavior.

Despite these advancements, significant questions remain about how to translate soft robotic principles into functional, reliable, and efficient TAH systems suitable for human implantation.

1.5. Research Gaps and Challenges

While early studies have demonstrated promising prototypes of soft robotic pumps and even preliminary soft TAH concepts [48–54], key technological challenges persist:

• **Size and volumetric constraints:** All TAH designs remain bulky because they require a 1:1 fluidic input-to-output volume ratio, necessitating large fluid reservoirs and high-powered pumps.

• **Power requirements and efficiency:** Current soft TAH prototypes often exhibit low energy efficiency, resulting in high power consumption, which poses significant challenges for developing practical, long-term implantable systems.

• **Complexity and reliability:** The intricate designs inherent to many proposed soft TAH systems increase mechanical and control complexity, leading to a higher probability of component failure and challenges in long-term reliability.

• **Biocompatibility and thrombogenicity:** The interaction of soft devices with blood flow poses risks of thrombus formation unless surface coatings or tissue-engineered linings are incorporated.

• **Wireless energy transfer:** Existing TAHs depend on percutaneous drivelines, posing infection risks and impairing patient freedom. Wireless Transcutaneous Energy Transfer (TET) systems could eliminate drivelines but require integration with soft robotic systems.

Addressing these challenges is crucial for advancing TAH technology toward the ultimate goal of destination therapy.

1.6. Scope and Aims of This Thesis

Against this backdrop, my PhD thesis, "Can soft robots donate their heart to humans? Emerging technologies in total artificial heart development," explores novel solutions to overcome the limitations of existing TAHs by harnessing the principles of soft robotics.

Specifically, this thesis investigates:

• The historical evolution and current state of TAH development, identifying technological hurdles and emerging opportunities.

• The mechanical and analytical modeling of soft robotic actuators—particularly elastic pouch motors—and their implications for actuation strategies in cardiac devices.

• A novel concept for a compact soft robotic TAH, termed the LIMO (Less In, More Out) heart, that leverages fluidic transmission to reduce device size and improve efficiency.

• The development and proof-of-concept of the Hybrid Heart, a soft robotic TAH platform that integrates soft actuation, biomimetic motion, tissue-engineered linings, and prospects for wireless energy transfer.

1.7. Objectives

The overarching aim of this thesis is to explore the potential of soft robotics in developing TAHs capable of replicating human cardiac function and ultimately serving as viable alternatives for heart replacement therapy. To achieve this aim, the following specific objectives are pursued:

• To conduct a systematic review of the evolution of TAH technologies, identifying key

design principles, challenges, and emerging trends, with a focus on the integration of soft robotic approaches.

• To model and analyze the mechanical behavior of elastic pouch motors, investigating how different material properties influence performance metrics relevant to its applicability as a cardiac device.

• To develop and evaluate a compact soft robotic artificial ventricle utilizing a soft fluidic transmission system inspired by pouch motors, assessing its ability to generate sufficient cardiac output against physiological afterloads.

• To propose and characterize the Hybrid Heart concept, integrating soft robotic actuation with biocompatible materials, and demonstrating its capacity to mimic physiological behaviors such as the Frank-Starling mechanism.

Collectively, these objectives aim to advance the understanding and technological foundation necessary for realizing soft robotic TAHs suitable for human application.

1.8. Outline of the thesis

The remainder of this thesis has the following structure.

In **Chapter 2**, a comprehensive review of the development of TAHs is presented, titled "The ongoing quest for the first TAH as destination therapy". This chapter examines the historical milestones, fundamental principles, and the limitations of current TAH technologies, such as high complication rates, device bulkiness, limited durability, and biocompatibility concerns. Additionally, it explores emerging innovations—including battery advancements, wireless energy transmission, novel biocompatible materials, and soft robotics—that hold potential for overcoming the barriers preventing TAHs from becoming viable destination therapy solutions. The chapter concludes with a discussion of current challenges and future perspectives in the field.

In **Chapter 3**, the thesis transitions into the modeling of soft robotic actuators in the study entitled "Modeling the behavior of elastic pouch motors". This chapter focuses on the analytical modeling of pouch motors, a class of soft actuators characterized by their low weight, large stroke, and ease of fabrication. Contrary to prior models that assume inextensible materials, this work incorporates material stretchability into the analysis, revealing how elasticity imposes critical limits on the maximum contraction and force generation of pouch motors. The developed model is evaluated through blocked-displacement experiments using various elastic materials, providing essential insights for optimizing soft actuator design for cardiac applications.

In **Chapter 4**, the research advances toward practical device development in the study "Toward developing a compact total artificial heart using a soft robotic fluidic transmission system". Here, the thesis introduces the LIMO heart, a novel TAH concept utilizing an efficient soft fluidic transmission mechanism. By leveraging thin-walled pouch actuators capable of achieving transmission ratios above one through circumferential shrinkage, the design achieves significant reductions in actuator volume and improvements in energy transfer efficiency. A rapid prototyping approach enabled swift iteration and testing. This chapter represents a pivotal step toward realizing a compact, soft robotic TAH for addressing end-stage HF.

In **Chapter 5**, the thesis presents an innovative device concept in the paper "A soft robotic total artificial hybrid heart". This chapter introduces the Hybrid Heart, a soft

robotic TAH designed to enhance biocompatibility and mimic native cardiac function. The device integrates a pneumatically driven soft robotic septum with a biocompatible inner lining derived from supramolecular polymers, which aim to reduce thrombogenicity and support tissue engineering.

In **Chapter 6**, a general discussion synthesizes the insights gained across all preceding chapters. This final chapter reflects on the progress achieved in leveraging soft robotics for TAH development, critically assesses remaining challenges, and outlines directions for future research. It discusses the feasibility and translational potential of soft robotic TAHs for clinical use, ultimately addressing the central question of whether soft robots can indeed donate their heart to humans.

2

The ongoing quest for the first total artificial heart as destination therapy

Abstract

Patients with end-stage heart disease die because of the scarcity of donor hearts. A total artificial heart (TAH), an implantable machine that replaces the heart, has so far been successfully used in over 2100 patients as a temporary life-saving technology for bridging to heart transplantation. However, after more than six decades of research on TAHs, a TAH that is suitable for destination therapy is not yet available. High complication rates, bulky devices, poor durability, poor biocompatibility and low patient quality of life are some of the major drawbacks of current TAH devices that must be addressed before TAHs can be used as a destination therapy. Quickly emerging innovations in battery technology, wireless energy transmission, biocompatible materials and soft robotics are providing a promising opportunity for TAH development and might help to solve the drawbacks of current TAHs. In this Review, we describe the milestones in the history of TAH research and reflect on lessons learned during TAH development. We summarize the differences in the working mechanisms of these devices, discuss the next generation of TAHs and highlight emerging technologies that will promote TAH development in the coming decade. Finally, we present current challenges and future perspectives for the field.

Based on: A. Vis, **M. Arfaee**, H. Khambati, M. S. Slaughter, J. F. Gummert, J. T. B. Overvelde, J. Kluin, *The ongoing quest for the first total artificial heart as destination therapy.* nature reviews cardiology, 2022 Dec;19(12):813-828

2.1. Introduction

Cardiovascular disease is the leading cause of death globally, and heart failure, one of the end points of cardiovascular disease, affects approximately 2% of the adult population worldwide [56]. The estimated prevalence of heart failure will increase markedly owing to the ageing global population. It is predicted that by 2030, more than 8 million people in the USA (1 in every 33) will have heart failure [57]. Heart transplantation is currently considered the gold standard treatment for end-stage heart failure. However, a tremendous shortage of donor hearts exists worldwide. In 2018, more than 2,500 patients were actively awaiting heart transplantation in the USA alone [58]. To compensate for this shortage, mechanical devices to support the failing heart, such as left ventricular assist devices (LVADs), have been widely implanted over the past two decades as an alternative therapy for end-stage heart failure. At present, over 3,000 LVADs are implanted in North America every year, either as a bridge to heart transplantation or as destination therapy [59]. LVADs are a treatment option for patients with left ventricular failure but are not suitable for patients with severe biventricular failure or other conditions that preclude the use of LVADs [60]. Furthermore, LVAD support is associated with poor quality of life and a risk of complications, such as thromboembolic events, bleeding and driveline* infections [61–64].

A total artificial heart (TAH) is a surgically implanted pump that provides blood circulation and replaces cardiac ventricles that are diseased or damaged [65]. The TAH is implanted in an orthotopic position and replaces both the left and right ventricle of the native heart. In 1969, a TAH was implanted in a patient for the first time [25]. However, TAHs have so far primarily been implanted as a temporary bridging therapy for patients with advanced heart failure who are awaiting heart transplantation. The SynCardia TAH (SynCardia Systems, Tucson, AZ, USA) is the TAH that is most frequently implanted as a bridge to heart transplantation therapy and is under investigation in a clinical trial to assess its applicability as destination therapy [66]. However, the limitations of the SynCardia device, which include bulkiness, short durability, high complication rates and low patient quality of life owing to the need for percutaneous hoses and frequent hospitalizations, have so far precluded its approval for this indication. An urgent need for destination therapies for (biventricular) end-stage heart disease exists because the majority of patients have no prospect of recovery with currently available therapies. The rapidly emerging technologies in wireless energy transmission, biocompatible materials and soft robotics provide a promising outlook for TAH development. Many teams across the world have tried different approaches to develop various types of TAHs, of which only a few are still under development. In this Review, we describe the historical milestones and lessons learned during TAH development and discuss the current generation of TAHs and the differences in their working mechanisms. We also highlight new technologies that will promote TAH development in the coming decade.

*Percutaneous cable that transmits electrical power from an external driver to the internally implanted device such as a TAH or LVAD.

2.2. History of TAH development

2.2.1. Animal experiments

The development of TAHs dates back to the previous century. One of the first experiments with a TAH was reported in 1958, when pioneers Willem Kolff and Tetsuzo Akutsu at the Cleveland Clinic (Cleveland, OH, USA) implanted a TAH in a dog after removing its native heart13. The TAH sustained blood circulation in the dog for 90 min [67]. More experiments in dogs were conducted at the Cleveland Clinic in the 1960s, including implantation of a mechanical TAH with two blood chambers that were alternately emptied by a motor pendulum [68] and implantation of two different pneumatically driven TAHs [69]. In the same period, Domingo Liotta (School of Medicine, Cordoba, Argentina) implanted a pneumatic TAH, named the Liotta Heart, in dogs [70]. These experiments inspired more researchers across the world to start developing TAHs. In Japan in 1963, Kazuhiko Atsumi (Tokyo University School of Medicine, Tokyo, Japan) developed several types of pneumatic and mechanical TAH and tested them in 56 dogs [71]. In 1964, a national artificial heart programme was initiated in the USA, sponsored by the National Heart, Lung and Blood Institute. This big nationwide project, led by Frank Hastings, aimed to develop novel technical advances (similar to the aims of the USA space programme) for generating TAHs. Boosted by the national artificial heart programme, TAH experiments were conducted in numerous research centres in the USA, such as at the Penn State Milton S. Hershey Medical Center [72] and the Cleveland Clinic [73].

2.2.2. First TAH implantation in humans

In 1969, Denton Cooley (Texas Heart Institute, Houston, TX, USA) performed the first TAH implantation in humans, implanting the Liotta-Cooley TAH in a patient aged 47 years11 (Fig. 2.1). The Liotta-Cooley device was a rigid pneumatic TAH with two ventricles implanted orthotopically. An external pump moved compressed air into a pneumatic chamber inside the ventricle, which pushed a diaphragm and caused the ejection of blood from the blood chamber on the other side of the membrane. The Liotta-Cooley TAH supported the patient for 64 h, after which the patient underwent heart transplantation [25]. The patient died owing to sepsis 32 h after the heart transplantation. Furthermore, the poor biocompatibility of the valves and the surfaces that were in contact with the blood might have contributed to haemolysis and renal impairment [25]. Therefore, although the first TAH implantation was ground-breaking, it was not considered a success [74]. However, this first implantation of a TAH in humans proved the concept that such technology could support a patient as a bridge to heart transplantation. However, the procedure sparked ethical and legal controversy regarding improper consent and experimentation [75]. In the years after the first implantation in humans, further research on TAH prototypes was conducted solely in large animal models by researchers from the University of Alberta (Edmonton, Alberta, Canada) [76]; the University of UTAH College of Medicine (Salt Lake City, UT, USA) [77–80]; the University of Mississippi Medical Centre (Jackson, MS, USA) [81, 82]; the Cleveland Clinic [83, 84]; the Baylor College of Medicine (Houston, TX, USA) [85]; and the US Atomic Energy Commission (University of UTAH, Salt Lake City, UT, USA) [86–88].

It took 12 years from the first TAH implantation in humans until the next human TAH implantation in 1981, again at the Texas Heart Institute, when the pneumatic Akutsu III

TAH was implanted as a bridge to transplantation in a man aged 36 years [89]. The Akutsu III TAH worked similarly to the Liotta-Cooley TAH, with two inflatable air sacs to displace blood. The Akutsu III TAH supported the patient for 55 h, after which the patient received heart transplantation. However, in the last 27 h before the transplantation surgery, the patient could not be fully supported by the TAH and died 7 days after the heart transplantation owing to multiorgan failure [89]. The third TAH implantation in humans occurred in 1982 at the University of UTAH, where William DeVries and Willem Kolff implanted the Jarvik-7 TAH as destination therapy in a patient aged 61 years with congestive heart failure [30]. The Jarvik-7 was a pneumatic device with a similar working mechanism to the Liotta-Cooley TAH. After implantation of the Jarvik-7 TAH, the patient was conscious and able to communicate with his family. Progressive circulatory shock led to his death 112 days after TAH implantation [30].

This first successful clinical outcome with the Jarvik-7 TAH encouraged many teams across the world to continue developing TAHs (Fig. 2.1). Most TAHs developed by the first pioneers were pneumatically or hydraulically driven; later, researchers developed TAHs with different working mechanisms. Currently available TAHs can be classified into three types on the basis of their working mechanism: fluid-driven TAHs, mechanical TAHs and continuous-flow TAHs (Fig. 2.2), which are discussed below.

2.3. Working mechanisms of TAHs

2.3.1. Fluid-driven TAHs

Fluid-driven TAHs are the oldest type of TAH, with a working mechanism similar to that of the Liotta-Cooley and Jarvik-7 TAHs. Fluid-driven devices have blood chambers separated by a membrane from a chamber filled with fluid (air or liquid). A pressure rise in the fluid chamber moves the flexible membrane so that the blood chamber empties and the blood is ejected (Fig. 2.2a). A pump is required to increase the pressure in the pneumatic or hydraulic chamber. Often, these pumps are placed outside the body, which requires percutaneous hoses to move the pressurized fluid from the pump to the TAH. Depending on the type of pump used in these pneumatic and hydraulic devices, the left and right chamber eject blood either simultaneously or alternatingly. More recently developed TAHs (such as the Carmat TAH (Aeson; Carmat, Vélizy-villacoublay, France)) are designed to have the pump implanted in the body, avoiding the need for percutaneous pneumatic or hydraulic pressure hoses. However, percutaneous cables to supply power to the TAH are often still needed.

Historical devices

Several pneumatic TAHs were developed in the 1980s, such as the Brno TAH (Vacord Bioengineering Research Company, Brno, Czech Republic) [98], Penn State pneumatic TAH (Pennsylvania State University, Hershey, Pennsylvania) [99], Phoenix (Southern Taiwan University, Tainan, Taiwan) [100, 101], Poisk TAH (Institute of Organ and Tissue Transplantation, Moscow, Russia) [102, 103], POLTAH (Artificial Heart Laboratory, Zabrze, Poland) [104] and Vienna TAH (University of Vienna, Vienna, Austria) [105]. In the same period, the electrohydraulic TAH (EHTAH) was developed in Japan (Artificial Organs Department, Osaka, Japan) [106]. Development of the hydraulically driven AbioCor (Abiomed, Danvers,

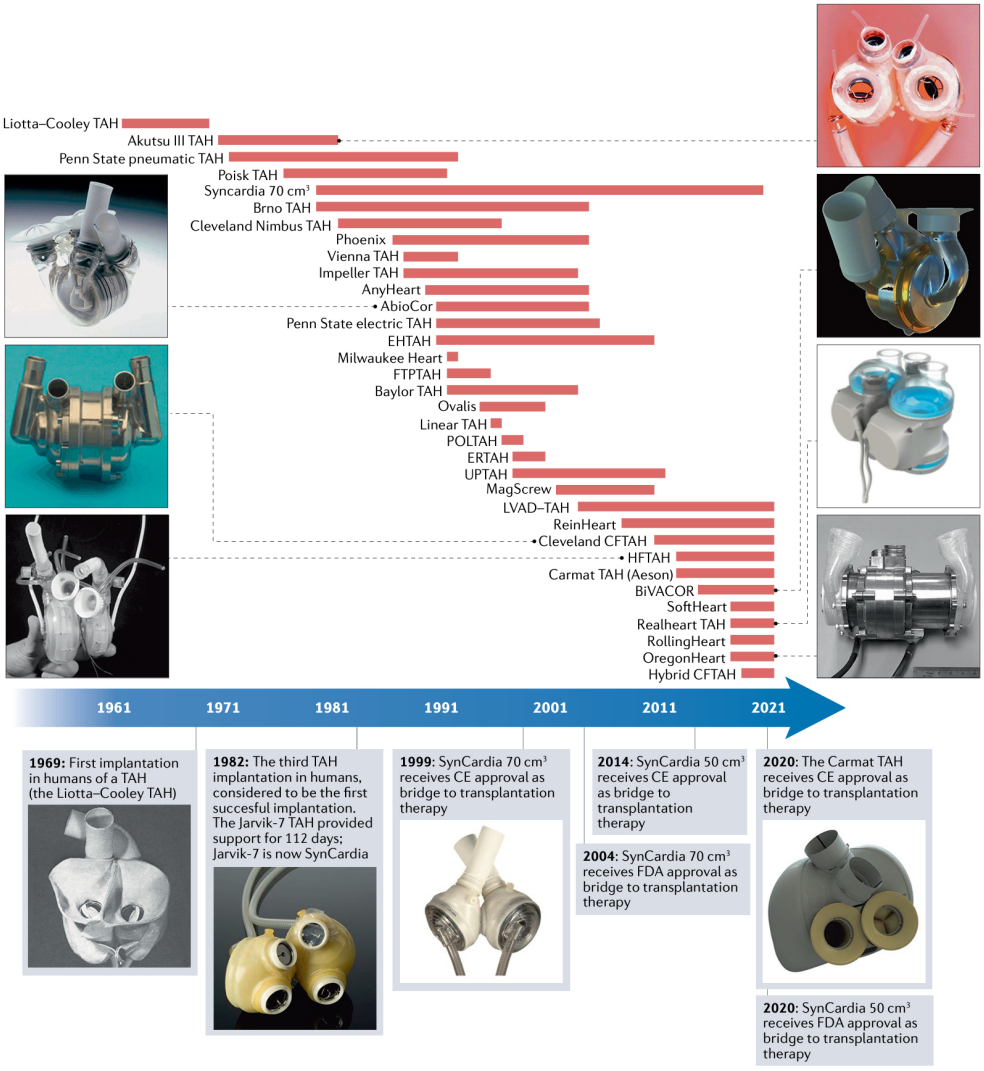

Figure 2.1 | Timeline of the milestones in the development of total artificial hearts. All current TAH devices and the most historically important TAH devices are shown. The red bars represent the period of development and/or reporting of testing results in literature for each TAH. CFTAH, continuous-flow total artificial heart; EHTAH, electrohydraulic total artificial heart; ERTAH, eccentric roller total artificial heart; FTPTAH, flow-transformed pulsatile total artificial heart; HFTAH, helical flow total artificial heart; LVAD-TAH, total artificial heart made with two left ventricular assist devices; UPTAH, undulation pump total artificial heart. Images reproduced with permission from ref.[90], Springer Nature (AbioCor); ref.[91], Science Museum Group/Academic (Akutsu III); ref.[92], Wiley (BiVACOR); ref.[27], Carmat/OUP (Carmat TAH); ref.[93], Springer Nature (Cleveland CFTAH); ref.[94], Wiley (HFTAH); The Board of Trustees of the Science Museum (Jarvik-7); ref.[25], Elsevier (Liotta-Cooley TAH); ref.[95], Wiley (OregonHeart); ref.[96], Wiley (Realheart TAH); and ref.[97], Elsevier (SynCardia).

MA, USA) started in the 1990s [91, 107, 108]. AbioCor was the first fully implantable system designed without any percutaneous cables; it consisted of four internal components and a transcutaneous energy transfer (TET) system*. The characteristics of all the TAHs discussed in this Review are summarized in Table 2.1.

Current devices

Two fluid-driven devices, SynCardia [34] and the Carmat TAH, are currently in use as a bridge to transplantation and are undergoing further evaluation as destination therapy. Another fluid-driven TAH, SoftHeart (ETH Zurich, Zurich, Switzerland) [50], is currently under development. The working mechanism of these three prototypes is very similar to the earliest devices, such as the Liotta-Cooley and Akutsu III TAHs.

The history of the development of SynCardia dates back 40 years to 1982, when Kolff and DeVries performed the first successful implantation of a TAH in a patient [30]. This TAH, the Jarvik-7, is now known as SynCardia. SynCardia is a pneumatically driven TAH consisting of two independent ventricles that collect and eject blood simultaneously in a pulsatile manner. A four-layer polyurethane membrane separates the blood in the ventricle from the pneumatic chamber. The pressures in the pneumatic chamber are generated by a pump placed outside the body and connected via percutaneous drivelines. SynCardia is the first TAH that received CE approval (in 1999) and FDA approval (in 2004) for temporary use as a bridge to heart transplantation in eligible candidates who are at risk of imminent death from end-stage biventricular failure [109]. This TAH has been implanted in over 2100 patients worldwide [110].

The Carmat system is a hydraulic TAH developed in France that received CE approval as a bridge to transplantation therapy in 2020. The Carmat TAH consists of left and right blood chambers separated from the hydraulic pressure chamber by a two-layer biocompatible membrane made from bovine pericardium. The pumps that pressurize the hydraulic pressure chambers of the Carmat TAH are built within the TAH itself, making this device larger than SynCardia. Furthermore, the Carmat TAH ejects blood from the left and right blood chambers alternatingly. Although percutaneous pressure hoses are not required to pressurize the hydraulic chamber, the Carmat system requires percutaneous cables to deliver the required electrical power to the TAH. The Carmat TAH has been implanted as a bridge to transplantation in 24 patients in clinical trials (as of February 2022) [111]. SoftHeart is a pneumatically driven TAH entirely made of silicone rubber (except for its mechanical heart valves), and is the only completely soft TAH developed so far. SoftHeart has been tested only in vitro [50, 52]. Although the durability of SoftHeart has been improved compared with earlier iterations, it is still limited to only 110,000 cycles (approximately 30 h) [50, 52].

*A wireless power delivery system that uses magnetic fields to transfer power across the skin without the need for direct electrical connectivity.

Table 2.1 | Baseline characteristics of total artificial hearts.

TAH	Region	Type	Dimensions (mm)	Weight (g)	Volume (ml)	Power supply	Valve types	Development stage	Refs
AbioCor	USA	Fluid-driven	85 × 85 × 100	907	723[a]	TET	Mechanical	Stopped	[34, 91, 108]
AnyHeart	South Korea	Mechanical	60×100×100	650	600	TET	Mechanical	Stopped	[112–114]
Baylor TAH	USA and Japan	Mechanical	97 × 97 × 83	620	510	TET	Biological	Stopped	[115, 116]
BiVACOR	USA	Continuous flow	NR	650	NR	Percutaneous	No valves	Animal models	[117, 118]
Brno TAH	Czech Republic	Fluid-driven	NR	NR	NR	Percutaneous	Mechanical	Stopped	[98]
Carmat TAH (Aeson)	France	Fluid-driven	NR	900	750	Percutaneous	Biological	Approved	[119]
Cleveland continuous-flow TAH	USA	Continuous flow	60 × 60 × 100	486	160	Percutaneous	No valves	Animal models	[93, 120]
Cleveland Nimbus	USA	Mechanical	90 × 97 × 134	NR	700	TET	Biological	Stopped	[121, 122]
Eccentric roller TAH	Japan	Mechanical	100×100×80	1,800	800[a]	Percutaneous	No valves	Stopped	[123]
Electrohydraulic TAH	Japan	Fluid-driven	NR	2,492	872	TET	Mechanical	Stopped	[106]
Flow-transformed pulsatile TAH	Japan	Continuous flow	NR	2,000	550	Percutaneous	Mechanical	Stopped	[124]
Helical flow TAH	Japan	Continuous flow	80 × 80 × 77	565	493[a]	Percutaneous	No valves	Animal models	[94]
Hybrid continuous-flow TAH	USA	Continuous flow	50 × 50 × 50b	NR	125[a,b]	Percutaneous	No valves	In vitro	[125]
Impeller TAH	China	Continuous flow	40 × 40 × 80	250	128[a]	TET	No valves	Stopped	[126]

Continuation of Table 2.1

TAH	Region	Type	Dimensions (mm)	Weight (g)	Volume (ml)	Power supply	Valve types	Development stage	Refs
Linear TAH	Japan	Mechanical	85 × 85 × 94	1,900	560	Percutaneous	Mechanical	Stopped	[127, 128]
LVAD-TAH	Various	Continuous flow	Various	Various	Various	Percutaneous	No valves	Clinical trials	
MagScrew	USA	Mechanical	NR	890	506	TET	Biological	Stopped	[129]
Milwaukee Heart	USA	Mechanical	83 × 83 × 62	600	490	Percutaneous	Mechanical	Stopped	[130]
OregonHeart	USA	Continuous flow	85 × 75 × 60b	NR	130	Percutaneous	No valves	In vitro	[95, 131]
Ovalis	Germany	Mechanical	75 × 75 × 95	950	560	Percutaneous	Mechanical	Stopped	[132]
Penn State electric TAH	USA	Mechanical	91 × 91 × 94	700	778[aa]	TET	Mechanical	Stopped	[133]
Penn State pneumatic TAH	USA	Fluid-driven	NR	NR	NR	Percutaneous	Mechanical	Stopped	[99]
Phoenix	Taiwan	Fluid-driven	70 × 70 × 130	NR	NR	Percutaneous	Mechanical	Stopped	[100, 101]
Poisk TAH	Russia	Fluid-driven	125×100×70	220	NR	Percutaneous	NR	Stopped	[102, 103]
POLTAH	Poland	Fluid-driven	NR	NR	NR	Percutaneous	Mechanical	Stopped	[104]
Realheart TAH	Sweden	Mechanical	148×126×96	800	1790[a]	TET	Mechanical	Animal models	[134, 135]
ReinHeart	Germany	Mechanical	87 × 87 × 90	940	550	TET	Mechanical	Animal models	[136]
RollingHeart	Switzerland	Mechanical	80 × 80 × 110	NR	704[a]	Percutaneous	No valves	In vitro	[137]
SoftHeart	Switzerland	Fluid-driven	NR	136	447	Percutaneous	Mechanical	In vitro	[52]
SynCardia 70cc	USA	Fluid-driven	NR	240	400	Percutaneous	Mechanical	Approved	[34]
Undulation pump TAH	Japan	Continuous flow	77 × 77 × 79	660	310	Percutaneous	No valves	Stopped	[138]
Vienna TAH	Austria	Fluid-driven	72 × 72 × 120	NR	622[a]	Percutaneous	Mechanical	Stopped	[105]

LVAD-TAH, total artificial heart made with two left ventricular assist devices; NR, not reported, TAH, total artificial heart; TET, transcutaneous energy transfer.
aCalculated with the reported dimensions. bReported target size (not the current prototype).

2.3.2. Mechanical TAHs

The functionality and clinical applicability of fluiddriven TAHs were demonstrated in the early 1990s, but some of their disadvantages also became apparent. These TAHs were bulky, had poor durability and required percutaneous air pressure hoses and external drivers, which led scientists to explore alternative working mechanisms and shift the focus to mechanically actuated TAHs [139]. Mechanically actuated TAHs have many similarities to fluid-driven TAHs: both have two chambers to collect and eject blood, and inlet and outlet valves to direct the flow (Fig. 2.2b). Like fluid-driven TAHs, mechanical TAHs have a moving membrane to empty the blood chambers. However, instead of emptying the blood chambers with the use of pressurized gas or liquid (as in fluid-driven devices), mechanically actuated TAHs have an electric motor that drives a pusher plate against the blood chambers. Compared with fluid-driven TAHs, mechanical TAHs are less bulky and, most importantly, do not require large external drivers.

Historical devices

Multiple mechanical TAHs were developed in the 1990s by different teams and institutions: AnyHeart (Seoul University, Seoul, South Korea) [112–114], Baylor TAH (Baylor College of Medicine) [115, 116], Cleveland Nimbus (Cleveland Clinic) [121, 122], eccentric roller TAH (Hiroshima University, Hiroshima, Japan) [123], Linear TAH (Shinshu University, Nagano, Japan) [127, 128], MagScrew (Cleveland Clinic) [129], Milwaukee Heart (Milwaukee Heart Project, Milwaukee, WI, USA) [130], Ovalis (Humboldt University, Hamburg, Germany) [132] and Penn State electric TAH (Pennsylvania State University) [133]. These TAHs can be classified on the basis of their working mechanism as TAHs with mechanical actuation parts with either linear or rotary motion.

Current devices

We have identified three mechanically actuated devices that are still under development: Realheart TAH (Linköping University, Linköping, Sweden) [134, 135], ReinHeart (Helmholtz Institute, Aachen, Germany) [136] and RollingHeart (University of Lausanne, Lausanne, Switzerland) [137]. None of these devices has been assessed in clinical trials. Realheart and ReinHeart are fully implantable systems, including a TET system and internal battery packs. Both TAHs are actuated with magnets and are being assessed in animal studies. The RollingHeart is a mechanically actuated TAH developed in Switzerland and has only been tested in vitro. This TAH has a spherical shape, and two moving disks divide the spherical cavity into four chambers. An electrical motor moves the disks and thereby changes the volume of the chamber over time, which enables the filling and ejection of the blood. The design is unique because it does not require any valves. However, issues in the design of this TAH related to the recirculation and mixing of oxygenated with deoxygenated blood need to be addressed [137].

2.3.3. Continuous-flow TAHs

A major disadvantage of the above-mentioned fluid-driven and mechanical devices is that they require several indispensable components, such as blood collecting chambers, flexible membranes and valves. As a result, these devices are often bulky and usually do not fit

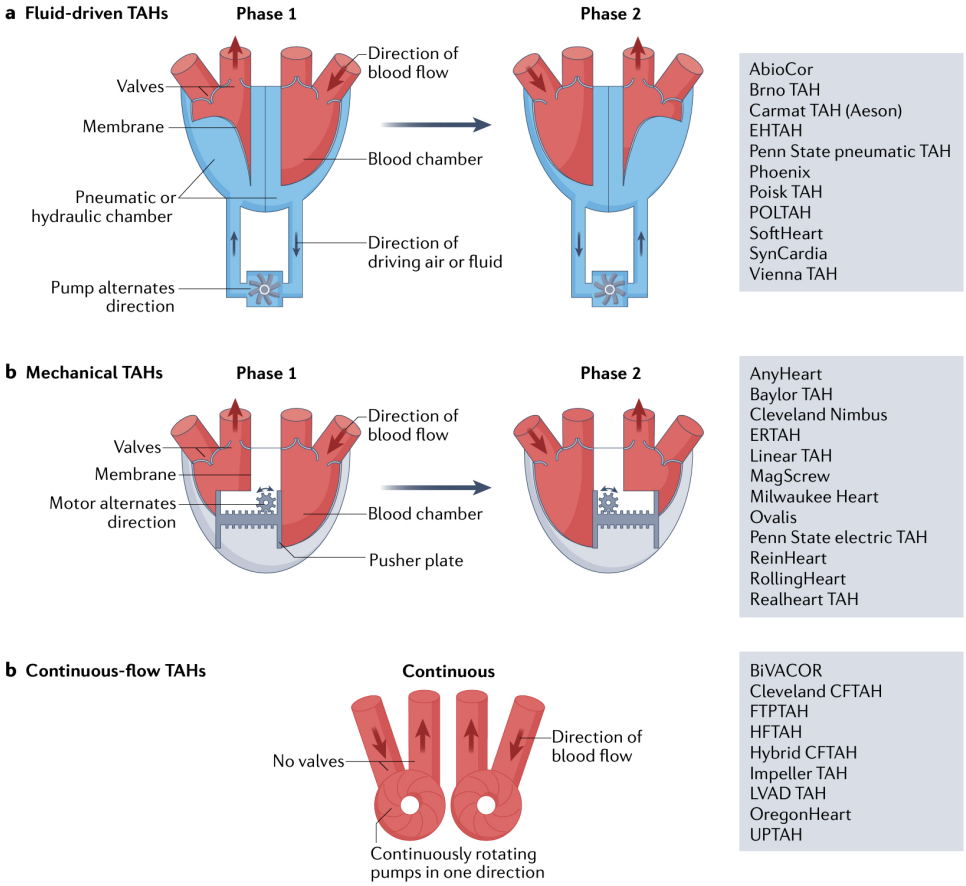

Figure 2.2 | Working mechanisms for different types of total artificial hearts. **a** | Fluid-driven total artificial hearts (TAHs) are composed of blood chambers and pneumatic or hydraulic chambers, which are separated by a membrane. A pump moves pressurized air or liquid into the pneumatic or hydraulic chambers, which moves the membrane and causes the ejection of the blood in a pulsatile manner. In the example shown in the figure, blood is ejected from both blood chambers alternately; however, some devices eject blood simultaneously from both chambers. The pump that moves the air or fluid can be implanted in the body or can be placed externally. For the latter, percutaneous hoses are required. Phase 1 shows the filling of the right blood chamber and the ejection of the left blood chamber. In phase 2, the pump rotates in the opposite direction, resulting in the filling of the left blood chamber and the ejection of the right blood chamber. **b** | Mechanical TAHs have two blood chambers and a mechanical motor, separated by a membrane. A motor pushes a mechanical part (pusher plate) against the membrane so that blood is ejected from that blood chamber. In the example, blood is ejected from the blood chambers alternately; however, some devices eject blood simultaneously from both chambers. In phase 1, the mechanical motor moves the pusher plate against the membrane of the left chamber, which ejects blood while the right chamber fills. In phase 2, the mechanical motor moves the pusher plate against the membrane of the right chamber, which ejects blood while the left ventricle fills. **c** | Continuous-flow TAHs have two continuous-flow pumps that pump blood continuously in one direction. Valves are usually not required. There is no filling or ejection phase because the blood is continuously being pumped. CFTAH, continuous-flow total artificial heart; EHTAH, electrohydraulic total artificial heart; ERTAH, eccentric roller total artificial heart; FTPTAH, flow-transformed pulsatile total artificial heart; HFTAH, helical flow total artificial heart; LVAD-TAH, total artificial heart made with two left ventricular assist devices; UPTAH, undulation pump total artificial heart.

inside petite patients, such as children and some women. The flexible membranes present in these devices are often prone to wear and tear because they deform with every heartbeat (about 35 million times a year). Continuous-flow pumps were introduced as an alternative to traditional pulsatile devices. Because blood is pumped continuously in these devices, they do not require valves, membranes or blood collecting chambers. Therefore, continuous-flow TAHs are smaller and lighter than other types of TAHs. In addition, their lifetime is longer owing to the absence of flexible membranes and the continuous rotation of their motors in a single direction. In the past two decades, substantial progress has been achieved in the field of continuous-flow LVADs, whose efficacy has been proved in clinical trials [140]. The longest reported duration of LVAD support without mechanical failure is 13 years [140, 141]. These positive results inspired many TAH researchers to use continuous-flow pumps for TAH development, mainly because of their superior power-to-size ratio and durability compared with fluid-driven and mechanical TAHs. After implantation of a regular continuous-flow LVAD, some blood flow pulsatility remains because the native heart is left in place. By contrast, continuous-flow TAHs eject blood continuously and generate a true continuous blood flow. Given that the physiological response to long-term continuous blood flow is unclear [142, 143], most of the investigators developing continuous-flow TAHs are exploring the possibility of modulating the flow to provide some level of pulsatilily. So far, achieving the same pulsatility index as with the native heart or the pulsatile TAHs has not been possible.

Historical devices

The first continuous-flow TAHs were developed in the 1990s. We have identified three continuous-flow TAH devices, which are no longer in use: the flow-transformed pulsatile TAH (University of Tokyo, Tokyo, Japan) [124], the undulation pump TAH (UPTAH) (University of Tokyo, Tokyo, Japan) [138] and the Impeller TAH (Jiangsu University, Zhenjiang, China) [126].

Current devices

Although LVADs were developed to assist the native left ventricle, these devices are powerful enough to take over the function of the native ventricle completely. Therefore, several research groups have investigated the efficacy of two commercially available LVADs (such as HeartMate II, Heartmate III, HeartWare HVAD, Jarvik 2000 and HeartAssist 5) combined into a TAH configuration after removing the native heart [144–153]. The configuration of two LVADs functioning as a TAH has been tested in animal studies and clinical trials [144–153]. In this Review, we refer to the configuration of two commercially available LVADs functioning as a TAH as LVAD-TAH. Many TAH developers have used continuous-flow pump technology to develop custom-built TAH devices. Several continuous-flow TAHs are currently under development: BiVACOR (BiVACOR, Houston, TX, USA) [117], Cleveland continuous-flow TAH (CFTAH) [93, 120] and helical-flow TAH (HFTAH) (University of Tokyo, Tokyo, Japan) [94] are being assessed in chronic animal experiments, and Hybrid CFTAH (Drexel University, Philadelphia, PA, USA) [125] and OregonHeart (OregonHeart, Portland, OR, USA) [95, 131] are undergoing in vitro testing.

2.3.4. Balancing right and left cardiac outputs of TAHs

A major issue that must be addressed for successful TAH implantation is the balancing of the right and left cardiac outputs [74]. In a physiological setting, the cardiac output of the left ventricle is slightly greater than the cardiac output of the right ventricle [154], because part of the oxygen-rich blood from the aorta goes into the bronchial arteries that supply the lung parenchyma, which then drains back to the left atrium [155, 156]. Therefore, part of the blood ejected by the left ventricle returns to the left atrium without passing through the right circulation, resulting in a larger systemic flow than pulmonary flow. In healthy individuals, the bronchial shunt* flow is approximately 1% of the cardiac output [155]. However, various pulmonary diseases increase the bronchial shunt flow to up to one-third of the left ventricular output [155]. A study showed that three out of five patients with an implanted AbioCor TAH had increases in bronchial flow of up to 1.4 l/min, which is 28% of a cardiac output of 5 l/min [157]. The native heart continuously balances the systemic and pulmonary flows by ventricular interdependence, via the Frank-Starling mechanism† [154], but this balancing mechanism is difficult to implement in TAHs. If a TAH cannot compensate for flow differences in venous return, severe complications such as lung oedema and respiratory failure will arise [74]. Therefore, balancing the outputs to the systemic and pulmonary circulations during TAH support is one of the biggest challenges in TAH design [74, 158].

Pulsatile TAHs can alter the stroke volume of one of the blood chambers if a sudden change in atrial pressure occurs. The stroke volume can be adjusted in two ways: by adjusting the filling volume inside the chamber or by adjusting the ejection fraction. This adjustment is an active process that requires either manual control or automatic control by feedback from incorporated sensors. In the Carmat system, many internal electronics, microprocessors and sensors are needed to constantly monitor different internal pressures, as well as an ultrasound transducer to monitor the position of the membrane [159]. In SynCardia, the system parameters are manually set to fill the ventricles to 70-85% of their capacity, to create a buffer that passively enables the augmentation of venous return [97]. As a result, SynCardia is sensitive to preload‡, demonstrating Frank-Starling-like behaviour under normal conditions [97]. Therefore, Syncardia can provide increased output in response to increased preload. However, the shape of the Syncardia Frank-Starling curve differs from that of the human heart, because this TAH is inelastic [97, 160]. ReinHearts design uses the concept of passive and active limitation of the right-sided filling, in combination with the right ventricle having a fixed volume that is 10% smaller than that of the left ventricle [161].

A balancing mechanism is also required for continuous-flow TAHs, because a sudden drop in atrial pressure quickly results in negative atrial pressures (suction event). Continuous-flow TAHs that have two separate pumps for the left and right circulation (such as in the LVAD-TAH, Hybrid CFTAH and HFTAH) have some inherent flow-balancing capacity [94, 125, 158]. However, a study testing the performance of several types of continuous-flow TAHs made from two separate pumps in an in vitro set-up in which systemic and pulmonary resistance were changed to mimic the human cardiovascular system

*The physiological passage of oxygenated blood from the aorta to the bronchial circulation. This blood returns directly to the left atrium, thereby bypassing the right side of the heart.

†This law states that the stroke volume of the heart increases in response to an increase in the volume of blood in the ventricles before contraction (the end diastolic volume), when all other factors remain constant.

‡The filling pressure of the ventricle at the end of diastole, which is determined by the atrial pressure.

during daily activities showed that, although all the devices had some flow-balancing capacity, none was able to accommodate all resistance settings [158]. Cleveland CFTAH, BiVACOR and OregonHeart use a single moving rotor to perfuse the pulmonary and systemic circulations. The rotor of the OregonHeart is typically set to pump 60% of each beat time to the left circulation and 40% to the right circulation, but this ratio can be adjusted manually to meet the needs of a wide range of physiological conditions101. BiVACOR incorporates an axial magnetic levitation system, which enables active control of the position of the single moving rotor [117]. A leftward shift of the rotor causes an increase in left-sided flow [117]. The Cleveland CFTAH uses a similar mechanism, but in this TAH, the rotor can have passive axial movements inside the stator[§], enabling the TAH to balance the left and right outputs passively, without any sensors [162]. The axial position of the rotor is determined by the pressure gradient between the left and right blood chambers. When the pressure drops in one of the blood chambers, the rotor passively moves to that side, which helps to prevent atrium wall suction and balances the cardiac outputs [162]. This low-complexity passive feedback mechanism inherently reduces the risk of device failure compared with the complex active feedback mechanisms in other TAHs.

2.4. Chronic animal trials

Chronic animal trials are an important step in the preclinical testing of new TAHs. Chronic animal trials have been conducted for AbioCor, AnyHeart, Baylor TAH, BiVACOR, Brno TAH, Carmat TAH, Cleveland CFTAH, Cleveland Nimbus, EHTAH, HFTAH, LVAD-TAH, MagScrew, Penn State electric TAH, Penn State pneumatic TAH, Phoenix, ReinHeart, SynCardia, UPTAH and Vienna TAH (Table 2.2). Calves are the most frequently used animal model for TAH implantation, followed by goats and sheep. In most of the older chronic animal trials, the animal was implanted with a TAH and was followed up until death. In contemporary studies, researchers often terminate the experiments after a given follow-up period (usually 30-90 days, according to FDA regulations), by taking out the TAH. For the latter studies, elective termination is assigned as the cause of death in Table 2.2. Nevertheless, the follow-up time in chronic animal trials is often short. Only ten TAH devices were associated with a maximum survival time exceeding 100 days (AbioCor [163], Brno TAH [98], Cleveland Nimbus [164], EHTAH [165], HFTAH [94], Penn State electric TAH [166], Penn State pneumatic TAH [99], SynCardia [79], UPTAH [138] and Vienna TAH [105]) and only one device was associated with a maximum survival time of over a year (Penn State electric TAH) [166]. Overall, the most frequently reported cause of death in chronic animal trials is mechanical failure of the device. Examples of mechanical failure that occurred in chronic animal trials include an electrical short circuit caused by fluid entering the electronics, dislocation of TET coils, obstruction of the inflow or outflow grafts of the TAH, membrane ruptures, air leakage in pneumatic devices, failure of the implantable battery and a defect or lock in pump bearings [80, 94, 129, 138, 152, 165, 167–170]. The second- and third-most frequently reported reasons of death are thromboembolic complications and respiratory failure, respectively.

[§]The stationary part of a rotary machine or device.

2.5. Clinical trials

Since the first successful implantation of a TAH in humans in 1982, a total of nine different TAH devices have been assessed in patients in clinical trials: AbioCor, Brno TAH, Carmat TAH, LVAD-TAH, Penn State pneumatic TAH, Phoenix, Poisk TAH, SynCardia and Vienna TAH (Table 2.3). These TAHs are pneumatic or hydraulic pulsatile devices, except the continuous-flow LVAD-TAH.

2.5.1. Early studies in humans

Several fluid-driven TAHs were tested in humans in the 1980s and 1990s. Overall, the outcomes were poor, and many patients died within the first days after receiving a TAH or could not successfully receive a heart transplant [31, 171, 172]. The Brno TAH, developed in the Czech Republic, was implanted in six patients [171]. All patients died of serious complications related to poor device biocompatibility, with a maximum survival of 10 days [171]. The Phoenix TAH was implanted in two patients [31, 173]. One patient received a heart transplant on the same day as TAH implantation but died 1 day after receiving the heart transplant [31]. The other patient was successfully bridged to heart transplantation after 15 days of support with the Phoenix TAH [173]. The Poisk TAH was developed in Russia and has been implanted in 13 patients [172]. Of these patients, 12 died during support with the Poisk TAH, for unknown reasons. The maximum period of support was 15 days [172]. The Vienna TAH was implanted in five patients, and three of these patients were successfully bridged to heart transplantation [105, 174]. The maximum duration of support was 22 days [105, 174]. The Penn State pneumatic TAH was implanted in three patients [99]. Two of the patients were bridged to heart transplantation, and the third patient did not receive a heart transplant because a suitable donor was not found. After 70 days of support, the patient had a cerebrovascular accident, manifested by aphasia. The TAH support stopped on day 379 when this patient had a respiratory arrest and could not be resuscitated [99].

2.5.2. Latest clinical trials

AbioCor, the first fully implantable TAH that used a TET system, was implanted in 14 patients between 2001 and 2003 [91]. The maximum duration of support was 512 days, which occurred in a patient who died owing to a membrane rupture in the device [175]. The most frequently observed causes of death were thromboembolic complications and multiorgan failure [175]. The development of AbioCor stopped in 2007 owing to concerns related to the high number of patients who died because of complications of stroke (caused by an ineffective anticoagulation regimen), the low quality of life of the patients and the poor commercial viability [74].

Since 2011, several teams worldwide have studied the use of a combination of two commercially available rotary LVADs (HeartMate II, HeartMate III or HeartWare HVAD) adapted to a TAH configuration to replace the native heart completely [145, 146, 148–150, 153]. These LVAD- TAHs have been implanted in nine patients [145, 146, 148–150, 153], with a maximum reported duration of support of 6 months [148]. The most frequently reported complications were related to thromboembolic and haemorrhagic events [145, 146, 148–150, 153].

Table 2.2 | Total artificial hearts assessed in chronic animal trials

TAH	Type	Study period	Number of animals	Maximum survival (days)	Most reported causes of death (n)	refs
AbioCor[a]	Fluid-driven	1990 – 2001	120	108	Elective termination (16), mechanical failure (5)	[74, 163, 168, 176, 177]
AnyHeart	Mechanical	1990	1	4	Respiratory failure (1)	[113]
Baylor TAH[a]	Mechanical	1993 – 1994	8	7	NR	[178, 179]
BiVACORa	Continuous flow	2017	15	90	NR	[118, 180]
Brno TAH[a]	Fluid-driven	1983 – 1995	168	314	Thromboembolic complications (6), mechanical failure (5)	[98, 170, 181, 182]
Carmat TAH (Aeson)	Fluid-driven	2014 – 2017	12	10	Thromboembolic complications (4), respiratory failure (2), bleeding (2),	[169, 183]
Cleveland CFTAH	Continuous flow	2015	17	90	Elective termination (4), bleeding (3)	[184]
Cleveland Nimbus	Mechanical	1992 – 1994	12	120	Mechanical failure (10), thromboembolic complications (1), infection (1)	[121, 164]
Electrohydraulic TAH[a]	Fluid-driven	1990 – 2003	57	159	Mechanical failure (14), thromboembolic complications (7), respiratory failure (7)	[165, 185–189]
Helical flow TAH	Continuous flow	2015	13	100	Mechanical failure (7)	[94]

Continuation of Table 2.2

TAH	Type	Study period	Number of animals	Maximum survival (days)	Most reported causes of death (n)	refs
LVAD-TAH	Continuous flow	2009 – 2021	40	92	Thromboembolic complications (23), elective termination (8)	[144, 147, 151, 152]
MagScrew	Mechanical	2001 – 2005	12	92	Mechanical failure (5), respiratory failure (3)	[129, 190]
Penn State electric TAH	Mechanical	1990 – 2000	54	388	Mechanical failure (17), respiratory failure (13)	[133, 166, 191–193]
Penn State pneumatic TAH[a]	Fluid-driven	1979 – 1989	47	353	Mechanical failure (22), thromboembolic complications (6)	[99, 194]
Phoenix	Fluid-driven	2001	41	60	Respiratory failure (22), thromboembolic (6), multiorgan failure (6)	[100]
Reinheart[a]	Mechanical	2015	12	2	NR	[136]
SynCardia	Fluid-driven	1979 – 1981	31	268	Thromboembolic complications (8), bleeding (5)	[79, 80]
Undulation pump TAH	Continuous flow	2000 – 2011	68	153	Mechanical failure (30), bleeding (15)	[138, 167, 195, 196]
Vienna TAH[a]	Fluid-driven	1991	15	180	Mechanical failure (3)	[105]

All devices that have been assessed in published chronic animal trials are listed. The cause of death of the animals was not always reported in the literature, especially for AbioCor, Baylor TAH, BiVACOR, Brno TAH, electrohydraulic TAH, ReinHeart, Penn State pneumatic TAH and Vienna TAH. LVAD-TAH, total artificial heart made with two left ventricular assist devices; NR, not reported; TAH, total artificial heart. [a]Devices with high numbers of missing animal data.

Table 2.3 | Total artificial hearts assessed in clinical trials

TAH	Type	Number of implanted devices	TAH support duration (days) Mean(max)	Number implanted as bridge to transplantation (%)	Number of deaths during TAH support (%)	Most reported causes of death during TAH support (%)	refs
AbioCor	Fluid-driven	11	142(512)	0 (0)	10 (100)	Thromboembolic complications (50), multiorgan failure (33)	[175]
Brno TAH	Fluid-driven	6	5(10)	0 (0)	6 (100)	Thromboembolic complications (50), bleeding (33)	[171]
Carmat TAH (Aeson)[a]	Fluid-driven	24	166(308)	(45)	(55)	Multiorgan failure (50), mechanical failure (33)	[197, 198]
LVAD-TAH	Continuous flow	9	92(180)	4 (44)	4 (44)	Multiorgan failure (50), bleeding (50)	[145, 146, 148, 150, 151, 153]
Penn State pneumatic TAH	Fluid-driven	3	135(379)	2 (67)	1 (33)	Aspiration pneumonia (100)	[99]
Phoenix	Fluid-driven	2	8(15)	2 (100)	0 (0)	–	[31, 173]
Poisk TAH	Fluid-driven	13	5(15)	1 (8)	12 (92)	Unknown	[172]
SynCardia[b]	Fluid-driven	>2100	94(4.5 years)	(65)	(33)	Multiorgan failure(40), thromboembolic complications (13), infection (10)	[199–206]
Vienna TAH	Fluid-driven	5	12(22)	3 (60)	2 (40)	Infection (50), multiorgan failure (50)	[105, 174]

All TAH devices that were implanted in patients are listed. LVAD-TAH, total artificial heart made with two left ventricular assist devices; TAH, total artificial heart. [a]The trial on the Carmat TAH is currently enrolling patients [207]; a total of 24 patients received the Carmat TAH (as of February 2022), of which data from only 11 patients are described in the literature; the mean duration of support, bridge to transplantation, death during TAH support and most reported causes of death are based on data from these 11 patients. [b]SynCardia TAHs have been implanted in over 2100 patients, of which only a fraction has been reported in the literature; we used data from eight clinical trials describing 574 patients implanted with a SynCardia TAH to calculate the mean duration of support, bridge to transplantation, death during TAH support and most reported causes of death [31, 167–169, 171–173]

The pneumatically actuated SynCardia, the first TAH that became commercially available as a bridge to transplantation therapy, is currently available in two sizes (70 cm3 or 50 cm3 ventricles), which enables its implantation in patients of various body sizes. The youngest recipient of a 50 cm3 SynCardia is a boy aged 10 years [208]. So far, Syncardia has been implanted in over 2100 patients worldwide, with a maximum reported duration of support of 4.5 years receiving permanent SynCardia support [110]. Despite the poor prognosis that the SynCardia recipients have before TAH implantation, the long-term survival of recipients of a heart transplant after temporary support with SynCardia is encouraging and comparable with the long-term survival of recipients of a heart transplant who did not receive SynCardia support [209]. Twelve months after the SynCardia implantation, 55% of the patients had received heart transplantation, 14% were still supported by the SynCardia device and 31% died before undergoing a heart transplantation [199]. SynCardia is currently being evaluated in an approved investigational device exemption[¶] clinical trial for use as destination therapy [66].

The care of patients receiving SynCardia support remains challenging [209]. The percutaneous hoses are frequently associated with driveline infections, and the TAH material itself often causes mediastinitis and constrictive pericarditis [209]. The period after heart transplantation is associated with a high risk of (temporary) haemodialysis owing to impaired renal perfusion and postoperative compression of the donor heart [209]. The risk of post-transplantation complications increases with prolonged TAH support [209]. The most frequently reported causes of death during support with a SynCardia device are multiorgan failure (40%), thromboembolic complications (13%) and infection (10%) [199–206]. Although minor device malfunctions are frequently described in the literature, severe device malfunctions that lead to death are rare (<2% of the deaths during SynCardia support) [199–206].

The hydraulic TAH developed by Carmat received CE approval as bridge to transplantation therapy in 2020, but the company is continuing clinical research with the aim of ultimately using the Carmat TAH as destination therapy [111]. The Carmat TAH has been implanted as a bridge to transplantation in 24 patients (as of February 2022) [197, 198, 207]. Patient enrollment for the second clinical trial on the Carmat TAH is ongoing56. Although the Carmat TAH was designed to promote biocompatibility, given that its diaphragms and valves are made from bovine pericardium, all patients must receive a strict anticoagulation regimen [198]. Thus far, the clinical outcomes of 11 recipients of the Carmat TAH have been described in the literature [197, 198], with a maximum support duration of 308 days [198]. Of these patients, six died during TAH support, and the other five were successfully bridged to heart transplantation[197, 198]. The causes of death were multiorgan failure (50%), mechanical failure (33%) and respiratory failure (17%). No thromboembolic complications were observed [197, 198].

To date, no TAH has been approved as destination therapy. Only the SynCardia and Carmat TAH are approved as temporary therapy to bridge a severely ill patient to heart transplantation. The percutaneous drivelines of both TAHs are associated with low quality of life and a high risk of infection128. Long-term support with the SynCardia TAH is associated with serious risks such as stroke and multiorgan failure [200–206, 209].

[¶]Type of FDA approval that allows the investigational device to be used in a clinical study in order to collect safety and efficacy data.

2.6. Technological advances and future perspectives

2.6.1. TET systems to improve quality of life

The TAHs currently available for clinical use (SynCardia and Carmat TAH) have percutaneous cables to supply power to the devices. Percutaneous drivelines are associated with a high risk of infection and reduce the patients quality of life owing to the limited freedom of movement of the patient. Therefore, TAH devices intended for approval as destination therapy should ideally omit these percutaneous cables. Percutaneous cables can be avoided when all TAH components are implanted inside the body and the electrical power is wirelessly transferred via a TET system.

A TET system transfers all the electrical power required by the TAH across the patients skin via an internal and external coil. Part of this energy is stored in internal battery packs, enabling the patient to have free-from-charging periods. In the past decade, batteries have become smaller and have longer battery life, enabling implantation in the body. In addition to small and high-capacity batteries, high efficiency of the TAH is also essential when energy is provided through a TET system. Figure 2.3 shows the efficiencies of all types of TAH. The methodology we used to calculate the efficiencies is described in Box 1.

Generally, fluid-driven TAHs are slow systems because they first have to move fluid or air to empty the blood-containing chambers. Therefore, emptying the chambers in fluid-driven systems is easier and more efficient at low beat rates than at high beat rates. Fluid-driven TAHs generally show a decline in efficiency at high beat rates. For example, the efficiency of the hydraulic EHTAH declines at cardiac outputs exceeding 6 l/min (Fig. 2.3a). Like fluid-driven TAHs, mechanical TAHs also have blood chambers, and higher cardiac output can be achieved by maximizing stroke volume and, if needed, by increasing the beat rate. In general, mechanical TAHs become more efficient at higher beat rates and, therefore, at higher cardiac outputs (Fig. 2.3b). The highest efficiency reported for mechanical TAHs is often reached at a cardiac output of approximately 10 l/min [112, 116, 121, 123, 129, 130]. Compared with pulsatile devices, continuous-flow devices do not have blood-collecting chambers because they pump blood continuously. In general, the efficiency of continuous-flow pumps increases with higher cardiac outputs. The optimal efficiency of most continuous-flow TAHs is at a much higher cardiac output than the average cardiac output of 5 l/min (Fig. 2.3c).

Prolonging the free-from-charging periods during support with TAHs using TET systems

Efficient TAHs prolong the period that the patient can engage in activities without charging the TAH, which will improve the quality of life of TAH recipients in the future. The most up-to-date battery technology used for TET systems in TAHs has been described by the team developing ReinHeart [210]. The ReinHeart system has implantable 12 volt lithium-iron-phosphate batteries with 1.1 Ah capacity [210]. We have used this battery as a standard to compare the running time (defined as the maximum time in which the TAH recipient can engage in activities without charging the TAH) of current TAHs if they hypothetically had TET systems with this specific internal battery capacity (Fig. 2.3d). The running time was calculated for a cardiac output of at least 5 l/min against a physiological

mean left afterload[‖] (≥90 mmHg). The data show that current TAH devices can hypothetically support the patients with a physiological cardiac output for approximately 1 h with the current battery technology (Fig. 2.3c; Table 2.4). For reference, the AbioCor (implanted for the first time in 2001) had the capacity to support the patient for up to 20 min without connection to a power source [108]. Our comparison results suggest that continuous-flow devices (Cleveland CFTAH and OregonHeart) are better than mechanically actuated devices in terms of their working time with internal batteries alone because continuous-flow TAHs require less input power than other TAH types to generate a higher cardiac output (Fig. 2.3d). Among continuous-flow devices, OregonHeart performs slightly better than the Cleveland CFTAH with regards to efficiency and the required input power (Fig. 2.3d). The mechanical ReinHeart has a relatively high power consumption (12.5 W) and provides less cardiac output than the other four TAHs analysed, resulting in the lowest efficiency (10.8%).

Box 1 | Calculation of TAH efficiencies

To compare the efficiency of the different types of total artificial heart (TAH) shown in fig. 2.3, we used a consistent measure of the power consumed by the TAH (input power) and the amount of work (output power) performed by the TAH to pump blood against physiological pressures. The numerical value of the output power is the product of the difference in outlet and inlet pressure (pressure head) and the flow of blood generated by the heart (cardiac output). For pulsatile TAHs, we calculated the pressure head as the difference between the mean afterload and the intraventricular pressure. We assume that during diastole, the pressure inside the TAH ventricle drops to near 0 mmHg, as in the native heart [211]. For continuous-flow TAHs, we calculated the pressure head as the difference between the mean afterload and the mean preload. We have used the following equation to calculate the output power of the TAHs:

$$Output\ power = Q_{sys}H_{sys} + Q_{pul}H_{pul}$$

where the output power is in watt, Q_{sys} and Q_{pul} are the resulting cardiac output (in m^3/s) for the systemic and pulmonary circulations, respectively, and H_{sys} and H_{pul} are the pressure heads (in N/m^2) for systemic and pulmonary circulations, respectively, against which the TAH must pump. The input power to the TAH is an individual number unique to the device. Therefore, we analysed only the TAHs that have the corresponding input power reported in the literature. We have used the following equation for calculating the efficiency (η) of a TAH on the basis of input power and output power:

$$\eta = \frac{Output\ power}{Tutput\ power} \times 1oo\%$$

Overall, we can conclude that for most TAHs, either the power consumption or the efficiency does not yet reach the levels required to use a TET system. To date, the AbioCor is the only fully implantable TAH that used a TET system that has been implanted in patients. The latest technological advances in TET systems are promising for future TAH

[‖]The amount of pressure that the ventricle needs to exert to eject the blood during ventricular contraction.

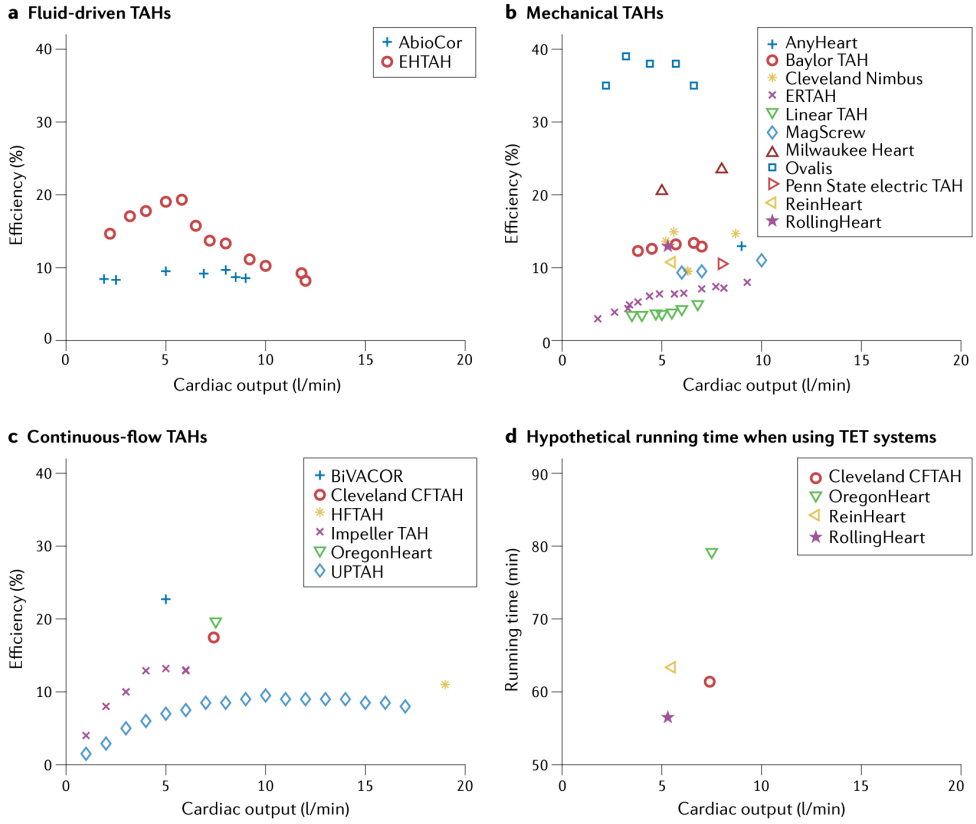

Figure 2.3 | Efficiency of total artificial hearts. Overall efficiencies of total artificial hearts (TAHs) are depicted against the cardiac output. The method of calculation for the overall efficiencies of the TAHs is explained in Box 1. All values are measured under physiological mean left afterload conditions (≥90 mmHg). If right afterload was not reported when tested in a double-sided mock loop, we assumed it to be 20 mmHg. For some TAH devices, we were not able to obtain data to calculate efficiencies. Data for ReinHeart were shared by the authors upon request. a | Overall efficiencies for fluid-driven TAHs [106, 213]. b | Overall efficiencies for mechanical TAHs [112, 116, 121, 123, 127, 129, 130, 132, 137, 214]. c | Overall efficiencies for continuous-flow TAHs [94, 117, 126, 184, 195, 212]. d | Running time (defined as the maximum time in which the TAH recipient can engage in activities without charging the TAH) of TAHs developed since 2015 [137, 184, 212], calculated as though these TAHs hypothetically had transcutaneous energy transfer systems with the internal battery capacity of the most recently available battery technology (from the ReinHeart system). CFTAH, continuous-flow total artificial heart; EHTAH, electrohydraulic total artificial heart; ERTAH, eccentric roller total artificial heart; HFTAH, helical flow total artificial heart; UPTAH, undulation pump total artificial heart.

Table 2.4 | Power requirements and efficiency of total artificial hearts

TAH	Type	Cardiac output (l/min)	input power (W)	output power (W)	Efficiency (%)	running time without charging (min)	Refs
Cleveland CFTAH	Continuous flow	7.4	12.9	1.7	13.3	61	[184]
OregonHeart	Continuous flow	7.5	10.0	1.7	17.5	79	[212]
ReinHeart	Mechanical	5.5	12.5	1.3	10.8	63	shared upon request[a]
RollingHeart	Mechanical	5.3	14.0	2.0	14.1	57	[137]

All TAHs currently being investigated with published power requirements are listed. For the TAHs not listed in the table, no power requirements have been reported in the literature. All parameters were measured at a physiological mean left afterload (90 mmHg). TAH, total artificial heart. [a]Data for ReinHeart was shared by the authors upon request.

development. Battery technology is rapidly evolving, resulting in more powerful and compact batteries. Powerful implantable batteries will prolong the time frame in which the patient can be free from having to use an electrical power source for the TAH. Furthermore, improving the overall efficiency of the TAH itself will help to use the stored energy of the internal battery packs more effectively. Therefore, we expect that transcutaneous charging of a fully implantable TAH with charging-free periods of >1 h will be feasible in the near future.

2.6.2. Bioinspired TAHs aim to improve biocompatibility

Since the beginning of TAH development in the 1960s, TAHs have been associated with limited biocompatibility resulting in frequently occurring pannus and thrombus formation. Although many attempts have been made to improve the design of TAHs, the biocompatibility issues could not be resolved. By the 1970s, the realization came that no implanted artificial material will ever come close to the anti-thrombogenic properties of the patients endothelium. Current TAH devices are still associated with numerous complications related to biocompatibility. A high number of thromboembolic events have been reported in clinical trials and animal studies. All TAH recipients require a strict anticoagulation regimen that results in a high risk of haemorrhagic events. Devices such as the Carmat TAH improved biocompatibility by using membranes and heart valves containing sheep pericardial tissue. The available data on the Carmat TAH suggest that patients receiving a Carmat TAH need less anticoagulation medication than patients receiving a SynCardia device [198]. Upcoming solutions to address biocompatibility issues can be found in new developments in biomaterials science. If growing endothelium derived from the patient

on the blood-contacting surfaces of the TAH becomes possible, this strategy would probably resolve many biocompatibility issues. The developers of the HybridHeart aim to grow a layer of patient-derived endothelium on the inside of the soft ventricles with the use of biofunctionalization** and in situ tissue-engineering techniques [215]. However, owing to the large surface area and the continuous movement of the TAH ventricles, applying tissue engineering techniques on TAH devices remains challenging. Even after five decades of research, we are still far from being able to create a living endothelium inside the ventricles of a TAH [216].

The interaction of rigid components with the blood is associated with many adverse effects. These effects have been most widely studied for the rotors in LVAD devices and include risks of thrombus formation and non-surgical bleeding caused by the device-altered haemostatic function [64, 217]. The artificial surface of the rotary blood pumps can induce platelet adhesion, which increases the risk of thrombosis, and the rotating parts can induce loss of haemostasis-related receptors on platelets, which increases the risk of bleeding [217]. Haemolysis is the second-most common LVAD-related complication, presumably caused by the destruction of erythrocytes in the rotating LVAD devices [218]. Problems related to the incompatibility between hard machines and soft human tissue might be solved if the machine is as soft as the human tissue. Soft robotics is an emerging research field that focuses on developing robots made of soft materials. In the past year, a few research groups have shifted their focus to developing TAHs that are completely soft on the inside and outside, such as SoftHeart and HybridHeart [50, 51, 219]. The primary benefit of developing soft TAHs is that they mimic the natural movement of the heart, potentially reducing the stress on the blood and thereby resulting in fewer adverse effects [52].

The second benefit of soft robotic cardiac devices is that they are compliant because they can stretch, contract or bend. As a result, soft robotic cardiac devices can promote both the contraction and the relaxation phases of the heart [53]. Owing to its elastic behaviour, the ventricle of a soft TAH has higher passive filling and contracts more forcefully at high filling pressures than at low filling pressures. Therefore, the soft robotic cardiac device passively ejects higher cardiac outputs at larger end-diastolic volumes, like the Frank-Starling mechanism of the native heart. This compliance is inherent to soft robotic cardiac devices [220] and works without the need for any sensors or manual control. A soft robotic cardiac sleeve developed in 2017, the first soft robotic cardiac assist device under development, shows Frank-Starling behaviour [53]. This Frank-Starling mechanism could mean that the expansible volume capabilities of future soft robotic TAHs can balance the left and right outputs to achieve Frank-Starling curve behaviour that resembles human physiology.

Given that TAHs need to work for a high number of cycles (one cycle for every heartbeat), achieving high durability and reliability remains a major challenge for TAH development. The SoftHeart had a maximum working duration of 110,000 cycles (approximately 30 h), after which a fatigue crack caused device failure [52]. Although current soft TAHs are at early development stages, with future optimization their benefits might outweigh those of traditionally rigid TAH devices.

**The modification of a material to add a biological function, such as replace or repair, while at the same time being accepted by the host organism.

2.7. Conclusions

After more than six decades of TAH research, TAHs have been successfully used in over 2200 patients as a bridge to heart transplantation, but a TAH suitable for destination therapy has not yet been developed. Some of the major drawbacks of current TAHs are high complication rates, bulkiness, short durability, poor biocompatibility and low quality of life for the patients. These issues need to be resolved before the potential of TAHs as destination therapy can be realized. Nevertheless, the field of TAH research is rapidly evolving, and various approaches are emerging that could potentially improve the quality of life of TAH recipients. With the development of TET systems and improved TAH efficiency, percutaneous cables will no longer be necessary to provide electrical power to the implanted TAH. The field of battery technology is continuously improving, delivering more compact batteries that are easier to implant internally and that prolong the period during which the patient can engage in activities without charging the TAH. New insights into soft robotics might result in the development of completely soft TAHs that reduce the occurrence of adverse effects associated with traditionally rigid TAHs. Meanwhile, smart biomaterials might solve current biocompatibility issues. In the future, these new technologies have the potential to enable the development of the first TAH approved for destination therapy.

3

Modeling the behavior of elastic pouch motors

Abstract

Pouch motors are one of the recently developed soft actuators, which are known particularly for their low-weight, ease of fabrication and large stroke. To date, several studies have been performed to develop and model new pouch motors designs to improve their functionality. All models assume that the material is behaving inextensibly, i.e. not stretchable. Here, we propose an analytical model for pouch motors where we consider the materials to be stretchable, and show that stretchability of pouch motors sets a limit for the maximum contraction and force, and therefore cannot be neglected even when using nearly inextensible materials. We evaluate our model qualitatively by conducting 'blocked-displacement' experiments on single pouches made of various materials with different elasticity.

Based on: **M. Arfaee**, J. Kluin, J.T.B. Overvelde, *Modeling the behavior of elastic pouch motors.* 2023 IEEE International Conference on Soft Robotics (RoboSoft), Singapore, 2769-4534 (2023)

3.1. Introduction

In the last decade, soft robots have become a popular alternative solution to rigid robots due to their capability of adapting to their environment. Their inherent adaptability makes them suitable for a wide range of applications in industry, health care, robotic surgery, assistive devices, and other areas [220, 221]. Soft robots are considered a reliable and safe solution for devices which are in contact with the human body [39], such as wearable devices [222, 223], rehabilitation devices [45, 224] and even implantable devices [225, 226]. Soft robots and their soft actuators are typically made from stretchable or flexible materials, which makes them relatively easy and inexpensive to manufacture, and makes them lightweight.

To date, several studies have been performed on developing and optimizing different types of soft actuators [227–229]. One of the recently developed soft actuators is referred to as the pouch motors, which is a thin-walled actuator typically fabricated by heat sealing [230]. Pouch motors can be driven using air, liquid, or both [230, 231] Some studies have been performed on modifying pouch motors, e.g. by pairing pouch motors to increase their contraction ratio and strength [232] and improving the contraction ratio and force output by developing new origami-based structures that use pouch motors [228]. Moreover, it has also been demonstrated that pouch motors can be driven by liquid-to-gas phase transition [231].

Typically, the pouch motors are fabricated from nearly inextensible materials, which has also enabled an analytical description of the behavior of linear and rotational pouch motors [230]. However, for some (medical) applications it could prove beneficial to use softer materials to fabricate pouch motors, to enable different stiffnesses in their actuated state. Currently, a model that describes the elastic behavior of pouch motors is missing and it is unclear how material stiffness affects the behavior of pouch motors. The aim of the present study is to develop a model that considers the effect of material stretchability and investigates pouch motors behavior under different loading conditions. In this paper, we propose an analytical model to describe the effect of material elasticity on the functionality of pouch motors. Using this model we show that the material elasticity of pouch motors has a significant effect on their functionality, which we validate using experiments on linear pouch motors made from three different materials. Therefore, material stretchability has to be considered in designing an optimized actuator for target applications.

The remainder of this paper is divided into the following sections. in the first section, we extend the model previously derived for inextensible pouch motors [230] to take material stretchability into account. Secondly, we discuss a 'blocked-displacement' setup to be able to effectively measure the behavior of elastic pouch motors. Thirdly, we perform blocked-displacement experiments on single pouches made from three different materials, for which we compare the results to our developed model. Finally, we conclude our findings and discuss implications for further research.

3.2. Elastic pouch model

3.2.1. General equations

We start from the derivation of a single inextensible pouch motor [230]. In order to consider stretching of the pouch motor, we assume that the material of the pouch motor can

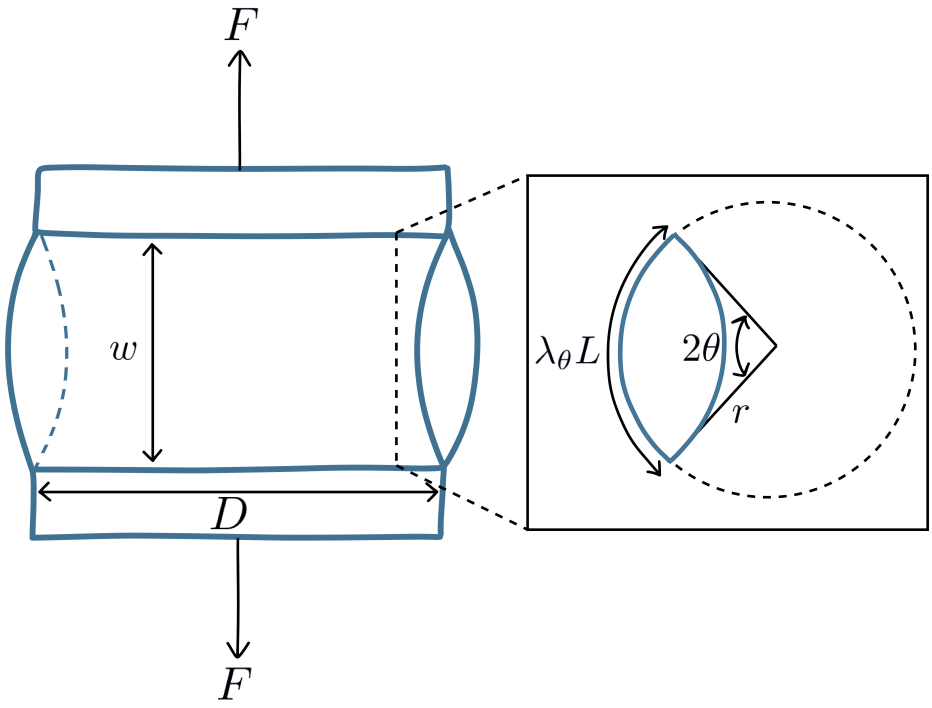

Figure 3.1 | Schematic view of a single stretchable pouch motor with dimensions.

deform, and assume that this deformation is uniform throughout the pouch motor. The state of the system can be described by three stretches: λ_θ, λ_r and λ_z, which are given by

$$\lambda_\theta = \frac{l}{L}, \quad \lambda_r = \frac{h}{H}, \quad \lambda_z = \frac{d}{D}. \tag{3.1}$$

Here l, h and d are the deformed length, thickness and depth of the pouch respectively, and L, H and D are the initial length, thickness and depth. Note that we will consider the materials to be incompressible (which is different than inextensible) [233], for which

$$\lambda_\theta \lambda_r \lambda_z = 1. \tag{3.2}$$

Using these definitions for the additional degrees of freedom that arise from assuming stretchable materials, we can describe the deformed state of the pouch. Specifically, the (arc) length of the pouch motors can be related to a radius r and angle θ of a circular segment. Following Fig. 3.1, we have

$$l = \lambda_\theta L = 2r\theta. \tag{3.3}$$

Moreover, given the assumption that the pouch deforms according to a circular segment, the width w (i.e. deformed length) of the pouch is given by

$$w = l\frac{\sin\theta}{\theta} = \lambda_\theta L\frac{\sin\theta}{\theta}. \tag{3.4}$$

Similarly, we can define the cross-sectional area of the pouch, a, as

$$a = 2\frac{r^2}{2}(2\theta - \sin 2\theta) = 2r^2(\theta - \sin\theta\cos\theta) = \frac{\lambda_\theta^2 L^2}{2}\frac{\theta - \sin\theta\cos\theta}{\theta^2}, \tag{3.5}$$

and the volume v inside the pouch as

$$v = ad = \frac{\lambda_\theta^2 L^2 \lambda_z D}{2}\frac{\theta - \sin\theta\cos\theta}{\theta^2}. \tag{3.6}$$

Now that we have defined the possible deformed states of the system, we need to specify the energy for each of those states. Here we consider three different types of energy contributions. First, an applied force F can change the width w of the pouch, leading to work done. This work is described by

$$E_{\text{force}} = F(w - W) = F(w - L), \tag{3.7}$$

where $W = L$ as we start from the flat state of the pouch. Second, inflation of the pouch by a pressure P also requires work, such that

$$E_{\text{pressure}} = P(v - V) = Pv, \tag{3.8}$$

where we have used $V = 0$ as the initial internal pouch volume. Finally, the elastic energy associated with stretching of the pouch material needs to be defined. Here we assume for simplicity that the material follows a Neo-Hookean hyperelastic material model [233], for which the strain energy density is defined by

$$\omega = \frac{\mu}{2}\left(\lambda_\theta^2 + \lambda_r^2 + \lambda_z^2 - 3\right), \tag{3.9}$$

such that the total elastic energy for both pouch walls is given by

$$E_{\text{material}} = 2lhd\omega = \mu LHD\left(\lambda_\theta^2 + \lambda_r^2 + \lambda_z^2 - 3\right), \tag{3.10}$$

where we have used the incompressibility condition from Eq. (3.2). The total energy is then given by

$$E = -E_{\text{force}} - E_{\text{pressure}} + E_{\text{material}} \tag{3.11}$$

$$= -F\left(\lambda_\theta L\frac{\sin\theta}{\theta} - L\right) - \frac{P\lambda_\theta^2\lambda_z L^2 D}{2}\frac{\theta - \sin\theta\cos\theta}{\theta^2} + \mu LHD\left(\lambda_\theta^2 + \lambda_r^2 + \lambda_z^2 - 3\right), \tag{3.12}$$

where we expressed all variables in terms of θ, λ_z, λ_θ and λ_r, and we consider F and P parameters that we specify. We can non-dimensionalize the energy, by dividing both sides of the above equation by μLHD, such that

$$\hat{E} = -\hat{F}\left(\lambda_\theta\frac{\sin\theta}{\theta} - 1\right) - \frac{\hat{P}\lambda_\theta^2\lambda_z}{2}\frac{\theta - \sin\theta\cos\theta}{\theta^2} + \left(\lambda_\theta^2 + \lambda_r^2 + \lambda_z^2 - 3\right), \tag{3.13}$$

and $\hat{E} = E/\mu LHD$, $\hat{F} = F/HD\mu$ and $\hat{P} = PL/H\mu$.

3.2.2. Plane strain solution

We now aim to find the equilibrium states of Eq. (3.13), and additional geometric constraints such as the one given in Eq. (3.2). If we assume plane strain conditions along the z-direction of the pouch, which means that no deformation occurs along z-axis, we have that

$$\lambda_z = 1. \tag{3.14}$$

Note that in experiments there will always be some force, and therefore some stretch, along the z-axis due to the closed ends of the sealed pouches. However, assuming plane strain conditions simplify the derivation considerably, and we will show that with plane strain conditions the results capture qualitatively the behavior observed in experiments.

We go ahead and plug both constraints into Eq. (3.12), such that

$$\begin{aligned}\hat{E} = &-\hat{F}\left(\lambda_\theta \frac{\sin\theta}{\theta} - 1\right) - \frac{\hat{P}\lambda_\theta^2}{2}\frac{\theta - \sin\theta\cos\theta}{\theta^2} \\ &+ \left(\lambda_\theta^2 + \lambda_\theta^{-2} - 2\right),\end{aligned} \tag{3.15}$$

where all variables can be expressed only in terms of θ and λ_θ. Equilibrium requires that the derivative of the energy with respect to the variables equals zero, such that

$$\begin{aligned}\frac{\partial \hat{E}}{\partial \theta} = &-\hat{F}\lambda_\theta \frac{\theta\cos\theta - \sin\theta}{\theta^2} \\ &+ \hat{P}\lambda_\theta^2 \frac{\cos\theta}{\theta}\frac{\theta\cos\theta - \sin\theta}{\theta^2} = 0,\end{aligned} \tag{3.16}$$

$$\begin{aligned}\frac{\partial \hat{E}}{\partial \lambda_\theta} = &-\hat{F}\frac{\sin\theta}{\theta} - \hat{P}\lambda_\theta \frac{\theta - \sin\theta\cos\theta}{\theta^2} \\ &+ 2\left(\lambda_\theta - \lambda_\theta^{-3}\right) = 0.\end{aligned} \tag{3.17}$$

From Eq. (3.16) we can extract the relation

$$\hat{F} = \hat{P}\lambda_\theta \frac{\cos\theta}{\theta}, \tag{3.18}$$

which can be plugged into Eq. (3.17), to give a relation between θ and λ_θ equal to

$$\theta = \frac{\hat{P}}{2\left(1 - \lambda_\theta^{-4}\right)}. \tag{3.19}$$

Following these results, we can determine the response of the elastic pouch motors upon inflation, given a force $\hat{F}$ applied to the pouch (e.g. a fixed weight attached to the pouch). In Fig. 3.2 we show the response of the pouch for a range of forces. If we compare the results to an inextensible pouch as shown in Fig. 3.3, we find that the elasticity of the material affects the behavior of the pouch especially for larger forces and pressures. Specifically, we observe a dramatic inflation for higher pressures that seems to indicate similar behavior to the inflation of a balloon. This sets a limit to the maximum contraction that can be achieved, which depends on the relation between the shear modulus of the material and the load applied to the pouch motors.

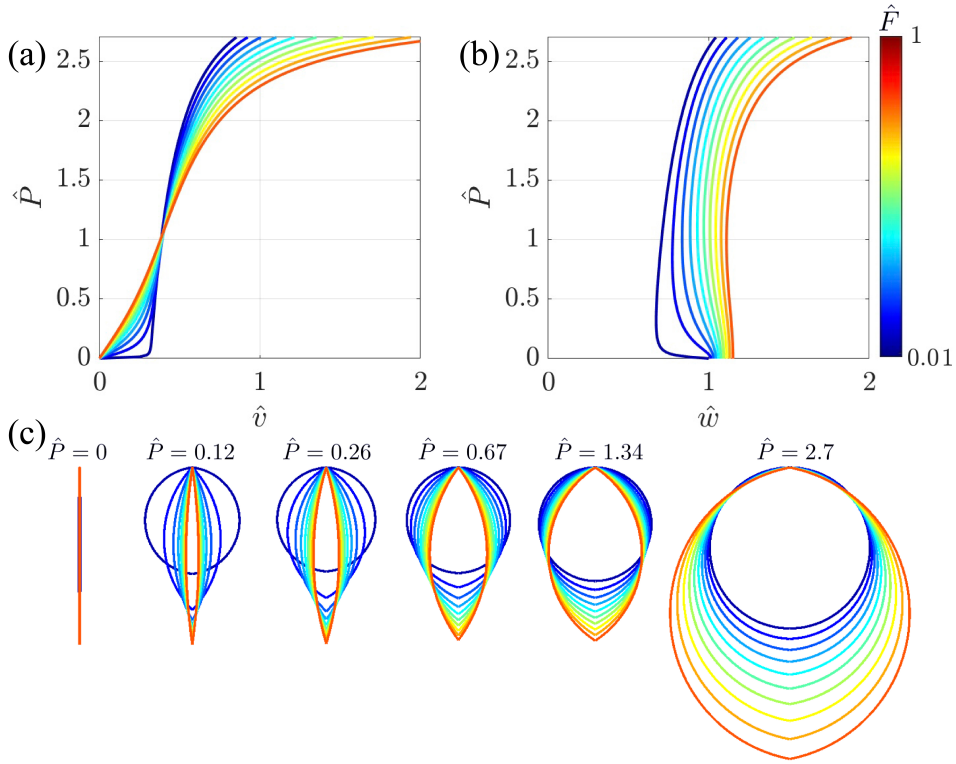

Figure 3.2 | Response of an individual elastic pouch upon inflation by an internal pressure P. Relation between (a) pressure $\hat{P}$ and volume $\hat{v}$, and (b) pressure $\hat{P}$ and width $\hat{w}$. (c) inflated state of the pouch for various pressure and forces.

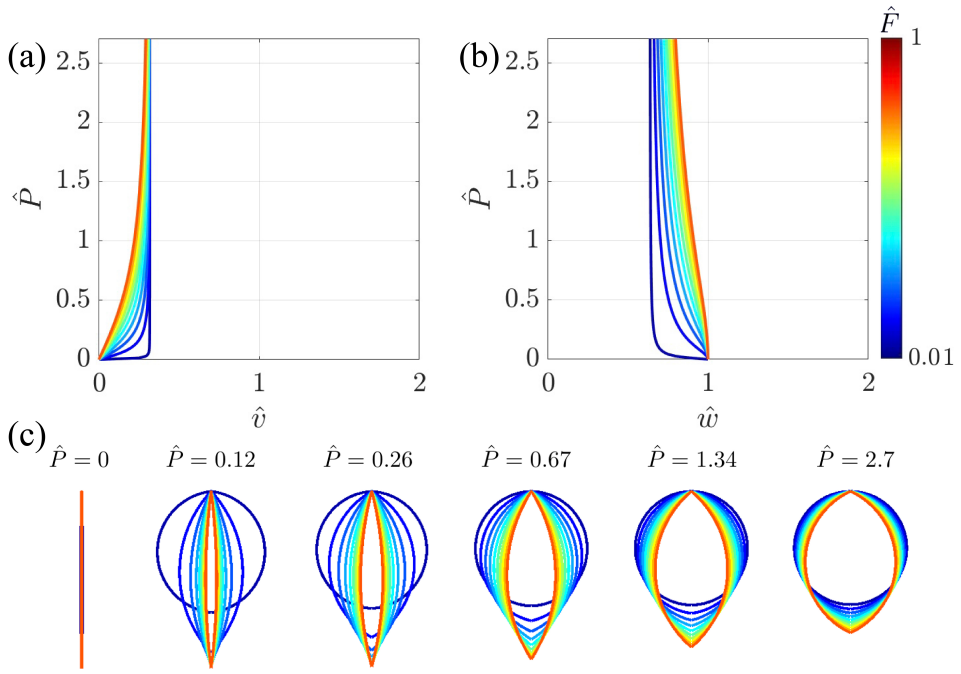

Figure 3.3 | Response of an individual inextensible pouch upon inflation by an internal pressure P. Relation between (a) pressure $\hat{P}$ and volume $\hat{v}$, and (b) pressure $\hat{P}$ and width $\hat{w}$. (c) inflated state of the inextensible pouch for various pressure and forces.

To compare the model to experiments that we will perform on three different pouches, we next define the 'blocked-displacement', which can be determined by inflating the sample while clamping it in its original configuration for which $w = L$. Note that this experiment can only be performed for extensible materials, as inextensible materials would simply not be able to inflate. For this condition, Eq. (3.4) gives us

$$\lambda_\theta = \frac{\theta}{\sin\theta}. \tag{3.20}$$

Moreover, for these specific blocked-displacement conditions, we find the following solution from our analytical model from Eq. (3.18) and Eq. (3.19)

$$\hat{P}_{\text{blocked}} = 2\theta\left(1 - \left(\frac{\theta}{\sin\theta}\right)^{-4}\right), \tag{3.21}$$

$$\hat{F}_{\text{blocked}} = \hat{P}_{\text{blocked}}\frac{\cos\theta}{\sin\theta}, \tag{3.22}$$

As shown by the results in Fig. 3.4, at $\hat{P} \approx 1.2$ we find that the maximum force the pouch can exert equals $\hat{F}_{\text{blocked}} \approx 0.65$, which thus depends on the shear modulus, the thickness and depth of the pouch. Moreover, at pressure $\hat{P}_{\text{blocked}} \approx 2.6$, we see that the pouch no longer contracts and pulls on the clamps, but starts to extend and push on the clamp. Note that at $\hat{P}_{\text{blocked}} \approx 2.6$ we find that $\lambda_\theta \approx \pi/2$, which for most materials already goes far beyond the elastic limit.

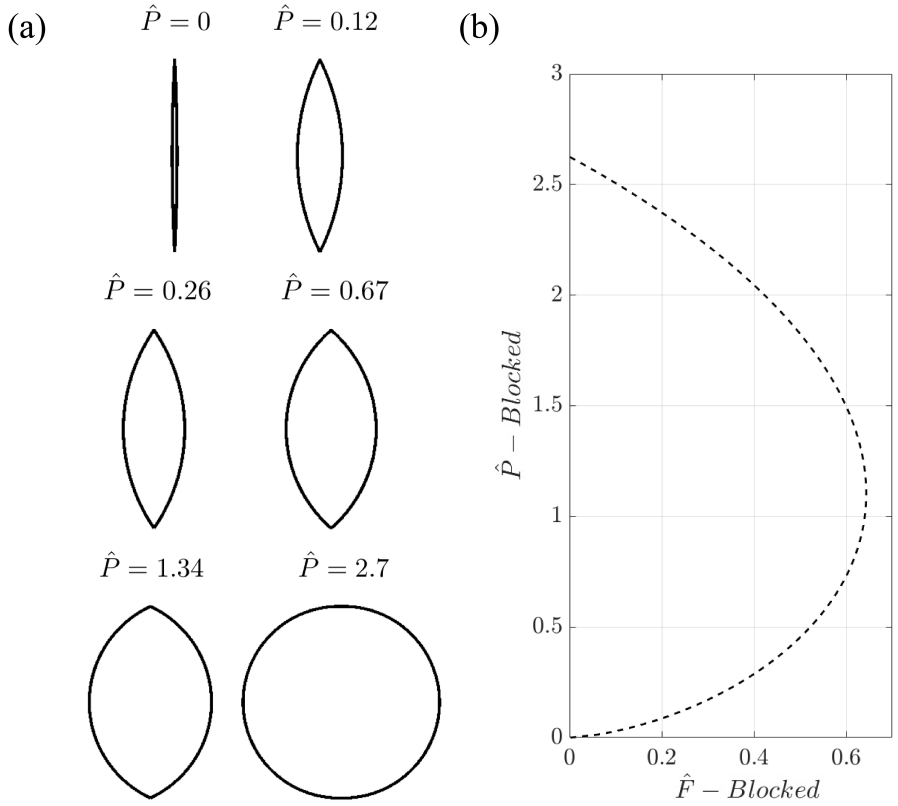

Figure 3.4 | Response of an individual pouch upon inflation by an internal pressure P, while constraining the width $w = L$ (blocked-displacement). (a) Inflated state of the extensible pouch for various pressure and forces. and (b) relation between normalized pressure $\hat{P}$ and normalized reaction force $\hat{F}$.

3.3. Experimental setup

To evaluate our model and explore the effect of material properties on the pouch motor behavior, we conducted blocked-displacement experiments on single pouches made of materials with different properties. We fabricated pouches from three different thermoplastic sheets with different stiffnesses, specifically SEBS sheet (Vreeberg Elastic Materials-0.2mm-white), TPU sheet (Airtech Stretchlonő 200-0.038mm-green) and TPU-coated Nylon fabric (extremtextil-70den-black), which are categorized from low to high stiffness, respectively. To be able to compare the model with the experiments, each material underwent tensile testing based on the ASTM-D882 standard. These tests were performed to determine the shear modulus of each material that is needed for further analysis. We derived the shear modulus of the sheets by fitting the uniaxial incompressible neo-hookean model to the stress-strain curve of the materials on the first 5% elongation of the total initial length (Fig. 3.5).

Next, all pouch motors were made using the same design that we heat sealed using an adapted 3D-printed (FELIX TEC4). The pouches have a length L=20mm and a despth D=60mm. The adapted printer moves a hot nozzle over the films at a specific speed and

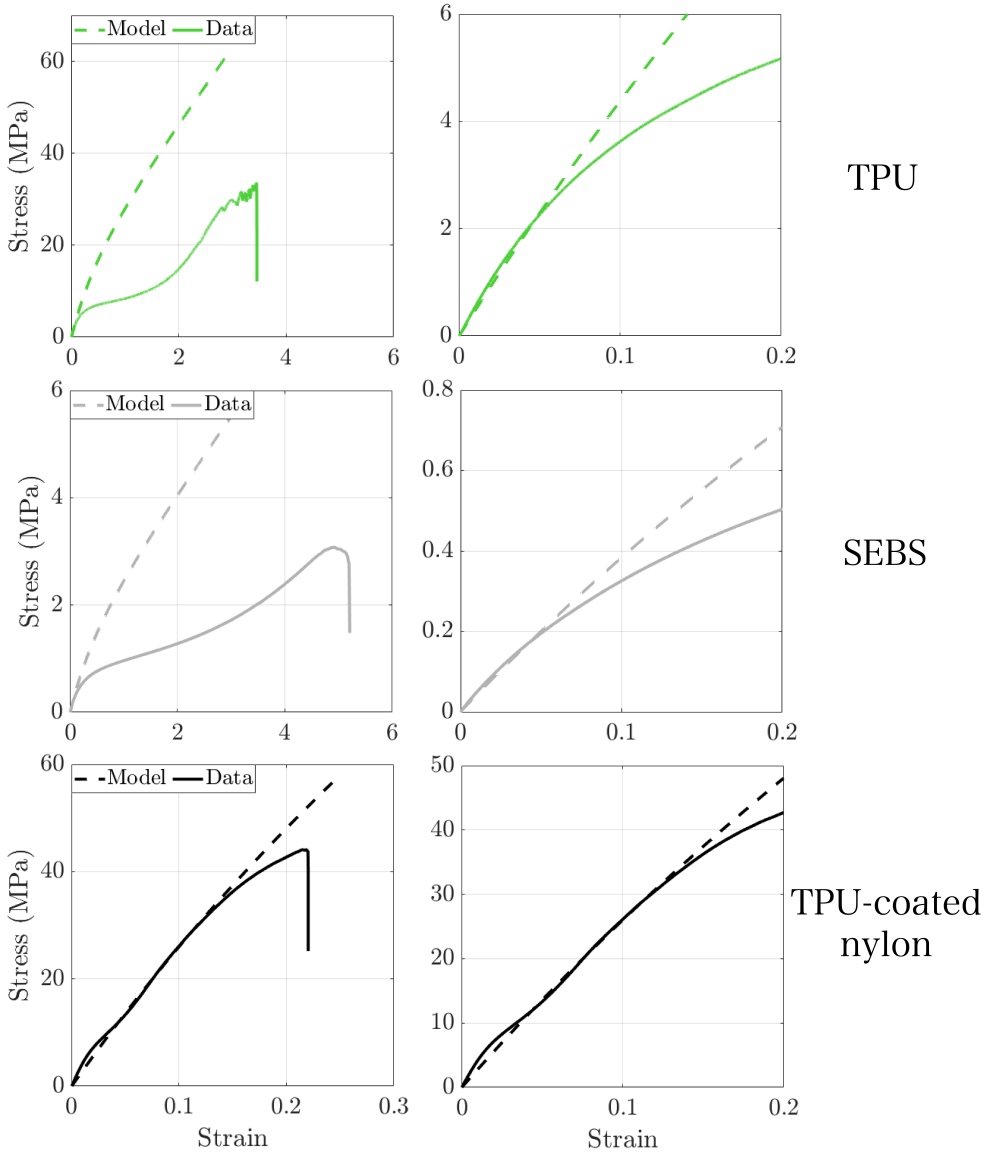

Figure 3.5 | Derivation of the shear modulus of three different materials (TPU, SEBS, and TPU-coated Nylon), by fitting an incompressible neo-Hookean model to the stress-strain response of the first 5% elongation of total initial length.

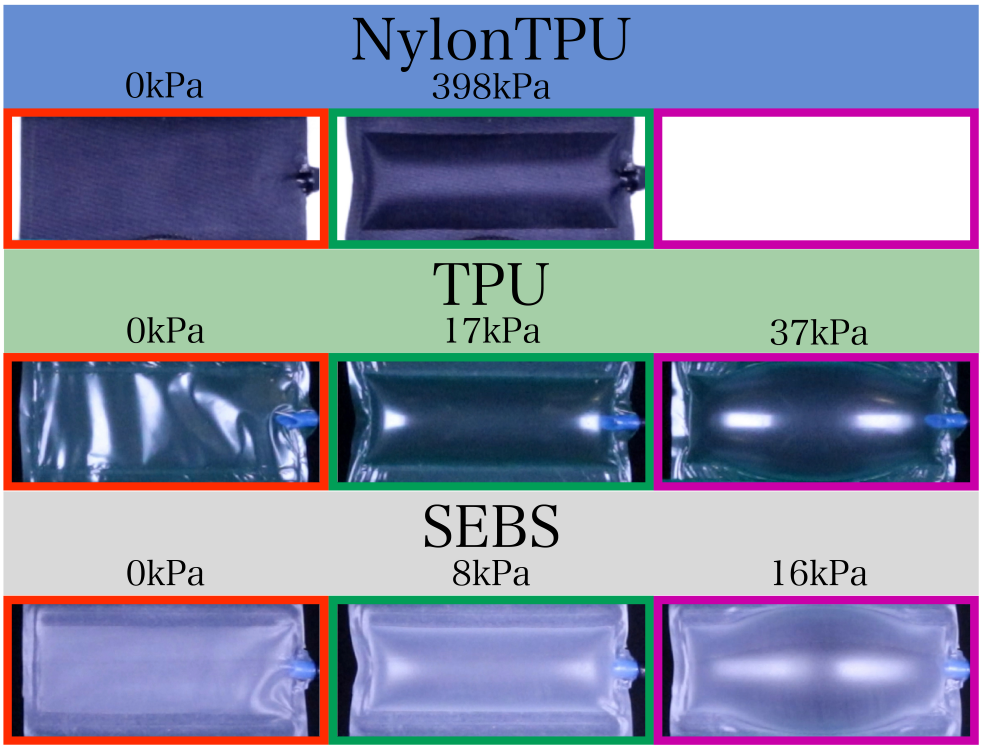

Figure 3.6 | Pouch motors at different states of inflation. First column: fully deflated. Second column: the pressure at which maximum force occurs for each sample. Third column: the pressure at which the sample start to push the clamps out.

axial pressure, sealing two layers of thermoplastic films together using a pre-designed pattern. The height and speed of the nozzle and the bed temperature should be adjusted according to the film melting point and its thickness to obtain a strong seal. After fabrication of the pouch motors, we performed the blocked-displacement experiments (Fig. 3.6). The pouches were clamped in a tensile testing machine (INSTRON 5965) using custom-designed grippers and were held at a fixed distance. The initial distance between the clamps was set equal to the uninflated pouch width, i.e. at $W = L$. Next, we slowly pressurized the pouch to a maximum pressure that we based on the material stiffness, where we pressurized the TPU and SEBS samples up to $P = 80$ kPa and we pressurized the TPU-coated nylon sample up to $P = 400$ kPa. We recorded the force applied by the pouch and the volume change in the pouch using the INSTRON machine and a bi-directional flow sensor (HAFBLF0750CAAX5, Honeywell) respectively.

3.4. Results and discussion

The measured response during the blocked-displacement experiments (Fig. 3.6) for the three different materials are shown in Fig. 3.7. It should be noted that the samples were pressurized until their failure point (except for TPU-coated nylon). We therefore did not

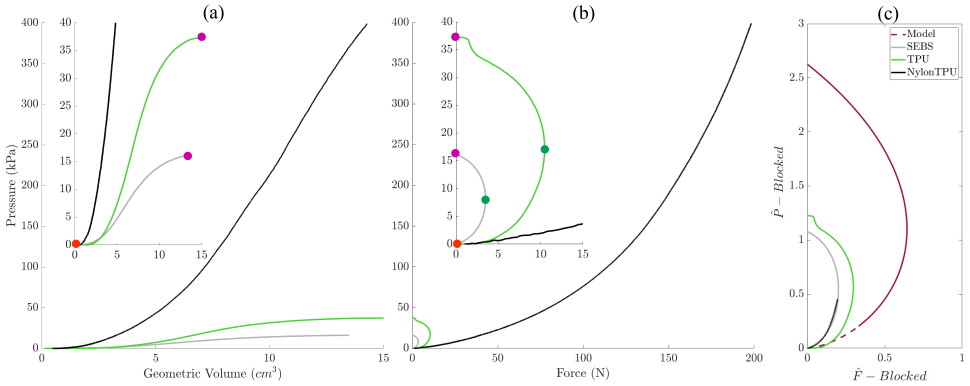

Figure 3.7 | Response of a single pouch to increase in pressure in a blocked-displacement test. (a) The relation between internal pressure and geometric volume of the pouches; The points on the curve of each sample correlate to a state of the pouch, demonstrated in Fig. 3.5 in a column with same color. (b) The real force-pressure curve, resulted from blocked-displacement experiment, for pouches made of SEBS (gray line), TPU (green line), and TPU-coated nylon (black line). (c) The force-pressure relationship of a single pouch. The model is shown in red, where the dashed line indicates the part of the response up till a stretch λ_θ<1.05, and all experimental results are normalized using $\hat{F} = F/HD\mu$ and $\hat{P} = PL/H\mu$ to be comparable to the model.

capture the cyclic behavior of the pouches, e.g., to observe potential hysteresis in the sample. Given the magnitude of the stretches in experiments, we do expect that the materials do not behave purely elastic. Overall, and by looking at the deformation of the pouch motors shown in Fig. 3.6, we observe that the pouch first deforms to approximately a cylinder as also assumed in our model (Fig. 3.2c). Interestingly, for higher pressures the pouches start to balloon, which is clearly an indication of the pouches being stretchable. Note that we could only observe this for the pouches made from SEBS and TPU, as the TPU-coated nylon pouch did not reach the state of generating maximum force, followed by ballooning, in its range of applied pressure. This ballooning for the SEBS and TPU pouch motors is also clearly observed when looking at the internal pressure (P) and volume (V) relation of the pouch (Fig. 3.7a). Here we find that the pressure reaches a peak, which indicates a ballooning instability.

The ballooning effect sets a limit to the maximum force that is generated by the pouch. As shown in Fig. 3.7c, at first the pressure increases in the pouch while the volume changes at lower rates. This state correlates to the increase in generated force, shown in Fig. 3.7b. However, once the pouch reaches the state of generating maximum force (green points on SEBS and TPU curves), the internal volume starts to increase at higher rates. This is due to stretchability and causes the decline in the generated force by the pouch. This decrease in force will continue until the pouch starts to push the clamps instead of pulling them (purple points on the Fig. 3.7b and c), unless it breaks before that.

One important result from the model is that the pouches demonstrate a maximum force that they can apply to the clamps (Fig. 3.4b). This maximum force is clearly indicated for the softer SEBS and TPU samples, which show a maximum force of $F \approx 4$ N and $F \approx 10$ N, respectively. Although the TPU-coated Nylon did not reach its maximum force at $P = 400$ kPa, we observe that the force-pressure curve achieved in all experiments follows same trend as the force-pressure curve derived from our model. The TPU-coated Nylon reached a relatively high force of $F \approx 200$ N at $P = 400$ kPa (Fig. 3.7b).

A more quantitative comparison is made in Fig. 3.7c, where we consider the normalized quantities $\hat{F}$ and $\hat{P}$. While we find the same qualitative trends, we do observe considerable differences (approximately a factor of 2) between experiments and simulations. These differences are likely the result of the material model used, which does not capture for example visco-elastic behavior (Fig. 3.5), but also the assumption of the plane strain condition likely does not perfectly hold as the pouch motors are sealed at the sides, which also introduces an additional axial force. However, it is surprising that even for materials with stiffnesses that span more than an order of magnitude, we can normalize the results to fall approximately on the same curve. Therefore, the model does capture the qualitative behavior of our samples, such that we can conclude that the the force scales with H, D and μ, and the pressure P scales with $1/L$, H and μ.

It should be noted that an uniaxial incompressible neo-hookean model is typically suited for elongations up to 30% [234] and we do not expect a precise fit for the larger strains that we observe in experiments. However, the experiments still demonstrate that our model captures the behavior of an extensible pouch qualitatively, and it does improve the overall fit compared to existing inextensible pouch models. To improve the quantitative predictability of our model, additional mechanical tests are needed to obtain material parameters under biaxial conditions, so that different hyperelastic models suitable for larger strains can be employed. Additionally, the model should be updated to include the additional forces generated by the internal pressure along the z-axis.

3.5. Conclusion

We proposed an analytical model to predict the behavior of pouch motors considering the effect of stretchability on their performance. Our model showed that the material elasticity influences the pouch motors output significantly and must be considered in designing an optimal actuator. An important finding is that elastic behavior is not only important for softer materials such as SEBS and TPU, but also occurs for stiffer sheets such at the TPU-coated Nylon (given sufficient load). Furthermore, we conducted blocked-displacement experiments on single pouches made of various materials with different properties. Although there is a deviation between the experimental results and the model due the material non-linearity and modeling limitations, we observed the same behavior trend in our proposed model and experimental results. Future work may include implementing the same modeling strategy to predict the behavior of pouch arrays and other pouch designs, and the possibility of developing new functionalities using the same technology as the pouch motors.

4

Towards developing a compact total artificial heart using a soft robotic fluidic transmission system

Abstract

Cardiovascular diseases are a leading cause of mortality, with limited possibilities for transplantation due to a critical shortage of donor hearts. Replacing the heart by total artificial hearts remains challenging, due to size constraints, and energy requirement, among others. To address this, we introduce the LIMO Heart, a compact total artificial heart (TAH) concept based on an efficient soft fluidic transmission system. By reducing actuator volume and enhancing energy transfer, LIMO enables a more compact and efficient design. We developed a soft ventricle prototype using thin-walled pouch actuators that achieve transmission ratios above one via circumferential shrinkage. A fast, cost-effective prototyping method accelerated testing. Experimental results showed high energy transfer efficiency (82–91%), and in vitro tests demonstrated promising cardiac outputs of 5.9 L/min against aortic, and 7.6 L/min against pulmonary pressures. These findings represent a step toward a more broadly applicable biventricular soft robotic TAH for treating end-stage heart failure.

Based on: **M. Arfaee**, L. C. van Laake, S. Zou, C. Bording, J. Kluin, J. T. B. Overvelde, Toward developing a compact total artificial heart using a soft robotic fluidic transmission system.Sci.Adv.11,eadv4854(2025).

4.1. Introduction

Cardiovascular diseases are a major cause of death globally, and as the population ages, the prevalence of heart failure is expected to increase [235, 236]. Heart transplantation remains the ideal treatment for severe heart conditions, but a critical shortage of donor hearts necessitates the development of alternative solutions like left ventricular assist devices (LVADs) and total artificial hearts (TAHs). While LVADs provide significant support, they are not suitable for patients with severe biventricular failure and carry risks of complications such as post-LVAD right ventricular failure, highlighting the need for TAH development [19].

Currently available TAHs that are approved as a bridge to transplant are the Syncardia and Carmat, both fluid-driven (either pneumatic or hydraulic) pulsatile devices [97, 237]. The popularity of fluid-driven systems in developing TAHs and the need for more biomimetic behavior has opened the door for soft robotics as an alternative solution to traditional driving systems [226]. Soft robotics is being used to develop different types of medical devices [39], such as wearable devices [45, 238, 239] and implantable devices [240, 241], among which cardiovascular devices have gained significant attention over the past few years [50, 52, 242]. Recent studies in the development of heart assistive devices [53, 243–246] and TAHs [50–52] utilizing soft robotics highlight a potential avenue to more closely mimic the natural behavior of the heart. In a recent study on developing a soft TAH, sufficient cardiac output of 8 l/min has been achieved in a prototype working for 30 hours [52].

Although the results of recent studies on developing a soft TAH warrant further investigation, an important problem of all the currently existing fluidically-activated TAH designs—including the soft TAH designs—remains their total size. The combination of the actuator, driving system, and power supply leads to bulky devices that cannot be fully implanted, therefore requiring percutaneous drivelines [236]. Existing devices require at least the same amount of volumetric input to the actuators compared to the volumetric (blood) output ejected. This means that the actuators need to displace a large amount of fluid (or air) that is identical to or larger than the volume of blood that needs to be pumped. Besides that, a reservoir is needed to store the actuation fluid that is not inside the actuators of the device. In comparison, in a natural heart the cardiac tissue only takes up approximately equal or slightly larger space compared to the total volume of blood that needs to be pumped in each cycle [247–250]. In addition, the membrane-based actuators of these soft TAHs work only effectively at relatively high pressures (150−200 kPa) [52], which is more than 10 times higher than the required blood pressure. This considerably limits the energy efficiency of soft TAHs, and increases the size of auxiliary components such as batteries and pumps.

As a result, the existing driving system for (soft) TAHs still requires a bulky driving system to work. In fact, this same problem limits both the miniaturization of the Syncardia and Carmat, since they classify as membrane-based systems that can reach a 1:1 fluidic transmission ratio (volumetric input/output) at best. Carmat only partially circumvents this problem by alternatingly activating the left and right ventricle, while Syncardias drive system can only be placed extracorporeally. Importantly, in mechanical or electrical systems this problem would normally be overcome by using a transmission system, such as mechanical gears or electrical transformers. Therefore, a natural question to ask is what different types of efficient soft fluidic actuation strategies can be employed that achieve

fluidic transmission, with the ultimate goal to reduce the size of the complete TAH system, and increase the application potential for TAHs in general.

We propose a soft ventricle that can be used in a fully soft Total Artificial Heart concept that we refer to as the LIMO (Less In, More Out) heart. The actuation of the ventricle is based on existing pouch motors [230, 231, 251]. Our concept consists of a blood collecting chamber (so-called ventricle) that is surrounded by flat pouches that transform into cylinders when actuated. The aim of our soft ventricle design is to achieve fluidic transmission with only limited energy loss (i.e., high efficiency). In essence, we aim to build a system where lower volumes of fluid (gas or liquid) are delivered at higher pressures as input to the actuators, which is then transformed into a larger blood output volume at the required reduced pressures. We anticipate that such an efficient pressure-volume transmission strategy reduces the total size of a TAH, as both the total fluidic volume (driving fluid and maximum stroke volume combined), and required pump power and battery size can be considerably reduced.

The remainder of this paper is divided into the following sections. First, we introduce our concept and an analytical model that theoretically explores the possibility of using only the geometry of the device design to achieve programmable fluidic transmission ratios that are higher than one. Second, we investigate experimentally the effect of geometry on the input pressure and force output of pouch arrays, and how the results can be translated to the application in a soft TAH concept. Third, we describe the fabrication method of a closed chamber based on pouch motors and experimentally prove its functioning as a pump in a static experimental setup with afterload. We finalize by reporting the results of testing a single ventricle in a single-sided mock circulation loop (MCL) against physiological conditions, to explore the effect of dynamics and cyclic loading on the system.

4.2. Rationale and design of the LIMO heart

We propose a model that consists of a cylindrical ventricle, surrounded by pneumatically actuated pouches that are aligned vertically. By pressurizing the pouches, they deform from a flat shape into a cylindrical shape, which causes their (arc-)length to decrease (Fig. 4.1.A). Therefore, the circumference of the cylindrical ventricle shrinks when the pouches are inflated, while maintaining effectively the same vertical height [252]. This global deformation accounts for the major proportion of the total volumetric shrinkage of the ventricle. In addition, approximately half of each pouch volume occupies the inner space of the ventricle which also causes reduction of the inner volume (Fig. 4.1.A).

Based on these two observations, we can derive a simplified analytical model to qualitatively investigate the behavior of the system, and to investigate the feasibility of attaining desired fluidic transmission ratios that are larger than one. The model assumes an idealized cylindrical initial shape of the ventricle, parametrized by height H, and number of pouches N of initial length L_0 that are separated by seams of width s (Fig. 4.1.B). We furthermore assume that the height H remains constant, and the material is inextensible, such that the deformed shape is fully described by the opening angle θ of the pouches [230]. The deformed length L and volume V_P of a single pouch can then be expressed as

$$\begin{aligned} L &= L_0 \sin\theta/\theta \\ V_\mathrm{P} &= L_0^2 H(\theta - \cos\theta \sin\theta)/\left(2\theta^2\right) \end{aligned} \tag{4.1}$$

.

We define $V_A = NV_P$ as the total actuator volume, i.e., the volume of all pouches combined. Based on Eq. (1), we can approximate the radius r_C and volume V_C of the cylindrical ventricle as

$$\begin{aligned} r_C &= N(L+s)/(2\pi), \\ V_C &= H\pi r_{C^2} - V_A/2. \end{aligned} \tag{4.2}$$

We can furthermore define the ejection fraction (EF), which is a common performance measure in the natural heart as well as in artificial heart devices.

$$\mathrm{EF} = -\Delta V_C / V_0 \times 100\% = (1 - V_C/V_0) \times 100\% \tag{4.3}$$

Where V_0 is the initial volume of the cylindrical ventricle before actuation. Excitingly, from this simplified geometrical model interpreted in Figure 4.1.C, we learn that the cumulative volume expelled from the ventricle ΔV_C can indeed exceed the cumulative volume introduced into the pouches ΔV_A. In fact, we can choose a desired fluidic transmission ratio

$$i = -\Delta V_C / \Delta V_A \tag{4.4}$$

by selecting the number of pouches N (Fig. 4.1.C). The fluidic transmission ratio i at full actuation (i.e., $\theta = \pi/2$) can theoretically be chosen arbitrarily large by increasing N. This is because, as N increases, ΔV_A approaches zero, while ΔV_C approaches $V_0\ (1 - 4/\pi^2)$ $\approx 0.59\ V_0$, resulting in EF > 59% for all values of N. Note that this relation is only valid if we assume that seam width s is negligible. We show the modeled effect of N and s on i and EF in Supplemental Figure S7. Next, we derive the required actuator pressure P_A that balances a given ventricular pressure P_C for different values of pouch opening angle θ. We assume static equilibrium, and find the pressure ratio $P^* = P_A/P_C$ by conservation of energy:

$$\begin{aligned} &P_A\, \mathrm{d}V_A + P_C\, \mathrm{d}V_C = 0 \\ &P^* = -\mathrm{d}V_C/\mathrm{d}V_A = -\left(\mathrm{d}V_C/\mathrm{d}\theta\right) / \left(\mathrm{d}V_A/\mathrm{d}\theta\right) \\ &P^* = \left(N/(2\pi\cos\theta)\right)\left(\sin\theta + \theta s/L_0\right) + 1/2 \end{aligned} \tag{4.5}$$

where we used expressions (1) and (2) for V_A and V_C. Using (1), (2), and (3), we determine the actuator input volume and pressure required to expel a representative physiological stroke volume and afterload delivered by a healthy left ventricle, equal to a volume ΔV_C = 90 mL from the ventricle, against a constant afterload of P_C = 112.5 mmHg (15 kPa), which are in the range of average values for a heart working in normal conditions [253, 254]. For these fixed output requirements of the cylindrical ventricle, varying the number of pouches reveals an expected trade-off between actuator pressure and volume, where an increasing number of pouches require less input volume but higher actuator pressure (Fig. 4.1.d). Taken together, our model informs a rational selection of N for given application requirements, based on analytical relations between ejection fraction EF, required actuation volume V_A, and required actuation pressure P_A. Practically, there may be additional considerations for choosing N, such as fabrication limitations or a minimum channel width that is required to avoid excessive viscous losses when driving fluid is forced in and out of the actuators.

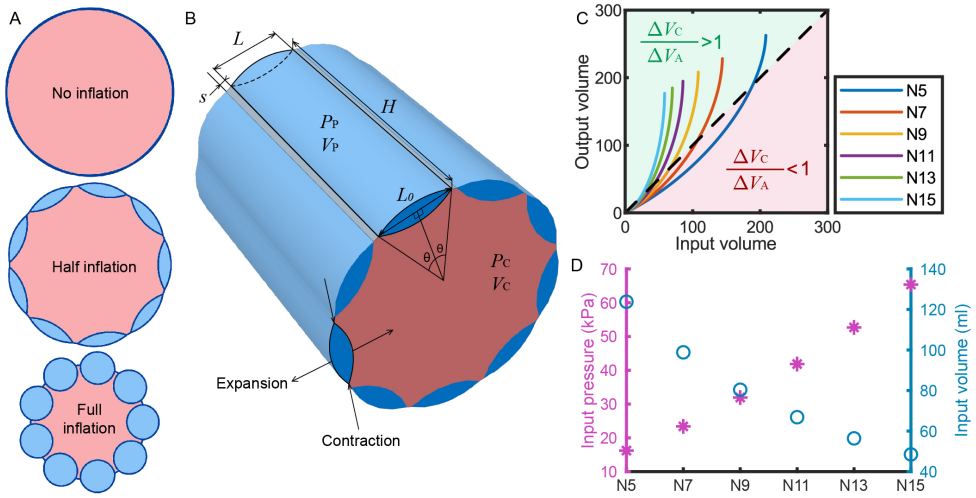

Figure 4.1 | Simplified working mechanism of the proposed fluidic transmission system. A. Cross-sectional view of a cylindrical chamber surrounded by vertical pouches, and the inner deformation after pouch inflation. B. Model of a single pouch with cylindrical surfaces. C. Output-Input geometrical volume relation obtained from analytical modeling. The fluidic transmission ratio is higher than one above the dashed line. D. Changing trend of input volume and pressure needed for samples with different number of channels to reach an output volume of 90 mL at 15 kPa, considering a cylindrical system with an initial diameter of 60 mm, height of $H = 100$ mm, and seam thickness of $s = 1.5$ mm.

4.3. The effect of channel size on the response of pouch arrays

To explore the feasibility of implementing the fluidic transmission ratio experimentally, we first focus on fabricating and measuring the performance of pouch arrays. We are specifically interested in the relationship between the pouch actuator pressure and resulting circumferential forces that can be delivered by the pouches. To determine if the number of pouches has an effect on the maximum force that can be delivered, we can layout the design of the proposed ventricles that are made from heat-sealing TPU-coated Nylon fabric (Riverseal 70 LW, 78Dtex, 170 g/m2, Rivertex, Culemborg, The Netherlands) with varying number of pouches N, to obtain flat arrays of pouch motors (Fig. 4.2) [230]. We designed and performed so-called blocked-displacement experiments [251], in which we clamp the samples in a tensile testing machine (INSTRON 5965, Norwood, United States) using custom-designed clamps which hold the pouch motors ends at a fixed distance, while we quasi-statically increase the pressure P_A in the pouch actuators.

Interestingly, the measured results in Fig. 4.2.A demonstrate that the number of pouches does not directly affect the ability to reach certain force levels. However, and as expected, as the surface area of the pouches is reduced for increasing N, we do require higher pressures in pouch arrays with more pouches to achieve these forces (Fig. 4.2.A). Importantly, the required higher pressures come with the benefit that less volume is needed to inflate the pouch motors for increasing N (Fig. 4.2.B). Therefore, this experiment demonstrates the transmission trade-off between the pressure and volume needed to reach a certain force in samples with different geometries. Thus, we can obtain different behaviors by just

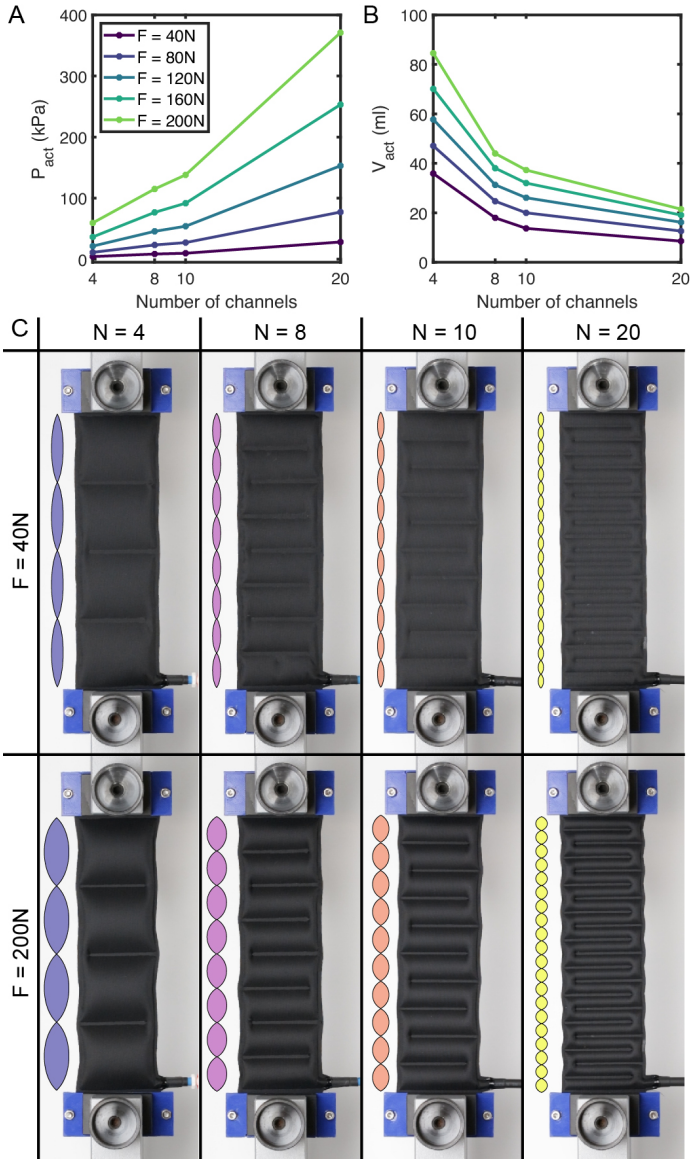

Figure 4.2 | Blocked-displacement testing of pouch arrays. A. Input pressure needed to reach certain forces for samples with different number of pouches (i.e. different pouch size). B. Input geometric volume needed to reach certain forces for samples with different number of pouches C. From left to right, pouch arrays with 4, 8, 10, and 20 pouches. Top and bottom rows show the samples exerting 40 N and 200 N to the jaws of the tensile testing machine. Pouch arrays with more (smaller) pouches require lower input volume to reach a certain force, at the cost of higher input pressure compared to pouch arrays with fewer (larger) pouches.

changing the design, while using the exact same amount of material (Fig. 4.2.C).

4.4. Fast and cost-effective prototyping method

While so far we have focused on a relatively simple geometry, fabricating a leak-proof soft artificial ventricle will lead to additional complexities that cannot easily be modeled. Given these complexities that are involved with soft and flexible components, it is beneficial to have a fast and cost-effective prototyping method to fabricate different designs of our pouch-based ventricle and investigate them experimentally. Therefore, we implemented a prototyping method that enables us to effectively fabricate several completely soft samples with different designs using only a customized 3D-printer CNC machine that can be used for both heat-sealing [230], and 3D-printing of TPU components.

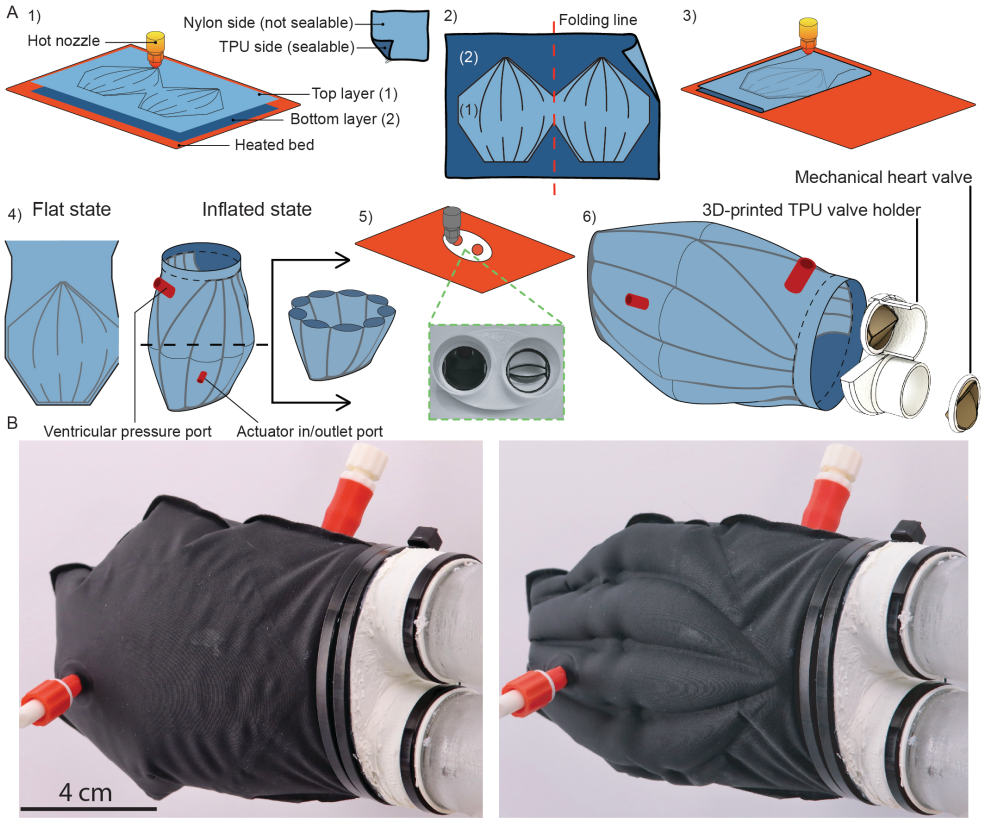

Figure 4.3 | Fast and cost-effective fabrication method for the LIMO Heart ventricle. A. 1) Heat-sealing two layers of TPU-coated nylon to create pouches. 2) Cutting leftovers from one side and folding the sample from its middle line. 3) Second heat-sealing step to create ventricle chamber. 4) Schematic 3D shape of the ventricle chamber after inflation. 5) 3D-printing a TPU soft housing that holds the inlet and outlet valves, and also acts as an interface between the prototype and the Mock-loop Circulation setup. 6) Exploded view of all components. B. LIMO ventricle in a relaxed and actuated state.

With this approach, we fabricate an artificial ventricle of our LIMO heart consisting of three major fabrication steps (Fig. 4.3): (*i*) heat-sealing two layers of fabric together to create the pouches; (*ii*) cutting the outline of the artificial heart and revealing a layer of heat-sealable fabric to perform a second round of heat-sealing to create the internal

ventricular chamber; (*iii*) 3D-printing soft TPU connectors and a soft TPU housing for mechanical heart valve prostheses (Sorin Bicarbon, Sorin Group, Milan, Italy), that are sealed or glued to the ventricle directly (Fig. 4.3.A). Note that to create the ventricle (Fig. 4.3.B), we use a 2D-fabrication method (heat-sealing) that results in an elliptic cross-sectional area, rather than a perfect cylinder considered in our analytical model (Fig. 4.1.B). The relaxed and actuated state of the ventricle are shown in Fig. 4.3.B.

It should be noted that although this technique is cost- and time-efficient, it can currently only be used in the proof-of-concept phase to evaluate the working mechanism. Using the same platform, we were also able to print soft valves that could directly be implemented in the ventricle to obtain a fully soft device (Figure S9). However, the material and heat-sealing technique used for prototyping are not yet adequate for producing durable samples capable of withstanding the extreme cyclic loading required for real-world TAH applications. Notably, all observed failures occurred near the sealing lines, particularly at the endpoints adjacent to the gaps functioning as air channels between pouches (Figure S10). In our case, we were able to obtain in the order of 1500−2000 cycles per sample fabricated. This was sufficient to prove the concept and perform all the required measurements. Further optimization of the design to limit stress concentrations at sealing lines is essential to further develop the demonstrated fluidic transmission concept towards a TAH concept.

4.5. In vitro quasi-static characterization of the artificial ventricle

We next aim to determine if our fabricated prototype for a soft artificial ventricle can achieve higher fluidic transmission ratios than one, as predicted by our analytical model (Fig. 4.1.C). We first conducted an experiment with a minimum afterload of 3.8 kPa (originating from the column of water) that we could achieve in our quasi-static experimental setup (Fig. 4.4). We tested a range of artificial ventricles that are identical in size (V_0 = 300 mL at relaxed state against minimum afterload), and only varied the number of pouches N = 5, 7, 9, 11, 13, and 15 by varying the length L_0 of the individual pouches, while keeping their height identical (Fig. 4.5, S3). Since the pouches occupy negligible space, the total volume of a biventricular LIMO heart made from two ventricles, while excluding the valves, is approximated to be 600−700 mL. This falls within the range of a normal adult heart volume of 490−910 mL [255]. The results clearly demonstrate that the ventricle size required to achieve a specific stroke volume (SV) can be adjusted by modifying the pouch size, which is ultimately constrained by factors such as the capacity of the actuation system. As shown by the results in figure 4.6.A and table 1, where we provide the same actuation pressure P_A to all prototypes, we observe that for fewer pouches we achieve a larger maximum volumetric output V_C, resulting in a higher EF. However, for fewer pouches we also require considerably higher actuation volume V_A.

Importantly, these results demonstrate experimentally that all samples could reach a fluidic transmission ratio higher than one, where for smaller and more pouches we achieve higher ratios, reaching a maximum of 2.19 for N15 that consequently has the lowest EF (39%) among the prototypes (Table 4.1). It should be noted that when determining the fluidic transmission ratio, we consider the geometric volume of the pouches, not the total uncompressed volume of the air used to actuate the pouches. Effectively, we therefore

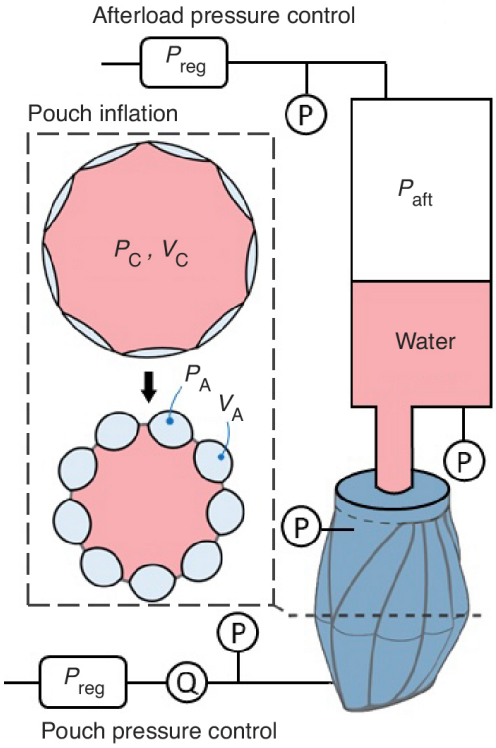

Figure 4.4 | Quasi-static experiments to evaluate transmission ratio and efficiency. Experimental setup, including a water tank, pressure regulators (P_{reg}), pressure sensors (P), and an air flow sensor (Q).

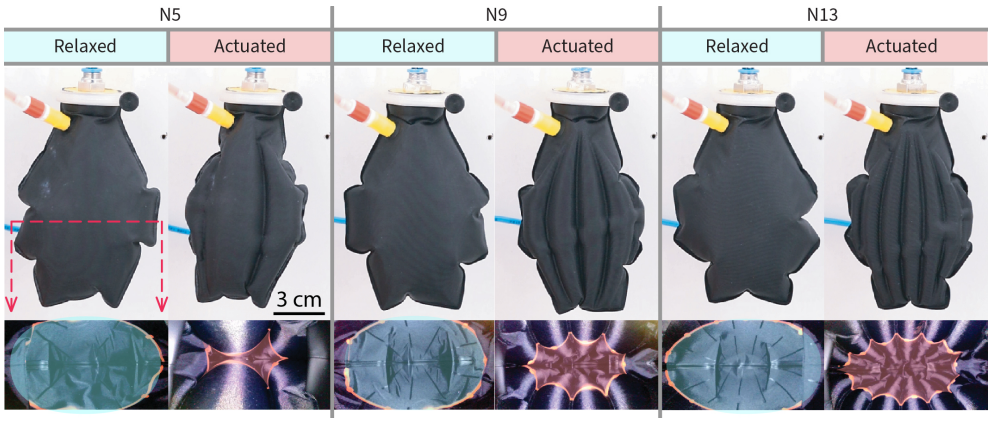

Figure 4.5 | Quasi-static experiments to evaluate transmission ratio and efficiency. Relaxed and actuated state of prototypes N5, N9, and N13, showing the difference in the internal deformation at maximum actuator pressure of P_A = 40 kPa against identical internal pressure of P_C = 10 kPa; light blue: inner surface area at relaxed state, light red: inner surface area at actuated state.

assume we are inflating the pouches using an incompressible fluid. Focusing on a SV of 90 mL that lies in the range of the SV of a healthy native heart (50–100 mL) [253], we observe

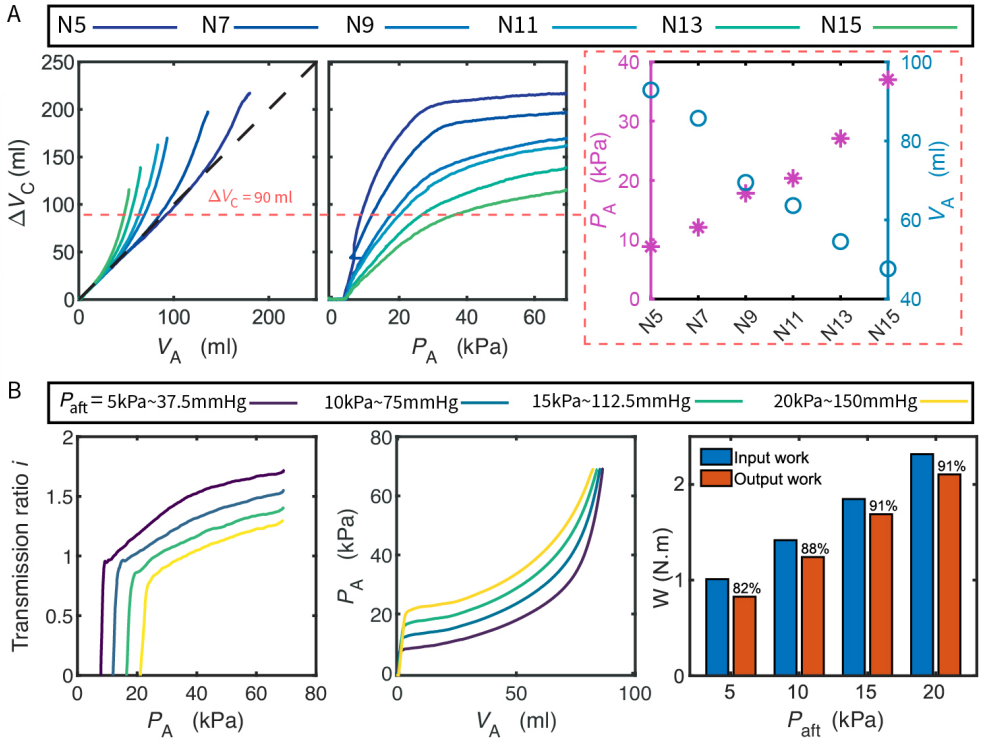

Figure 4.6 | Quasi-static experiments to evaluate transmission ratio and efficiency. A. Experimental results of quasi-static testing of samples with different number of pouches against minimum afterload (3.8 kPa); Change of volumetric output (V_C) at various actuator volumes (V_A) and pressures (P_A), showing the trade-off between V_A and P_A required to reach a certain volumetric output of 90 ml in different samples. B. Experimental results of quasi-static testing of prototype N9 against various afterloads (P_{aft}) between 5−20 kPa (37.5−150 mmHg).

Sample	Input volume (ΔV_A)	Output volume (ΔV_C)	Ratio i at P_C = 70 kPa	EF (%)
N5	180	216	1.2	72
N7	135	195	1.44	65
N9	93	170	1.83	57
N11	83	162	1.95	54
N13	65	140	2.15	47
N15	53	116	2.19	39

Table 4.1 | Fluidic transmission ratio i of LIMO ventricles with different number of pouches. Input volume (ΔV_A), output volume (ΔV_C) and fluidic transmission ratio i and ejection fraction EF of samples with different number of pouches against minimum afterload of 3.8 kPA.

that all artificial ventricles can reach this output volume, and all ventricles reach a fluidic transmission ratio higher than one except for N5 (Fig. 4.6.A). In addition, we observe that prototypes with 11 or fewer pouches (N11, N9, N7, and N5) could reach an EF between 54−72% (Table 1), which equals to SV of 162−216 mL, against minimum pressure of 3.8 kPa (~28 mmHg). Although the size and EF of current models are comparable to the normal values of our native ventricle (52−72%) [255, 256], the obtained values of SV (162−216 mL)

are significantly higher than for a native heart. This gives us further opportunity to tune the design to adjust and minimize the size of the device further. It should be noted that the EF is measured against a minimum afterload of 3.8 kPa (~28 mmHg), which is comparable or slightly higher than pulmonary artery systolic pressure [257]. As such, for a biventricular device distinct design parameters must be considered for each side to ensure balanced cardiac output, as the left ventricle operates against significantly higher afterloads [254].

We next study the afterload sensitivity of the artificial ventricle, i.e., how an increasing afterload affects the fluidic transmission ratio at given actuator pressures. To do so, we conducted similar in vitro quasi-static experiments as before, while increasing the afterload (P_{aft}) in the range of 5−20 kPa (37.5−150 mmHg) above the minimal afterload of 3.8 kPa (Fig. 4.4). These are pressures in the range of those generated by a native heart. We focus on an artificial ventricle with 9 pouches (N9) that we believe shows most potential for dynamic testing, as samples with fewer pouches do not reach fluidic transmission ratios that are significantly higher than $i = 1$, while more pouches require higher actuation pressure, and lead to narrow channels which limit the air flow in high frequency actuation. It should be noted that the ventricle with 11 pouches (N11) also shows similar trends.

Figure 4.6.B shows the test results of the ventricle with 9 pouches under different afterloads. Interestingly, we observe that the fluidic transmission ratio only starts to increase after the pressure in the pouches surpasses the pressure in the ventricle. As a result, for an increasing afterload from 5 kPa to 20 kPa we find that the fluidic transmission ratio at $P_{\text{A}} = 70$ kPa drops from 1.68 to 1.30. Even though the afterload influences the fluidic transmission ratio at a specific actuation pressure, the pressure-volume response of the pouch actuator seems to indicate that the afterload mostly shifts the pressure, such that this affect can be circumvented by increasing the actuation pressure further to again increase the fluidic transmission ratio.

Afterload	**Ratio** i		**Input work (N·m)**		**Output work (N·m)**		**Efficiency (%)**	
P_{aft} (kPa)	**N9**	**N11**	**N9**	**N11**	**N9**	**N11**	**N9**	**N11**
5	1.32	1.46	1.01	1.01	0.83	0.80	81.87	78.94
10	1.28	1.36	1.42	1.45	1.24	1.23	87.51	84.97
15	1.25	1.34	1.85	1.88	1.69	1.62	91.48	86.49
20	1.21	1.30	2.32	2.33	2.10	2.10	90.83	90.48

Table 4.2 | Fluidic transmission ratio i and energy efficiency of N9 and N11 LIMO ventricles. Measured at ΔV_{C} = 90 mL, and mechanical efficiency of the LIMO ventricles against different P_{aft} above minimum afterload.

Besides providing sufficient cardiac output, efficient transfer of energy is crucial for any transmission system. To evaluate the mechanical efficiency of work transmission in the soft artificial ventricle, we characterize the ratio of the work done by the ventricle and compare it to the input work supplied to the pouch actuator. Since mechanical work is represented by the integration of pressure over geometric volume, the input and output work are determined from the pressure-volume curves of the pouch actuator and the ventricle, respectively (Figure S5). From our analysis we find that for a given output volume of ΔV_{C} = 90 mL the mechanical efficiency increases from 82% to 91% as the P_{aft} increases from 5 kPa to 20 kPa above the minimum afterload of 3.8 kPa, indicating that the LIMO ventricle transforms the energy more effectively under higher afterload. We also find that the LIMO ventricle with 9 pouches has a slightly higher efficiency than the LIMO ventricle with 11

pouches (Figure S5, Table 4.2). We believe this is because the pouch fabric undergoes stretching during actuation, consuming part of the input energy. In the LIMO ventricle with more pouches, higher pressure is required in the pouches to achieve a given output volume, resulting in greater stretching and therefore slightly more energy consumption, compared to the LIMO ventricle with less pouches. Although these materials are nearly inextensible, previous modeling results still demonstrate some stretching that occurs in the pouches at these pressures [251].

4.6. In vitro dynamic test bench performance

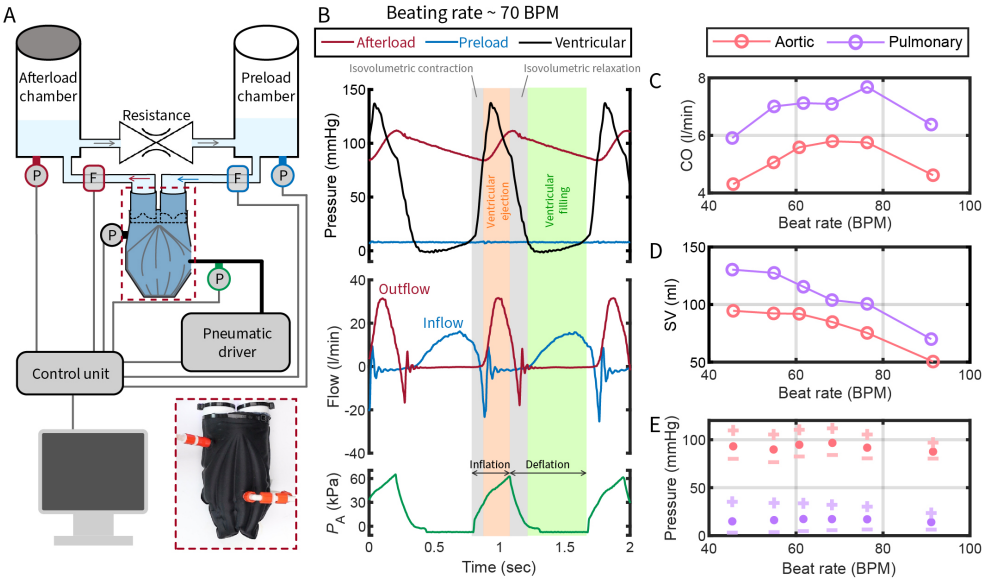

Figure 4.7 | In vitro evaluation of a single ventricle in a single-sided MCL. A. Single-sided MCL setup, pressure sensors (P), and flow sensors (F). B. Prototype N9 functioning against aortic condition at 70 BPM. C. Total cardiac output (CO) from a single ventricle against aortic and pulmonary condition. D. Stroke volume (SV) at different beating rates against aortic and pulmonary conditions. E. Systolic (+), diastolic (-) and average (·) pressures at different beating rates against aortic and pulmonary conditions.

To assess the behavior of the LIMO ventricle under physiological conditions and cyclic loading, we performed an in vitro experiment in a single-sided MCL (Fig. 4.7.A). The MCL consists of two compliance chambers that mimic the afterload and preload, with a manually controlled restriction in between that is used to tune the setup for desired conditions (Figure S6). Real-time data is collected and stored using pressure sensors in the preload chamber, afterload chamber and ventricle, and by using flow sensors before and after the ventricle to measure the cardiac inflow and outflow. These experiments were done to measure the generated cardiac output by the developed prototype (N9) against aortic and pulmonary afterloads, and to investigate the dynamic behavior of the system by applying cyclic loading and increasing the beating rate from 45 to 90 beats per minute (BPM). Both the aortic and pulmonary conditions are considered independently, to which we tune the MCL. For the aortic condition, we pump against afterloads in the range of 105 ± 6.4 and

78 ± 2.1 mmHg as, respectively, the peak-systolic and end-diastolic pressures, which is characterized by a mean aortic pressure of 87.3 ± 2.6 mmHg. This is comparable to the pressures of the left side of a healthy human heart [258]. For the pulmonary condition, we pump against mean afterload of 14.3 ± 0.7 mmHg that is comparable to the normal working condition of the right side of the human heart, with a mean value between 11 and 17 mmHg [259]. It should be noted that we use mean afterload as the control parameter for MCL tuning. However, due to our MCL limitations, the peak-systolic and end-diastolic pressures (31.8 ± 3.8, 5.5 ± 1.5) are higher and lower, respectively, than physiological levels.

Focusing first on the aortic conditions, we find that similar to a native heart, a full cardiac cycle of the LIMO ventricle consists of four stages (Fig. 4.7.B). A cardiac cycle starts with a very short duration of isovolumetric contraction at which the ventricular pressure (P_v) is increasing without generating cardiac flow, as the afterload is higher than P_v. Once P_v becomes higher than the afterload, the outlet valve opens, and fluid is pumped out of the ventricle. This causes an increase in the afterload as well. Once the inflation phase stops, P_v starts to decline rapidly and the outlet valve closes, which results in an isovolumetric relaxation until P_v dives below the preload pressure, where the inlet valve opens, and the ventricle fills up. It is important to note that the misalignment between afterload pressure and ventricular pressure occurs because the afterload pressure sensor is positioned below the afterload chamber. The distance between the afterload chamber and the LIMO ventricle introduces a delay in the peak systolic pressure of the aorta relative to ventricular pressure (Fig. 4.7.B).

We find that against aortic pressures the maximum SV of 95 mL against mean afterload of 93 mmHg occurred at the lowest beating rate of 46 BPM that we tested (Fig. 4.7.C). In general, we found that an increase in heart rate (HR) reduces the stroke volume (SV). While this could be an effect of less effective pumping due to internal flow in the ventricle, we observe a decline in the maximum pressure in the pouches (Table S2) by increasing the beating rate (Fig. 4.7.C). This indicates that the driving system we used cannot supply the pressures fast enough to maintain a higher SV that is measured in quasi-static conditions. Despite that decline, we could obtain sufficient CO up to 5.9 l/min at 70 BPM (P_A = 61 kPa), after which the *CO* decreases (Fig. 4.7.D). Our LIMO ventricle could maintain mean afterloads of 88-97 mmHg pumping at the rate of 4.3-5.9 l/min (Fig. 4.7.D, 4.7.E). In future work, to address the reduction in SV at higher frequencies, the actuation system should be engineered to consistently reach the desired target pressure across all operating frequencies, as our setup currently did not allow to determine the effectiveness of the LIMO ventricle concept at higher frequencies. To achieve this, adopting a hydraulically-driven system could provide significant advantages by enabling volume-controlled actuation, resulting in more precise, reliable, and consistent performance.

Next, to resemble pulmonary circulation, we set the manual valve in the single-sided MCL between the chambers to its fully open position. Nevertheless, we observe that the resistance is still slightly high as the peak systolic pressure goes above 30 mmHg. Despite higher resistance, we were able to achieve a maximum CO of 7.6 l/min at 76 BPM (P_A = 39 kPa). Our LIMO ventricle could maintain mean afterloads of 14-17.3 mmHg pumping at the rate of 6-7.6 l/min (Fig. 4.7.D). It should be noted that the actuator pressure was reduced to 50 kPa in this setting, since the afterload is also lower than aortic condition and we wanted to avoid overloading the system. Despite that, we observed that the CO in pulmonary condition is still higher than the CO against aortic condition.

4.7. Discussion

In this study, we proposed a fluidic transmission system with volume output/input ratios that exceed current existing solution that are inherently limited due to their membrane-based design. We demonstrated that in our system that showed relatively low energy losses (Table 4.2), smaller actuator volumes at higher pressures are transformed to larger volume at lower pressures (Fig. 4.6.A, Table 4.2). This characteristic is essential in the next generation of fluidically driven TAHs, where the size of the device can be reduced to enable full implantation of both the artificial heart and the systems required to control and power it.

Overall, the fluidic transmission system with 9 pouches around its circumference has an energy transfer between 82% and 91%, which means that less than 1.22W of net fluidic input power needs to be supplied to the system to output 1W of fluidic power to the blood, corresponding to a CO = 5 l/min, against a mean afterload of 90 mmHg. Note that this is a lower bound on energy input, since there are necessarily additional losses in the driving fluid supply system, including viscous losses and efficiency losses of the driving pump. Still, this is a promising energy transfer efficiency that is needed in development of a fully implantable control and battery system in the future.

Moreover, while here we only validated a single ventricle at both aortic and pulmonary conditions, we did not test our LIMO heart with two ventricles in a double-sided MCL. At the moment, a full TAH could for example be obtained by using two separate ventricles, actuated either simultaneously, as in the Syncardia design, or alternately, as in the Carmat system. It is too early to conclude what the best approach is for our LIMO concept. We hypothesize that in the case of simultaneous actuation, which mirrors the function of the native heart, integrating both ventricles into a single structure could enhance the fluidic transmission ratio, as a portion of the pouches can be incorporated into the shared septal wall to assist in contracting both the left and right sides of the TAH. However, this configuration would require an additional volume to store the driving fluid during diastole. When considering alternating actuation, an additional volume is not necessary, allowing for a more compact system. The trade-off, however, is that a larger volume must be displaced in each cycle, compared to the simultaneous actuation approach. Future work will focus on the development of a biventricular device and the optimization of its actuation mechanism, taking into account these considerations to achieve an optimal balance between system size, efficiency, and physiological performance.

Moreover, each side of our native heart is pumping against different pressures. In developing a TAH with two ventricles, one of the primary challenges will be to ensure a balanced output between the left and right ventricles, which is a vital factor for the successful mimicry of the heart's natural mechanical function. Towards that challenge, we demonstrated that by tuning the design of pouch geometries, we can achieve different cardiac outputs against similar afterload, or similar cardiac output against different afterloads. It enables us in future studies on biventricular TAH development to optimize the geometry of pouches and ventricles, to obtain equal cardiac output, despite their different afterloads. In addition, an important consideration for a TAH is that it must dynamically adjust ventricular output in response to changes in the circulatory system to maintain healthy blood pressure. This requires each ventricle to exhibit preload sensitivity, which underlies the Frank-Starling mechanisms that describes the ability to accommodate increased filling volume without a significant rise in pressure when unactuated. Soft materials and structures inherently support this functionality. In fact, we already observe preload sensitivity

in our samples (Figure S5.b, e) even though we did not specifically design our ventricle to demonstrate this effect. Yet, further design optimization should be employed when working towards a biventricular device. Further enhancement of this feature could be achieved through improved design and the use of more stretchable fabrics, which will be essential in future developments.

While this study demonstrates the proof of concept for our efficient fluidic transmission system, we acknowledge several directions that need to be further investigated to advance this technology toward TAH development. First, the proposed fabrication method and materials are optimized for cost-effective and rapid prototyping, enabling the essential experiments conducted in this study. However, to ensure long-term durability, further advancements in both materials and fabrication techniques are necessary, as the system must withstand millions of cycles over a lifetime of operation. Second, biocompatibility was not considered in this study, yet it is a critical factor influencing both material selection and device design. Future research should address these aspects to ensure safe and reliable long-term implantation. Additionally, pouch configuration should be further investigated to optimize flow patterns, minimizing stagnation points and reducing the risk of thrombosis. Third, in our experiments, the device was pneumatically actuated using air, which is not a viable option for an implantable device due to safety concerns and air compressibility limitations that restrict higher cardiac outputs at increased frequencies. Future iterations should incorporate a hydraulic actuation system, which would not only improve control reliability but also enable volume-controlled actuation for more precise performance. Finally, our MCL has limited capabilities in replicating a wide range of hemodynamic conditions, which are essential for evaluating a TAH. Therefore, future studies on a biventricular device should be conducted using a more advanced MCL, capable of simulating both healthy and pathological conditions for comprehensive evaluation.

4.8. Materials and Methods

4.8.1. Design and fabrication

To mimic the natural movements and characteristics of a human heart more closely, we design and fabricate a soft artificial ventricle, employing a novel way of blood ejection. In this concept, we use parallel cylindrical pouches along the height of the ventricle as soft artificial muscles. The pouches inflate and deflate using a pneumatic driving system that provides positive and negative pressure during respectively inflation and deflation. To construct the pouches, we use a heat-sealing technique to bond two layers of thermoplastic sheets together using specific patterns designed in 2D. For this purpose, we customized a 3D CNC machine (TEC4, FELIX, IJsselstein, the Netherlands) by adding a hot rolling tip as the end effector. Using the G-code generated for a 2D pattern, the machine moves the hot tip on sheets at a low speed (200 mm/min) to seal them together. The nozzle and bed temperatures are set to respectively 275 °C and 70 °C in order to seal two layers of nylon coated with thermoplastic polyurethane (TPU-coated nylon) (Riverseal 70 LW, 78Dtex, 170 g/m2, Rivertex, Culemborg, The Netherlands). It is a nearly inextensible material, yet flexible and thin. The 2D patterns are designed in Adobe illustrator software (Adobe Illustrator, Adobe, California, United States) (Figure S1.a). In our design, all pouches are placed within a frame and are separated from each other by a sealing line. There is a gap between each sealing line to let the air reach all pouches. As a result, we do not need sepa-

rate opening for each pouch, and they all are connected (Figure S1). After that, we cut the leftovers from only one side of the prepared pouches, and fold the prepared pouch arrays along the middle line, and then do another heat-sealing using a 2D pattern that creates the ventricle chamber. We leave a single opening at the top of the ventricle that is filled with a 3D-printed TPU part which holds two mechanical heart valve prostheses with opposing orientation, creating an inlet and an outlet (Figure 3, Figure S1.b). In a variation on this design, we created ventricles with two, smaller openings (Figure S1.c), and we used this design in our quasi-static experiments, where we connected the ventricle to the water chamber with a single port used for both inlet and outlet. In both cases, we made a hole in one pouch on each side of the ventricle to insert 3D-printed soft TPU connectors that are used for air inlet and outlet. A larger 3D-printed soft TPU connector is also placed in the ventricle wall to measure ventricular pressure (Fig. 4.3).

4.8.2. Blocked-displacement testing of pouch arrays

For our cylindrical model, if we make a cut from one of the seam lines and unwrap the ventricle, we will have an array of pouches that is known as a soft actuator called pouch motors [230]. To explore the possibility of getting the same result in various designs, we performed a blocked-displacement experiment on four pouch arrays (N4, N8, N10, N20) with different number of pouches (4, 8, 10, 20), each with a constant total height of H = 20 centimeter. All samples have a width of W = 6 centimeter. The total height of the pouch arrays is divided equally between the pouches and the pouches are separated by seal lines (seams) of approximately 2 mm wide. Therefore, a single pouch has a height of respectively 48, 23, 18 and 8 mm. Samples are made by heat-sealing two layers of TPU-coated nylon (Riverseal 70 LW, 78Dtex, 170 g/m2, Rivertex, Culemborg, The Netherlands) together using a 2D-pattern designed in a sketching software (Adobe Illustrator, Adobe, California, United States) (Figure S2).

Samples are then clamped in a tensile testing machine (INSTRON 5965, Norwood, United States). The initial length between the top and bottom clamps is set to 20 cm, equal to the total height of the samples. Before pressurizing the pouches, we apply a relatively low negative pressure of -5 kPa to ensure that the initial geometric volume of the pouches is zero. Then, the pouches are pressurized up to 4 bars in 5 minutes at a constant rate, after which the pressure is reduced back to -5 kPa at the same rate. Meanwhile the force applied to the jaws is measured by the INSTRON machine. We refer to this experiment as a blocked-displacement experiment [251]. Thus, the jaws do not move during the test. The air pressure and air flow are measured by respectively an air pressure sensor (MPX5100DP, NXP, Eindhoven, The Netherlands), and a low-range flow sensor (HAFBLF0750CAAX5, Honeywell, North Carolina, United States). Geometrical volume change (Vact) of the samples is calculated using pressure and mass flow data obtained by the sensors, considering the ideal gas law.

4.8.3. In vitro quasi-static characterization against no afterload

Although we could assess our concept theoretically by the proposed model, there are some factors affecting the behavior of the device that are not considered in the model, such as the exact geometry, and the deformation in the material due to its elasticity. Therefore, to explore the behavior of the system in a physical setup and to proof the fluidic transmission

concept experimentally, an in vitro setup was designed and built, enabling us to perform quasi-static experiments to evaluate and characterize the prototypes. The setup consists of a chamber containing colored water. A pressure sensor (RS PRO 828-5726, London, England, UK) is placed below the chamber to measure the pressure of the water column by which we could also measure the volume displaced from the prototypes to the chamber, extracting the volume of the chamber. The aim of this experiment was to assess the behavior of samples with different number of channels against almost no afterload. Thus, no air pressure is applied to the top of the chamber to simulate afterload, and the only minimum afterload that is applied to the system is caused by the height of the water column. A digital pressure controller (VEAB-L-26-D13-Q4-V1-1R1, Festo, Esslingen am Neckar, Germany) is used to actuate the samples. Six samples underwent this experiment; so called N5, N7, N9, N11, N13 and N15 with respectively 5, 7, 9, 11, 13, and 15 pouches distributed around the circumference of the prototype (Figure S1, S3). The prototypes have equal initial circumference of 22 cm. therefore, the higher the number of pouches, the smaller the size of each individual pouch. The samples that are tested in the quasi-static setup have a single opening that is connected to the bottom of the water chamber, through which water flows into and out from ventricle. To run the system, we slowly increase the pressure linearly from -5 kPa to 70 kPa in 90 seconds (0.83 kPa/s) to make sure that there are no dynamic effects. The pressure inside the pouches is measured by a pressure sensor (MPX5100DP, NXP, Eindhoven, The Netherlands) during the cycle. In order to measure volume displacement of the pouches, we employed a one-directional thermal mass flow sensor (AWM5101VN, Honeywell, North Carolina, United States) measuring mass of air into and out from the pouches. To use only one sensor for measuring both inflow and outflow, we put it in a circuit by which we could change the flow direction using manual valves, so that the flow is always passing through the flow sensor in the same direction, whether it is inflow or outflow (Figure S4). We wait 10 seconds between each step to let the system settle, and to change the flow direction. Volume displacement of the pouches is then calculated by the pressure and mass flow, considering the ideal gas law.

4.8.4. In vitro quasi-static characterization against physiological afterloads

To evaluate the prototypes working against afterloads comparable to physiological pressures, two of the samples (N9, N11) were chosen to undergo quasi-static experiments with applied afterload above the water chamber. In this experiment, the chamber was closed off, and the air pressure above the chamber was set and controlled by a digital pressure controller (VEAB-L-26-D13-Q4-V1-1R1, Festo, Esslingen am Neckar, Germany) and monitored by a pressure sensor (RS PRO 828-5726, London, England, UK). The pressure controller was used to maintain the pressure above the water constant during each test. The samples were tested four times against respectively 5, 10, 15, and 20 kPa. It should be noted that these are values to which we set the pressure controller, above the minimum pressure of 3.8 kPa. Thus, the pressure inside the ventricle is slightly higher than that because of the water height. We used the data from the pressure sensors (RS PRO 828-5726, London, England, UK) on top and bottom of the chamber to calculate water displacement. A full actuation cycle consists of inflating the pouches from -5 kPa up to 70 kPa linearly in 90 seconds (0.83 kPa/s) by a proportional pressure controller (VEAB-L-26-D13-Q4-V1-1R1, Festo, Esslingen am Neckar, Germany), then waiting for ten seconds to settle and deflating

the pouches back to -5 kPa. We repeat each cycle 3 times against each afterload condition. We used a thermal mass flow sensor (AWM5101VN, Honeywell, North Carolina, United States) and a differential pressure sensor (MPX5100DP, NXP, Eindhoven, The Netherlands) to characterize the flow and pressure in the pouch, respectively. The geometric volume of the pouch actuator V_A was calculated by

$$V_{\mathrm{A}} = \frac{P_{\mathrm{atm}} V_{\mathrm{p\_o}}}{P_{\mathrm{A}} + P_{\mathrm{atm}}} + \frac{\int Q dt \cdot T_{\mathrm{room}}}{P_{\mathrm{A}} + P_{\mathrm{atm}}} \cdot \frac{P_{\mathrm{atm}}}{T_{\mathrm{zero}}}, \tag{4.6}$$

where Q is the mass flow rate (at standard temperature and pressure) measured by the flow sensor, P_{A} is the pouch actuator pressure (relative to atmosphere pressure Patm) measured by the pressure sensor, $V_{\mathrm{P\_0}}$ is the initial geometric volume of the pouch at atmosphere pressure, $T_{\mathrm{room}} = 293\ K$ and $T_{\mathrm{zero}} = 293\ K$ represent the room and zero temperature, respectively. We assume that $V_{\mathrm{P\_0}} = 0$ since the pouch was vacuumed at -5 kPa in each test. Therefore, the geometric volume change of the pouch was calculated by

$$\Delta V_{\mathrm{A}} = V_{\mathrm{A}} - V_{\mathrm{P\_0}} = V_{\mathrm{A}}. \tag{4.7}$$

We used a pressure sensor (RS PRO 828-5726, London, England, UK) to measure the water pressure inside the ventricle P_{C} (relative to atmosphere pressure). We placed two pressure sensors (RS PRO 828-5726, London, England, UK) at the top and bottom of the water cylinder, respectively, in order to measure the change of the height of the water column $\Delta H_{\mathrm{water}}$. The geometric volume change of the ventricle ΔV_{C} was calculated by:

$$\Delta V_{\mathrm{C}} = \pi R^2 \Delta H_{\mathrm{water}}\,, \tag{4.8}$$

where, R is the radius of the water cylinder.

The input work done by the air in the pouch can be calculated by

$$W_{\mathrm{in}} = \int P_{\mathrm{A}} d\Delta V_{\mathrm{A}} \tag{4.9}$$

Note that we assume that the initial work done by loading the ventricle is negligible compared to the input work done by the pouch actuator. The output work done on the ventricle can be calculated by

$$W_{\mathrm{out}} = \int P_{\mathrm{C}} d\Delta V_{\mathrm{C}} \tag{4.10}$$

The mechanical efficiency of the LIMO heart is defined as

$$\eta = \frac{W_{\mathrm{out}}}{W_{\mathrm{in}}} \times 100\% \tag{4.11}$$

Figure S5 shows the test results of the artificial ventricles with 9 pouches and 11 pouches, respectively. The input work is calculated by equation (S4), which corresponds to the area under the pressure-volume curves of the pouch actuator (Figure S5.a, d). The output work is calculated by equation (S5), which corresponds to the area under the pressure-volume curves of the ventricle (Figure S5.b, e). The mechanical efficiencies of N9 and N11 ventricle are calculated by equation (S6) at various afterloads (Figure S5.c, f). Both N9 and N11 ventricles show higher mechanical efficiency with increasing afterloads. The N9 ventricle shows slightly higher efficiencies than the N11 ventricle. Note that the rise and fall in the pressure-volume curves of the ventricle in Figure S5.b and e are due to the flow resistance present in the experimental setup.

4.8.5. In vitro evaluation in a dynamic test bench

Actuation method: The pouches are actuated pneumatically using a digital pressure controller (VPPE-3-1-1/8-2-010-E1, Festo, Esslingen am Neckar, Germany) in a pulsatile manner. Their inflation induces systole, followed by their deflation to create diastole. The heart rate is determined by the timing of systolic (t_{sys}) and diastolic (t_{dia}) phase. To drive the pouches, two digital solenoid valves (MHE2-MS1H-5/2-QS-4-K, Festo, Esslingen am Neckar, Germany) connect them to either a pressure containing pressurized air at a fixed pressure adjusted by the pressure regulator, or a tank with fixed negative pressure (-7 kPa) generated by a vacuum pump (VN-14-L-T4-PQ2- VQ3-RO2, Festo, Esslingen am Neckar, Germany). Inflation occurs when the pouches are linked to pressurized air, and deflation occurs when connected to the vacuum tank. Control over the solenoid valves allows for adjustments in the beating frequency as well as the timing of systolic and diastolic phase, facilitating the exploration of the LIMO hearts performance under various conditions. The maximum pressure inside the pressure tank in these experiments is set to 70 kPa and 50 kPa, when working against respectively aortic and pulmonary conditions. However, we observed that the pouch actuator pressure does not always reach the set value due to the circuit resistance at elevated actuation frequencies. This results in a reduction in stroke volume for increasing the beating rate, which is not intrinsic to the LIMO heart design, but is a result of the LIMO heart integrated with its pneumatic control system.

Mock circulatory loop (MCL): The prototype N9 was tested in vitro in a single-sided MCL designed according to the Windkessel model (Figure S6). Our MCL replicates various aortic and pulmonary afterloads and preloads, along with peripheral resistances and compliances for both conditions. The systemic and pulmonary arterial circulations (afterloads) are modeled with a two-element Windkessel consisting of a compliance chamber followed by a manually adjustable resistance valve (Type 3232 2/2 way diaphragm valve, Burkert, Ingelfingen, Germany). The compliance in these chambers can be adjusted by changing the water level. A pinch valve is employed to replicate vascular resistance for both pulmonary and aortic conditions separately. Venous compliances and preloads for the right or left sides are represented using a chamber open to air, where water levels are adjustable. Pressure under both preload and afterload chambers is monitored by electronic pressure sensors placed under each chamber (RS PRO 828-5726, London, England, UK). Cardiac outflow and inflow are measured using ultrasonic flow sensors (DIGIFLOW-EXT1, Emtec, Finning, Germany) that are clamped on hoses (Tygonő formula E-3603 laboratory tubing Z765139, Saint Gobain, La Défense, France) coming out of the device. For in vitro testing, tap water was used. All sensor data were captured using a NI-DAQ card (USB-6218, National Instruments, Austin, Texas, United States).

We tested the N9 prototype under pulmonary and aortic conditions at frequencies set to 50-100 BPM in steps of 10. Inflation time (t_{sys}) and deflation time (t_{dia}) are set approximately to 1/3 and 2/3 of the whole cycle duration respectively. Note that the actual beating rate is less than that what we set due to a delay caused by the software in compiling the driving script line by line (Table S1).

To analyze experimental data obtained from the MCL experiment and to determine the actual beating rate, stroke volume, and total cardiac output, a set of data including 5 consecutive cycles is taken out from the steady-state working period that is reached after adjusting the MCL. The average stroke volume (SV_{avg}) is measured by integrating the outflow (Q_{water}) curves of these five cycles during systole phase and averaging them. How-

ever, for some of the experiments, we had to use inflow curves during diastole to measure stroke volume, since the peak outflow was higher than the normal measuring range (up to 32 l/min) of our sensors.

$$\mathrm{SV} = \int Q_{\mathrm{water}}\,\mathrm{d}t \tag{4.12}$$

Beating rate (HR) is determined by dividing the total time of these cycles by five and then, the total cardiac output (CO) is calculated by:

$$\mathrm{CO} = \mathrm{HR} \times \mathrm{SV}_{\mathrm{avg}}\,. \tag{4.13}$$

5

A soft robotic total artificial Hybrid Heart

Abstract

End-stage heart failure is a deadly disease. Current total artificial hearts (TAHs) carry high mortality and morbidity and offer low quality of life. To overcome current biocompatibility issues, we propose the concept of a soft robotic, hybrid (pumping power comes from soft robotics, innerlining from the patients own cells) TAH. The device features a pneumatically driven actuator (septum) between two ventricles and is coated with supramolecular polymeric materials to promote anti-thrombotic and tissue engineering properties. In vitro, the Hybrid Heart pumps 5.7 L/min and mimics the native hearts adaptive function. Proof-of-concept studies in rats and an acute goat model demonstrate the Hybrid Heart's potential for clinical use and improved biocompatibility. This paper presents the first proof-of-concept of a soft, biocompatible TAH by providing a platform using soft robotics and tissue engineering to create new horizons in heart failure and transplantation medicine.

Based on: **M. Arfaee***, A. Vis*, P.A.A. Bartels, L.C.V. Laake, L. Lorenzon, D.M. Ibrahim, D. Zrinscak, A.I.P.M. Smits, A. Henseler, M. Cianchetti, P.Y.W. Dankers, C.V.C. Bouten, J.T.B. Overvelde, J. Kluin, *A soft robotic total artificial Hybrid Heart.* Nat Commun 16, 5146 (2025). (* contributed equally)

5.1. Introduction

End-stage heart failure has a high mortality rate [260], and while heart transplantation is the best treatment [261], donor hearts are scarce [262]. This limitation has led to the development of total artificial hearts (TAHs) and left ventricular assist devices (LVADs). However, the clinical application of currently available TAHs and LVADs is largely hampered by their poor biocompatibility [263], mainly caused by their non-physiological way of propelling blood and the use of non-autologous materials [39]. These factors can induce thromboembolic complications and bleeding complications due to acquired von Willebrand disease or due to the inherent anticoagulation regimen [64]. Another limitation of the current generation of devices is the use of percutaneous drivelines required for actuation, that carry a high infection risk and significantly impact the patients' quality of life [59]. Due to the high complication rate and low quality of life, the currently clinically available TAHs, SynCardia (SynCardia Systems, Tucson, AZ, USA) and Carmat (Aeson; Carmat, Vélizy-villacoublay, France), are sparsely implanted [236, 264].

We hypothesize that a TAH in which the pumping (beating) power comes from soft robotics can propel the blood in a physiological way. Combined with supramolecular coatings to prevent blood clots and integrate with the patient's cells this could then result in a hybrid TAH. Here, we describe the development of the Hybrid Heart as a proof of concept of a soft robotic heart with some biomimetic properties, such as tissue-engineered inner lining, electronics-free control of the heartbeat, and wireless energy transfer. As such, the Hybrid Heart provides a platform to tackle the multiple issues currently associated with TAHs, with the aim to come closer to the ultimate goal of providing destination therapy for end stage heart failure. (Figure 5.1).

5.2. Results

5.2.1. Rational and design of the Hybrid Heart

As no TAH is as good as a donor heart [236], we believe that the new generation of TAH should as closely as possible mimic the anatomy and function of the human heart. As the human blood vessels and organs are designed to perform under pulsatile blood flow, pulsatile flow seems to be beneficial over continuous flow in long term [265, 266]. In addition, propelling the blood in a physiological way is key in preventing thrombotic complications that are currently seen with LVADs and TAHs. The use of soft materials can create bio-inspired motions [243, 267] (including passive Frank-Starling like behavior), and safe interaction with blood and the surrounding tissues [39]. The ideal TAH should therefore be free from any thrombotic complications. The human heart has two blood chambers (ventricles), separated by a septum, that eject blood simultaneously at each heartbeat. During systole, the ventricular walls and the interventricular septum contract synchronously, resulting in ejection of blood from both chambers. The contraction of the septum is responsible for 40% of the left ventricular output and is the major force of ejection for the right ventricular output [268]. To mimic the human heart contraction closely, an ideal TAH should have two ventricles and a working septum that contributes to the cardiac output. In general, a TAH must deliver the same cardiac output as the human heart during resting and performing light activities, which is 5-6 L/min at a heart rate of 60-100/min [269].

Given the importance of the septum in cardiac function, we conceptualized this in the

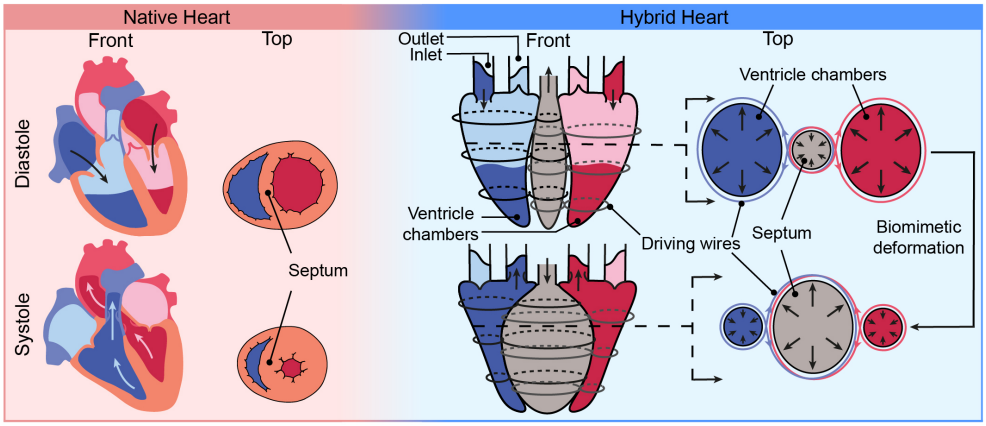

Figure 5.1 | The Hybrid Heart design. The Hybrid Heart is a soft robotic pulsatile TAH that enables a soft contractile motion like the human heart. It is actuated by a pneumatic actuator (septum) positioned between the ventricles, surrounded by wires that wraps around both septum and each ventricle in a shape of (∞).

Hybrid Heart design. The Hybrid Heart has two blood collecting chambers like those in the human heart, which we refer to as "ventricles". Both artificial ventricles are similar in shape and size and can hold a maximum volume of 140 ml each. In between the ventricles of the Hybrid Heart, one soft pneumatic muscle is placed, which we refer to as the septum with a maximum volume of (~)160 ml. The septum is inflated and deflated using relative positive or negative air pressure. Multiple inextensible wires, wrapped around the septum and ventricles in a closed-loop infinity symbol (∞), distribute the forces over the surfaces of both ventricles of the Hybrid Heart (Figure 5.1). Importantly, when the septum inflates, its internal diameter increases, and more length of each wire goes around the septum. As the total length of each wire is constant, they squeeze the ventricles, resulting in ejection of fluid from the ventricles (i.e., blood). Moreover, when the septum is pressurized, it also pushes against the ventricular walls attached to it. Note that the length of each wire and the number of wires around each ventricle dictate the stroke volume ejected by the Hybrid Heart. A deflated septum represents diastole, enabling the passive filling of the ventricles. This process is further supported by the native atria, which remain intact just before the inlet valves, functioning similarly to the ventricles in our native heart [270].

Typically, soft robotic devices are fabricated using extensible materials, such as silicones and soft polyurethanes [52, 53], as their functionality often relies on their material extensibility. However, the durability of these materials when stretching them for as much as 3 billion times in a lifetime at frequencies ranging from 60 to 100 Hz, is a major issue. Here, we opted to develop a concept, in which we can also use thin and flexible yet almost inextensible materials, exploring another material type and actuation method, and expanding the library of soft robotic techniques used in implantable applications. Although its improved durability is yet to be confirmed by more studies and also design optimizations to prevent stress concentrations, this approach fundamentally reduces wall stretch as the softness originates from bending rather than stretching, thereby creating an optimal condition for in situ tissue engineering. We used nylon with a coating of thermoplastic polyurethane (TPU, 70 den, 170 g/qm, extremtextil, Dresden, Germany) for the ventricles and the septum.

Each ventricle has one inlet and one outlet for blood, which can be fitted with any valve type to direct the blood flow. In this proof of principle, we opted for mechanical heart valves for pragmatic reasons, as they are easy to sanitize and can be stored in a dry stage. The Hybrid Heart weighs 62 g including both ventricles, the pneumatic muscle, wires and four mechanical heart valves (when empty). The length from valves to apex is 11 cm and the maximum width is 10 cm.

5.2.2. In vitro quasi-static experiments

In the in vitro quasi-static experiments, we found that the Hybrid Heart only started to contract after the septum pressure reached a critical value, and only returned to its initial shape at a significantly lower critical value, indicating hysteresis in the mechanical response (Figures B.3, B.4, B.5, B.6). Importantly, this effect mainly originates from mechanical hysteresis intrinsic to the Hybrid Heart design and not from friction between wires and the fabrics, which we concluded from a simplified analytical model (Figures B.7, B.8, B.9). The hysteresis results in a slow buildup of pressure in the ventricles and leads to a fast actuation and contraction of the ventricles. Note that this slow buildup of pressure inside the ventricles (isovolumetric contraction phase) and rapid increase during contraction resembles the pumping physiology of the human heart [263].

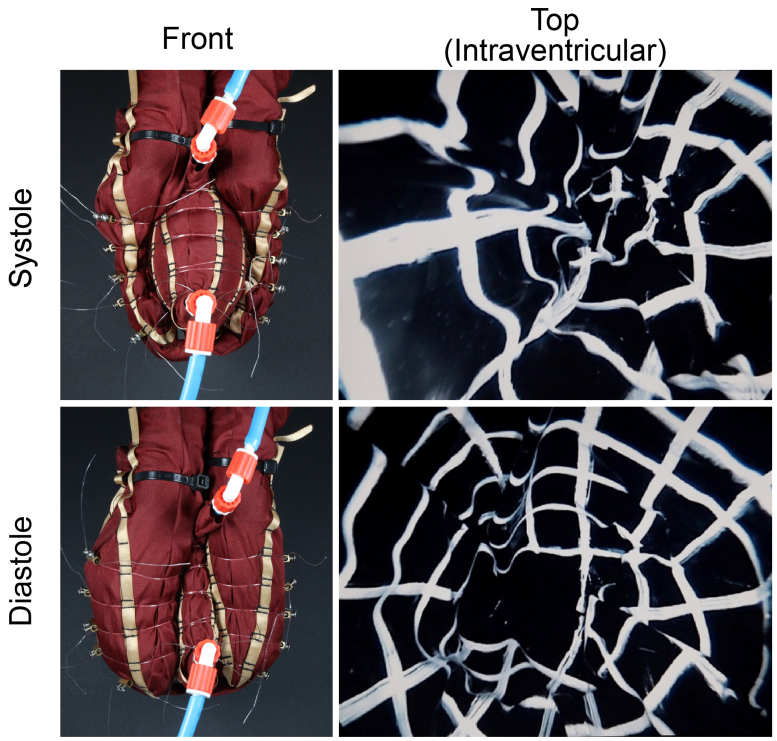

Figure 5.2 | Hybrid Heart in front view (left images) and the view inside the ventricle, captured by a laparoscope (right images), during systole and diastole.

5.2.3. Dynamic test bench performance

Dynamic behavior of the Hybrid Heart was evaluated in a mock circulatory loop (MCL) (Figures B.11, B.12). Figure 5.2 shows the Hybrid Heart prototype at end systolic and end diastolic conditions. We found that, under physiological conditions (Figure 5.3.a), the left ventricle of the Hybrid Heart has a maximum cardiac output of 5.71 ± 0.04 L/min at 60 beats per minute (bpm) (Figure 5.3.b). Since a portion of blood ejected by the left ventricle is shunted directly to the left atrium via the bronchial circulation [154], higher ventricular outputs of the left ventricle are needed compared to the right ventricle. Therefore, we set the right ventricular output to a lower value of 5.02 ± 0.08 L/min. We were able to decrease the right ventricular output relatively to the left ventricular output by adjusting the length of the wires around the right ventricle.

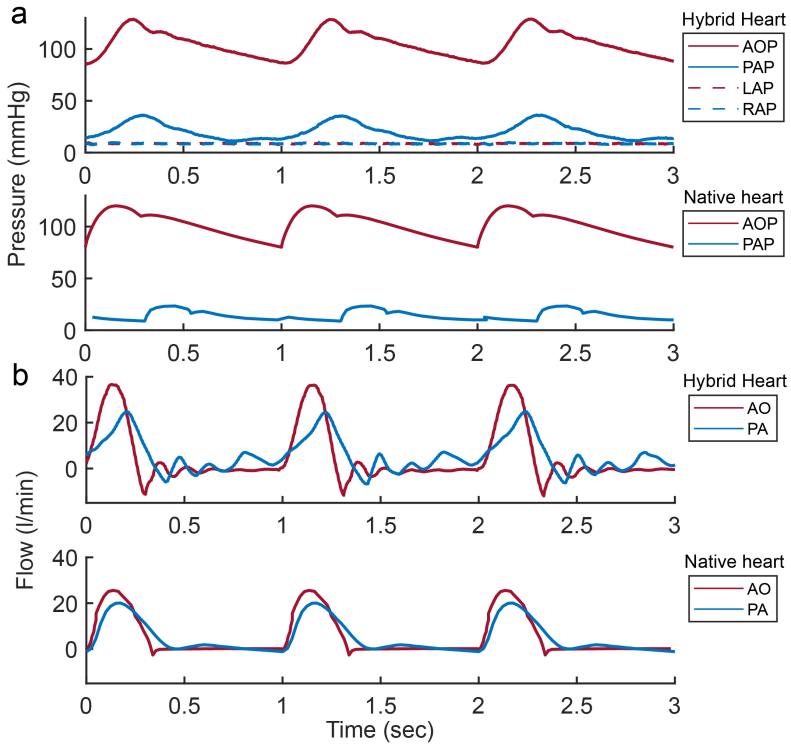

Figure 5.3 | In vitro test results of the Hybrid Heart. All tests were performed in the double MCL. a) On top, pressure curves measured during hybrid heart operation in the MCL, followed by pressure curves of the native heart below. AOP: aortic pressure, PAP: pulmonary artery pressure, LAP: left atrial pressure, RAP: right atrial pressure. b) Flow curves measured during hybrid heart operation in the MCL, followed by flow curves of native heart below [271, 272]. AO: blood flow in aorta, PA: blood flow in pulmonary artery.

The human heart automatically balances its cardiac output through the Frank-Starling mechanism [273]. A TAH needs to have a similar mechanism that allows for increased cardiac output when the preload increases, otherwise severe complications such as respiratory failure can occur. Ideally, this mechanism should be passive, to avoid the use of additional hardware and sensors that are often prone to failure [274]. In the Hybrid Heart, we solely use inextensible materials that are inherently non-compliant in comparison to the

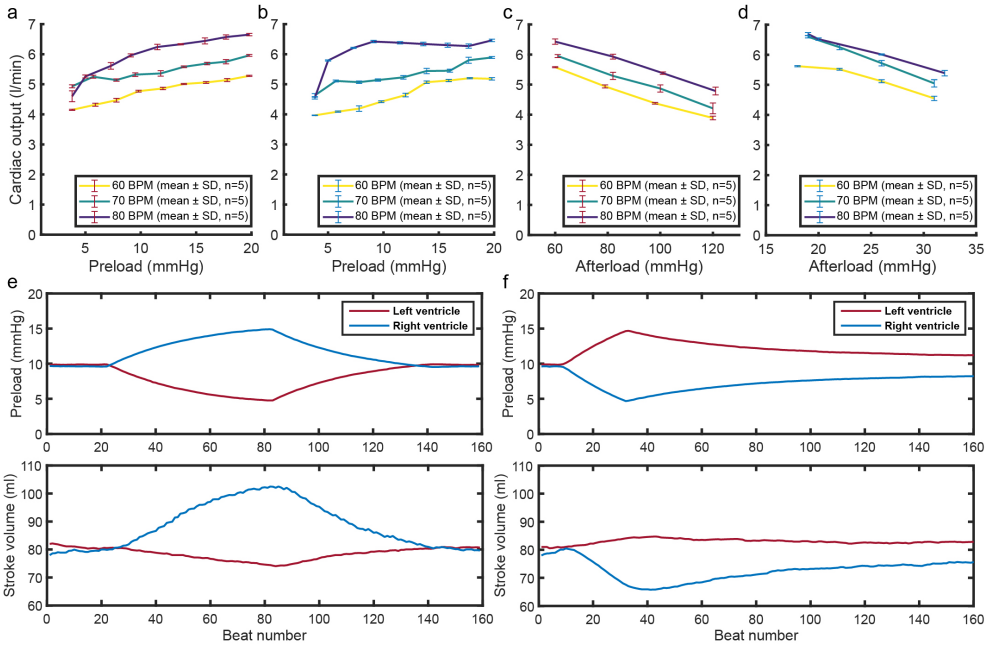

Figure 5.4 | In vitro characterization of Hybrid Hearts preload and afterload sensitivity. All tests were performed in the double MCL at different heart rates of 60, 70, and 80 BPM. Data are presented as mean ± SD of n = 5 cycles. a) The relation between varying left preload (4-20 mmHg) versus left cardiac output. b) The relation between varying right preload (4-20 mmHg) versus right cardiac output. c) The relation between varying left afterload (MAoP) (60-120 mmHg) versus left cardiac output. d) The relation between varying right afterload (MPAP) (15-35 mmHg) versus right cardiac output. e) Hybrid Hearts reaction to left-to-right preload imbalance of approximately 12 mmHg. f) Hybrid Hearts reaction to right-to-left preload imbalance of approximately 12 mmHg.

stiffness of the human heart. However, in our design the ventricles can be compliant because of their geometry and the compliance of the air in the septum. With the laparoscopic camera, we observed that during contraction, multiple folds and wrinkles are formed in the ventricles (Figure 5.2). In addition, the laparoscopic test (Figures B.24, B.25) showed that the ventricles do not completely distend during diastole, allowing for a buffer volume inside the ventricles for increased venous return (preload sensitivity). In case of a rise in venous return, the folds straighten, resulting in an increased stroke volume. Preload sensitivity of the left and right ventricles is illustrated in figures 5.4.a and 5.4.b as a function of preload and heart rate. At the heart rates of 60 and 70 bpm, cardiac output seems to increase almost linearly by increasing the preload on both sides. Preload sensitivity of 0.0701 and 0.0894 L/min/mmHg are measured respectively for left and right ventricles at 60 bpm. By increasing the heart rate to 70 bpm, both left and right preload sensitivity decreases slightly to respectively 0.0577 and 0.0674 L/min/mmHg. However, we observe different behavior at higher heart rate of 80 bpm, where we can identify two distinct region of preload sensitivity for right ventricle. From 4 to 8 mmHg, right CO increases from 4.55 L/min to 6.2 L/min, resulting in a preload sensitivity of 0.4354 L/min/mmHg, after which CO remains approximately constant at 6.36 ± 0.07 L/min. Same trend is observed for left side as well, where the CO of 80 bpm at 4 mmHg is lower than CO at 70 bpm, and increases rapidly by

increasing the preload. However left preload sensitivity can be divided into three regions. Firstly, from 4 to 6 mmHg where the Hybrid Heart ejects 0.550 L/min extra for each mmHg of preload rise. Between 6-12 mmHg and 12-20 mmHg, left preload sensitivity decreases to respectively 0.1538 L/min/mmHg and 0.0511 L/min/mmHg. In general, the mean preload sensitivity of the left ventricle is calculated as 0.176 ± 0.213 L/min/mmHg. Regarding afterload sensitivity, we found that the Hybrid Hearts left ventricle ejects 28 ś 1 mL/min less, for each mmHg afterload rise. As illustrated in figure 5.4.c, heart rate has almost no effect on afterload sensitivity of the Hybrid Heart on both sides. Same trend applies to the right-side afterload sensitivity (Figure 5.4.d). While, it has higher afterload sensitivity by ejecting 104 ± 23 mL/min less, for each mmHg afterload rise. It should be noted that we could not have perfect control over right afterload at higher frequencies due to the limitations of our MCL. However, we assumed that it is not affecting the characterization of the afterload sensitivity, as CO decreases quite linearly by increasing the afterload (Figure 5.4.c, 5.4.d).

Figures 5.4.e and 5.4.f demonstrate the ability of the Hybrid Heart to passively adjust the left and right CO in case of acute imbalance in left and right preloads. As shown in figure 3.e, by increasing right preload from 10 to 16 mmHg, and decreasing left preload from 10 to 4 mmHg, right SV increased dramatically up to 25%, while left SV also decreases 10%, resulting in balancing the preloads after approximately 60 beats. However, the Hybrid Heart was not able to fully maintain balanced output in reverse scenario, where right preload is decreased from approximately 10 to 4 mmHg, and left preload is increased from 10 to 15 mmHg (Figure 5.4.f). This can be due to different preload sensitivity of right and left ventricle in the preloads ranged between 4-16 mmHg at 60 bpm. As illustrated in figures 5.4.a and 5.4.b, right-side preload sensitivity becomes higher at 10-16 mmHg (0.1256 L/min/mmHg) than 4-10 mmHg (0.0734 L/min/mmHg), while on the other side, left-side preload sensitivity is higher at 4-10 mmHg (0.1009 L/min/mmHg) than 10-16 mmHg (0.0504 L/min/mmHg). This can explain the better performance of the Hybrid Heart at 60 BPM, when right preload becomes higher than left preload.

4D flow magnetic resonance imaging results revealed that the flow during the filling and ejection phases of the Hybrid Hearts ventricles is laminar (Figure B.13).

5.2.4. Acute animal experiment

As a proof of concept, we assessed the performance of the Hybrid Heart in an acute goat animal model, excluding the use of a biocompatible coating, and implantable driving system. Prior to the animal trial, we conducted an in vitro experiment against physiological pressures using the exact same prototype for more than two hours (>7000 cycles), to ensure its durability within the time range of an acute animal experiment. During open heart surgery, we placed the goat on cardiopulmonary bypass. After removal of the native goats ventricles, we surgically implanted the Hybrid Heart in the pericardial space. After deairing and weaning from cardiopulmonary bypass, the Hybrid Heart was fully responsible for all blood flow in the goat during a 50 min testing period. We actuated the Hybrid Heart at 65 bpm, and we obtained $2.275 \pm 0.035\ L/min$ of cardiac output on both the left and right ventricles (average stroke volume 35 ml) (Figure 5.5). Throughout the testing period, we recorded a mean aortic pressure of 49 mmHg and a mean pulmonary artery pressure of 17 mmHg from the data of two pressure sensors in the ascending aorta and the pulmonary artery. An additional pressure sensor in the iliac artery recorded systemic blood pressures between 70/35 mmHg and 105/46 mmHg (Figure 5.5.e). After 50 minutes we had to stop

the experiment due to a leakage in the pneumatic septum. The leakage was because of the delamination between TPU (inner layer) and nylon (outer layer) at the heat-sealing line.

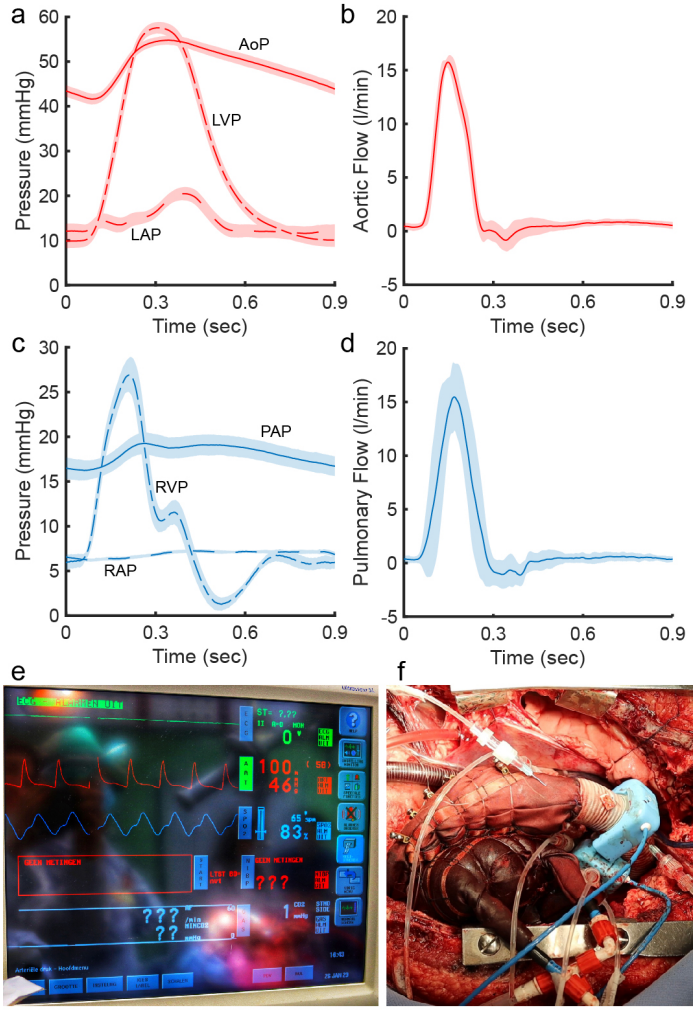

Figure 5.5 | Test results of the Hybrid Heart in vivo experiment in an acute goat experiment. All data corresponds to the period during which the Hybrid Heart was providing all the blood flow in the animal, without additional support of the cardiopulmonary bypass. Data are presented as mean ± SD of n = 20 cycles with shaded error bars. a) Systemic pressures measured during the in vivo experiment. AOP: aortic pressure, LVP: intra ventricular pressure of the left ventricle, LAP: left atrial pressure. b) Aortic flow during the animal experiment. c) Pressures of the pulmonary circulation measured during the animal experiment. PAP: pulmonary artery pressure, RVP: intra ventricular pressure of the right ventricle, RAP: right atrial pressure. d) Pulmonary flow during the acute goat experiment. e) Screen capture of the monitor during the animal experiment. Red line shows the blood pressure measured in the iliac artery (100/46 mmHg, mean 58 mmHg). f) Photo of the Hybrid Heart implanted in the goat.

5.2.5. Biocompatible coating

The biocompatibility of the blood contacting surfaces of the Hybrid Heart was achieved by functionalizing a polycaprolactone bisurea (PCL-BU) coating with heparin to create an anti-thrombogenic surface. To bind heparin onto the TPU-coated nylon material, a heparin binding peptide was added to the system through coupling to a bisurea linker (BU-HBP) allowing incorporation into the bisurea stacks formed in the system (Figure 5.6). Incorporation of 20 mol% of BU-HBP in the supramolecular coatings showed a reduction in water contact angle (Figure 5.7.a).

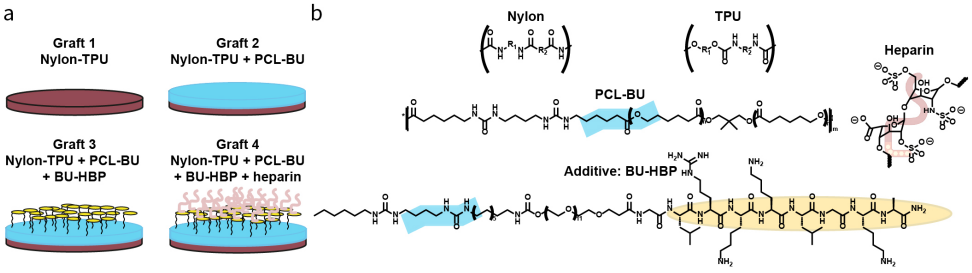

Figure 5.6 | The biocompatible inner lining for the Hybrid Heart, In vitro studies on coated and uncoated TPU-coated nylon. a) Schematic overview of the different grafts used in the in-vitro and in-vivo rat studies. b) Chemical structures of Nylon, TPU, PCL-BU, heparin and BU-HBP.

This increased hydrophilicity was expected because of the polar amine side chains and amide bonds of the BU-HBP molecule. To evaluate the heparin binding to these surfaces, they were incubated in a solution containing heparin coupled with fluorescein isothiocyanate dye for 2 hours. When the BU-HBP concentration was increased to 20 mol%, the fluorescence intensity of that solution dropped (Figure 5.7.b), which indicated that heparin-FITC had specifically adsorbed to this coating. 24 hour testing with human umbilical vascular endothelial cells showed no cytotoxicity of the raw PCL-BU material, nor of the PCL-BU + BU-HBP coating (Figure 5.7.c) Thereafter, the anti-thrombogenic properties of the heparin functionalized coatings were investigated by incubating the materials with human blood plasma for 60 min and scanning electron microscopy analysis afterwards.

On the uncoated TPU-coated nylon material, large platelet aggregates were observed. The TPU-coated nylon with a heparin-functionalized PCL-BU + BU-HBP coating, led to a reduction in platelet adhesion (Figure 5.8). Secondly, we assessed the biocompatiblity of the supramolecular coatings on the TPU-coated nylon base material during an in vivo trial in rats. We fabricated vascular grafts from TPU-coated nylon that we implanted as interposition grafts in the rat abdominal aorta (n=20) (Figure B.17). The rats were randomly allocated to the experimental groups. The investigators were blinded to group allocation during data analysis. By comparing the biocompatibility of vascular grafts made from i) uncoated TPU-coated nylon, ii) TPU-coated nylon coated with PCL-BU or with PCL-BU + BU-HBP (without heparin), and iii) TPU-coated nylon coated with PCL-BU + BU-HBP functionalized with heparin, a high number of thrombotic incidents with the uncoated TPU-coated nylon grafts was observed. However, the addition of PCL-BU + BU-HBP + heparin as a coating showed positive results, with the majority of grafts remaining patent (Figures B.18, B.19, B.20, B.21, B.22, B.23, B.24, B.25). These findings suggest that supramolecular coatings based on bisurea polymers modified with heparin via heparin-

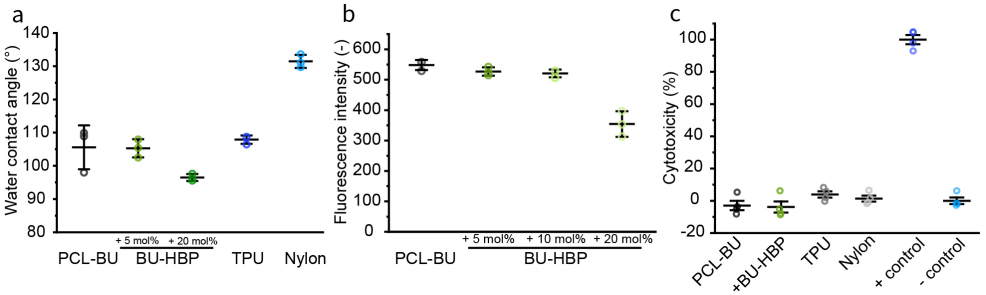

Figure 5.7 | a) water contact angles of TPU-coated nylon material with and without PCL-BU coating with or without 5 or 20 mol% BU-HBP. Data are presented as mean ± SD of n = 3 groups, each containing 3 samples. b) Fluorescence of solution taken from TPU-coated nylon coated with PCL-BU with or without 5, 10 or 20 mol% BU-HBP. Data are presented as mean ± SD of n = 3 samples. c) Cytotoxicity determined from LDH assay of TPU-coated nylon material with and without PCL-BU coating with or without 5 mol% BU-HBP. Data are presented as mean ± SD of n = 4 samples.

binding additives reduce the thrombogenicity of TPU-coated nylon.

To implement the supramolecular coating in the Hybrid Hearts ventricles, we coated its entire blood contacting surface (TPU-side) with PCL-BU through solution-casting. We characterized, by means of chemical analysis, the TPU-coated nylon materials surface with the PCL-BU coating before and after conducting tests in the MCL. We found that after conducting the experiments in the MCL, the PCL-BU coating was still present on the inside of the ventricles (Table B.4). This proves that the supramolecular coating is firmly attached to the Hybrid Heart ventricle even when exposed to flow hemodynamics simulating physiological conditions.

5.2.6. Fully implantable control system exploration

During all above-mentioned in vitro and in vivo experiments, the Hybrid Heart prototype was actuated using an open pneumatic system that is suitable for extra-corporeal operation only. For future translation to the clinic, our objective is to develop a closed fluidic driving system, that is completely implantable. Towards this future driving system, we explored if it is possible to provide the required pressure profile to the Hybrid Hearts septum using a recently developed soft robotic actuation mechanism (including a hysteretic valve) that does not depend on electronics to generate a beating sequence [275]. This actuation system, the hysteretic valve, autonomously and passively transforms the constant flow provided by a continuous flow air pump into pressure pulses that generate the heartbeat for the Hybrid Heart (Figure 5.10.a). This method greatly simplifies the driving system and reduces the number of failure-prone components such as electromechanical valves. The envisioned total pneumatic driving system consists of an implanted continuous flow air pump, an air container, and a soft hysteretic valve, connected to the septum in a closed circulation (Figure 5.10.c).

By furthermore integrating the closed fluidic system to a transcutaneous energy transfer (TET) system, the electrical energy to the pump is provided wirelessly, eliminating the need for external drivelines (Figures 5.10.c, B.15). An external battery or power supply powers the external coil of the TET system, that is placed on the patients skin. The external TET coil generates an electromagnetic field which transmits power to the subcutaneously

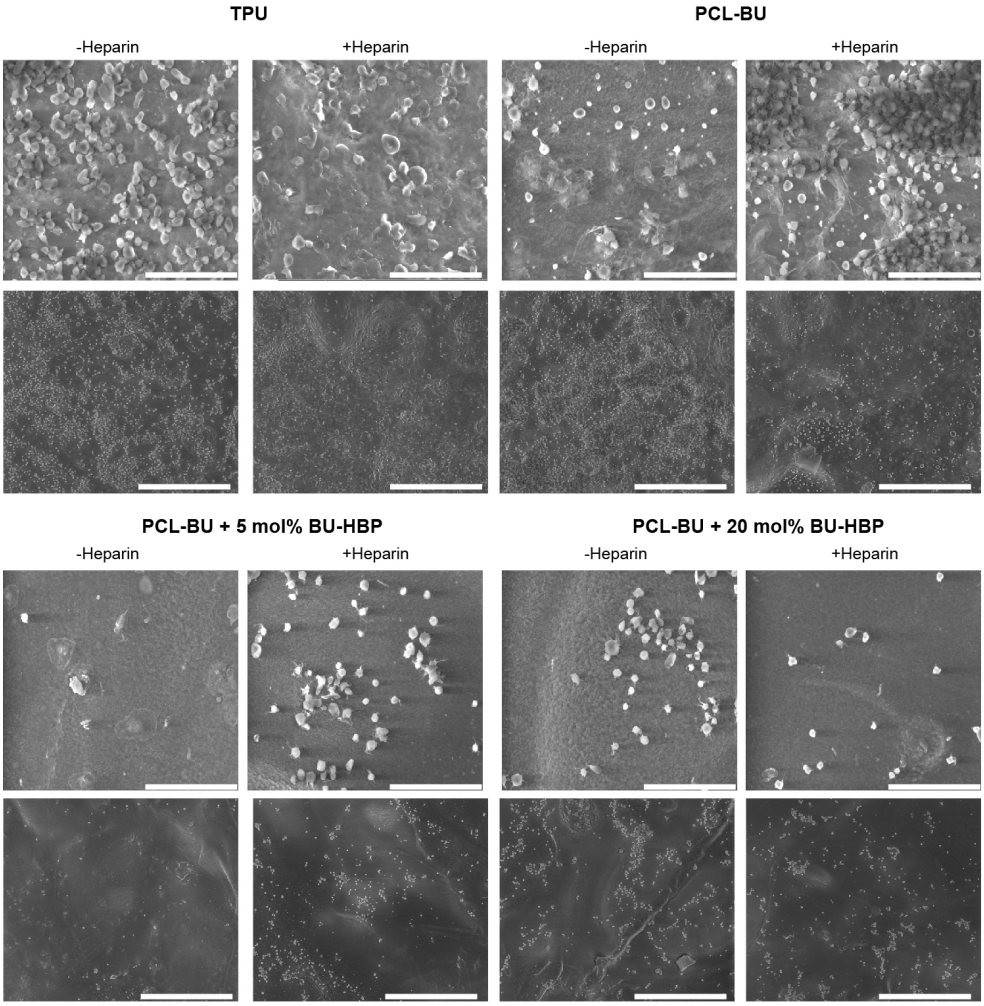

Figure 5.8 | SEM images of platelets adhered to the TPU-coated nylon materials with and without PCL-BU coating with or without 5 or 20 mol% BU-HBP either with heparin functionalization or without.

implanted internal TET coil, while leaving the skin intact. The internally implanted controller provides a stable output voltage to the implanted continuous flow air pump and the implantable battery packs. This approach reduces the risk of infection and enhances quality of life, as it allows future patients to temporarily detach from a power source and freely engage in activities like showering or swimming.

We performed an initial integration experiment to demonstrate the feasibility of this powering and actuation concept. In this experiment we used a TET system to transfer power to a continuous flow air pump connected to a closed fluidic circuit, that actuated the Hybrid Heart connected to the MCL (Figures 5.10.c, B.16). Upon powering the continuous flow air pump, the Hybrid Heart automatically starts to beat at a heart rate of 35 bpm. The beat rate and applied pressure profile are not real-time controlled, but resulted

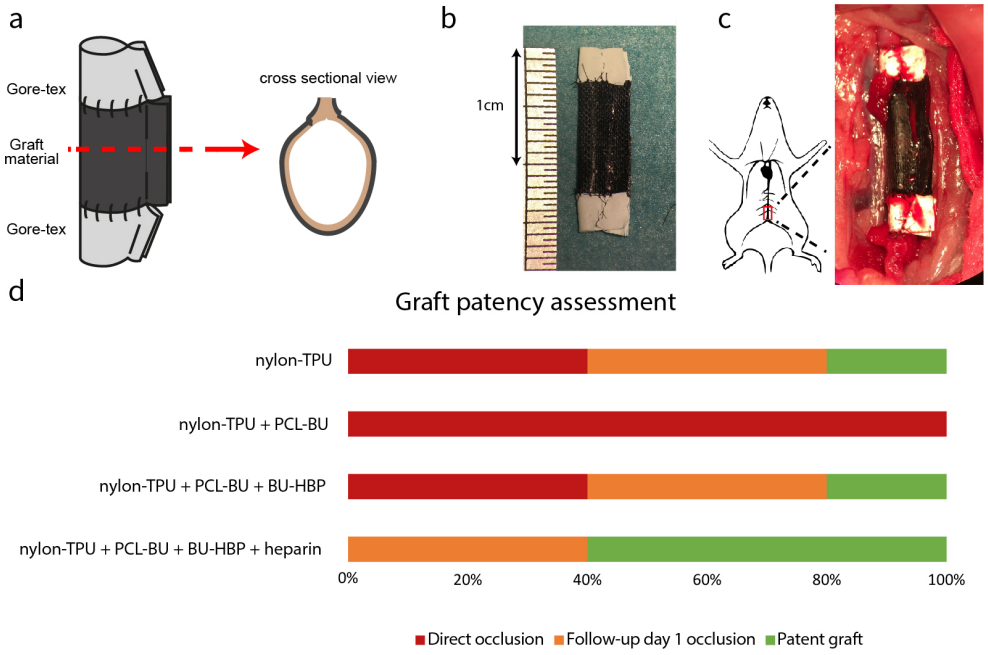

Figure 5.9 | Pre-clinical assessment of the grafts. a) Schematic drawing of the graft design with cross sectional view as well. b) Picture of fabricated graft. c) Picture of implanted graft in rat aorta. d) Assessment of the grafts in terms of occlusion based on hind leg movement and explantation.

from the air chamber, septum, and hysteretic valve properties. In this particular configuration, it provides a left stroke volume of 31 mL against a mean afterload of 66 mmHg, and a right stroke volume of 59 mL against a mean afterload of 12 mmHg. The difference in cardiac output is compensated by a shunt connected between the left and right preload chambers. Importantly, by varying the power supplied to the continuous flow air pump, we can modulate the cardiac output while the system is running, enabling periodic tuning or even real-time feedback control in the future. Note that pump speed mainly affects heart rate, not stroke volume (Figure 5.10.b). While these results demonstrate the concept, it should be mentioned that the cardiac output is still low. That is because in this initial experiment, compared to the traditional driving system, we are limited by the available power provided by the TET system. This is not a limitation of the TET system as such, nor a limitation of the valve and fluidic circuit itself, as higher input energy will result in a higher cardiac output (Figure 5.10.b). Therefore, we aim to improve the energy efficiency of the control system in combination with the Hybrid Heart in the future.

5.3. Discussion

We are on the brink of a new era in which soft robotic technologies are making significant advancements. We present first evidence that soft robotic techniques can be successfully utilized to create a TAH capable of delivering adequate cardiac output under physiological hemodynamic conditions in vitro, and can be successfully, though for now still with

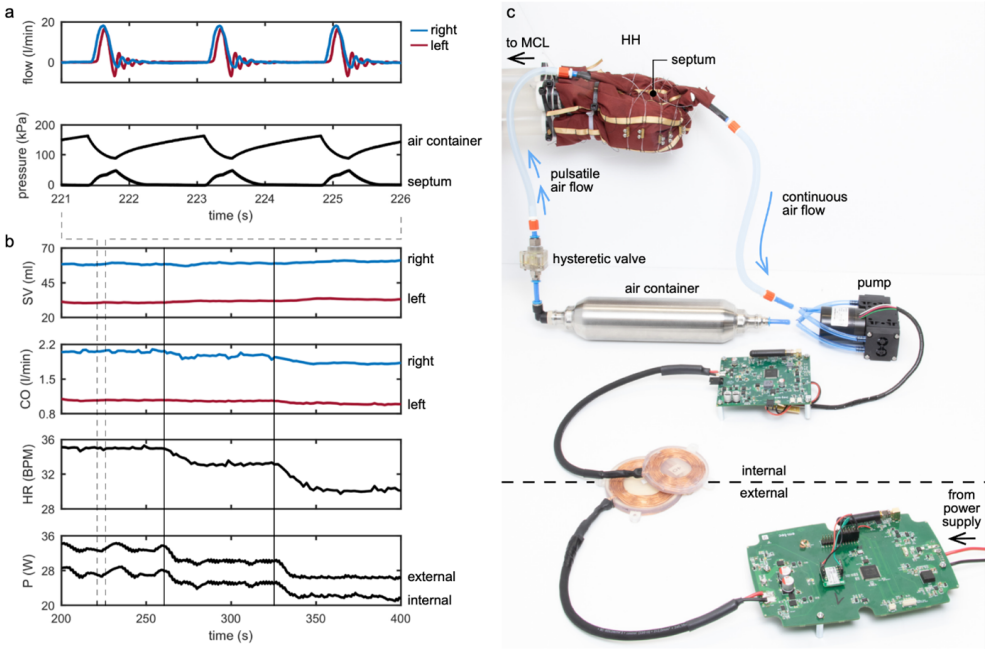

Figure 5.10 | Integration test with implantable control system. a) Left and right ventricular output flow (top panel) as a result of pressure pulses provided to the septum (bottom panel). b) (all panels show 10-beat moving average values). Two vertical solid lines indicate two instances where input power is manually decreased to demonstrate the effect of electrical input power on hybrid heart output. SV = stroke volume, CO = cardiac output, HR = heart rate, P = electrical power. c) Components of the experimental setup, showing how the septum of Hybrid Heart is connected in line with the sealed air circulation of the implantable control system. The ventricles of the Hybrid Heart are connected to a MCL. A horizontal dashed line demarcates the division between the internal and external components of the TET system.

subphysiological performance, implanted and actuated in the acute animal model. Our research has shown that the arrangement of wires, including their number and length, has impact on the ventricular performance, thereby making this technology potentially applicable to patients with various pathologies (Table B.1). For instance, patients with pulmonary hypertension could benefit from wire adjustments to the right ventricle, that allow the right ventricular contractile force to be equal or even outperform the force of the left ventricle to overcome the pathological high pressures in the pulmonary circulation. Indeed, further studies are essential to characterize the effect of wire configuration (number, length, and position) on the cardiac output, which enable us to create a more robust design and utilize this adjustability as a solution for patients with different pathologies.

On itself, the Hybrid Heart shows preload sensitive behavior due to its geometry, varying from 0.0510 to 0.550 L/min/mmHg (0.176 ± 0.213 L/min/mmHg) at different preloads (Figure 5.4.a, 5.4.b), which is somewhat lower than the values reported for native human heart varying from 0.213 to 0.241 L/min/mmHg 23,24. Regarding afterload sensitivity, comparing the right and left side, for a mmHg increase in the arterial pressure, right CO reduction is 3 to 4 times more than the reduction in left CO (Figure 5.4.c, 5.4.d), which is comparable with human heart performance [275, 276]. By developing and implementing additional mechanisms that enhance preload sensitivity, the Hybrid Heart will ulti-

mately be able to adapt to a larger range of hemodynamic conditions, while maintaining balanced cardiac output at different conditions. One possible approach is the implementation of origami [277, 278] folds in the ventricles to allow for additional buffer volume for increased venous returns, while keeping the end systolic volume constant. Such origami folds may also positively affect blood-material interactions, similar to corrugations in the endocardium arterial lumen [279]. These adjustments may also be tailored to the patients specific needs. For example, patients with a large bronchopulmonary shunt flow may benefit from extra buffer volume in the left ventricle. Another benefit of soft artificial hearts in general, is that the patient may be resuscitated via chest compressions until the patient is connected to extracorporeal membrane oxygenation (ECMO), in case of an acute emergency. This is impossible with the currently available LVADs and TAHs.

Balancing left and right ventricular outputs in a TAH is challenging due to dynamic hemodynamic changes and the higher afterload on the left ventricle, which limits its stroke volume. Failure to maintain this balance can result in severe complications, such as lung edema and respiratory failure, which are common causes of death in chronic animal trials with TAHs [280]. Existing TAH designs use various methods to achieve balanced output, including compliant ventricular materials, passive shunts, active control mechanisms, and size adjustments of the right ventricle [280], among which Passive preload-sensitive mechanisms offer advantages over sensor-based systems, which are prone to malfunctions [236]. Our studies illustrates that the Hybrid Heart is able to provide balanced output by adjusting the wire length around each ventricle, and due to its preload sensitivity, it can inherently balance the output in case of any acute changes in the system (Figure 5.4.e, 5.4.f). However, we are aware that it is still limited to a few conditions and can probably not cover all possible condition that may happen in the human body. Therefore, our aim for future studies is to identify, explore, and employ the inherent properties of soft materials and structures for passive ventricular filling and output regulation, leading to a sensorless and robust system.

To enhance its biocompatibility, we introduced the concept of a Hybrid Heart by combining soft robotics that deliver contraction, with supramolecular coatings that are modular and have the potential for dual functionalization to combine anti-thrombogenic properties while stimulating endogenous endothelialization through in situ tissue engineering to ensure long-term hemocompatibility, potentially without the long-term use of anticoagulants. These materials allow for the incorporation of functional additives, such as peptides or extra cellular matrix derived molecules through a mix-and-match approach [280, 281]. Such biomaterials have proven suitable for in situ tissue engineering in clinical and large animal trials for cardiovascular applications such as heart valves [215, 282, 283], vascular grafts [284] and cardiac patches [285], which also proves their scalability to larger models. These cell-free constructs made from biomaterials are designed to induce regeneration upon implantation, directly at the functional site [286]. Our proof-of-concept in vitro and in vivo (rat) experiments show that supramolecular coatings can potentially be used to improve the biocompatibility of the blood contacting surfaces of the Hybrid Heart.

The presence of folds may be an important finding for further optimization of the supramolecular coatings to grow an endothelial monolayer, as folds have been suggested as mechanostructural cues to modulate cell fate and the initial infiltration of immune cells (such as neutrophils) upon implantation in vivo [287]. Future research, by means of e.g., computational fluid dynamics (CFD)-CT, needs to assess if these folds result in blood stasis or not. The native human heart also has folds on the inside that probably are at the

same location at every heart cycle and do not result in stasis of blood; usually blood stasis only occurs in areas with no contractility (e.g., ventricular aneurysm following myocardial infarction). To further enhance the biocompatibility of the Hybrid Heart, a coating that promotes the recruitment of host cells to initiate endogenous colonization of the ventricular surfaces, ultimately forming a functional endothelial monolayer [288] could be used. Previously, we have found that the binding of endothelial cells to supramolecular materials can be further improved through functionalization with vascular endothelial growth factor (VEGF) [288]. A next step is to translate the cell-binding properties to the BU supramolecular system, that is used for the coating of the Hybrid Hearts ventricles. Ultimately, the potential dual activity of the Hybrid Hearts blood-contacting surfaces will be investigated, both as an anti-thrombogenic surface (e.g., heparin) and as an inducer of endothelial monolayer formation (e.g., VEGF).

Use of a TET system reduces the risk of infection and enhances quality of life, as it allows patients to temporarily detach from a power source and freely engage in activities like showering or swimming. We aim to improve the energy transfer of the actuator to the blood, redesign the architecture of the fluidic circuit, and develop pneumatic pumps specifically designed for the hybrid heart. By further optimizing the integral system design, we aim to achieve an efficiency, such that the system can provide sufficient cardiac output using 25 W of electrical energy, the power that our TET system can continuously supply. This research represents a collaborative effort across multiple disciplines, establishing a platform that facilitates future investigations. Though, it is important to note that all ingredients together still have to be tested in (chronic) large animal studies. In conclusion, soft robotics technology can be a game-changer in developing TAHs by enabling biomimicry designs that have the potential to evolve into more efficient, biocompatible and blood friendly devices. This paper presents the first proof-of-concept of a soft, biocompatible TAH and, as such, creates a new horizon in the treatment of heart failure and transplantation medicine that is not currently available or anticipated.

Limitations and future perspective

It is important to note that this study presents a first important step in bridging several fields, yet all ingredients together still have to be improved and tested in animal studies. For practical reasons, we did not use medical-grade materials yet. The material used here for prototyping the ventricles and the septum (TPU-coated nylon) was chosen for its cost-effectiveness and ease of use. Moreover, the heat-sealing technique is also utilized only as a fast-prototyping method that enable us fabricate and test the samples easier and faster for further improvements. Future studies will be performed on developing and evaluating new fabrication methods employing durable and biocompatible materials.

Since the Hybrid Heart is soft, it is crucial to consider the interaction between the device and its surrounding organs after implantation and how the device responds in different conditions. This includes some optimizations on its size, design, and also anatomical shape. Moreover, the whole device including the full fluidic circuit, electronics and the TET system are not yet fully implantable. Future studies and developments are needed to assess and increase energy efficiency of the system, by which we hope to minimize the size of the whole system and bring it closer to a fully implantable device.

In this study, pneumatic actuation was selected for in vitro experiments due to its simplicity and ease of use. However, it is not an ideal long-term solution, as it poses safety

concerns and limits device controllability. Additionally, air compressibility restricts the device from providing higher outputs at higher frequencies, as we observed that the cardiac output starts to decline after reaching a certain beating rate (Figure B.10). To overcome these limitations, future research should focus on developing a hydraulic septum and actuation system, enabling more precise volume-controlled experiments both in vitro and in vivo. It should be noted that the Hybrid Heart already demonstrates a very limited effect of heart rate on afterload sensitivity (Figure 5.4.c, 5.4.d), suggesting the potential for a simpler control system.

5.4. Methods

5.4.1. Design and fabrication

We customized a CNC machine (Felix Tec4, FELIXprinters, Ijsselstein, The Netherlands) to heat-seal two layers of TPU-coated nylon together using a specifically pattern designed in a 2D design software (Adobe illustrator, Adobe, California, United states) (Figure B.1.a, B.1.b). We then inserted the TPU-coated nylon ventricles and septum (Figure B.1.c) into a polyester fabric sleeve that is used to guide the wires and keep them in plane (Figure B.2). Multiple inextensible wires (100% Fluorocarbon, 0.46mm, SavagaGear, Gadstrup, Denmark), wrapped around the septum and ventricles in a closed-loop infinity symbol (∞), distribute the forces over the surfaces of both ventricles of the Hybrid Heart (Figure 5.2). We used four mechanical valve prostheses (Sorin Bicarbon, Sorin Group, Milan, Italy) as inflow and outflow valves with diameters of 21 mm and 27 mm respectively.

5.4.2. Actuation method for in vitro and in vivo experiments

The septum is inflated to induce systole and then deflated to create diastole. For driving the septum in the MCL and the in vivo experiments, two digital solenoid valves (MHE2-MS1H-5/2-QS-4-K, Festo, Esslingen am Neckar, Germany) connects the septum to either pressurized air or vacuum. By controlling the opening and closing of the solenoid valve, we are able to adjust the beat rate and also the systole and diastole timing to explore and investigate the working behavior of Hybrid Heart under different conditions. The air pressure is set by a digital pressure regulator (VEAB-L-26-D18-Q4-V1-1R1, Festo, Esslingen am Neckar, Germany). The vacuum is generated continuously, using a vacuum generator (VN-14-L-T4-PQ2- VQ3-RO2, Festo, Esslingen am Neckar, Germany). The maximum pressure inside the septum can be set according to the preferences and is normally in the range of 70 to 100 kPa.

5.4.3. Quasi-static in vitro experiments

In the experiments to determine the mechanical characteristics of Hybrid Heart, we measure pressures in each of the chambers directly with a pressure sensor (MPX5100DP, NXP, Eindhoven, The Netherlands). Concurrently, we measure bidirectional flow into and out of each of the chambers and integrate to obtain volumes. To measure flow, we place custom-built restrictions in line with the air connections to the chamber and we measure the pressure drop over these restrictions to obtain standard flow rates. In a separate experiment we calibrated the pressure drop over the restrictions against known standard flow rates

produced by a mass flow controller (SLA5850, Brooks Instrument, Hatfield, Pennsylvania, USA), at various absolute pressures.

In all quasi-static in vitro experiments, we pressurize the left and right ventricle with pressure controllers (VEAB-L-26-D13-Q4-V1-1R1, Festo, Esslingen am Neckar, Germany), each set to its individual setpoint pressure. Then, in pressure-controlled experiments, we cycle septum pressure (using a third pressure controller (same type as for the ventricles). We first pressurize the ventricles and let them settle for 30 s. Then, we increase the septum pressure from 0 to 80 kPa in 20 s, we hold the septum pressure for 15 s, and decrease from 80 kPa to 0 in 20 s, while monitoring all pressures and volumes.

In volume-controlled experiments, we use a mass-flow controller (MFC) (SLA5850, Brooks Instrument, Hatfield, Pennsylvania, USA) to inflate the septum at a controlled (quasi-static) rate of 0.2 SLPM (standard liter per minute). Thereto, we connect the outflow of the MFC to the septum via a solenoid-operated three-way valve. To deflate the septum, we connect a restriction (918050-TE, Metcal, Menlo Park, CA, USA) to the septum via a solenoid-operated two-way valve. We turn on the MFC at the desired flow rate and let the flow stabilize, while the three-way valve is set to vent the air to the surroundings. Then, we switch the valve so that the air inflates the septum. After 50 s, we switch the three-way valve to its initial position, to stop inflow. After another 5 s, we switch the two-way valve, such that the septum deflates, for 100 s.

5.4.4. Evaluating the dynamical behavior of the Hybrid Heart

Mock circulation loop: Our double MCL (Figure B.11, B.12) can mimic various systemic and pulmonary afterloads and preloads, as well as systemic and pulmonary peripheral resistances and compliances. The pulmonary and systemic arterial circulations (afterloads) are both simulated using a two element Windkessel containing a compliance chamber followed by an adjustable resistance valve (Type 3232 2/2 way diaphragm valve, Burkert, Ingelfingen, Germany). These afterload chambers are sealed with a lid, and the compliance can be adjusted by altering the water level in the chamber. The resistor valves are manually adjustable and are used to simulate vascular resistance (for pulmonary and systemic sides separately). Venous compliances and preloads are simulated using an open to air chamber for right and left side separately, in which the water level can be altered. All preload and afterload pressures are measured by electronic pressure sensors in each compliance chamber (XMLP500MC11F, Schneider Electric, Rueil-Malmaison, France). Left and right cardiac output were measured using two ultrasonic clamps on liquid flow sensors (DIGIFLOW-EXT1, Emtec, Finning, Germany). In vitro testing has been conducted with 40% glycerol solution in tap water, as well as with 100% tap water.

Actuation method: The septum is pneumatically actuated in a pulsatile manner using a digital pressure controller (VPPE-3-1-1/8-2-010-E1, Festo, Esslingen am Neckar, Germany). Inflation of the septum induces systole, while deflation creates diastole, with the heart rate determined by the timing of these phases. To drive the septum, two digital solenoid valves (MHE2-MS1H-5/2-QS-4-K, Festo, Esslingen am Neckar, Germany) alternately connect it to a pressure tank with regulated pressurized air or a vacuum tank maintained at -10 kPa by a vacuum pump (VN-14-L-T4-PQ2-VQ3-RO2, Festo, Esslingen am Neckar, Germany). When connected to the pressurized air source, the septum inflates, and when linked to the vacuum tank, it deflates. By controlling the solenoid valves, both the beating frequency and the timing of systolic and diastolic phases can be adjusted, al-

Table 5.1 | Parameter values, set in MCL for characterization of Hybrid Hearts preload and afterload sensitivity.

Parameter	Unit	Value
MAP	mmHg	60, 80, 100, 120
PAP	mmHg	15, 20, 25, 30
AP	mmHg	4, 6, 8, 10, 12, 14, 16, 18, 20
Heart rate	BPM	50, 60, 70, 80
Systole/diastole timing	_	~1/2

lowing for the evaluation of the Hybrid Hearts performance under different conditions.

We calculated the average cardiac output by multiplying average stroke volume to beating rate. To determine the stroke volume, we measured the area below the flow curves, obtained from flow sensors that are placed after outlet valves right before the afterload chambers. To obtain the stroke volume, we conducted three separate experiments under identical conditions using the same prototype. From each experiment, we analyzed five random cycles selected from the regions where the device operated steadily. Therefore, the reported values for cardiac output are based on 15 cycles taken out from three separate experiments on same prototype. To study the deformation of the ventricles during contraction in in vitro tests, we inserted a laparoscope (HOPKINS II 26003 BA, KARL STORZ, Tuttlingen, Germany) into the Hybrid Heart ventricles.

5.4.5. In vitro characterization of the Hybrid Heart's preload and afterload sensitivity

Table 5.11 specifies the parameter variations used for in vitro characterization of the Hybrid Hearts preload and afterload sensitivity, over which we have control using our mock circulation loop. These experiments were conducted in the same MCL as mentioned above. Also, same actuation method was used as explained above using an alternative vacuum pump (AMEB71FY4R3N1Q4, AEG, Berlin, Germany). Mean aortic pressure (MAP) and pulmonary artery pressure (PAP) was used respectively to control systemic and pulmonary resistances. Different levels of afterload in the systemic and pulmonary circulation were achieved by manually adjusting the systemic and pulmonary resistance valves to maintain the reference MAP and mean PAP, as specified in Table 5.1. The left and right atrial pressures (AP) were held constant at 10 mm Hg for afterload sensitivity experiments. For preload sensitivity experiments, we kept the afterload constant to a mean AoP of 100 mmHg and a mean PAP of 25 mmHg. The preload was then changed by adding water to the preload chambers in steps of 2 mmHg, starting from 4 mmHg up to 20 mmHg.

For demonstrating the Hybrid Heart capability of balancing the cardiac outputs to compensate left and right preload difference, the imbalance between left and right preloads were created by using a roller pump (505S, WATSON MARLOW, Rotterdam, The Netherlands) on a shunt between the two preload chambers. The pump can displace water in both directions, causing pressure to rise in one chamber while simultaneously decreasing in the other. Therefore, in each experiment, consisting of a total of 200 cycles, the Hybrid Heart runs for a few initial cycles before activating the pump to displace water. The displacement occurs either from left to right preload (Figure 5.3.e) or from right to left preload (Figure 5.3.f). The initial mean AoP and PAP are set at 100 and 25 mmHg, respectively, and

the preload is set at 10 mmHg on both sides. Once the pump is activated, it operates until the preload reaches approximately 16 mmHg in the increasing-preload chamber and 4 mmHg in the decreasing-preload chamber. At this point, the pump is turned off, and the system continues running until the experiment concludes. All data is recorded throughout the whole process and then analyzed cycle by cycle in MATLAB (R2024b, MathWorks).

5.4.6. In vivo experiment

For in vivo testing the acute goat model was used. The goat is a frequently used animal model for TAH testing [196, 236, 289]. The body weight and hemodynamics of large adult goats are comparable to those of humans [138, 290, 291]. In addition, the hemodynamics of a large adult goat does not change over time, as the adult goat does not grow. This is a clear advance over the use of calves as animal model for long term trials, where the growth of calves leads to increasing cardiac demands during the follow-up period. First, we tested the device prototype in MCL to confirm its performance. Thereafter, four mechanical heart valves were sutured in a continuous fashion to the TPU-coated nylon inner layer and polyester outer layer (5-0 Prolene C1, Ethicon, Somerville, US). We used 19mm mechanical outflow valves and 25mm mechanical inflow valves (Sorin Bicarbon, Sorin Group, Milan, Italy). Woven vascular prostheses (22mm diameter; Gelweave, Vascutek, Inchin- nan, United Kingdom) were sutured to the outflow valves for easy implantation to the native aorta and pulmonary artery. Atrial cuffs were fabricated using two Hemagard strips per cuff (Hemagard Carotid Patch 25x150mm; Getinge, Gotenburg, Sweden) and sutured to the mechanical inflow valves (Figure B.14). Approval for the animal studies was obtained by the Amsterdam University Medical Centers Animal Care Ethics Committee (AVD1180020209766) and was in agreement with the current Dutch law on animal experiments (WOD). In total 2 female Dutch white goats underwent acute implantation with our Hybrid Heart prototype, of which the second experiment is reported here. The first experiment was a try-out to practice the surgical procedure. For the reported acute experiment, we used a 2,5-year-old female white goat of 65kg. We used propofol to induce anesthesia (24 mg/kg IV; propofol 20 mg/mL, Fresenius Kabi, Bad Homburg, Germany) and to maintain anesthesia (20 mg/kg/h IV) during surgery. We used sufentanil (5 mcg/kg/h IV, Sufentanil-Hameln 50 mcg/mL, Hameln, Gloucester, UK) as pain relief during surgery. We added a single dose of amiodarone hydrochlorine (300 mg IV, cordarone 50 mg/mL, Sanofi, Paris, France) in the saline infusion bag before starting cardiopulmonary bypass (CPB). The animal was placed in the dorsal position. A 25 Fr venous cannula (Maquet, Rastatt, Germany) was inserted in the left jugular vein following the Seldinger technique. A midline sternotomy was performed and the pericardium was opened. We placed a 20 Fr arterial cannula (Edwards Lifescienes, Irvine, US) in the ascending aorta and a 24 Fr venous cannula (Maquet, Rastatt, Germany) in the inferior caval vein. We placed the goat on CPB after heparinization (15000-20000IU IV, Heparine 5000IU/mL, LEO, Ballerup, Denmark). We used CPB flow rates between 4-4.5 L/min. An activated clotting time > 400 seconds was maintained during CPB and arterial blood gas analyses were performed. The animal was cooled down to 30řC. The ascending aorta was clamped just proximal to the junction of the brachiocephalic trunk. We administered 455 mL of St Thomas Hospital Cardioplegic Solution number 1 to arrest the heart. We excised the native ventricles, leaving a rim of approximately 2cm of the ventricular wall from the mitral and tricuspid annulus in situ. The leaflets of the mitral valve and the tricuspid valve were excised. The native

atria were kept intact. The TAH was first sutured to the atrioventricular junctions and then to the pulmonary artery and aorta, using continuous sutures (5-0 Prolene RB, Ethicon, Somerville, US) and carefully de-aired. The animal was rewarmed and the aorta clamp was removed. The TAH was actuated. During actuation of the TAH, the weaning from extracorporeal circulation was initiated until the extracorporeal circulation was stopped. Phenylephrine was administered intravenously as vasoconstrictive medication at an infusion rate of 1500-2500ţg/hour. The cardiac output of the TAH was measured by two ultrasonic flow sensors (MC24PAU and MC28PAU COnfidence Flowprobes, Transonic, Ithaca, New York, US) clamped on the vascular grafts to the aorta and pulmonary artery. We measured pressure in the aorta, pulmonary artery, left and right atrium, and inside the left and right ventricles. We left the chest of the goat open during the full length of the experiment. At the end of the experiment the animal was exsanguinated under full anaesthesia, after which the implanted TAH was explanted.

5.4.7. Control system

To determine the performance of Hybrid Heart when actuated by the soft robotic fluidic circuit and TET system (Figure B.16, we connected a high-performance membrane pump (NMP850.1.2KPDC-B4 HP, KNF Verder B.V., Utrecht, the Netherlands), a 400 mL air container (CRVZS-0.4, Festo, Esslingen am Neckar, Germany), and a hysteretic valve (24) in a 3D printed holder, in a closed circulation with the septum, using PU tubing (PUN-H-6X1-BL , Festo, Esslingen am Neckar, Germany), silicone tubing (SFM3-4050, Trelleborg Healthcare and Medical, Trelleborg, Sweden) and Nordson connectors (MLRL035-1, FS-LLR, FTLL035-1, Nordson Medical, Westlake, Ohio, USA) (Figure B.17). An external power supply was used to provide electrical power to the external electronics of the TET system. The external and internal coils were positioned with respect to each other using a 3D printed holder and were separated by an air gap (6 mm air gap). The internal controller of the TET system conditioned the received electrical power and provided 17.5V to the pump (NMP850.1.2KPDC-B4 HP, KNF Verder B.V., Utrecht, the Netherlands). A control voltage (Vctrl = 0 to 5V) was supplied to the pump via a custom, manually adjustable power supply to set the target pump speed. The internal voltage, as well as the internal and external power were monitored with a sample rate of 1.2 Hz.

5.4.8. Biocompatible innerlining

In vitro tests

Polycaprolactone bisurea (PCL-BU), whose synthesis has been described previously [292], was dissolved with or without 5,10 or 20 mol% BU-HBP in 1,1,1,3,3,3-hexafluoro-2-propanol at a concentration of 20 mg/mL. Heparin functionalization of the materials was performed in 96-wells plates by incubating the materials with 100 ţL of sterile heparin solution (100 mg/mL) for two hours and afterwards washing the samples twice in PBS prior to the experiments.

X-ray photoelectron spectroscopy (XPS) spectra were recorded to determine the atom composition of the supramolecular coatings on TPU-coated nylon with a Thermo Scientific K-Alpha spectrometer equipped with a 180ř double-focusing hemispherical analyser with a 128- channel detector.

For the Heparin FITC assay, 100 L of Heparin-FITC (100 mg/mL) was added. The

samples were incubated for two hours at 37 °C. Afterwards the solutions were removed from the samples and transferred to a new 96-wells plate. The fluorescence of this plate was measured with a fluorescence spectrometer using 495 nm excitation and 520 nm absorbance wavelength.

In vitro cell culture

Cytotoxicity assay was conducted using human umbilical vein endothelial cells (HUVECs, Lonza). HU- VECs were cultured in endothelial cell growth medium 2 (ECGM-2, PromoCell) supplemented with 2% (v/v) fetal calf serum (FCS, PromoCell), growth factors (ECGM- 2, bullet kit, PromoCell) and 1% (v/v) penicillin and streptomycin (P/S) (Gibco) in a humidified incubator at 37 °C and 5% CO2. HUVECs were used at passage 3, and medium was changed every 2-3 days, when cells were 90% confluent, they were detached using accutase (STEMCELL Technologies). Cells were seeded in 96 well plate at seeding density of 3×104 cells/cm2 and incubated in culture medium from different tested material as referred to later.

The cytoxicity of coated and uncoated TPU-coated nylon was determined using the CyQUANT LDH Cytotoxicity Assay (Invitrogen, Thermo Fisher Scientific, Waltham, US) following the manufacturer protocol. The samples were placed in 96-wells plates and fixed in place with an O-ring on top. The samples were incubated in endothelial cell growth medium 2 (ECGM-2, PromoCell) supplemented with 2% (v/v) fetal calf serum (FCS, PromoCell), growth factors (ECGM-2, bullet kit, PromoCell) and 1% (v/v) penicillin and streptomycin (P/S) (Gibco) for 24 h at 37 °C. The next day this medium was removed and added to the HUVECs for 24 hours. The negative control of this experiment were HUVECs cultured according to a standard protocol. For the positive control groups (maximum death of cells), lysis buffer 1:10 was added to HUVECs for 45 minutes. The following day 50 µL from all experimental groups was transferred to a new 96-wells plate and 50 µL of the reaction mixture from the CyQUANT LDH Cytotoxicity Assay was added. These solutions were incubated for 30 minutes and terminated by adding stop solution. Absorbance of the solutions was measured at 490 and 680 nm. The absorbance reading at 490 was subtracted from the reading at 680 to eliminate the background signal. The cytotoxicity percentage was calculated following the formula:

$$\%Cytotoxicity = [\frac{(Compound-treatedLDHactivity-SpontaneousLDHactivity)}{(MaximumLDHactivity-SpontaneousLDHactivity)}] \times 100$$

Platelet adhesion assay

Human peripheral blood buffy coats were obtained from healthy donors with informed consent (Sanquin, Nijmegen, The Netherlands). These buffy coats were centrifuged for 20 minutes at 200 g. The top layer, consisting of platelets rich plasma (PRP), was collected for the platelet adhesion assay. All the material conditions were functionalized with heparin by incubating them with 100 µL of sterile heparin solution (100 mg/mL) for two hours at 37 °C. Afterwards the samples were washed twice with PBS. 100 µL of PRP was added to the samples and they were incubated under gentle shaking condition (50 RPM) for 1 h in a humidified incubator at 37 °C and 5% CO2. The solutions were removed from the samples, and they were washed three times with PBS. Next, the samples were fixated in 4% (v/v) formaldehyde for 15 minutes and washed with PBS.

Scanning electron microscopy (SEM) was used to provide an overview for platelet adhesion and morphology.

in vivo study in rats

Fabrication of the grafts

Rectangular pieces measuring 18×10 mm were manually cut for all three materials (1 uncoated TPU-coated nylon, 2 TPU-coated nylon + PCL-BU, and 3 TPU-coated nylon + PCLBU + BU-HBP). These rectangular pieces were folded and sutured together with interrupted sutures (8-0 ethilon, Ethicon, Raritan, New Jersey), resulting in a 10mm long graft with 2mm internal diameter (Figure 5.9.a, 5.9.b). To prevent transanastomotic cell ingrowth into the graft [293]) and to facilitate the suturing to the native aorta, we added Goretex (Preclude 1PCM102, Gore Medical, Newark, Delaware) strips on both sides of the grafts. The grafts were sterilized with ethylene oxide (Synergy Health, Venlo, The Netherlands) after fabrication.

In vivo study

Every experiment involving animals, human participants, or clinical samples have been carried out following a protocol approved by an ethical commission. Approval for the animal studies was obtained by the Amsterdam University Medical Centers Animal Care Ethics Committee (AVD1180020209766) and is consistent with the current Dutch law on animal experimentation (WOD). In total, 22 male Sprague-Dawley rats were used with a mean weight of 386 (±13) grams and a mean age of 105 (±4) days. Rats were randomly allocated into four groups of N=5 animals, while 2 rats were kept for potential replacements in case of deaths during surgery. The follow-up time was 24 h. No anticoagulant was given during the follow up period.

For experimental groups 1-3, grafts were implanted as fabricated, without further functionalization or treatments (1. uncoated TPU-coated nylon, 2. TPU-coated nylon + PCL-BU, and 3. TPU-coated nylon + PCL-BU + BU-HBP). For experimental group 4, sterile TPU-coated nylon + PCL-BU + BU-HBP grafts were submerged in heparin solution (100µg/ml, Heparin Sodium H4784-1G, Merck Group, Darmstadt, Germany), during 2 hours prior to implantation under sterile conditions. After 2h, the grafts were flushed with sterile saline and implanted immediately thereafter.

Animals were anesthetized using isoflurane gas (2.5 %/L). Buprenorphine (0.05 mg/kg SC; Temgesic 0.3 mg/ml, Chesterfield, Virginia) was administered as general analgesic and a mix of lidocaine (1 mg/kg SC; Lidocaine 20 mg/ml, Fresenius Kabi, Bad Homburg vor der Höhe, Germany) and levobupivacaine (1.5 mg/kg SC; Levobupivacaine 2.5 mg/ml, Fresenius Kabi) was given as local analgesic at the incision site. Midline laparotomy was performed, and the abdominal viscera were lateralized for exposure of the abdominal aorta and the inferior caval vene. All side branches of the segment of the abdominal aorta between the renal arteries and the aortic bifurcation were ligated (8-0 silk suture, Ethicon, Raritan, New Jersey). Next, the abdominal aorta was occluded with microvascular clamps. The aorta was transected, and 1.5 cm of the native abdominal aorta was removed. The proximal and distal lumen of the aorta were flushed with heparin (10 IU, heparin 5000 IU/mL, LEO, Ballerup, Denmark) to remove any clots. The graft composite was sutured with end-to-end anastomosis at both the proximal and distal ends of the Gore-Tex sheets, using interrupted sutures (10-0 ethilon, Ethicon, Raritan, New Jersey). Af-

terwards, vascular clamps were removed, and the blood flow through the abdominal aorta was restored. The abdominal muscular layer was closed with running sutures (4-0 vicryl, Ethicon, Raritan, New Jersey) and the skin was closed with intracutaneous running sutures (4-0 monocryl, Ethicon, Raritan, New Jersey).

Assessments

When the rat had pale and cold hind legs that were not moving or dragging when walking after more than 1 hour after surgery, a human end point was reached and the rat was euthanized.

To evaluate vessel patency, animals underwent in vivo MR imaging (MRI) at 24 h after implantation on a preclinical 7.0T MRI scanner (MR Solutions, Guilford, UK) under full anesthesia (3% isoflurane in medical air). Due to unforeseen technical issues with the MRI scanner during the course of our studies, we could not make all planned MRI scans. We could only make MRI scans for n=6 animals on POD1 (grafts 1.1, 1.2, 3.1, 3.4, 4.1 and 4.5). Furthermore, we obtained MRI scans for n=3 animals on the same day of the surgery in animals that had to be killed early due to immobile hind legs after surgery (grafts 1.5, 2.3 and 3.5). For the remaining N=11 rats, no MRI scan was taken.

After MRI scanning, the rats were transferred to the surgery table and the abdomen was opened under full anesthesia. The grafts were explanted, and the animal was sacrificed by exsanguination under full anesthesia. The grafts were cut in half and were fixated in 3.7% formalin for 24 h and washed in phosphate buffered saline (PBS).

Sections were stained for hematoxylin and eosin (H&E; HT1079 and HT110116, Sigma-Aldrich, Saint Louis, US).

6

General Discussion

The development of total artificial hearts (TAHs) has been a long-standing ambition in the field of cardiovascular medicine, dating back to the first implantation of a mechanical heart in 1969. Over the decades, multiple generations of TAHs have emerged, ranging from the pneumatically driven SynCardia to more recent electromechanical and hydraulically actuated systems such as Carmat, BiVACOR, and RealHeart. These devices were designed to serve as life-saving options for patients with end-stage biventricular heart failure, particularly as a bridge to transplantation. However, despite substantial engineering advances and more than 1,700 successful implants globally, no TAH has yet been approved or widely adopted as a viable destination therapy. This gap is due in large part to persistent challenges including high complication rates (notably thromboembolic events and driveline infections), device bulk, limited durability, and poor quality of life for recipients. These limitations underscore a fundamental disconnect between rigid mechanical solutions and the complex, adaptive behavior of the human heart.

In recent years, the emergence of soft robotics has introduced a paradigm shift in biomedical engineering, offering the potential to address these limitations by mimicking the heart's natural biomechanics in a safer and more adaptable way. Soft robotic actuators that are built from compliant materials capable of large, reversible deformations are uniquely positioned to replicate cardiac motion while minimizing trauma to surrounding tissues and blood components. Nevertheless, the translation of soft robotic principles into functional, clinically viable TAHs remains in its infancy. Few studies have moved beyond bench testing or partial prototypes, and no existing system fully integrates the mechanical, and biological requirements for a long-term implantable heart. As such, there remains a critical unmet need for artificial heart systems that can deliver physiologically relevant performance, adapt to changing circulatory conditions, minimize device-related complications, and support long-term use without reliance on rigid structures or complex control systems.

This thesis investigated the potential of soft robotics to overcome long-standing challenges in TAH development, centered on the guiding question: "Can soft robots donate their heart to humans?" By integrating literature review, analytical modeling, device prototyping, and early-stage testing, the work presented here advances the field of mechanical circulatory support by introducing new frameworks, technologies, and insights into the development of soft robotic TAHs. This chapter provides a comprehensive synthesis of the research findings, discusses their scientific and translational significance, identifies limitations, and outlines future directions. To support a clear and structured analysis, the discussion is organized into five sections: (1) integration of key findings, (2) scientific and technological contributions, (3) limitations and challenges, (4) future research opportunities, and (5) broader implications for the field of heart replacement therapies.

6.1. Overview Of Key Findings

The research presented in this thesis followed a progressive logic, beginning with a critical analysis of the historical and current state of TAH development and concluding with the conceptualization and in vivo testing of a novel soft robotic platform. Each chapter contributes a foundational layer to the overarching goal of designing a TAH that is efficient, adaptive, and biocompatible.

Chapter 2 laid the groundwork through a systematic review of more than six decades of TAH research, it becomes clear that while over 2100 patients have benefited from TAHs as

a bridge to transplantation, no device has yet met the clinical and technical requirements for destination therapy. The review identified five persistent challenges that continue to hinder progress in this field: high complication rates (particularly thromboembolic events and driveline infections), excessive device size, limited long-term durability, poor biocompatibility, and a reduced quality of life for recipients. An in-depth analysis of leading commercial and investigational TAHs including SynCardia, Carmat, BiVACOR, and RealHeart, revealed that despite employing a range of actuation principles and design philosophies, each system remains limited by one or more of these critical issues. This chapter underscores the ongoing need for a next-generation TAH that more closely mimics the native hearts structure and function, with the goal of minimizing complications and ultimately offering a reliable, long-term treatment option for patients with end-stage heart failure. Notably, the chapter identified soft robotics, tissue engineering, and wireless energy transfer as promising but underdeveloped areas of innovation that could transform the field.

Chapter 3 addressed the actuator-level modeling challenge, focusing on elastic pouch motors—a class of soft pneumatic actuators previously modeled under the assumption of inextensibility [230]. A new analytical model was proposed that accounts for the stretchability of the materials, revealing how ballooning instabilities at higher pressures limit both contraction and force output. The study experimentally validated the model using three materials: SEBS, TPU, and TPU-coated nylon. Key observations included (i) a ballooning transition that correlates with a decline in force after peak contraction, (ii) qualitative agreement between model predictions and experimental trends, and (iii) stretch-induced limitations even in stiffer materials previously assumed inextensible. This modeling work highlighted the importance of material selection and predictive modeling in soft robotic design, offering practical tools for optimizing actuator performance for cardiac workloads.

Chapter 4 moved toward device-level innovation with the development of the LIMO (Less In, More Out) heart—a compact soft robotic ventricle that leverages a fluidic transmission system. The LIMO design utilized multiple circumferential pouch motors that convert high-pressure, low-volume input into low-pressure, high-volume output. Experimental testing demonstrated cardiac outputs of up to 7.6 L/min against physiological afterloads and energy transfer efficiencies between 82% and 91%. However, limitations remained, including single-ventricle testing, pneumatic actuation, and lack of biocompatibility considerations. The LIMO heart demonstrated that soft fluidic actuators could meet the functional and energetic demands of a compact TAH, but further development was needed for full-body integration.

Chapter 5 introduced the Hybrid Heart—a soft robotic total artificial heart that integrates supramolecular polymeric coatings to enhance biocompatibility and enable future tissue engineering. The design used a pneumatically driven septum between two ventricles and incorporated adjustable wire constraints to tune left and right cardiac outputs. In vitro testing showed balanced biventricular output and a cardiac output of 5.7 L/min. Preload sensitivity was evident and comparable to native heart by replicating frank-starling behavior. In vivo studies in an acute goat implantation demonstrated successful actuation and cardiac support, though not yet at physiological rates or under chronic conditions. Supramolecular coatings showed promise for promoting endothelialization and reducing thrombogenicity, particularly through dual-functionalization with VEGF and antithrombotic agents. The Hybrid Heart brought together mechanical performance, physiological adaptability, and biological interface design, offering a vision for a fully soft and biointegrated TAH system.

6.2. Scientific and Technological Contributions

This thesis makes several significant contributions to the field of artificial heart development, particularly in the context of soft robotics, by advancing fundamental understanding of soft actuator mechanics, proposing energy-efficient and compact system architectures, integrating biofunctional materials to enhance biocompatibility, and demonstrating proof-of-concept prototypes through both bench testing and preliminary in vivo validation.

6.2.1. The Role of Material Selection in Soft Actuator Performance

Material selection plays a pivotal role in the design and performance of soft actuators, especially in applications such as TAHs where precise mechanical behavior, durability, and energy efficiency are critical. Traditionally, soft robotic actuators have relied on highly elastic materials such as silicone elastomers, thermoplastic polyurethanes (TPUs), or rubber-based composites to achieve large deformations under relatively low driving pressures. This intrinsic elasticity enables the actuators to mimic the natural expansion and contraction of cardiac muscle, providing gentle interactions with surrounding tissues. However, while this stretchability supports bioinspired motion, it also introduces important challenges. Excessive extensibility can lead to uncontrolled deformations (e.g., ballooning), reduced force output, and mechanical inefficiencies, particularly at higher actuation pressures. These issues are especially problematic in cardiovascular applications, where the actuator must perform under high cyclic loads and resist fatigue over millions of cycles. Thus, the design of soft artificial hearts calls for a reassessment of conventional material paradigms, moving beyond the sole use of stretchable elastomers.

To address these limitations, recent research has explored the use of deformable yet inextensible materials in soft actuation systems. These materials allow shape change through controlled folding, bending, or pressurization, without undergoing significant stretch. Such an approach not only limits ballooning and geometric instabilities but also enhances mechanical efficiency by losing less energy due to material elasticity. Analytical modeling performed in the context of pouch motors—key component in the design of the LIMO ventricle—has confirmed that material extensibility plays a crucial role in performance. Models incorporating stretchable material properties predict a decline in force output once ballooning occurs, a phenomenon that was validated experimentally. In contrast, actuators constructed from inextensible or low-stretch materials maintain their structural integrity across a broader range of pressures, resulting in greater contraction forces and more efficient fluid displacement. These insights underscore the necessity of carefully tuning material stiffness, elasticity, and thickness to optimize actuator output while avoiding failure modes like ballooning. Moving forward, the development of hybrid materials and composite layers that combine flexibility with inextensibility will be essential for advancing soft robotic artificial hearts toward clinical viability.

6.2.2. Compact and Energy-Efficient Design: A Prerequisite for Full Implantability

Achieving full implantability of a TAH hinges critically on two interdependent parameters: minimizing total device size and maximizing energy efficiency. Unlike bridge-to-transplant devices that may rely on external power supplies and tethered control units, a total artificial heart that can be ultimately used as destination therapy must be entirely implantable to support patient autonomy, reduce infection risks, and restore quality of life. This demands not only a compact pumping unit but also the minimization and integration of auxiliary components such as actuation systems, control electronics, fluid reservoirs, and energy transfer units within the anatomical confines of the thoracic cavity. Traditional rigid systems often struggle to meet these volumetric constraints, limiting their applicability to larger patients. In contrast, soft robotic systems offer improved conformability to the body, yet still require precise spatial and functional optimization to accommodate the full system within the body.

Energy efficiency plays a pivotal role in enabling such compact integration. A more efficient actuator reduces the required input energy for each heartbeat, allowing for smaller and lighter components such as pumps, batteries, and transcutaneous energy transfer (TET) coils. For instance, the LIMO heart presented in this thesis demonstrated energy transfer efficiencies exceeding 80%, meaning that less than 1.22 W of fluidic power input is needed to produce 1 W of blood flow output—a substantial reduction compared to earlier designs [52, 54, 55]. This level of efficiency directly impacts system miniaturization, as it lowers the size and weight demands of power storage and conversion systems while minimizing heat generation within the body. Furthermore, energy-efficient actuation reduces the strain on battery life and improves the feasibility of operating continuously within the power budget of TET systems (typically ~20-25 W). Therefore, compactness and efficiency are not merely parallel goals but deeply interconnected design imperatives. Optimizing both simultaneously is essential to develop a fully implantable soft robotic TAH capable of long-term, autonomous operation in a wide range of patients.

6.2.3. Soft Actuation as a Pathway to Biomimetic Cardiac Function

One of the most transformative advantages of soft robotic systems lies in their capacity to replicate native biological function through inherent material and structural properties rather than through rigid mechanical components or complex electronics. In the context of total artificial hearts, soft actuation enables the design of systems that more naturally emulate the dynamic, adaptive, and compliant nature of the human heart. Unlike traditional mechanical pumps that operate with fixed stroke volumes and require active sensor feedback to adjust flow rates, soft robotic systems offer the possibility of embedding physiological responsiveness directly into the mechanics of the device. This shift from control by computation to control by compliance represents a fundamental reimagining of how artificial hearts can achieve truly biomimetic performance.

The potential of soft actuation to replicate native cardiac behavior was clearly demonstrated in Chapter 5 with the development of the Hybrid Heart. This system incorporated a pneumatically driven septum and deformable ventricular walls that were capable of mimicking the Frank-Starling mechanism—a fundamental physiological principle by which

the heart adjusts its stroke volume in response to changes in preload (ventricular filling). In the Hybrid Heart, this adaptive response emerged not from active feedback control but from the intrinsic deformability and geometry of the device. The ventricle expanded passively with increased venous return and subsequently generated higher output, without requiring real-time sensing or algorithmic intervention. This preload sensitivity closely parallels the behavior of the native myocardium and demonstrates that, with proper material selection and structural tuning, soft robotic hearts can adapt to hemodynamic changes in a purely mechanical manner.

The implications of this passive biomimicry are profound. By embedding adaptability into the mechanical architecture of the artificial heart, it becomes possible to reduce or even eliminate the need for complex sensor arrays, signal processing units, and real-time control algorithms traditionally required to balance left and right ventricular output. This is especially critical in biventricular support systems, where small mismatches in output can lead to dangerous complications such as pulmonary congestion or systemic hypotension. The Hybrid Hearts ability to achieve balanced biventricular function through adjustable wire constraints and soft material properties suggests a viable pathway toward a sensorless, self-regulating TAH. Such a design paradigm offers enhanced robustness, reduced system complexity, and improved implantability, all while more closely mirroring the natural dynamics of the human heart.

Looking ahead, further optimizations in soft actuator geometry, material composition, and compartmental coupling may enhance the precision and range of this passive adaptability. Strategies such as tunable stiffness zones, compliant origami-inspired folds, and pre-strained materials could allow fine-tuning of ventricular responses to changing circulatory demands. Additionally, intelligent mechanical design could enable selective modulation of right versus left ventricular compliance, offering tailored support in pathologies like pulmonary hypertension or unbalanced cardiac failure. These advances would further reduce the dependency on electronic sensing and control systems, streamlining the artificial heart into a more elegant, robust, and body-friendly device. In this light, soft robotics does not simply offer a new actuation mechanism but a fundamentally different path to replicating cardiac function.

6.2.4. Biocompatibility and Endothelialization: Toward Blood-Friendly Artificial Hearts

One of the most critical challenges in TAH development has been the interface between synthetic materials and circulating blood. Despite significant advances in pump mechanics and device miniaturization, most current TAH systems—including SynCardia, BiVACOR, and RealHeart—continue to rely on non-hemocompatible materials or rigid surfaces that make direct contact with blood. These foreign materials trigger a cascade of adverse biological responses, including platelet activation, thrombus formation, hemolysis, and inflammatory reactions. To mitigate these effects, patients are often required to undergo lifelong anticoagulation therapy, which itself introduces serious risks such as bleeding complications, poor wound healing, and stroke. Furthermore, the mechanical design of traditional devices, with abrupt flow transitions and non-physiological shear forces, exacerbates blood trauma and contributes to device-related morbidity. As a result, thrombogenicity remains a leading cause of TAH-associated complications, limiting the durability and widespread acceptance of these systems as destination therapy.

Recognizing these limitations, the need for biologically compatible blood-contacting surfaces has become increasingly urgent. While some devices, such as Carmat, have taken a step in this direction by using a layer of bovine pericardium on the blood-contacting surface of their membrane to improve hemocompatibility, such passive biological interfaces remain limited in function. Rather than merely attempting to reduce adverse interactions through pharmacology or static coatings, a more transformative approach lies in the integration of tissue-engineered linings that actively cooperate with the bodys natural healing and regulatory mechanisms. In particular, the incorporation of a biocompatible inner lining that can serve as a substrate for endothelialization—the process by which a functional monolayer of endothelial cells forms on the surface—is a promising strategy to replicate the anti-thrombotic and regulatory properties of native blood vessels. Such a strategy shifts the paradigm from passive blood compatibility to active biological integration, offering the potential to drastically reduce reliance on systemic anticoagulation while improving long-term hemocompatibility and healing outcomes.

In this context, the Hybrid Heart developed in Chapter 5 introduces a novel approach by using supramolecular polymeric coatings as blood-contacting materials. These coatings are designed to be not only hemocompatible but also biofunctional—capable of being functionalized with bioactive molecules such as vascular endothelial growth factor (VEGF), heparin, or extracellular matrix-derived peptides. This modular surface enables a mix-and-match strategy to tailor the biological response for specific patient needs or pathological conditions. In vitro and in vivo studies in this thesis have shown that these surfaces can support early-stage endothelial cell adhesion and show potential to guide in situ tissue regeneration, creating the conditions for a functional endothelium to form directly on the artificial surface. Such endogenous endothelialization transforms the blood-contacting surface from a source of risk to a biologically active layer with natural antithrombotic and anti-inflammatory properties.

The implications of this approach extend far beyond thromboresistance. A living, endothelialized inner surface can dynamically regulate coagulation, respond to flow changes, interact with immune cells, and release vasoprotective factors—much like the native vascular endothelium. This could improve the long-term biocompatibility of TAHs, reduce device-related complications, and open the door to safer, more personalized artificial heart systems. Moreover, this strategy aligns with the emerging field of regenerative prosthetics, where the goal is not just mechanical replacement but functional biological integration. By engineering a soft robotic TAH that not only mimics cardiac motion but also recreates a native-like blood interface, this thesis contributes to a new generation of cardiovascular devices—devices that are not just tolerated by the body, but are actively integrated into its physiology.

6.3. Integration of Key Findings Across Chapters

The research presented in this thesis brings together multiple dimensions of TAH development, ranging from actuator mechanics to physiological mimicry and biological integration, and collectively supports a vision for the future of heart replacement technology. Through analytical modeling, prototyping, and early biological testing, this work demonstrates the unique potential of soft robotics to overcome long-standing limitations of conventional TAH systems. While current technologies remain constrained by rigid designs, high complication rates, and limited biocompatibility, the findings here point toward a

promising new direction grounded in compliant materials, energy-efficient actuation, and regenerative surface engineering.

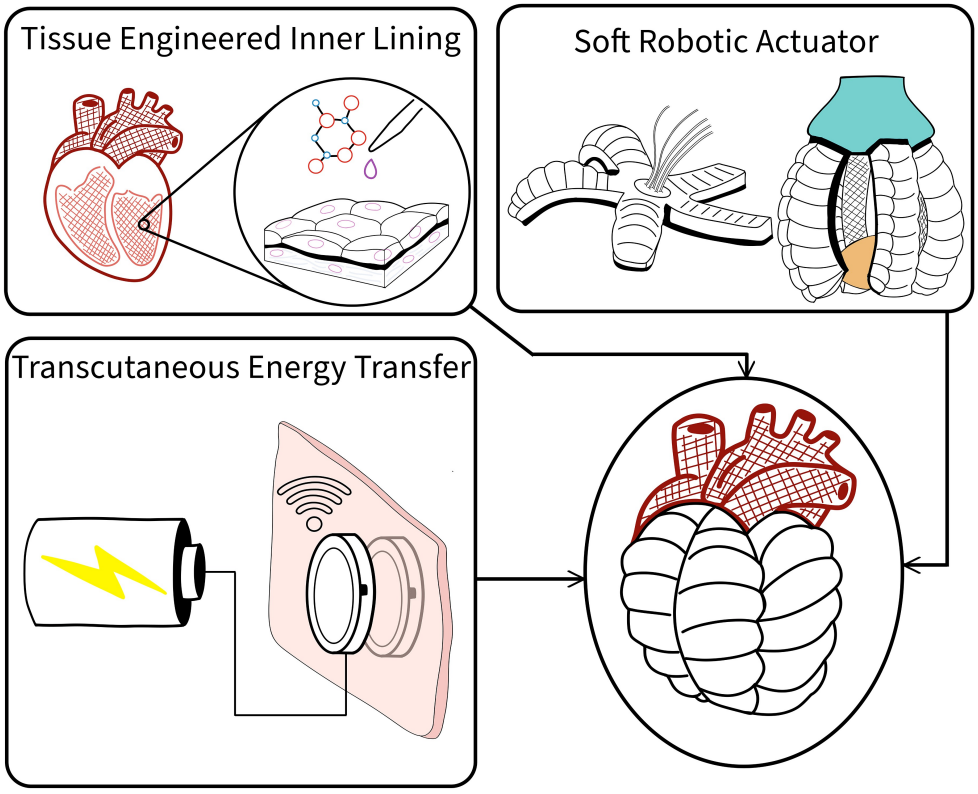

Figure 6.1 | The future of TAHs. A TAH made of soft robotic actuators and biocompatible materials with tissue engineered inner lining, powered by a transcutaneous energy transfer system.

Together, these findings support a forecasted vision for the next generation of TAHs: a fully implantable soft robotic artificial heart driven by energy-efficient actuation, powered by wireless transcutaneous energy transfer, and lined with tissue-engineered, biofunctional surfaces (Figure 6.1). Such a system would not only replicate cardiac motion, but also adapt to physiological demands and integrate biologically with the host. It must be emphasized, however, that this vision is not yet realized. Numerous challenges remain; from long-term durability and control optimization to full-scale clinical validation. Yet, this thesis offers a tangible blueprint and technological foundation for pursuing that future-one in which soft robotics and regenerative materials converge to create artificial hearts that are not just machines, but responsive, body-integrated systems capable of transforming end-stage heart failure treatment.

6.4. Limitations and Challenges

While this thesis presents promising advances toward the development of a soft robotic TAH, several limitations and challenges remain, underscoring the early-stage nature of

the proposed technologies and the considerable work required for clinical translation.

1. Long-term durability and material selection

Both Chapter 4 and Chapter 5 rely on rapid prototyping techniques and non medical-grade materials (e.g., TPU-coated nylon), chosen for their ease of use and affordability in early design iterations. While suitable for proof-of-concept experiments, these materials are not optimized for the mechanical fatigue resistance, chemical stability, and long-term durability required for chronic implantation. Future efforts must focus on identifying and validating biocompatible, fatigue-resistant materials that can withstand millions of actuation cycles over several years of continuous use without performance degradation.

2. Lack of biocompatibility and hemocompatibility testing

Neither the LIMO heart nor the Hybrid Heart prototypes presented in this thesis were fabricated from clinically approved or hemocompatible materials. Although the Hybrid Heart introduces the concept of a tissue-engineered, endothelializable inner lining, experimental validation of this feature remains limited. Critical studies such as long-term in vivo hemocompatibility, thrombus formation risk, and immune response are essential before the concept can be considered viable for clinical translation.

3. Limitations of actuation systems and control

In both studies, pneumatic actuation was used due to its simplicity in experimental setups. However, compressed air is not a feasible long-term solution for implantable devices due to safety concerns, lack of precise control, and performance limitations caused by air compressibility—especially at high heart rates. Transitioning to hydraulic actuation is a necessary next step to enable volume-controlled pumping, greater responsiveness to physiological changes, and safer chronic use. Additionally, further refinement is needed to develop compact, implantable control and feedback systems that can maintain adaptive performance across variable circulatory demands.

4. Incomplete implantability and system integration

Although the core pumping mechanisms were validated in vitro, neither system has yet achieved full integration into a self-contained, fully implantable unit. The electronics, energy transfer components, and fluidic systems remain external or loosely coupled. Key system-level challenges include miniaturizing the actuation hardware, integrating TET systems, and packaging components within a volume suitable for implantation in the thoracic cavity without compromising performance or safety.

5. Limited physiological testing and system-level evaluation

The mock circulatory loops used in this thesis were sufficient for initial functional assessment but lacked the sophistication to replicate a wide range of hemodynamic conditions, particularly in disease states or during rapid changes in preload and afterload. Additionally, while some in vivo testing was initiated in Chapter 5, the studies remain limited in scope and duration. Comprehensive long-term animal studies in anatomically relevant models will be critical to validate device performance under physiological conditions, assess biological integration, and ensure systemic safety.

6. Anatomical fit and soft-tissue interaction

Given the deformable nature of the Hybrid Heart, further studies are needed to understand its mechanical interaction with surrounding organs post-implantation. Optimizations in anatomical geometry, compliance matching, and physical constraints will be necessary to ensure proper fit, avoid compression of adjacent structures, and maintain consistent positioning during cardiac cycles.

6.5. Future Directions

Building on the foundational work presented in this thesis, several key pathways emerge for future research and development. Advancing the concept of a soft robotic total artificial heart toward clinical application will require a multidisciplinary effort across biomechanics, materials science, robotics, physiology, and translational medicine. The following directions outline priority areas that can significantly accelerate the Hybrid Hearts evolution into a viable, long-term solution for patients with end-stage heart failure.

1. Toward Fully Implantable, Energy-Efficient Architectures

A critical milestone in artificial heart development is achieving full implantability. This involves the integration of compact, energy-efficient actuation systems (e.g., hydraulic drives) with onboard electronics and wireless power transfer technologies. The actuation method must not only deliver adequate flow and pressure, but also do so with minimal power consumption, enabling downsizing of both the power unit and internal components like batteries and heat management systems. Ongoing efforts must focus on improving overall energy efficiency, including actuator output per watt and minimizing fluidic losses in the system. A more efficient design would also allow the use of smaller TET coils and enable more flexible anatomical placement, further improving implantability and patient comfort.

2. Dynamic Hemodynamic Control

The heart is a dynamic organ that constantly adapts to the body's metabolic demands during various physiological states, such as rest, exercise, or stress. Therefore, future iterations should incorporate both passive and active control mechanisms to allow for real-time adaptation of stroke volume, heart rate, and pressure output without relying solely on external sensors or complex feedback systems. Strategies such as geometry-based preload sensitivity (as demonstrated in the Frank-Starling behavior of the Hybrid Heart) could be paired with selectively tunable compliance or integrated low-power control electronics for more nuanced modulation of output. This hybrid control model would enhance physiological responsiveness while maintaining simplicity and robustness.

3. Anatomical Design Optimization and Valve Alignment

As the developed device advances toward preclinical and clinical stages, compliance with anatomical constraints will become increasingly critical. Future designs must be tailored to fit within the confined geometry of the thoracic cavity, considering not only overall device size but also the spatial arrangement and orientation of key features such as inlet/outlet ports and valve mechanisms. Misalignment of valves can lead to abnormal flow trajectories, turbulence, and stagnation zones, increasing the risk of thrombosis and hemolysis. Additionally, asymmetrical shapes or poor fit may cause mechanical interference with surrounding organs and hinder surgical placement.

4. Advanced Computational Modeling and Geometric Optimization

The design of soft robotic hearts presents complex challenges in fluidstructure interaction and nonlinear material behavior. The use of finite element modeling (FEM) and computational fluid dynamics (CFD) should be expanded to simulate wall deformation, stress distribution, flow path streamlining, and energy transfer under varied physiological loading conditions. Specifically, optimization of pouch geometry, actuation sequence, and chamber compliance will be vital to achieving stable, thrombosis-resistant flow patterns with minimal energy loss. Coupling these simulations with experimental validation will help refine both mechanical efficiency and biocompatibility.

5. Transition to Medical-Grade and durable Materials

While the prototypes developed in this work used accessible and rapidly manufacturable materials (e.g., TPU-coated nylon), long-term implantable systems will require biocompatible, medical-grade materials with proven fatigue resistance, hemocompatibility, and sterilizability. Future studies must explore materials such as medical-grade silicones, polyurethanes, or composite laminates, as well as fabrication techniques compatible with regulatory standards for implantable devices. Additionally, scalable and repeatable manufacturing processes—such as laser welding, overmolding, or 3D printing with biocompatible materialsshould be investigated to facilitate preclinical testing and eventual clinical translation.

6. Engineering of Inner Lining for Long-Term Biocompatibility

The inner blood-contacting surfaces must be optimized not only for thrombogenic resistance but also for long-term biological integration. The next phase of development should focus on refining and testing tissue-engineered linings that promote endothelializationthe formation of a native-like endothelial cell layer. This can be achieved through the use of supramolecular polymer coatings, bioactive surface functionalization, and materials that support autologous cell adhesion and growth. Achieving a stable, living endothelium on the device surface could substantially reduce the need for lifelong anticoagulation and mitigate thromboembolic risks, offering a true leap in hemocompatibility.

7. Chronic Large Animal Studies and Long-Term Validation

To transition from proof-of-concept to clinical relevance, it is essential to develop and test a fully integrated and implantable prototype in chronic large animal models. These studies should assess device performance under clinically realistic hemodynamic conditions over extended periods, monitoring parameters such as biocompatibility, flow dynamics, tissue response, and structural durability. Furthermore, actuation should shift from pneumatic to hydraulic or volume-controlled systems to reflect the conditions of a practical implant. These long-term studies are a prerequisite for regulatory approval and form the foundation for eventual first-in-human trials.

A

Appendix: Supplemental Information to Chapter 4

Based on: **M .Arfaee**, L. C. van Laake, S. Zou, C. Bording, J. Kluin, J. T. B. Overvelde, Toward developing a compact total artificial heart using a soft robotic fluidic transmission system.Sci.Adv.11,eadv4854(2025).

A

Supplementary materials

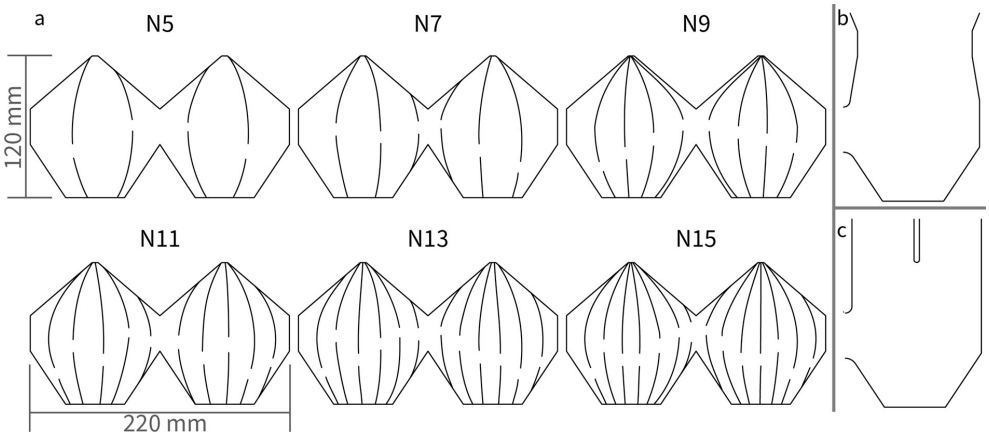

Figure A.1 | 2D pattern of pouches of LIMO ventricles. a) 2D heat-sealing pattern of pouches of the artificial ventricles with different number of channels, ranging from 5 to 15. b) 2D heat-sealing pattern of the second sealing step to create a single-opening ventricle. c) 2D heat-sealing pattern of dual-opening ventricle.

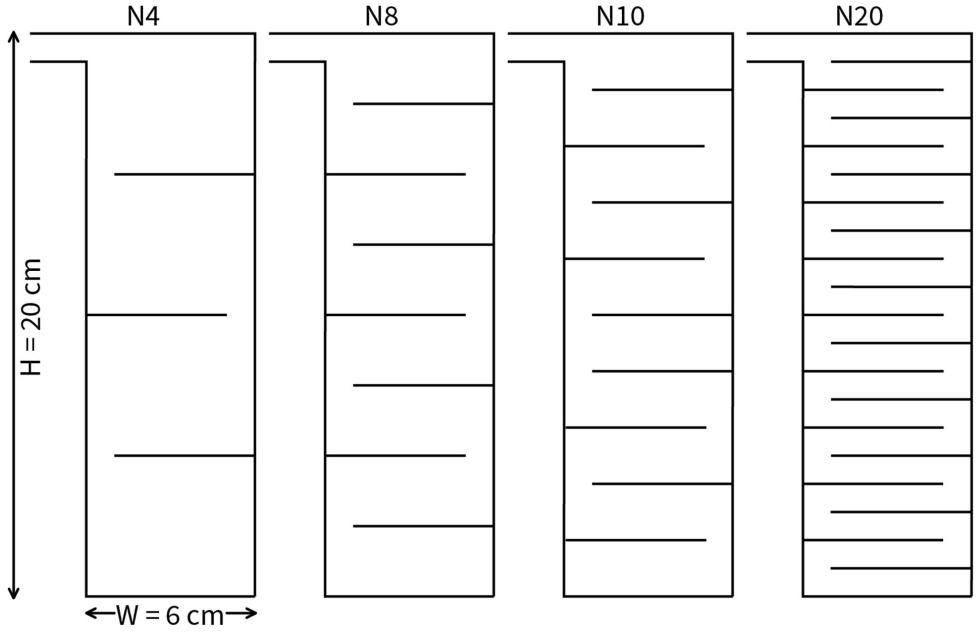

Figure A.2 | 2D pattern of pouch arrays. These patterns are used for heat-sealing and creating pouch motor samples.

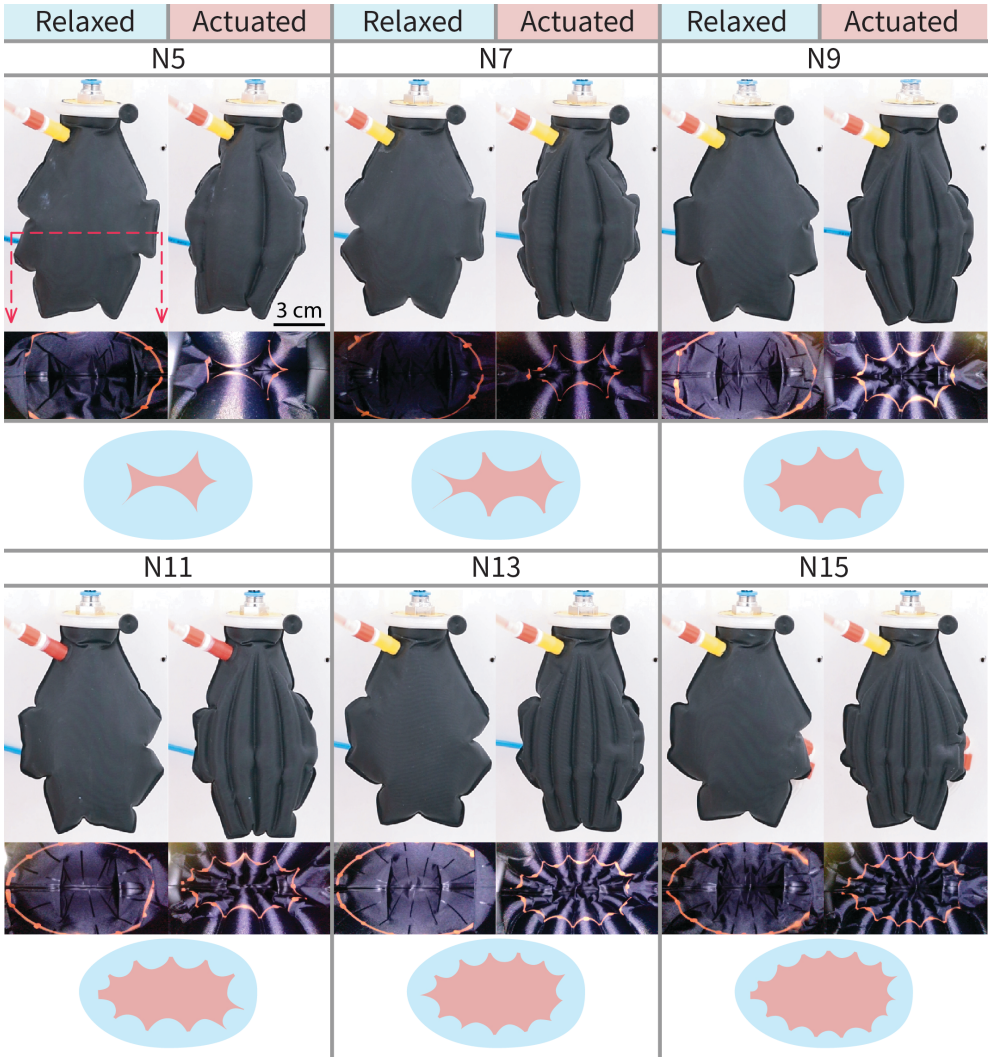

Figure A.3 | Relaxed and actuated states of prototypes with different number of pouches. Demonstrating the difference in intraventricular deformation resulting in various fluidic transmission ratios i and ejection fractions EF. Intraventricular deformations are shown at maximum actuator pressure of P_A = 40 kPa against identical internal pressure of P_C = 10 kPa; light blue: inner surface area at relaxed state, light red: inner surface area at actuated state.

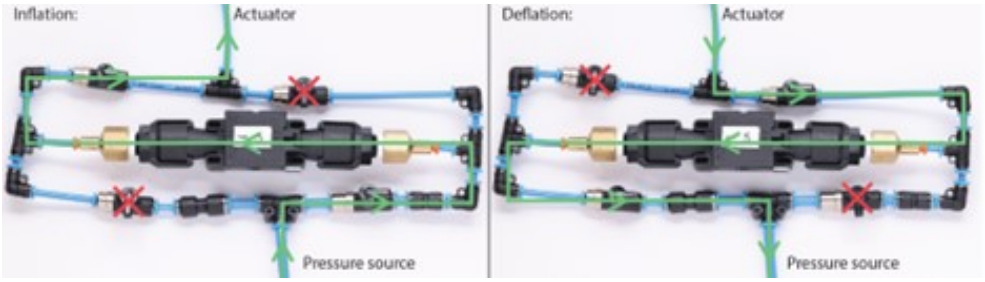

Figure A.4 | Volume change measurement. Mass flow sensor circuit configuration at inflation and deflation phase.

A.1. In vitro quasi-static characterization against physiological afterloads

Figure A.5 shows the test results of the artificial ventricles with 9 pouches and 11 pouches, respectively. The input work is calculated by equation (4), which corresponds to the area under the pressure-volume curves of the pouch actuator (Figure A.5.a, A.5.d). The output work is calculated by equation (5), which corresponds to the area under the pressure-volume curves of the ventricle (Figure A.5.b, A.5.e). The mechanical efficiencies of N9 and

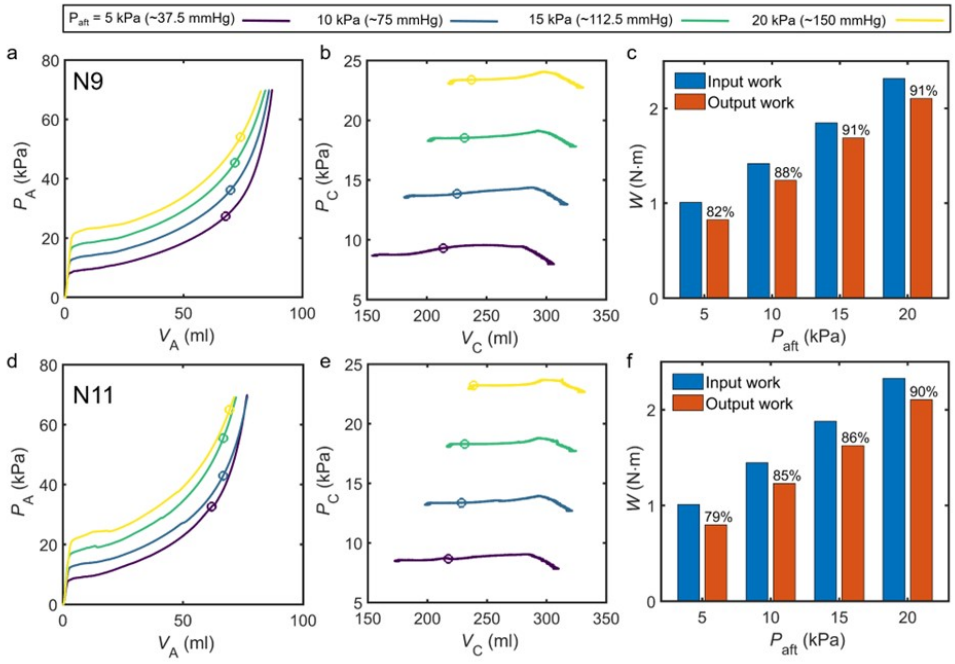

Figure A.5 | Volume change measurement. Mass flow sensor circuit configuration at inflation and deflation phase.

Table A.1 | Dynamic test condition. Set and actual beat rate per minute (BPM), and the maximum pressure reached against each condition.

Beating rate (BPM)		Maximum pouch actuator pressure (kPa)	
~Set	~Actual	Pulmonary (set to 50 kPa)	Aortic (set to 70 kPa)
50	46	50.2	71.7
60	55	48.6	67.9
70	61	46.6	61.9
80	69	42.7	63
90	75	38.8	56
100	91	31.8	46.4

N11 ventricle are calculated by equation (6) at various afterloads (Figure A.5.c, A.5.f). Both N9 and N11 ventricles show higher mechanical efficiency with increasing afterloads. The N9 ventricle shows slightly higher efficiencies than the N11 ventricle. Note that the rise and fall in the pressure-volume curves of the ventricle in figure A.5.b and e are due to the flow resistance present in the experimental setup.

Figure A.6 | The single-sided mock circulatory loop. The setup used for testing the dynamic performance of the N9 prototype.

A.2. Analytical model, effect of seam width and number of pouches

Our simplified analytical model assumes an initial cylindrical shape of the ventricle with internal volume V_0, and N pouches of length L_0, equally distributed around the perime-

ter and separated by seams of width s. Since the material is assumed to be inextensible, the pouch opening angle $0 \leq \theta \leq \pi/2$ fully describes the systems deformed shape. Here, we expand on the key results described in the main text, equations (1)–(3) and figure 4.1. Specifically, we provide analytical expressions for the fluidic transmission ratio i and ejection fraction EF at full actuation ($\theta = \pi/2$),

$$i_{\theta=\pi/2} = \frac{2NS_L - 2N + \frac{N\pi^2}{2} - S_L\pi^2 + \pi^2 - 2\pi NS_L + \frac{NS_L\pi^2}{2}}{2\pi^2(1-S_L)} \tag{A.1}$$

$$\mathrm{EF}_{\theta=\pi/2} = \frac{2(1-s_L)\left(2Ns_L - 2N + \frac{N\pi^2}{2} - s_L\pi^2 + \pi^2 - 2\pi Ns_L + \frac{Ns_L\pi^2}{2}\right)}{N\pi^2} \times 100\% \tag{A.2}$$

where we define dimensionless seam width $s_L = s/(s+L_0)$, $0 \leq s_L \leq 1$.

These expressions are further simplified when we assume seam width is negligeable ($s_L = 0$),

$$i_{\theta=\pi/2,s_L=0} = \frac{\frac{N\pi^2}{2} - 2N + \pi^2}{2\pi^2}, \tag{A.3}$$

$$\mathrm{EF}_{\theta=\pi/2,s_L=0} = \frac{2\left(\frac{N\pi^2}{2} - 2N + \pi^2\right)}{N\pi^2} \times 100\%, \tag{A.4}$$

from which we arrive at the conclusions about i and EF that we present in the main text,

$$\lim_{N\to\infty} i_{\theta=\pi/2,s_L=0} = \infty, \tag{A.5}$$

$$\lim_{N\to\infty} \mathrm{EF}_{\theta=\pi/2,s_L=0} = \left(1 - \frac{4}{\pi^2}\right) \times 100\% \tag{A.6}$$

We illustrate the modeled behavior in figure A.7. For non-negligible seam width, as s_L increases, seam width s increases at the expense of pouch length L_0. Interestingly, selecting relatively wider seams increases i (and decreases EF), as does increasing the number of pouches N (Figure A.7.a, A.7.b). However, the asymptotic behavior differs significantly. Ever wider seams ultimately result in a fully passive ventricle, such that the ejection fraction vanishes (Figure A.7.c). In contrast, for negligeable seam width, increasing the number of pouches results in a linear increase of the fluidic transmission ratio i, while the ejection fraction EF approaches 59.5% (Figure A.7.d).

A.3. Blocked-displacement testing of pouch arrays

In these experiments, samples N4, N8, and N10 broke before reaching the maximum set pressure of 400 kPa, at respectively 159.5, 249.9, and 241.3 kPa (P_{max}). The samples generated maximum force (F_{max}) of 319.7, 310.2, and 270.1 N, respectively. Sample N20 did not fail and could generate the maximum force of 208.3 N at an actuator pressure of 398 kPa (Table. A.2). As predicted, by increasing the number of the pouches, i.e., by reducing the size of the individual pouches, the pressure required to reach a certain force increases

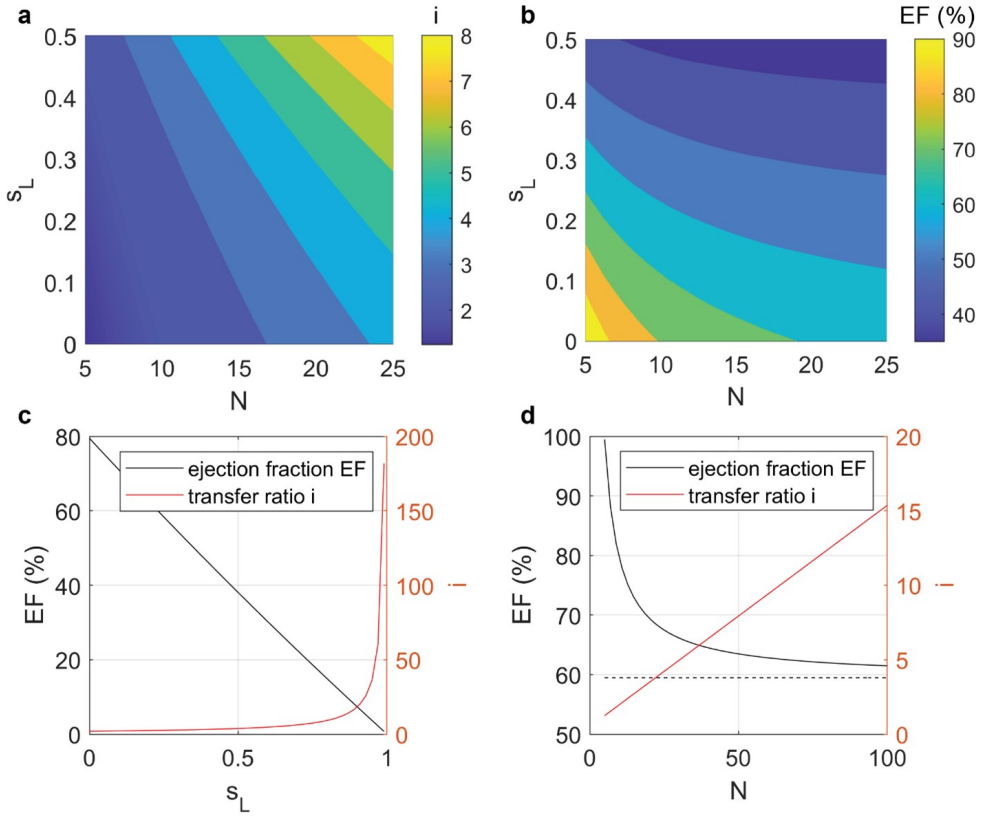

Figure A.7 | Idealized model-based effect of number of pouches N and dimensionless seam width s_L. a) Effect on fluidic transmission ratio i. b) Effect on ejection fraction (EF). c) Effect of s_L for $N = 10$. d) Effect of N for $s_L = 0.01$, dashed line indicates asymptotic value EF = 59.5%.

while the geometric volume reduces. We observed a general trend where smaller pouches typically withstand higher pressures than larger pouches (Figure A.8). However, among samples with relatively minor differences in pouch size, imperfections caused by our heat-sealing technique could cause failure points that deviate slightly from this trend, as all samples ruptured near the sealing lines.

A.4. Fully soft prototype utilizing 3D-printed prosthetic valves as inlet and outlet

Although mechanical heart valve prostheses are reliable and being used as a therapy for heart valve treatments, they require lifelong management with anticoagulants and regular follow-up to monitor for complications that mainly concern their biocompatibility [294]. In this study, we used mechanical heart valve prostheses in our LIMO heart as a practical and repeatable solution suitable for in vitro trials. To show the feasibility of making a fully soft LIMO heart, we made a prototype by employing two 3D-printed prosthetic valves for inlet and outlet (Figure A.9.a). The valves have an inner diameter of 30 millimeter and

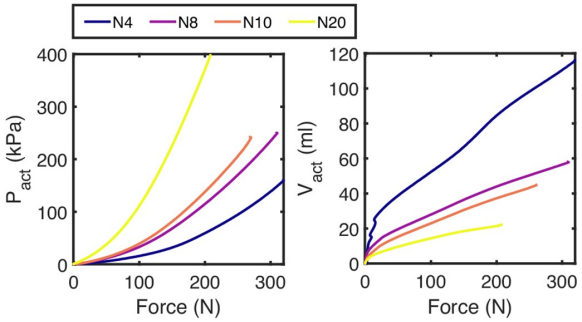

Figure A.8 | Force response of pouch arrays with 4, 8, 10, and 20 pouches. Left: Force-Actuator pressure ($F - P_{act}$). Right: Force-Actuator volume ($F - V_{act}$).

Table A.2 | Pressure, volume and generated force of each pouch array just before failure.

Sample	P_{max} before failure (kPa)	V_{max} before failure (mL)	F_{max} before failure (N)
N4	159.5	116	319.7
N8	249.9	57.9	310.2
N10	224.2	45.1	261.6
N20*	398.8	22.2	208.3

*N20 did not fail, and survived the whole experiment.

coaptation height of 5 millimeters to avoid any back flow [295]. They are printed from thermoplastic polyurethane (TPU) shore 60A filament using a FDM 3D-printer (TEC4, FELIX, IJsselstein, the Netherlands). For this prototype, we fabricated the ventricle using the sealing pattern shown in figure A.1.c. It has two openings that hold inlet and outlet valves. Interestingly, this prototype could deliver maximum cardiac output CO = 8.8 l/min at 81 BPM against pulmonary condition (35/9 mmHg). However, it failed working against aortic condition (Figure S9.b). The rupture happened at the bottom of U-shape sealing path that separates the inlet and outlet (Figure A.1.c, A.9.c) that indicates the high stress concentration at that point. It should be noted that the sealing lines are more generally weak points of the samples, as the sheets are heated up to 275 °C and compressed. A full summary of stroke volume and cardiac output of both models against aortic and pulmonary settings at various beating rates is presented in table A.3. Using a single housing for both inlet and outlet valves seems to constrain the ventricle, leading to a reduction in SV resulting in 1.2 l/min reduction in total cardiac output. Future studies need to be performed to optimize the design to maximize the cardiac output as well as improving durability by reducing stress concentrations.

A.5. Life-time evaluation of current LIMO heart prototype

Each sample tested in the mock circulation loop (MCL) under short-term dynamic conditions was able to operate for approximately 1500−2000 cycles before failure. However, since the experiments were not conducted continuously, this does not provide a realis-

Table A.3 | In vitro results of N9 LIMO ventricle in dynamic test bench. Stroke volume (SV) and cardiac output (CO) of LIMO heart and fully soft LIMO heart against pulmonary and aortic conditions at various beating rates (HR).

		HR (BPM)	SV (mL)	CO (l/min)
Mechanical heart valves	Pulmonary	46	130.3	6
		55	127.5	7
		62	115.4	7.2
		69	103.9	7.2
		76	100.6	7.6
		91	70	6.4
	Aortic	45	94.5	4.3
		55	92.3	5.1
		61	91.9	5.6
		70	84.8	5.9
		76	75.3	5.7
		91	50.5	4.6
Soft valve	Pulmonary	46	135.6	6.3
		55	130.6	7.2
		64	124.9	8.1
		73	113.7	8.3
		81	108.6	8.8
		91	89	8.1

Figure A.9 | Fully soft prototype. a) Inlet and outlet valves 3D-printed from TPU. b) Placement of the valves in two separate openings. c) Rupture at the bottom of the U-shaped sealing line that separates the inlet and outlet valves.

tic estimate of the actual lifetime, as fatigue effects are largely overlooked in short-term testing. To assess the durability of our current fabrication method and prototypes and identify areas for future improvement, we conducted fatigue testing on the prototype with nine pouches (N9), made from TPU-coated nylon (Riverseal 70, 78Dtex, 70 g/mš, Rivertex, Culemborg, The Netherlands). The prototype underwent cyclic testing in the MCL at 60 BPM against mean afterload of 20 mmHg. Failure in this sample began after approximately 800 cycles (~13 minutes), evidenced by the appearance of air bubbles moving from the ventricle to the afterload chamber in the MCL. The failure point is indicated in figures A.10.a and A.10.b. Following this, a slight reduction in maximum actuator pressure was observed (Figure A.10.a), along with alterations in the afterload peak and minimum values, likely due to changes in flow dynamics and air leakage into the circuit.

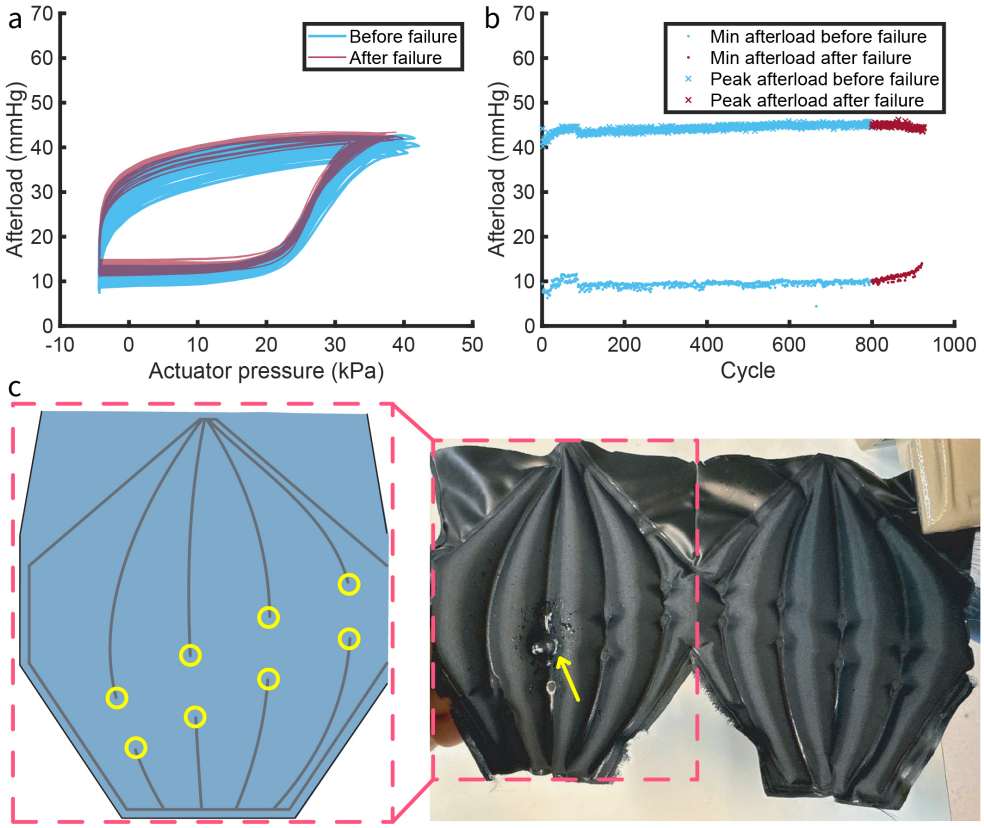

Figure A.10 | Results of fatigue experiments on N9 prototype. a) Change of actuator pressure and afterload after failure. b) Afterload peak and minimum values before and after failure. c) Points along the sealing line where the prototype is prone to tearing. We manually opened the ventricle after the fatigue experiment to observe the failure point on the inside of the ventricle.

The failure was caused by a small tear in the TPU layer near the sealing line (Figure A.10.c), which allowed air to leak through nylon layer into the water stream. We consistently observed that among all the samples, tested during our study, a tear is occurring where the sealing line ends near the gaps for air channels as indicated in figure A.10.c, suggesting a critical weak point. These findings indicate that, even with the current fabrication method, durability can be improved by eliminating gaps in the sealing lines and using individual air valves for each pouch to avoid stress concentrations at vulnerable points.

B

Appendix: Supplemental Information to Chapter 5

Based on: **M. Arfaee***, A. Vis*, P.A.A. Bartels, L.C.V. Laake, L. Lorenzon, D.M. Ibrahim, D. Zrinscak, A.I.P.M. Smits, A. Henseler, M. Cianchetti, P.Y.W. Dankers, C.V.C. Bouten, J.T.B. Overvelde, J. Kluin, *A soft robotic total artificial Hybrid Heart.* Nat Commun 16, 5146 (2025). (* contributed equally)

Supplementary materials

B.1. Hybrid Heart Prototype Fabrication

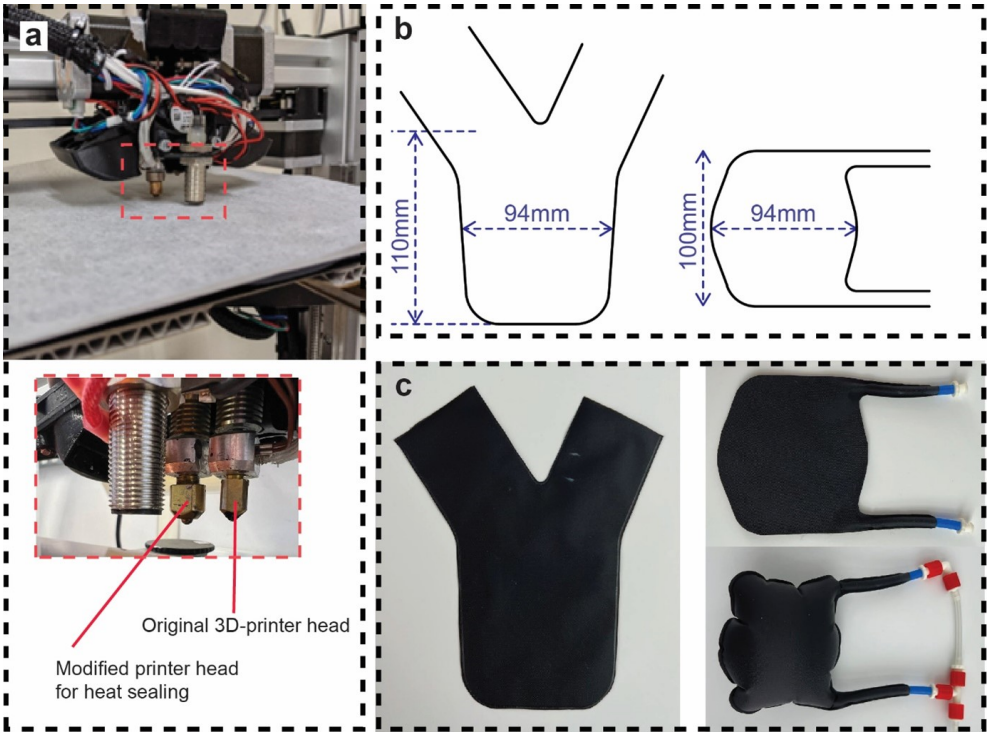

Figure B.1 | Fabrication of TPU-coated nylon ventricles and septum by means of heat sealing. a) A conventional 3D printer was modified by replacing the original 3D printer head by a modified head for heat sealing. b) 2D Patterns of the ventricle and the septum, used to heat seal TPU-coated nylon sheets together. c) On left, a TPU-coated nylon ventricle that was heat sealed in the desired shape. It has two channels for inlet and outlet. On right, a TPU-coated nylon septum that was heat sealed in the desired shape. It has two inlet/outlets for inflation and deflation. The deflated state is shown on top and the inflated state on bottom.

Each part of Hybrid Heart prototypes are made of two layers. The inner layer of the septum and ventricles is made by heat sealing two layers of TPU-coated nylon. We used this material and technique to make air and water sealed chambers for, respectively septum and ventricles. (See figure B.1) The outer layer of septum and ventricles is made by sewing polyester fabrics in the same shape as inner layer. The outer layer consists several tunnels to guide wires and keep them in place along the length of the septum and ventricles. The TPU-coated nylon inner layers within the ventricles and septum are inserted into the polyester fabric housing and then sewn together. Two mechanical heart valve prostheses (Sorin Bicarbon, Sorin Group, Milan, Italy) are positioned at the outlets of each ventricle. The septum also has two outlets and is linked to a pneumatic system (Festo, Esslingen am Neckar, Germany). We employed fishing line (100% Fluorocarbon, 0.46mm, SavagaGear, Gadstrup, Denmark) as driving wires around septum and ventricles, threading it through tunnels on the fabric's outer layer. A metal clamp was used to fasten both ends of each

wire. To mount the prototype to the mock circulatory loop, we used a 3D-printed PLA interface for each outlet, which on one side holds the valve prosthesis and the other side goes into the tube coming from the mock circulatory loop. A silicone ring around this part helps to make it water sealed. Figure B.2 shows a schematic of all components and their arrangement.

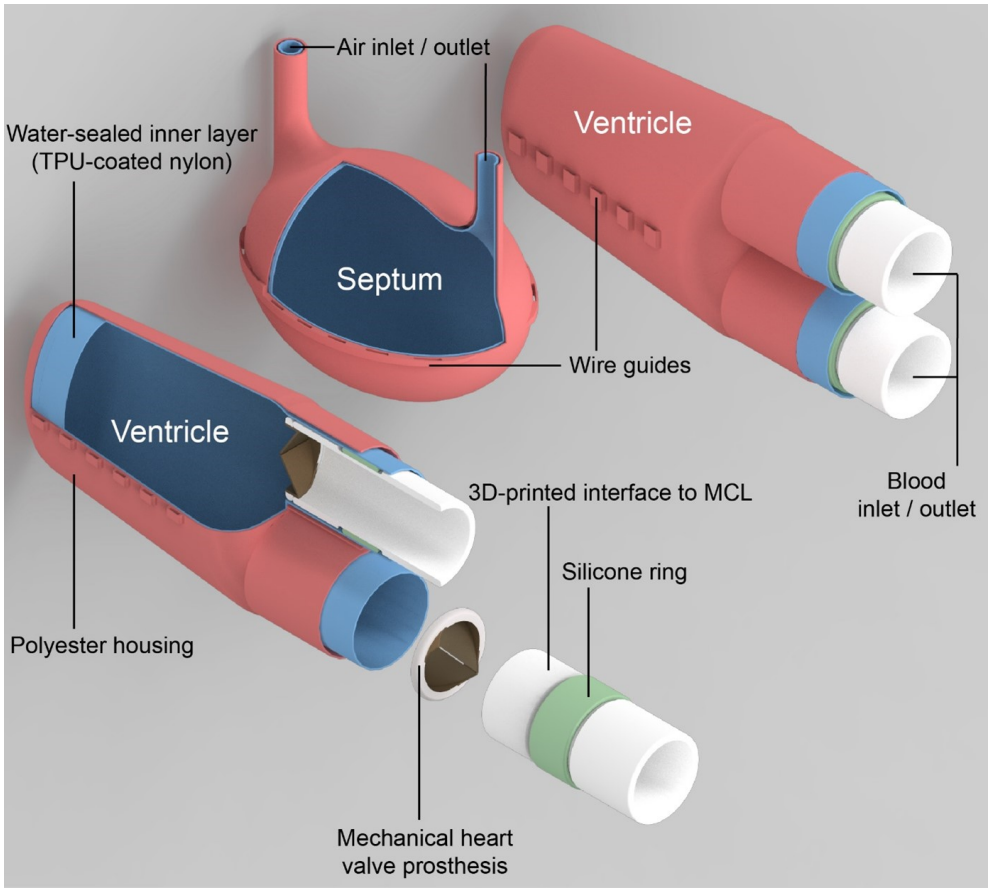

Figure B.2 | Exploded view of the schematic 3D model of the Hybrid Heart. The ventricles and septum has made of two thin layers. Inner layer is made of TPU-coated nylon to be air/water-sealed. Outer layer is made of polyester fabric to keep the wires in place. Two mechanical heart valve prostheses are incorporated in each ventricle as inlet and outlet valves.

B.2. Quasi-static characterization of the Hybrid Heart using a pneumatic ventricle load

To measure the complete mechanical characteristics of the Hybrid Heart, we need to monitor the volumes and pressures of its three chambers (the septum, left ventricle, and right ventricle) at the same time, at various conditions. We vary the conditions by quasi-statically actuating the septum, either by controlling septum pressure, or by controlling

septum volume, while we keep the ventricles at predetermined pressures (see Methods).

B.2.1. Septum pressure control

In a first experiment, we pressurize the left and right ventricle, each to its individual set point pressure. Then we cycle septum pressure between 0 and 80 kPa, while monitoring all pressures and volumes. Pressures are regulated using three individual pressure controllers (VEAB-L-26-D13-Q4-V1-1R1, Festo).

Figures B.3 and B.4 show the sample in different stages of the test for different ventricle pressures. Figure B.5 shows the measured pressure and volume response of the septum in this experiment. The panels in figure B.5 are showing results for different combinations of ventricle loads.

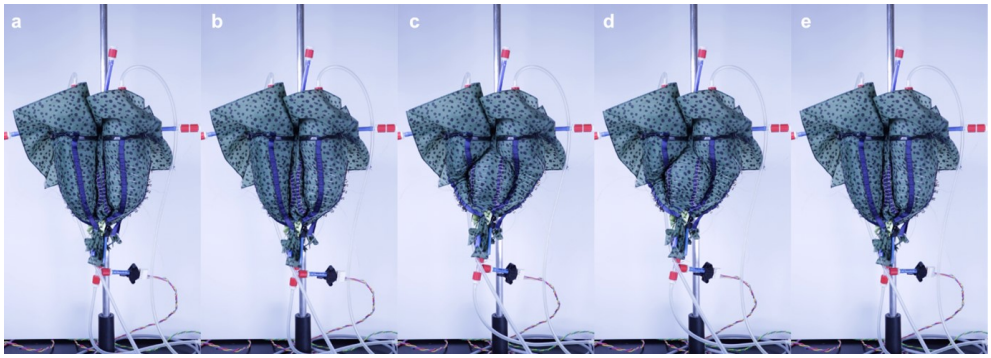

Figure B.3 | Quasi-static pressure-controlled experiment on a Hybrid Heart prototype, p_L= 23 mmHg, p_R= 75 mmHg. Photographs are taken a) after ventricle pressurization, before septum pressurization (p_s=0 kPa); b) at a intermediate septum pressure (p_s=40 kPa); c) at maximum septum pressure (p_s=80 kPa); d) at an intermidate pressure during deflation of the septum (p_s=20kPa); e) at the end of one complete cycle (p_s=0 kPa).

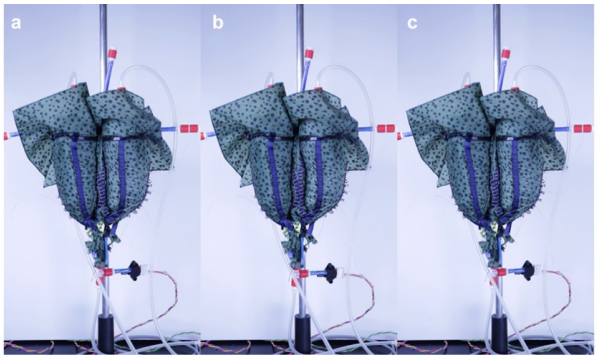

Figure B.4 | Quasi-static pressure-controlled experiment on a Hybrid Heart prototype, p_L= 105 mmHg, p_R= 75 mmHg. Photographs are taken a) after ventricle pressurization, before septum pressurization (p_s=0 kPa); b) at maximum septum pressure (p_s=80 kPa); c) at the end of one complete cycle (p_s=0 kPa).

Firstly, we conclude that the effect of ventricle load is additive, i.e., that the response for different combinations of ventricles loads that add up to the same sum are comparable.

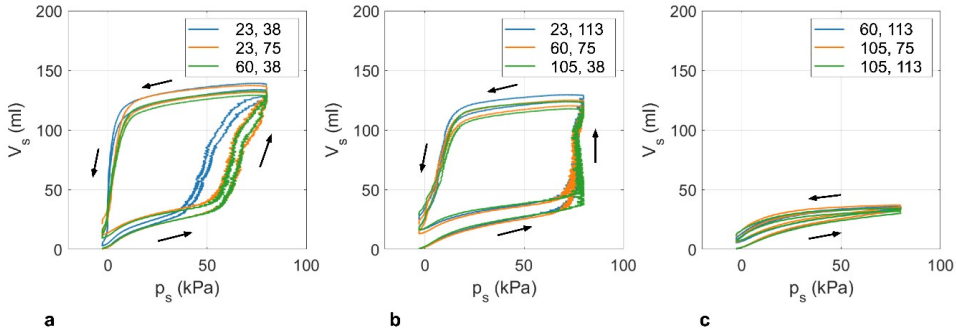

Figure B.5 | Quasi-static pressure-controlled experiment on a Hybrid Heart prototype. Geometric septum volume V_S as a function of septum pressure p_S for various pressures in the left (p_L) and right (p_R) ventricles. a) p_L+p_R=60 or 98 mmHg, b) p_L+p_R=135 or 143 mmHg, c) p_L+p_R=173, 180 or 218 mmHg.

This can be seen for example from the orange and green curves in figure B.4.a, and the orange and blue lines in figure B.4.b.

Secondly, and even more importantly, there is a striking hysteresis in the pressure-volume behavior of the septum. As pressure increases, initially there is limited increase in the septum volume. Then, at a pressure value that depends on the sum of the ventricle loads, there is a sudden increase in septum volume (and, not shown here for clarity, an associated decrease in ventricle volumes). Similarly, upon depressurization the septum volume remains almost constant at its maximum volume, until there is a sudden deflation at a (very) low septum pressure. Moreover, for high enough pressures in the ventricles ($p_L + p_R \geq 173$ mmHg) there is no expansion of the septum even at the maximum septum pressure (80 kPa in this experiment). This behavior is indicative of a mechanical instability.

B.2.2. Septum volume control

To better understand the hysteresis loop that we observed in the pressure-controlled experiment, we perform a volume-controlled follow-up experiment. Instead of a pressure controller, we now attach a mass flow controller (SLA5850, Brooks Instrument, Hatfield, Pennsylvania, USA) to the septum and quasi-statically inflate the septum, while all other connections and sensors remain the same. Figure B.6 shows the results for different ventricle pressure loads. Here, we apply identical loads to both ventricles, as we observed that the cumulative pressure is most important to determine the load needed to be applied by the septum. The results conclusively show that there is indeed an instability in the system, which can be seen from the portion of the pressure-volume relation that has a negative slope, i.e., where for increasing volume, the pressure decreases. When controlling the pressure input to the septum, these results show that when reaching the critical peak the instability would result in a sudden large change in volume, as also observed in the pressure control experiments. While there is likely still some friction between the wires and the septum and the ventricles that could result in some hysteresis, the main hysteresis in the system originates from the geometrical design of the Hybrid Heart.

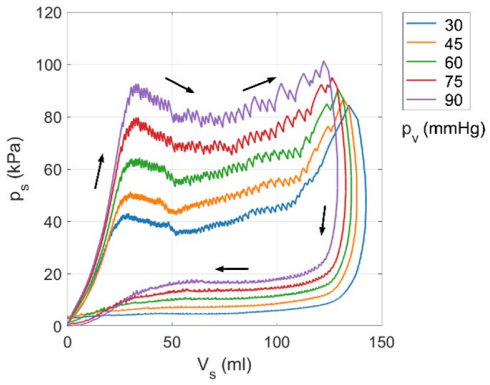

Figure B.6 | Quasi-static volume-controlled experiment on a Hybrid Heart prototype. Septum pressure p_s as a function of geometric septum volume V_s for various pressures in the ventricles (equal in left and right ventricle). Legend shows (equal) pressure applied to the left and right ventricles.

B.2.3. Analytical model of the Hybrid Heart

To understand why there is an instability in the Hybrid Heart, and how this can be the result of the geometrical design, we create an idealized analytical description. We assume that both the ventricles and the septum can be modeled as perfect cylinders, with instantaneous radius r_v and r_s, respectively, and constant height H. Figure B.7 shows a simplified model of the Hybrid Heart in the initial (a) and a deformed state (b). Note that the model is not meant to perfectly describe the quantitative behavior of the Hybrid Heart, but is implemented to understand the origin of the instability that occurs in the Hybrid Heart.

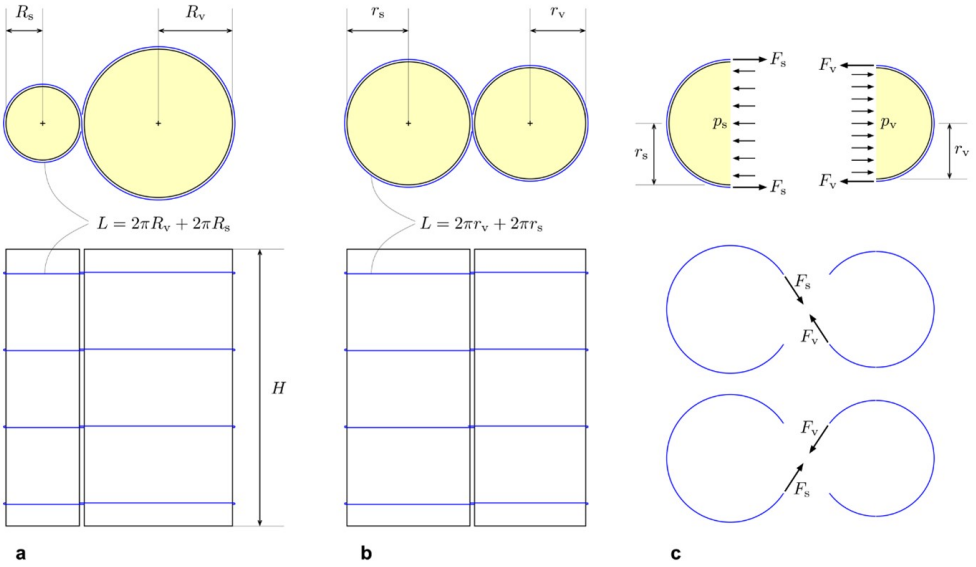

Figure B.7 | Analytical model of Hybrid Heart. a) Initial state, b) deformed state. c) Force balance. Top: balance between wire tension and septum (left) and ventricle (right) pressure. Bottom: force balance in wires.

To construct the model, we first consider the septum and a single ventricle. The initial radii of the ventricle and septum are given by R_v and R_s, respectively, such that the initial length L of the wires wrapped around the ventricle and septum in a figure eight is given by

$$L = 2\pi R_\mathrm{v} + 2\pi R_\mathrm{s}. \tag{B.1}$$

We assume that the wires are inextensible, such that we have the following constraint for the deformed state

$$L = 2\pi r_\mathrm{v} + 2\pi r_\mathrm{s}, \tag{B.2}$$

where r_v and r_s are the radii of the deformed state of the ventricle and septum, respectively. As a result, we have that

$$R_\mathrm{v} + R_\mathrm{s} = r_\mathrm{v} + r_\mathrm{s} \implies r_\mathrm{v} = R_\mathrm{v} + R_\mathrm{s} - r_\mathrm{s} \tag{B.3}$$

We next define the instantaneous transmission ratio α as an infinitesimal volume dV_v pushed out of the ventricle, with respect to an infinitesimal dV_s pumped into the septum. To determine α, first we take the derivative of volumes with respect to the radii:

$$V_v = \pi r_v^2 H, \tag{B.4}$$

$$\frac{dV_v}{dr_v} = 2\pi H r_v, \tag{B.5}$$

$$V_s = \pi r_s^2 H, \tag{B.6}$$

$$\frac{dV_s}{dr_s} = 2\pi H r_s. \tag{B.7}$$

Then we calculate the instantaneous transmission ratio

$$\alpha = -\frac{dV_v}{dV_s} = -\left(\frac{dV_v dr_s}{dr_v dV_s}\right)\left(\frac{dr_v}{dr_s}\right) = -\left(\frac{r_v}{r_s}\right)\left(\frac{dr_v}{dr_s}\right). \tag{B.8}$$

Using the previously derived expression for r_v, we find that

$$\frac{dr_v}{dr_s} = -1. \tag{B.9}$$

Therefore, we can conclude that the instantaneous transmission ratio is simply equal to the instantaneous ratio of the radii

$$\alpha = \frac{r_v}{r_s}. \tag{B.10}$$

Note that that the transmission ratio is not constant, but depends on the deformed state. Next, we define θ as the pressure ratio between ventricle and septum for which the system is in equilibrium.

$$\theta = \frac{p_v}{p_s}. \tag{B.11}$$

where p_v and p_s are pressures with respect to atmospheric pressure. To determine the pressure ratio θ, we first write tensile forces in the wires as a function of pressure for the ventricle $F_v(p_V)$, and the septum $F_s(p_s)$.

$$2r_s p_s H = 2F_s H,\ 2r_v p_v H = 2F_v H. \tag{B.12}$$

If we assume for simplicity of the model that friction is negligible, equilibrium is given by

$$F_s = F_v, \tag{B.13}$$

which results in

$$\theta = \frac{p_v}{p_s} = \frac{r_s}{r_v} = \frac{1}{\alpha}. \tag{B.14}$$

We can equivalently write α and θ using the square root of the ratio of volumes, which is more convenient for the analysis of the pressure-volume relation

$$\alpha = \sqrt{\frac{V_v}{V_s}}, \quad \theta = \sqrt{\frac{V_s}{V_v}}. \tag{B.15}$$

To show the results obtained by our simplified analytical model, in Figure B.7.a we show α and θ as a function of septum volume, for geometrical parameters approximately representing the Hybrid Heart prototype. Note that the volume in the septum and ventricle vary by as much as a factor 10 as the deformation progresses from the minimum septum volume (maximum ventricle volume) to the maximum septum volume (minimum ventricle volume). In Figure B.7.b we show the corresponding radii. Note that due to the inextensible wire, the sum of the radii remains constant.

B.2.4. Septum and (single) ventricle PVR

These results enable us to determine the equilibrium pressure ratio, i.e., the equilibrium pressure in the ventricle as a fraction of the septum pressure, and vice versa, for different instantaneous deformation states, i.e., for different combinations of V_s and V_v. By our assumption of inextensibility of the wires, r_s and r_v (and thus also V_s and V_v) are geometrically constrained, such that for any septum radius (or volume), we know the corresponding ventricle radius (or volume), and vice versa. In other words, we can now write the pressure-volume relations of the ventricle and septum as function of the septum pressure, and vice versa.

However, this relation no longer holds if the ventricle or the septum reach their as-produced size, since they are also made of inextensible material, like the wires. If the ventricle reaches this maximum size, the ventricle starts acting as a rigid container. In that case, the force balance in the wire no longer holds and the pressures cannot be related as previously derived. Instead, for incompressible medium (water, blood), the ventricle volume will be fixed at $V_{\mathrm{v,max}}$ for any pressure above atmospheric. For compressible medium (e.g., air), even though the geometrical volume is fixed, we can define a pressure-volume relation in terms of the standard or pressure-equivalent volume $V_{\mathrm{v,PE}}$, i.e., the volume the medium would have if it were at atmospheric pressure

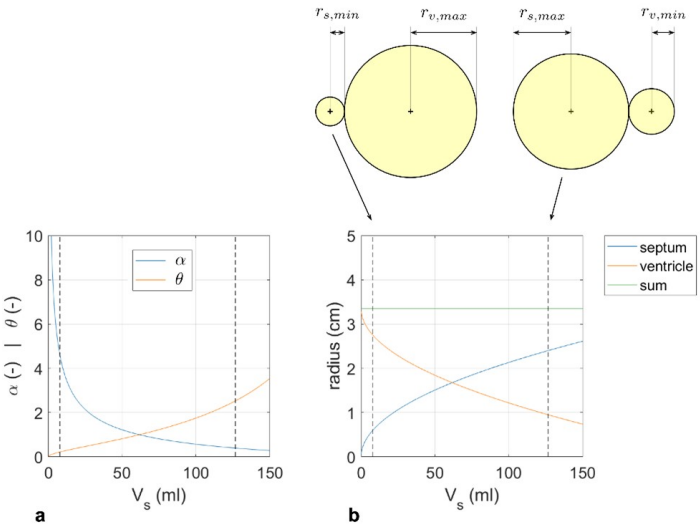

Figure B.8 | Resulsts analytical model of Hybrid Heart. a) α and θ as a function of septum volume V_s, b) radii as a function of septum volume V_s. Top shows sections of septum and ventricle (to scale) in initial and fully deformed states. $H = 7$ cm, r_s,min=0.6 cm, r_s,max=2.4 cm, r_v,min=0.95 cm, r_v,max=2.75 cm

$$p_v = \frac{V_{v,PE} p_0}{V_{v,max}} - p_0, \tag{B.16}$$

where we use atmospheric pressure as the reference pressure p_0.

We assume that in the initial state, the ventricle is fully inflated, i.e., that it is at its maximum volume $V_{v,\max}$. Therefore, its maximum volume is identical to its initial volume

$$V_{v,\max} = H\pi(r_{v,\max})^2 = \pi R_v^2 \tag{B.17}$$

Conversely, if the septum reaches its maximum volume, while the ventricle pressure is above atmospheric, but below the equilibrium pressure, the ventricle will act as a rigid container having its minimum volume, where the *minimum* volume is

$$V_{v,\min} = H\pi(\frac{L}{2\pi} - r_{s,\max})^2. \tag{B.18}$$

In that case volume is fixed at $V_{v,\min}$ for an incompressible medium, while for compressible medium we define the pressure volume relation as

$$V_{s,\max} = H\pi(r_{s,\max})^2, \quad r_{s,\max} < R_s. \tag{B.19}$$

B.2.5. Two (identical) ventricles

Based on the findings we obtained in the pressure-controlled septum inflation experiment (Figure B.3), and the fact that the effect of ventricle pressure on the septum is additive, we can expand this model to represent two ventricles by placing the two ventricles in parallel

to the same septum. The septum pressure is simply the sum of the pressure contributions from each of the ventricles. Therefore, the septum pressure equals

$$p_s = \frac{p_L}{\theta_L} + \frac{p_R}{\theta_R} = p_L\sqrt{\frac{V_L}{V_s}} + p_R\sqrt{\frac{V_R}{V_s}}, \tag{B.20}$$

where subscripts L and R refer to left and right ventricle, respectively. The pressures in the individual ventricles are

$$p_L = \theta_L p_s = p_s\sqrt{\frac{V_s}{V_L}}, \quad p_R = \theta_R p_s = p_s\sqrt{\frac{V_s}{V_R}} \tag{B.21}$$

Note that the volume of one ventricle determines the volume of the septum, while the septum volume sets the volume of the other ventricle, such that in this model, the ventricles always have identical volumes, as long as pressures are above atmospheric. Therefore, the left and right equilibrium pressure-volume relations are identical.

Based on these assumptions, and by taking geometrical parameters that are comparable to the prototype, we can determine the equilibrium ventricle pressure-volume relation for different septum pressures. Equivalently, we can determine the equilibrium septum pressure-volume relation for different cumulative ventricle pressures. We show the pressure-volume relation of the idealized system for a single ventricle, and for the septum, in figure B.8.

We can clearly see in all pressure-volume relation curves a region with negative slope, similar to what we observed in experiments. As in the model friction was assumed to be negligible, the instability and hysteresis observed in experiments must be the result of the mechanical behavior that originates from the design of the Hybrid Heart. The observed instability can thus be explained from the unstable part of the pressure-volume relation intrinsic to this system.

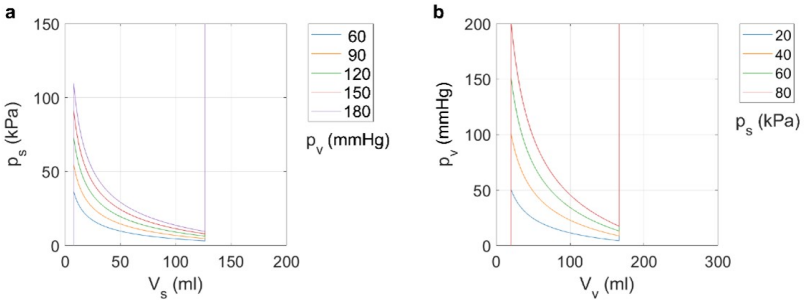

Figure B.9 | Results analytical model of Hybrid Heart. a) (geometrical) septum PVR. b) (geometrical) ventricle PVR. $H = 7$ cm, r_{S},min=0.6 cm, r_{S},max=2.4 cm, r_{V},min=0.95 cm, r_{V},max=2.75 cm

B.3. Mock circulatory loop setup and test results

B.3.1. Influence of wire arrangements on ventricular outputs in double mock circulatory loop

We have studied the influence of wire arrangements on the ventricular outputs during various tests in the double circulatory mock loop. Due to the challenging hemodynamic conditions of the systemic circulation versus pulmonary circulation (high left afterloads compared to low right afterloads), it is more difficult to obtain high stroke volumes for the left artificial ventricle. In addition, the bronchopulmonary shunt flow causes increased venous return to the left atrium compared to the right. Due to both factors, ideally, the left ventricular stroke volume should be larger than the right ventricular stroke volume. The Hybrid Heart prototype, as described in the main text, has similar sized ventricles. We aimed to decrease right stroke volume compared to the left volume by changing the wire length of the right ventricle. We used a full-fill/partially-eject compensation mode to obtain lower right stroke volumes. We have tested three prototypes, that we intended to be exact copies of each other. First, we have tested these prototypes with similar wire configurations, and similar wire length for both ventricles. Each ventricle had 5 wires in parallel, spaced apart with similar distances. We tested these prototypes in the double circulatory mock loop under physiological conditions, where we noticed that the measured stroke volumes varied per prototype (Table B.1). The left stroke volumes were 76 ml, 68 ml and 91 ml respectively for the three prototypes and the right stroke volumes were 84 ml, 76 ml and 125 ml respectively. It should be noted that all prototypes were fabricated by hand, which likely explains the performance differences. Furthermore, it should be noted that with similar wire configurations for the left and right ventricle, all three prototypes had larger right ventricular outputs compared to the left. We tried to reduce the right sided stroke volumes by loosening the wires of the right ventricle. This would result in complete filling of the right ventricle, and reduced ejection. We found that with loosening the wires, we could successfully decrease the right sided stroke volume to 79, 66 and 83 ml respectively (Table B.1). Interestingly, by loosening the wires of the right ventricle, the stroke volume of the left ventricle increased in all cases, 79, 84 and 95 ml respectively (Table B.1).

Similar configuration left and right ventricles						
	SV L ml	**SV R ml**	**CO L L/min**	**CO R L/min**	**Aft L mmHg**	**Aft R mmHg**
HH v1	76	84	4.5	5.0	98	30
HH v2	68	76	4.1	4.6	85	32
HH v3	91	125	5.5	7.5	100	27
Loosening wires of the right ventricle						
	SV L ml	**SV R ml**	**CO L L/min**	**CO R L/min**	**Aft L mmHg**	**Aft R mmHg**
HH v1	79	79	4.7	4.7	100	27
HH v2	84	66	5.0	3.9	89	26
HH v3	95	83	5.7	5.0	105	20

Table B.1 | The effect of wire arrangement on stroke volumes. HH: Hybrid Heart. V: version. SV: stroke volume. L: left. R: right. CO: cardiac output. Aft: mean afterload

B.3.2. Influence of beating rate on left cardiac output using pneumatic actuation system

In order to assess the pneumatic actuation system of our test bench, we tested the Hybrid Heart at beating rates of 30 to 100 BPM in steps of 10. During the experiment, both systemic and pulmonary resistance were kept constant, and Both preloads were set to 5 mmHg. The maximum pressure, reached in the septum was set to 80 kPa. We observed that the highest SV of 91.7 ± 0.3 was obtained at 30 BPM, yet cardiac output (2.75 L/min) was still quite low (Figure B.10). Increasing heart rate resulted in a decline in SV, while the cardiac output increased to 4.7 L/min at 70 BPM, after which it dropped to 4 L/min at 100 BPM. This shows that with current actuation system of our test bench, we can achieve the optimal performance at the heart rates of 60-80 BPM, and we are limited at the highest achievable beating rate while maintaining enough cardiac output.

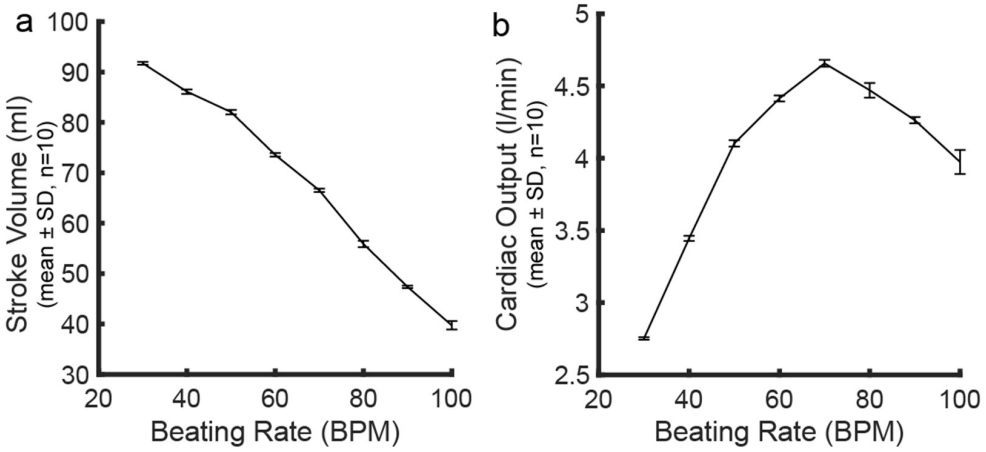

Figure B.10 | Effect of beating rate on left ventricular output. a) Left stroke volume measured at beating rates ranging from 30 to 100 BPM. b) Corresponding left cardiac output across the same range of beating rates. Data is presented as mean values ± SD of n = 10 cycles.

B.4. 4D flow MRI measurements

The biomimetic motion of the Hybrid Heart during relaxation and contraction was assessed by means of 4D flow magnetic resonance imaging (Philips Medical Systems, Best, the Netherlands with a 32-channel matrix head coil). Cardiac gating was performed using a simulation ECG set to 30 bpm. Velocity encoding (VENC) was set to 100 cm/s. Valvular flow was visualized and quantified using semi-automated retrospective valve tracking including automatic phase off- set correction through CAAS MR Solutions 4D Flow (Pie Medical Imaging BV, Maastricht, the Netherlands). Valve tracking was performed on 2D cine steady-state free precession (SSFP) images. To enable MRI scanning, we used plastic pinch valves as resistors to mimic the systemic vascular resistance and the pulmonary vascular resistance in the MRI compatible mock circulatory loop. We replaced all four mechanical heart valves of the Hybrid Heart prototype with bioresorbable Xeltis polymer

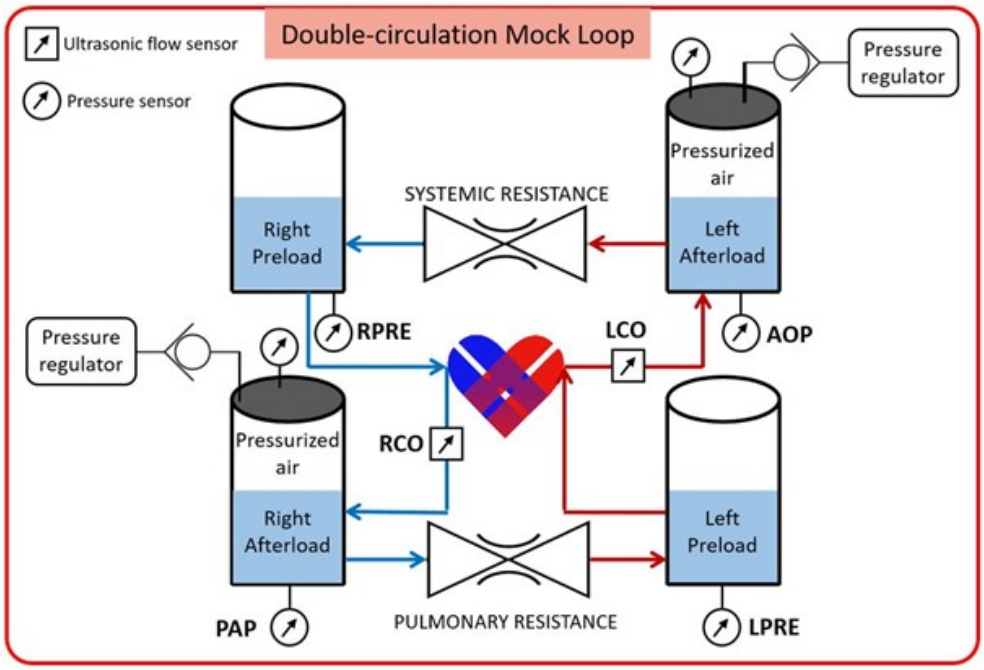

Figure B.11 | Mock circulation loop schematic. RPRE: right preload, RCO: right cardiac output, PAP: pulmonary artery pressure, LCO: left cardiac output, AOP: aortic pressure, LPRE: left preload

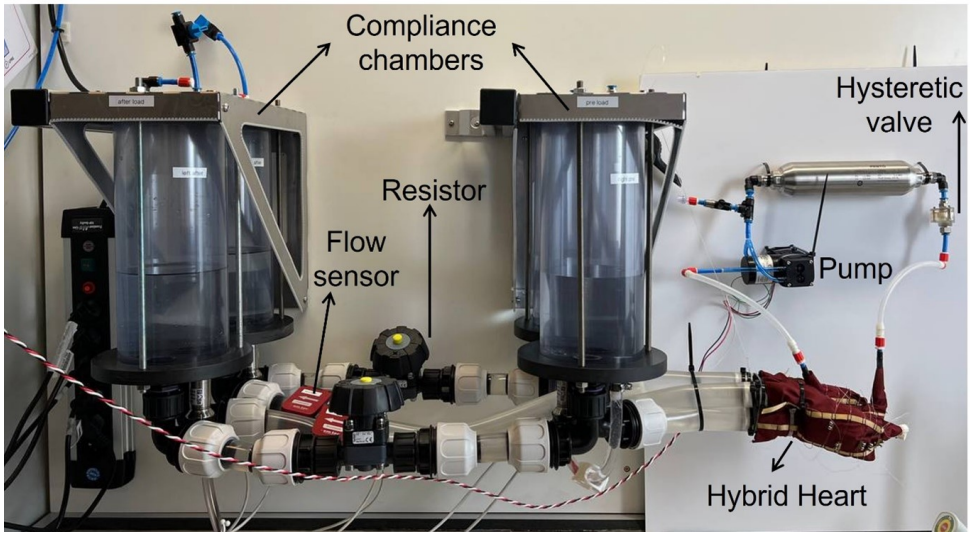

Figure B.12 | The Hybrid Heart in the mock circulation loop. The Hybrid Heart is actuated with closed-loop circuit including an air pump, and the hysteretic valve.

valved conduits (Xeltis pulmonary valveXPV, Eindhoven, the Netherlands).

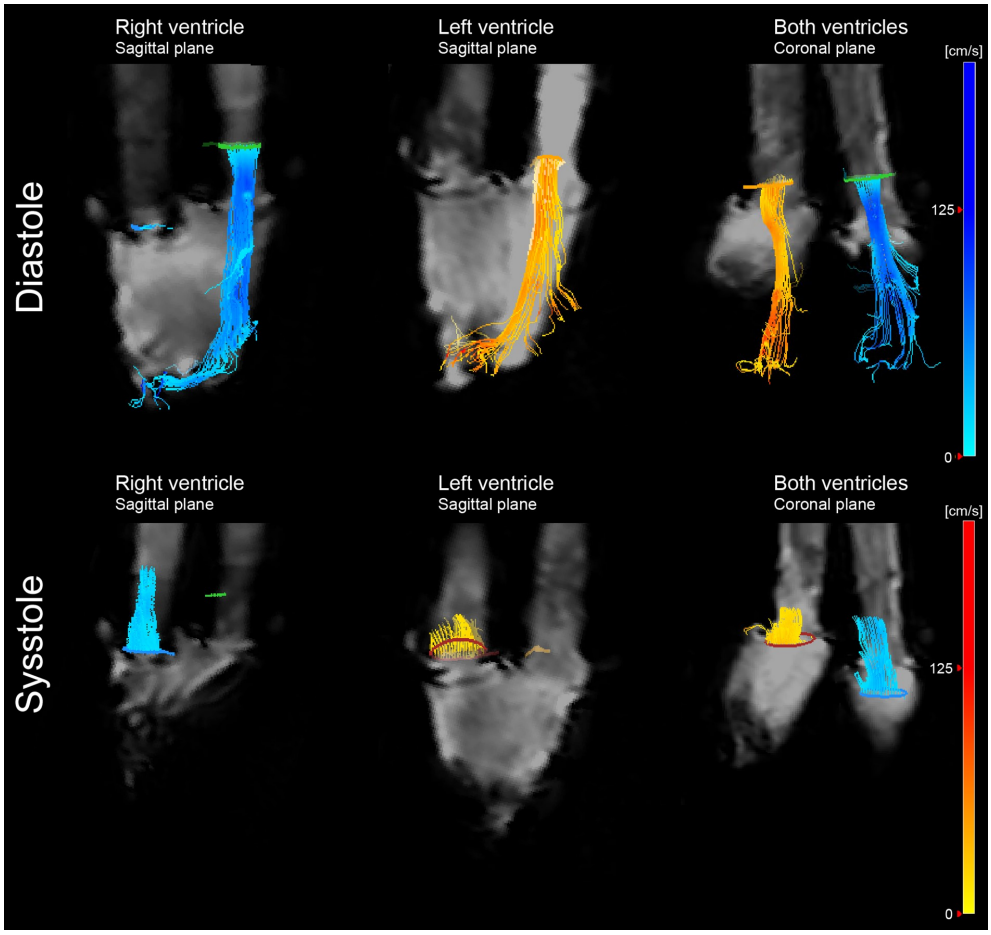

Figure B.13 | Hybrid Heart during 4D flow MRI measurements. Blue color depicts flow in the right ventricle, orange color depicts flow in the left ventricle. Laminar flow is observed during the filling and ejecting phases of both ventricles.

B.5. Hybrid Heart for in vivo implantation

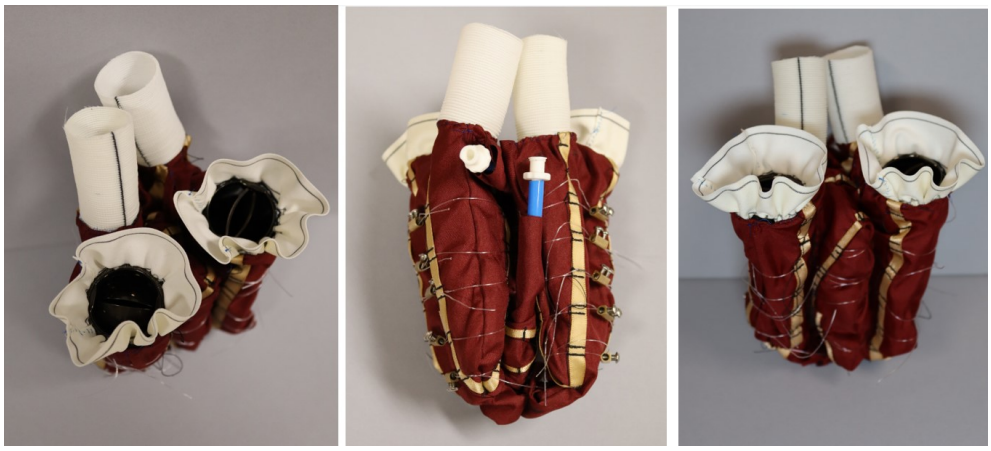

Figure B.14 | The Hybrid Heart prepration for in vivo implantation. In this prototype, mechanical heart valves are sutured to the ventricular ports. GORE-TEX grafts are attached to each valve to facilitate connection to the arteries and atria.

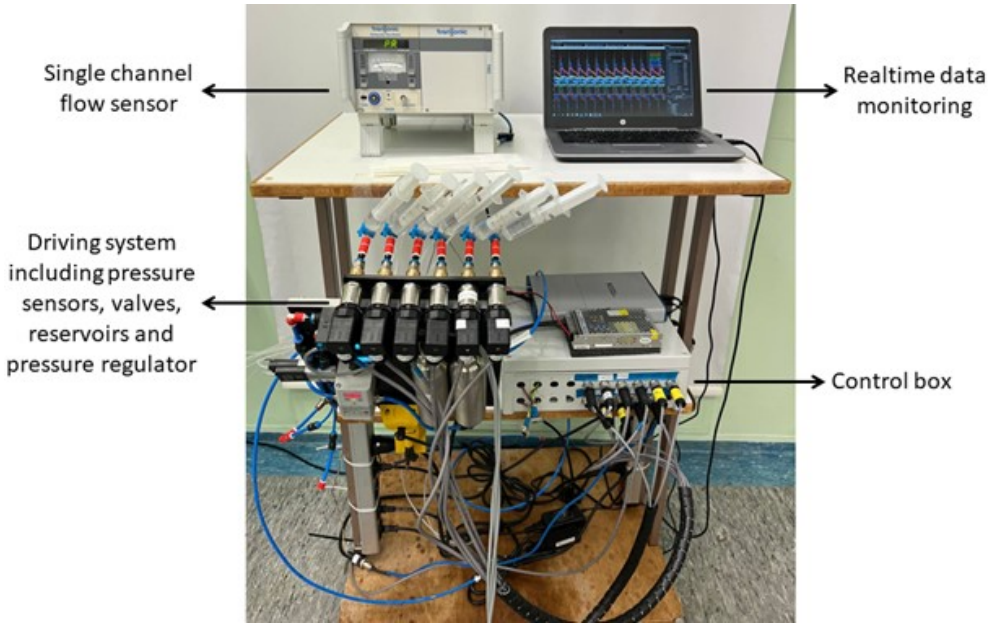

Figure B.15 | The control system used in the operation room to run the Hybrid Heart and collect data. It includes pressure and flow sensors, driving system and data acquisition units.

B.6. Transcutaneous energy transfer system

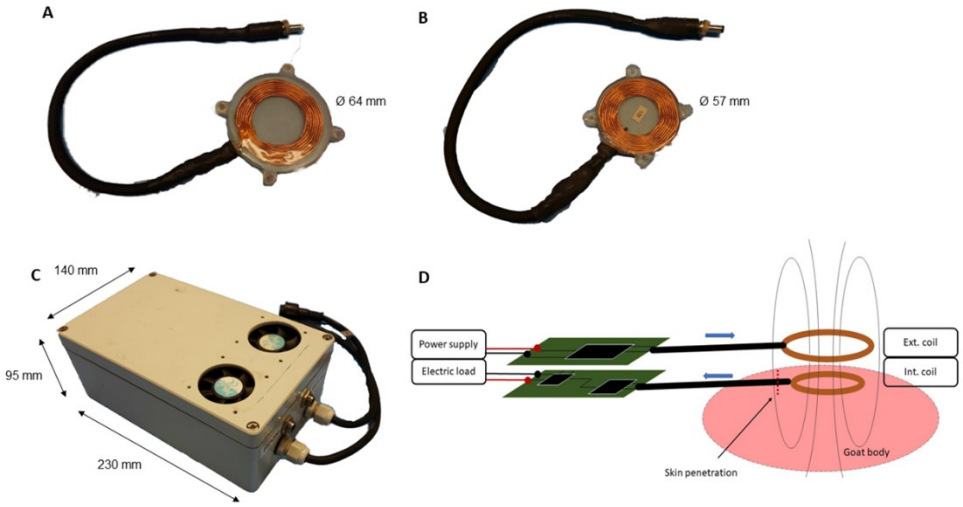

Figure B.16 | TET system overview. A) The external TET coil. B) The internal TET coil. C) The control box containing controllers for both coils and electric load. Fans are placed on top for temperature management. D) Schematic overview of the TET system after implantation. Power supply and electric load are put in the control box on the back of the goat. Power is transmitted from the external coil to the internal coil transcutaneous and goes to the electric load via a cable and skin incision.

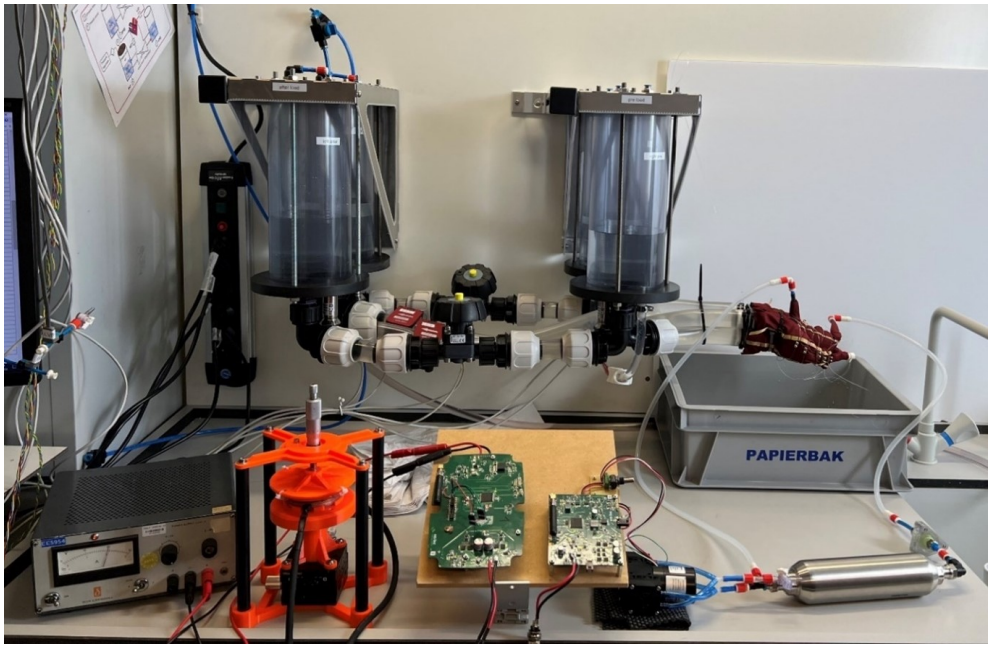

Figure B.17 | Integrating the TET system to evaluate the power transmition. The Hybrid Heart is driven using an air pump and a hysteretic valve in a close loop circuit, powered by a TET system.

B.7. Hemocompatibility assessment of TPU-coated nylon vascular grafts with heparin-functionalized supramolecular coatings in a rat aorta model

We expected that TPU-coated nylon itself would induce thrombus formation when in contact with blood and would therefore need functionalization of its surface to create an anti-thrombogenic layer. To this end, we used supramolecular polymeric systems as a coating, because these materials allow for the incorporation of functional additives, such as peptides or other ECM-derived molecules, through a mix-and-match approach [296–298]. The segmented block copolymer polycaprolactone bisurea (PCL-BU) (Figure 5.5.a, 5.5.b) is a supramolecular polymeric system that has been employed in various biomedical applications, including heart valves [215], vascular grafts [299–301], and cardiac patches [286]. We aimed to develop an anti-thrombogenic surface on the TPU-coated nylon through applying a PCL-BU coating that is functionalized with heparin (Figure 5.4.a). Heparin binds to antithrombin enhancing its inhibitory effect to both factor Xa and thrombin that are important factors in the coagulation pathway [302]. To bind heparin onto the materials, a heparin binding peptide [282, 303] was added to the system by coupling this to a bisurea linker (BU-HBP) (Figure 5.5.b) and then incorporating it into the bisurea stacks formed in the system.

We investigated whether the addition of BU-HBP and heparin to the PCL-BU based supramolecular coatings on the TPU-coated nylon would lead to fewer thrombotic incidents. To answer these research questions, we first studied the feasibility of applying

coatings to the TPU-coated nylon in vitro. Next, the thrombogenicity and cytotoxicity of the TPU-coated nylon with and without the various coatings were explored in vitro. The surface of the TPU-coated nylon was analyzed after coating with x-ray photoelectron spectroscopy to investigate the presence of the coating. The TPU-coated nylon materials were sutured into a vascular graft (Figure 5.5.a) before sterilization and subsequent use in the in vivo study. To this end, the vascular grafts made from TPU-coated nylon, with and without the different supramolecular coatings on the luminal side of the graft, were implanted as abdominal aortic interposition grafts in rats with a follow-up time of 24h (Figure 5.6.c). The patency of the graft after 24h was determined based on clinical presentation, and further evaluated by magnetic resonance imaging, scanning electron microscopy and histological analyses.

B.7.1. Feasibility of coating the TPU-coated nylon

The TPU-coated nylon was coated with PCL-BU through solution-casting. Comparing the surface atom composition, determined from XPS measurements, before and after coating revealed an increase in C and N atom percentages from 73 to 86.5 and 0.9 to 1.9 respectively, and a decrease in O atom percentage from 26.1 to 11.5 (Table B.3).

B.7.2. In vitro cytotoxicity and thrombogenicity

Cytotoxicity of the materials was assessed by a lactate dehydrogenase (LDH) release assay with human umbilical vascular endothelial cells (HUVEC). After 24 hours of HUVEC culture, no evidence of cytotoxicity was observed for either the nylon side or the TPU side of the TPU-coated nylon material. Similarly, no cytotoxic effects were detected when evaluating the cytotoxicity of the TPU-coated nylon coated with PCL-BU or with PCL-BU + BU-HBP (Figure 5.5.a). Thrombogenicity was investigated through incubating the materials with platelet-rich plasma for an hour, followed by assessing adsorption of platelets to the surface. On the TPU-coated nylon material with and without PCL-BU coating platelets readily adhered and spread, irrespective of heparin functionalization. Platelets were observed in all different stages of activation, from round to dendritic, to fully activated [304]. Less platelets were observed on the surfaces functionalized with the BU-HBP peptide. On the 5 mol% BU-HBP surface some platelets showed a different activation stage and spread morphology, but on the 20 mol% BU-HBP surfaces predominantly round platelets were observed. After heparin functionalization of these surfaces, no spreading of platelets was observed, while less platelets were present compared to before functionalization (Figure 5.5.f). Therefore, we selected 20 mol% BU-HBP to proceed with the in-vivo rat study, due to its optimal performance in binding heparin.

B.7.3. Surgery

Mean duration of the surgery was 2h11min (±13min) and mean clamp time was 50min (±3min). Two rats died during surgery. The first per-operative death occurred within 10 minutes after clamping the aorta, during implantation of the graft (graft type 1). There was no bleeding event, therefore we believe the rat died as a response to the anesthetics. The second rat died shortly after implant of graft type 4. This was the first graft implant that was treated with heparin, and after declamping the aorta a bleeding occurred that could not be stopped. After this incident, we rinsed all type 4 grafts with saline prior to

implantation. We replaced the two perioperative deaths by two new rats, using n=22 rats in total. The surgery was completed without complications for the other 20 implantations. For each group, n=5 rats survived the surgery.

B.7.4. Clinical assessment and explant

For graft type 1, two rats did not use their hind legs directly after surgery, which indicated immediate clotting of the graft. They were euthanized on the same day as the surgery. The three other rats were in good clinical condition with normal leg movement after surgery. On post-operative day (POD) 1, two of them did not use their hind legs at the next morning, which indicated complete graft occlusion. One rat remained in good clinical condition until the end of the follow up period (Figure 5.5.b, Table B.2). All five rats that received type 2 grafts did not use their hind legs after surgery, indicating immediate occluded grafts. All rats were euthanized on the day of surgery.

With grafts of type 3 one rat had an uncomplicated surgery but died during the recovery due to unclear reasons (graft 3.2). During explant no thrombus was seen in the graft. One other rat did not use its hind legs directly after surgery and was euthanized on the same day. Three of the rats were in good health on the day of surgery, but on the next morning one was found dead and another had immobile hind legs. One rat remained in good clinical condition, with normal leg movement until the end of the follow up period.

All rats with grafts of type 4 stayed in good health with normal leg movement on the same day of the surgery. However, two rats did not use their hind legs the next morning, indicating late graft occlusion. The other three rats stayed in good health with normal leg movement until the end of the follow up period.

At explant, large thrombi were found in occluded grafts (except for graft 3.2) that typically extended from the proximal to distal anastomosis. Even in patent grafts, small thrombi were often visible at the spot where the sheet was sutured together (Figure B.19).

B.7.5. Magnetic resonance angiography

The MRI analysis of the grafts measured (n=9) in animals revealed that three grafts were patent on POD1 (grafts 1.1, 3.1 and 4.5). This matched the clinically good state of all three animals that were using their hind legs normally. The other six MRI scans (three grafts taken from POD0: 1.5, 2.3 and 2.3, and three from POD1: 1.2, 3. and, 4.1) revealed that blood flow was absent distally from the renal branch. This matched the clinically poor state in which the animals were not using their hind legs in all six cases (Figure B.18, Table B.2). On MRI images of the three patent grafts, the transition of the native artery to the Gore-Tex strip was clearly seen due to a narrowed vessel diameter, both proximal as well as distal (Figure B.18). One open graft showed a small thrombotic region inside the graft, which was located proximally around 1/3rd of the graft length, that regionally caused a narrowed lumen (diameter of 0.4 mm) inside the graft (graft 4.5). It could not be determined if this thrombotic region was at the interface from the Gore-Tex to the coated TPU-coated nylon or in the coated TPU-coated nylon part. In the other two grafts (1.1 and 3.1) no blood flow obstructions were seen. In the patent grafts, the mean lumen diameter of the graft was 1.9 mm ± 0.1 mm, and the lumen of the proximal native aorta was 1.8 mm ± 0.3 mm (Table B.2).

B.7.6. Histology

All histological slices showed a thrombus in the lumen of the grafts except for two, graft 4.5 and 1.5. Most of the thrombi were located at the junction where the sheet was sutured together (Figures B.20, B.21). Only two thrombi were found at other locations. Graft 1.1 had a thin and elongated thrombus in the curvature of the lumen. Graft 4.3 had a round shaped thrombus in the middle of the lumen. All thrombi had a heterogeneous composition of red blood cells, fibrin and white blood cells. Thrombi in the grafts that were explanted within 1-3 hours after surgery were mainly composed of erythrocytes, but also some fibrin depositions were observed. Neutrophilic granulocytes infiltrated the erythrocyte sections but were not present inside the fibrin depositions in these early thrombi. Thrombi in grafts explanted after the 24 h follow-up period were composed of erythrocytes and larger fibrin areas compared to the grafts that were explanted at the day of surgery. The grafts that were explanted after 24 h showed more mature thrombi, with a mix of intact and degraded neutrophilic granulocytes present inside the fibrin regions (Figures B.20, B.21). On the H&E stained histological samples, no smooth muscle cells in the thrombi and no cell infiltration inside the graft material were observed. In group 1, the TPU layer could be clearly defined as a separate layer from the woven nylon fibers (Figures B.20, B.21). For all coated samples (group 2, 3 and 4), the TPU layer was not clearly distinguishable. Here, the supramolecular coating seemed to be fused with the TPU layer and formed one dense mass on top of the nylon fibers (Figures B.20, B.21).

B.7.7. Scanning electron microscopy

All grafts showed some clot formation composed of erythrocytes adhering to the material and clustering together (Figure B.20). In most of the grafts clearly fibrin could be observed, except for the grafts 1.1, 3.2, 3.3 and all grafts from type 4. In some grafts like 3.1 only some fibrin was observed, while in others like the grafts of type 2, a full plaque layer could be observed of interwoven fibrin and erythrocytes. Overall, no clear distinctions in number of adsorbed erythrocytes were found between the occluded grafts of the different conditions based on visual inspection. The patent grafts seemed to have less erythrocytes adsorbed to the material compared to the occluded grafts (Figure B.20). In the patent grafts from group 4 seemingly less erythrocytes were observed; especially on graft 4.5 barely any cells were found. However, it is hard to draw conclusions as only small sections from the grafts were analyzed and some of the clots may have fallen off before SEM imaging. Both of the materials that were explanted at the day of surgery, and the ones explanted at 24 h looked similar with SEM analysis. The SEM analysis also indicated that after the 24 h follow up there was no cell infiltration into the graft material, which was in line with the histology analysis. Most thrombi were located around the sutures, which could indicate that this is a point of origin for the clot formation. In some samples clusters of erythrocytes were found on the Gore-Tex material (Figures B.22, B.23).

B.7.8. Interpretation of the results

The results of this study indicate that a TPU-coated nylon small diameter vascular graft may benefit from a PCL-BU supramolecular coating functionalized with heparin to reduce its thrombogenicity. However, the variability within most groups in combination with the small number of animals used in this study complicated the ability to draw conclusions

on the thrombogenicity of the individual materials tested.

The functionalization with heparin of vascular grafts is a well-known strategy to prevent thrombus formation [305–308]. In the present study, we found that in the three study groups without heparin functionalization (groups 1-3), at best, one out of five grafts remained patent. The TPU-coated nylon grafts with PCL-BU coating alone (graft type 2) showed occlusion in all grafts within two hours after surgery. Possibly, the addition of PCL-BU coating worsens the hemocompatibility of the TPU-coated nylon material. The reason why the PCL-BU coating would be more thrombogenic than the TPU layer itself is not known. Previously, grafts consisting of a similar polymer as PCL-BU have been successfully implanted in animal models in various trials. In a study of Hong et al. [299] a blend of the polymer with poly(2-methacryloyloxyethyl phosphorylcholine-co-methacryloyloxyethyl butylurethane) (PMBU) was used as electrospun graft for implantation in rat aortas. This study showed that 67% of the PMBU grafts were patent after 8 weeks compared to 40% without PMBU. However, the rats were given anti-platelet therapy during follow-up. In a study from Seifalian et al. [300], poly(carbonate-urea)urethane electrospun grafts were implanted in the aorta-iliac position in beagle dogs. This study showed that with this similar polymer no thrombotic effects were observed up to 36 months, but the grafts in this study had a larger diameter. Duijvelshoff et al. [309], fabricated electrospun PCL-BU aortic grafts that were implanted in rats with a follow up duration up to 56 days. In this study no thrombogenic events were reported, without administrating anti-coagulation therapy during the follow-up. The above-mentioned studies all reported fewer thrombotic events with comparable supramolecular materials, however they either used antithrombotic therapy, large animal models or fibrous graft constructs (by means of electrospinning), and are therefore not one-to-one comparable to our results. Still, we argue that one potential reason for the thrombogenicity observed in this study with the PCL-BU coating (group 2) could be related to the fact that we used solution casting to apply the PCL-BU instead of fabricating a porous PCL-BU electrospun graft. This should be further investigated in future studies.

In contrast to groups 1-3, in the group of rats that received heparin-coated grafts (group 4), three out of five grafts remained patent during the 24 h follow-up period. However, we did observe an increased occurrence of bleeding through the suture lines after the removal of the aortic clamps in the heparin-functionalized grafts. This bleeding was more pronounced compared to the other three graft types that were not functionalized with heparin, which exhibited relatively less bleeding. To mitigate the bleeding issue associated with heparin-functionalized grafts, we implemented an effective measure: rinsing the lumen of the grafts with saline to remove any residual heparin solution before implantation. This step proved successful in managing the bleeding and minimizing its occurrence during the procedure. The increased bleeding observed in grafts functionalized with heparin, in addition to the higher number of patent grafts after 24 h follow up, suggests that the heparin functionalization may have had the desired antithrombotic effect at least shortly after surgery.

We chose a 24 h follow-up time to study the thrombogenicity of the four selected materials in vivo. However, this follow-up time is too short to effectively assess the long-term activity of the developed coatings. Free circulating unfractionated heparin molecules have an elimination half-life of 1.5 hours [310], thus their effect is fully eliminated after 6-7.5 hours. We found that after 24 hours, the heparin-functionalized grafts had less thrombotic complications than the other types of grafts, which indicates that the heparin func-

tionalization was still active. We attempted to investigate the functionalization upon explantation by studying the chemical composition of the surfaces of the explants with x-ray photoelectron spectroscopy. However, we could not reliably study the composition of the material due to the influence of the proteins and cells that had adsorbed to the material. Therefore, we could not prove that the heparin was still retained on the coating after completing the follow-up time of 24 h. To eventually use a heparin functionalization strategy for blood contacting surfaces of MCS devices, the bonding method and long-term function of heparin play crucial roles. Longer follow-up times are needed to investigate if the effect of heparin functionalization is sustainable.

Generally, this study was marked by the high number of thrombotic complications, which occurred in all study groups. Even in patent grafts, we found evidence that small thrombi were present in the lumen. MRI analysis revealed an obstruction in the blood flow of a patent graft that is likely to be caused by a thrombus in the lumen (graft 4.5). Histology and SEM analysis showed that in multiple patent grafts, thrombi were found around the sutures inside the grafts (Figures B.19, B.20, B.21). Histological analysis revealed that almost all thrombi were located to the site of the graft where the two ends of the TPU-coated nylon sheet were conjoined with sutures (Figure B.20). Due to our fabrication method and the use of flat TPU-coated nylon sheets, the lumen of the grafts was not round, but was tapered on one side (Figure B.6.a). We hypothesize that this tapered shape has played a role in the formation of the thrombi. Potentially, in the area where the sheet was sutured together, there was turbulent or partially stagnant blood flow that may have initiated thrombus formation [311, 312]. A future recommendation for a similar study is to develop a new fabrication method in which the lumen of the graft is fully round in shape. An example of such a fabrication would be round knitting/weaving or electrospinning a nylon tube and applying TPU and supramolecular coatings afterwards. However, the small diameter of the vascular grafts makes coating of the lumen challenging. Alternatively, a TPU-coated nylon sheet could be folded to a tubular shape, the ends placed next to each other and glued or heat-sealed together, so that a round graft lumen is formed.

Additionally, the small diameter (2 mm) of the grafts may have played a large role in the high number of thrombotic indications. Typically, the rat abdominal graft model is used to investigate the biocompatibility of novel biomaterials [301, 313]. This animal model has also been used extensively in earlier studies of our research group [282, 301]. Given the small diameter of the rat aorta, the fabricated grafts had to possess an inner diameter of 2 mm. To enhance future studies exploring vascular graft constructs where two ends of a flat sheet are joined using sutures, it would be advantageous to consider an animal model with larger vessel diameters, such as rabbits. Larger diameter grafts would result in a smaller junction site relative to the overall lumen diameter, potentially reducing its impact on thrombus formation.

The in vitro thrombogenicity test showed that many platelets adhered to the uncoated TPU-coated nylon (group 1) and to the nylon TPU + PCL-BU coating (group 2), while very few platelets adhered to the nylon TPU with PCL-BU + BU-HBP (group 3), and to the coating that was functionalized with heparin (group 4). However, during the in vivo experiment, 4/5 grafts of the PCL-BU + BU-HBP (group 3) and 2/5 grafts functionalized with heparin (group 4) were occluded by a large thrombus. This considerable difference between in vitro and in vivo results in terms of thrombogenicity further strengthens the hypothesis that the graft design played a role in the thrombus formation during the in vivo study.

In conclusion, Supramolecular coatings based on bisurea polymers modified with heparin via heparin binding additives showed a reduction in thrombogenicity of TPU-coated nylon grafts. This study establishes a first step toward the fabrication of TPU-coated nylon materials with functional supramolecular coatings for blood-contacting surfaces of (soft robotic) devices.

	Atom percentage (%)		
PCL-BU on TPU-coated nylon	**C**	**N**	**O**
Before	73	0.9	26.5
After	86.5	1.9	11.5

Table B.2 | Atom percentages determined by XPS measurements of TPU-coated nylon surface before and after coating with PCL-BU.

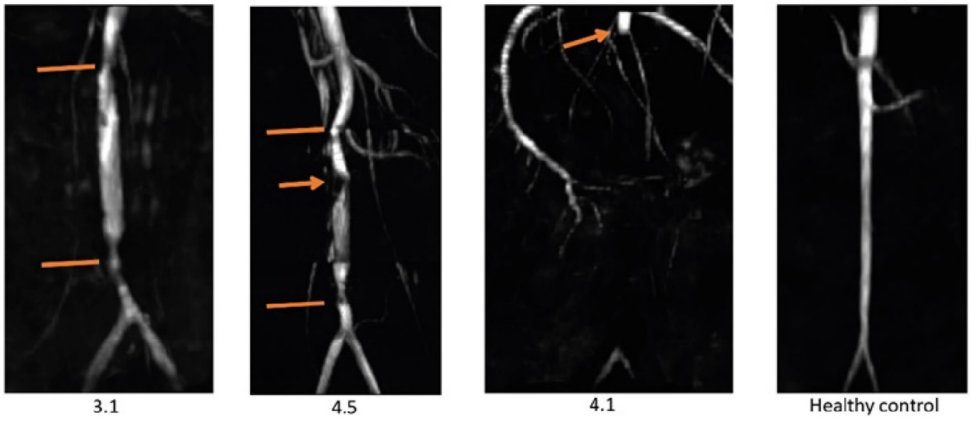

Figure B.18 | Pre-clinical assessment of the grafts. MRI images of grafts in the rat abdominal aorta (3.1, 4.5 and 4.1) as well as the native rat aorta. Horizontal lines indicate the proximal (top) and distal (bottom) anastomosis. Arrow indicates thrombi inside the lumen.

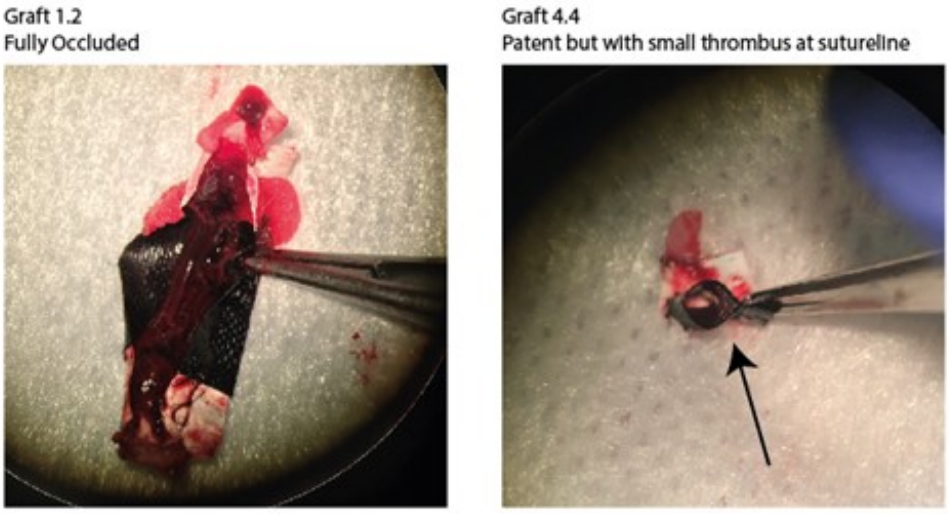

Figure B.19 | photos of two exemplary grafts at explant. Left image shows a fully occluded graft of a rat that had immobile hind legs one day after surgery. Typically, thrombi were seen that covered the full length of the graft. Right image shows a patent graft that has a small thrombus in the section where the TPU-coated nylon sheet is sutured together.

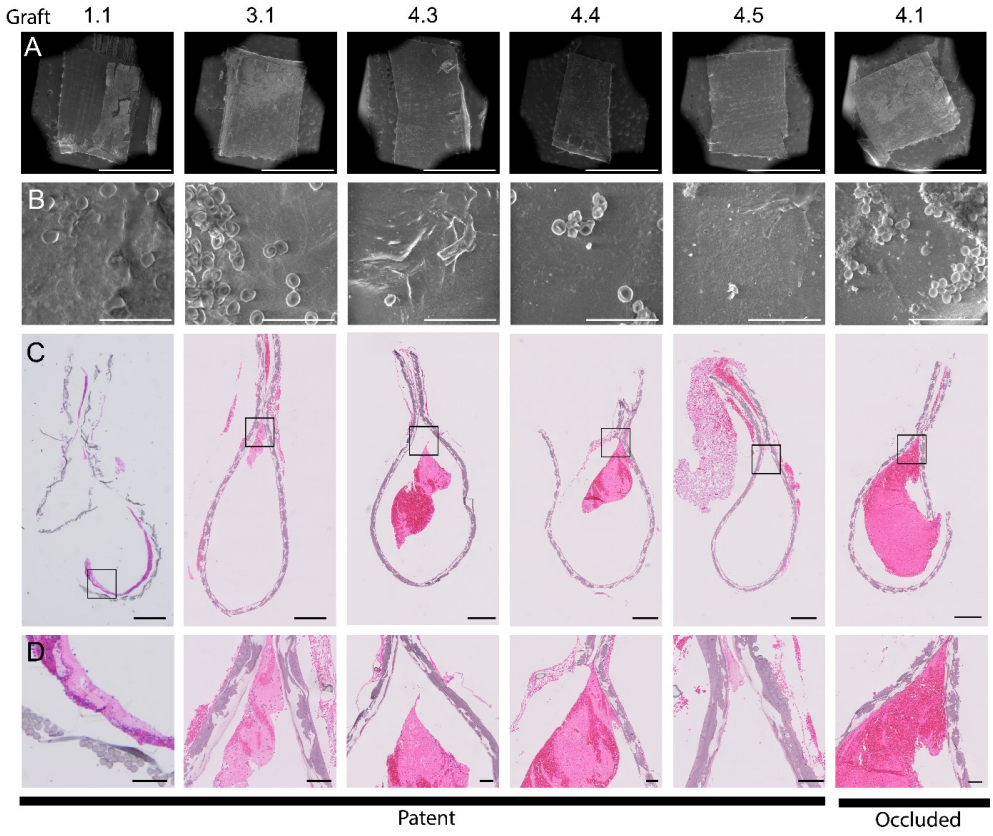

Figure B.20 | Visualization of explanted grafts. SEM images of part of the explanted grafts from graft 1.1, 3.1, 4.3, 4.4, 4.5 and 4.1. Scale bars represent 3 mm and 20 µm for A and B, respectively. Fluorescent images of an overview of a coupe (C) and a zoom-in (D), region where is zoomed is highlighted, from the explanted grafts from graft 1.1, 3.1, 4.3, 4.4, 4.5 and 4.1 stained with hematoxylin and eosin. Scale bars represent 500 and 100 µm for C and D, respectively.

Table B.3 | Clinical assessments and MRI analysis for all rats included in this study. POD= Post Operative Day.

Graft type	POD0 hind leg movement	POD1 hind leg movement	Follow up duration (hours)	graft status after 24h	MRI assessment graft	Lumen graft diameter (mm).		
						Prox	Mid	Dist
1.1	Yes	Yes	24	Patent	Patent	2,0	1,6	1,8
1.2	Yes	No	24	Occluded	Occluded			
1.3	No	NA	4	Occluded	NA			
1.4	Yes	No	18	Occluded	NA			
1.5	No	NA	3	Occluded	Occluded			
2.1	No	NA	1	Occluded	NA			
2.2	No	NA	0	Occluded	NA			
2.3	No	NA	4	Occluded	Occluded			
2.4	No	NA	6	Occluded	NA			
2.5	No	NA	3	Occluded	NA			
3.1	Yes	Yes	24	Patent	Patent	2,0	2,0	2,0
3.2	No	NA	1	Unclear	NA			
3.3	Yes	No	24	Occluded	NA			
3.4	Yes	No	24	Occluded	Occluded			
3.5	No	NA	4	Occluded	Occluded			
4.1	Yes	No	24	Occluded	Occluded			
4.2	Yes	No	20	Occluded	NA			
4.3	Yes	Yes	24	Patent	NA			
4.4	Yes	Yes	24	Patent	NA			
4.5	Yes	Yes	24	Patent	Patent	1,1	0,4	1,9

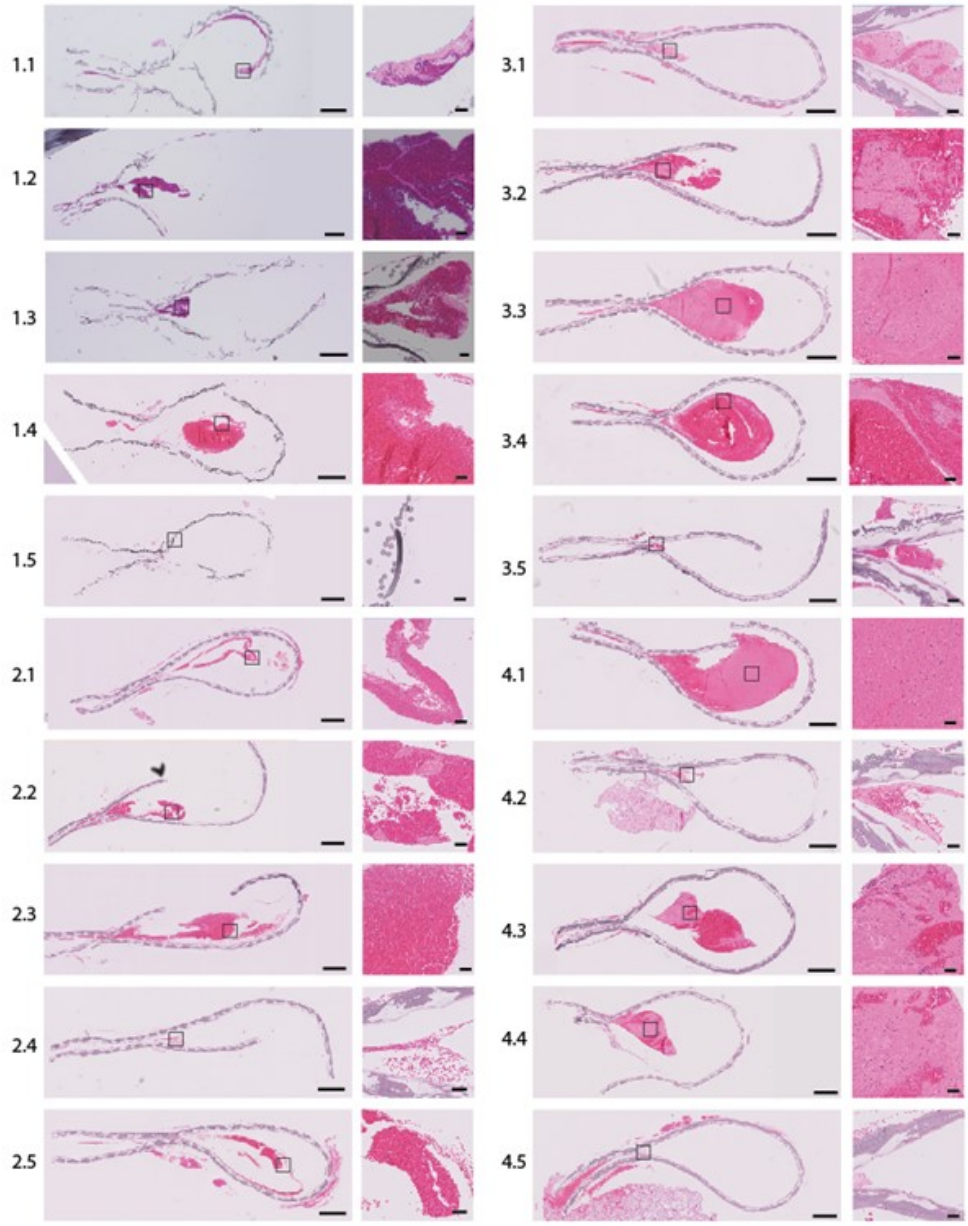

Figure B.21 | Histological images of an overview of a coupe and a zoom-in region, from all the explanted grafts stained with hematoxylin and eosin. Scalebars zoom-out images represent 500 μm. Scalebars zoom-in images represent 50 μm.

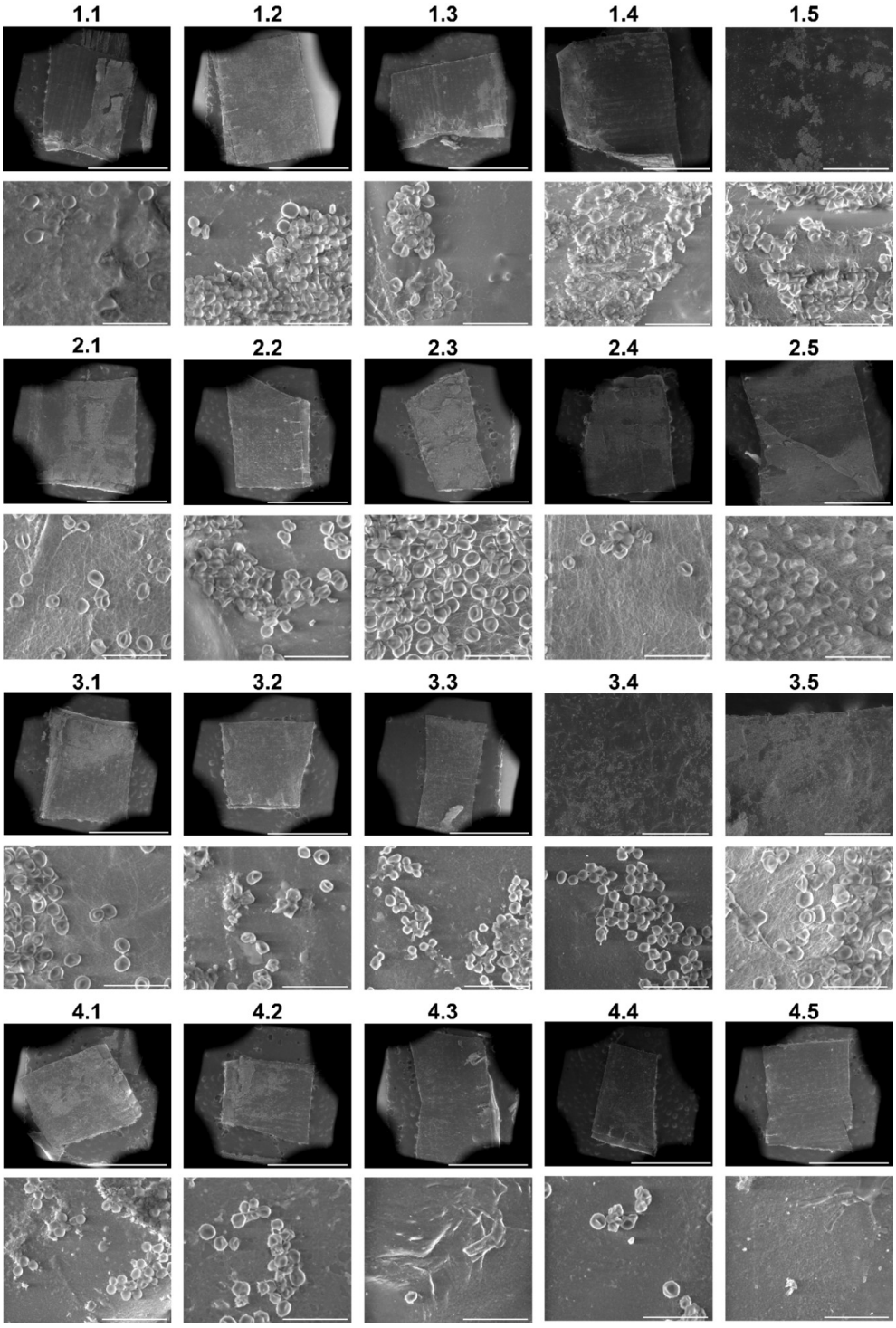

Figure B.22 | SEM images of zoom-out and zoom-in at 5000x magnification of part of all the explanted grafts. Scale bars represent 3 mm and 20 μm for the zoom-out and zoom-in images respectively.

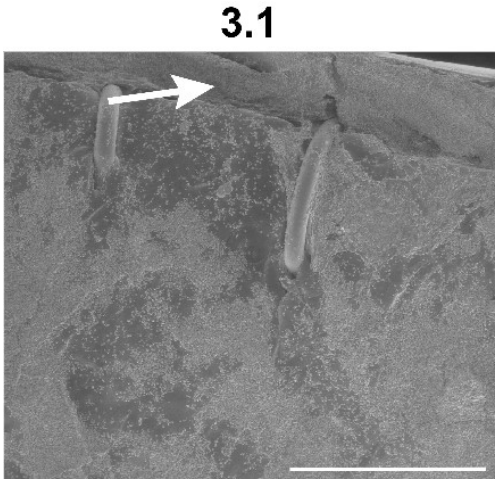

Figure B.23 | SEM image of 3.1 graft highlighting erythrocytes adsorption to gore-text material. Scale bar represent 500 μm.

	Atom percentage (%)		
PCL-BU on TPU-coated nylon	**C**	**N**	**O**
Before mock-loop	81.6	1.8	16.6
After mock-loop	79.6	17.5	2.8

Table B.4 | Atom percentages determined by XPS measurements of TPU-coated nylon and PCL-BU coating on TPU-coated nylon materials after being exposed to the mock loop set-up with the laparoscope experiments.

B.8. Investigating the intraventricular deformations

Considering that the deformation of the inner layer of the Hybrid Heart is strongly influenced by the hydraulic pressure of the ventricle chamber, we conducted experiments using a laparoscope to visually investigate the intraventricular deformations at different conditions and examine ventricle behavior. A Hybrid Heart prototype was connected to a mock circulation and the videos of the deformation were acquired. The description of the experiment and its results are reported in the following sections.

B.8.1. Hybrid Heart design and assembly and set-up description

To be able to insert the laparoscope in the Hybrid Heart, the external fabric was cut to create a small hole in between the valves. In addition, the design of the ventricle was slightly modified, and a straight central canal was added for the insertion and fixing of the laparoscope tip (Figure B.24).

The laparoscope tip was inserted in the prototype from a small hole that was created in between the inlet and the outlet valves of one of the two ventricles. This position for the laparoscope was chosen because the portion of the prototype to which the valves are

fixed is stable and shows only small movement and deformation during contraction. In addition, this position allowed a clear and wide view of the inner surface of the ventricle, from the base to the apex of the prototype.

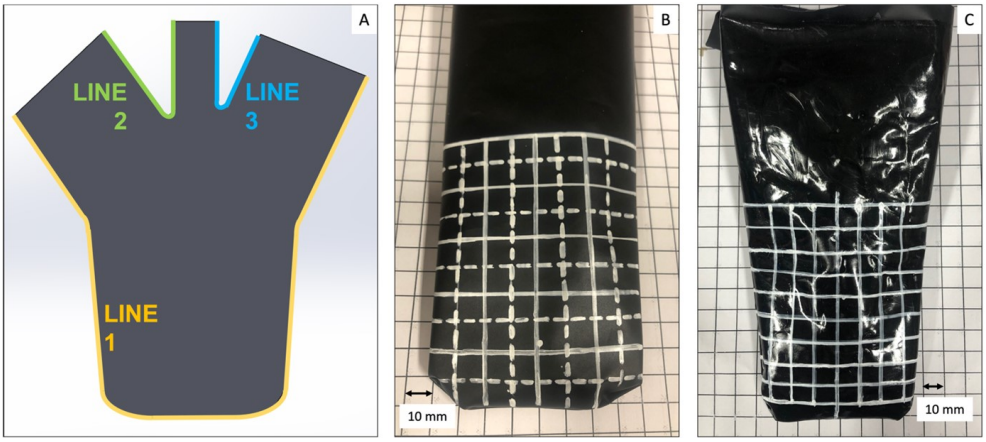

Figure B.24 | Coated and uncoated TPU ventricles. A) 2D path (colored lines) used for heat-sealing, B) inner surface of a TPU ventricle, with drawn grid, C) inner surface of a TPU ventricle with coating, and drawn grid.

To allow the manual drawing of a grid on the inner surface of the TPU ventricle, the heat-sealing procedure for the manufacturing of the TPU ventricle was modified as follows:

1. Two TPU sheets are placed on the bed of a modified 3D printer for heat-sealing. The path described by LINE1 is sealed.

2. The TPU sheet is reversed, and a 10 mm spaced grid is manually drawn on the TPU surface (See figures B.24.B, B.24.C). A white waterproof pencil was used to draw the lines.

3. The TPU sheet is reversed again and placed back on the bed of the modified 3D printer to do the sealing of LINE2 and LINE3 (see figure B.24.A).

The prototype and the laparoscope in position are shown in figure B.25. As can be seen from the figure, the Hybrid Heart was connected to the mock circulatory loop. A 27 mm and a 24 mm inner diameter mechanical valves were used at the inlet and the outlet ports of each ventricle, respectively. The vision system connected to the laparoscope was placed on side, and videos were recorded with a camera.

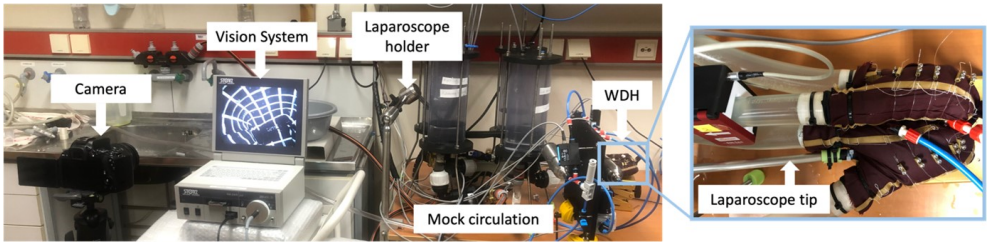

Figure B.25 | Intraventricular deformation investigation. Experimental setup used to study the deformation of the inner layer of the Hybrid Heart, when connected to the mock circulatory loop. On the right, a close-up on the Hybrid Heart shows how the laparoscope accesses the prototype.

B.8.2. Experimental procedure

The experiments were conducted as follows:

1. The ventricle of interest (the one with the access for the laparoscope) is inserted in the external fabric. The other ventricle is assembled as usual.

2. The Hybrid Heart is connected to the mock circulatory loop.

3. The laparoscope tip is inserted in the ventricle. The water tightness is obtained by placing a silicone ring around the laparoscope and the fabric and securing with zip-ties.

4. The mock circulation is filled with water. At this point, the wires of the Hybrid Heart are tightened.

5. The vision system of the laparoscope is switched on. The laparoscope is moved until a satisfying view of the inner surface of the ventricle is achieved. The laparoscope holder is then fixed.

6. The Hybrid Heart is actuated at 30 bpm, reaching a maximum pressure in the septum of 80 kPa. The videos of both the prototype contraction and of the deformation of the inner surface of the TPU ventricle are recorded.

Importantly, the settings in the mock loop are switched to test alternatively pressure conditions that are referred either to a right or a left ventricle, without changing the position of the laparoscope.

Bibliography

[1] M. Di Cesare, P. Perel, S. Taylor, C. Kabudula, H. Bixby, T. A. Gaziano, D. V. McGhie, J. Mwangi, B. Pervan, J. Narula, D. Pineiro, and F. J. Pinto, "The heart of the world," *Glob Heart*, vol. 19, no. 1, p. 11, 2024.

[2] B. Bozkurt, T. Ahmad, K. Alexander, W. L. Baker, K. Bosak, K. Breathett, S. Carter, M. H. Drazner, S. M. Dunlay, G. C. Fonarow, S. J. Greene, P. Heidenreich, J. E. Ho, E. Hsich, N. E. Ibrahim, L. M. Jones, S. S. Khan, P. Khazanie, T. Koelling, C. S. Lee, A. A. Morris, I. Page, Robert L., A. Pandey, M. R. Piano, A. T. Sandhu, J. Stehlik, L. W. Stevenson, J. Teerlink, A. R. Vest, C. Yancy, and B. Ziaeian, "Hf stats 2024: Heart failure epidemiology and outcomes statistics an updated 2024 report from the heart failure society of america," *Journal of Cardiac Failure*, vol. 31, no. 1, pp. 66–116, 2025.

[3] P. Shams, A. Malik, and L. Chhabra, *Heart Failure (Congestive Heart Failure)*. Treasure Island (FL): StatPearls [Internet], 2025.

[4] A. Groenewegen, F. H. Rutten, A. Mosterd, and A. W. Hoes, "Epidemiology of heart failure," *European Journal of Heart Failure*, vol. 22, no. 8, pp. 1342–1356, 2020.

[5] O. Domengé, A. Fayol, M. Ladouceur, K. Wahbi, L. Amar, C. Carette, A. Hagège, and J.-S. Hulot, "Trends in prevalence of major etiologies leading to heart failure in young patients: An integrative review," *Trends in Cardiovascular Medicine*, vol. 34, no. 2, pp. 80–88, 2024.

[6] H. Shih, B. Lee, R. J. Lee, and A. J. Boyle, "The aging heart and post-infarction left ventricular remodeling," *JACC*, vol. 57, no. 1, pp. 9–17, 2011.

[7] V. Papademetriou, "From hypertension to heart failure," *The Journal of Clinical Hypertension*, vol. 6, no. s10, pp. 14–17, 2004.

[8] B. J. van Essen, J. E. Emmens, J. Tromp, W. Ouwerkerk, M. D. Smit, C. A. Geluk, L. Baumhove, N. Suthahar, R. T. Gansevoort, S. J. L. Bakker, K. Damman, P. van der Meer, R. A. de Boer, D. J. van Veldhuisen, and A. A. Voors, "Sex-specific risk factors for new-onset heart failure: the prevend study at 25 years," *European Heart Journal*, vol. 46, pp. 1528–1536, 12 2024.

[9] P. A. Heidenreich, N. M. Albert, L. A. Allen, D. A. Bluemke, J. Butler, G. C. Fonarow, J. S. Ikonomidis, O. Khavjou, M. A. Konstam, T. M. Maddox, G. Nichol, M. Pham, I. L. Piña, and J. G. Trogdon, "Forecasting the impact of heart failure in the united states a policy statement from the american heart association," *Circulation. Heart failure*, vol. 6, no. 3, pp. 606–619, 2013.

[10] G. M. C. Rosano, P. Seferovic, G. Savarese, I. Spoletini, Y. Lopatin, F. Gustafsson, A. Bayes-Genis, T. Jaarsma, M. Abdelhamid, A. G. Miqueo, M. Piepoli, C. G. Tocchetti, A. D. Risti, E. Jankowska, B. Moura, L. Hill, G. Filippatos, M. Metra, D. Milicic,

T. Thum, O. Chioncel, T. Ben Gal, L. H. Lund, D. Farmakis, W. Mullens, S. Adamopoulos, M. Bohm, A. Norhammar, A. Bollmann, A. Banerjee, A. P. Maggioni, A. Voors, A. C. Solal, and A. J. S. Coats, "Impact analysis of heart failure across european countries: an esc-hfa position paper," *ESC Heart Fail*, vol. 9, no. 5, pp. 2767–2778, 2022.

[11] R. S. J. Goh, B. Chong, J. Jayabaskaran, S. M. Jauhari, S. P. Chan, M. T. W. Kueh, K. Shankar, H. Li, Y. H. Chin, G. Kong, V. V. Anand, K. A. Chan, I. Sukmawati, S. A. Toh, M. Muthiah, J.-W. Wang, G. Tse, A. Mehta, A. Fong, L. Baskaran, L. Zhong, J. Yap, K. K. Yeo, D. J. Hausenloy, J. W. C. Tan, T.-F. Chao, Y.-H. Li, S. L. Lim, K. H. Chan, P. H. Loh, P. Chai, T. C. Yeo, A. F. Low, C. H. Lee, R. Foo, H. C. Tan, J. Yip, S. Rao, S. Honda, S. Yasuda, T. Kajiya, S. Goto, B. P. Yan, X. Zhou, G. A. Figtree, M. A. Mamas, Y. Kim, Y.-H. Jeong, M. H. Kim, D.-W. Park, S.-J. Park, A. M. Richards, M. Y. Chan, G. Y. H. Lip, and N. W. S. Chew, "The burden of cardiovascular disease in asia from 2025 to 2050: a forecast analysis for east asia, south asia, south-east asia, central asia, and high-income asia pacific regions," *The Lancet Regional Health Western Pacific*, vol. 49, 2024.

[12] F. Epelde, "Impact of exercise on physiological, biochemical, and analytical parameters in patients with heart failure with reduced ejection fraction," *Medicina*, vol. 60, no. 12, 2024.

[13] H. Winkler, D. Riedlinger, A. Figura, L. Schenk, M. Möckel, and T. Reinhold, "Characteristics, health care utilization and cost of patients hospitalized with heart failure," *Frontiers in Health Services*, vol. Volume 5 - 2025, 2025.

[14] T. Bodenheimer and A. Fernandez, "High and rising health care costs. part 4: can costs be controlled while preserving quality?," *Ann Intern Med*, vol. 143, no. 1, pp. 26–31, 2005.

[15] L. A. Allen, L. W. Stevenson, K. L. Grady, N. E. Goldstein, D. D. Matlock, R. M. Arnold, N. R. Cook, G. M. Felker, G. S. Francis, P. J. Hauptman, E. P. Havranek, H. M. Krumholz, D. Mancini, B. Riegel, and J. A. Spertus, "Decision making in advanced heart failure," *Circulation*, vol. 125, no. 15, pp. 1928–1952, 2012.

[16] J. Maciver and H. J. Ross, "A palliative approach for heart failure end-of-life care," *Current Opinion in Cardiology*, vol. 33, no. 2, pp. 202–207, 2018.

[17] S. Mangini, B. R. Alves, O. M. Silvestre, P. V. Pires, L. J. Pires, M. N. Curiati, and F. Bacal, "Heart transplantation: review," *Einstein (Sao Paulo)*, vol. 13, no. 2, pp. 310–8, 2015.

[18] R. Jain, E. P. Kransdorf, J. Cowger, V. Jeevanandam, and J. A. Kobashigawa, "Donor selection for heart transplantation in 2025," *JACC Heart Fail*, vol. 13, no. 3, pp. 389–401, 2025.

[19] N. Melton, B. Soleimani, and R. Dowling, "Current role of the total artificial heart in the management of advanced heart failure," *Current Cardiology Reports*, vol. 21, no. 11, p. 142, 2019.

[20] C. M. Moeller, A. F. Valledor, D. Oren, G. Rubinstein, G. T. Sayer, and N. Uriel, "Evolution of mechanical circulatory support for advanced heart failure," *Progress in Cardiovascular Diseases*, vol. 82, pp. 135–146, 2024.

[21] C. H. Selzman, J. L. Madden, A. H. Healy, S. H. McKellar, A. Koliopoulou, J. Stehlik, and S. G. Drakos, "Bridge to removal: a paradigm shift for left ventricular assist device therapy," *Ann Thorac Surg*, vol. 99, no. 1, pp. 360–7, 2015.

[22] M. Melendo-Viu, D. Dobarro, S. Raposeiras Roubin, C. Llamas Pernas, C. Moliz Cordón, M. Vazquez Lamas, M. Piñón Esteban, M. Varela Martínez, E. Abu Assi, R. Pita Romero, J. J. Legarra Calderón, and A. Íñiguez Romo, "Left ventricular assist device as a destination therapy: Current situation and the importance of patient selection," *Life (Basel)*, vol. 13, no. 4, 2023.

[23] C. B. Patel, L. Blue, B. Cagliostro, S. H. Bailey, J. W. Entwistle, R. John, V. Thohan, J. Cleveland, Joseph C., D. J. Goldstein, N. Uriel, X. Su, S. I. Somo, P. Sood, and M. R. Mehra, "Left ventricular assist systems and infection-related outcomes: A comprehensive analysis of the momentum 3 trial," *The Journal of Heart and Lung Transplantation*, vol. 39, no. 8, pp. 774–781, 2020.

[24] N. McNamara, H. Narroway, M. Williams, J. Brookes, J. Farag, D. Cistulli, P. Bannon, S. Marasco, E. Potapov, and A. Loforte, "Contemporary outcomes of continuous-flow left ventricular assist devicesa systematic review," *Annals of Cardiothoracic Surgery*, vol. 10, no. 2, 2021.

[25] D. A. Cooley, D. Liotta, G. L. Hallman, R. D. Bloodwell, R. D. Leachman, and J. D. Milam, "Orthotopic cardiac prosthesis for two-staged cardiac replacement," *The American journal of cardiology*, vol. 24, no. 5, pp. 723–730, 1969.

[26] D. G. Tang, K. B. Shah, M. L. Hess, and V. Kasirajan, "Implantation of the syncardia total artificial heart," *J Vis Exp*, no. 89, 2014.

[27] P. Mohacsi and P. Leprince, "The carmat total artificial heart," *European Journal of Cardio-Thoracic Surgery*, vol. 46, pp. 933–934, 09 2014.

[28] D. Timms, J. Fraser, M. Hayne, J. Dunning, K. McNeil, and M. Pearcy, "The bivacor rotary biventricular assist device: Concept and in vitro investigation," *Artificial Organs*, vol. 32, no. 10, pp. 816–819, 2008.

[29] L. Fresiello, A. Najar, N. Brynedal Ignell, K. Zieliski, M. Rocchi, B. Meyns, and I. L. Perkins, "Hemodynamic characterization of the realheartő total artificial heart with a hybrid cardiovascular simulator," *Artificial Organs*, vol. 46, no. 8, pp. 1585–1596, 2022.

[30] D. Wc, J. L. Anderson, L. D. Joyce, F. L. Anderson, E. H. Hammond, J. Rk, and W. J. Kolff, "Clinical use of the total artificial heart," *The New England journal of medicine*, vol. 310, no. 5, pp. 273–278, 1984.

[31] J. G. Copeland, M. M. Levinson, R. J. H. Smith, T. B. Icenogle, C. Vaughn, K. Cheng, R. A. Ott, and R. W. Emery, "The total artificial heart as a bridge to transplantation: A report of two cases," *JAMA*, vol. 256, no. 21, pp. 2991–2995, 1986.

[32] A. Razumov, M. Burri, A. Zittermann, D. Radakovic, V. Lauenroth, S. V. Rojas, H. Fox, R. Schramm, J. Gummert, M. A. Deutsch, and M. Morshuis, "Outcomes after syncardiaő temporary total artificial heart implantation: A 20-year single-center experience in 196 patients," *Artif Organs*, vol. 49, no. 2, pp. 266–275, 2025.

[33] G. Torregrossa, M. Morshuis, R. Varghese, L. Hosseinian, V. Vida, V. Tarzia, A. Loforte, D. Duveau, F. Arabia, P. Leprince, V. Kasirajan, F. Beyersdorf, F. Musumeci, R. Hetzer, T. Krabatsch, J. Gummert, J. Copeland, and G. Gerosa, "Results with syncardia total artificial heart beyond 1 year," *ASAIO Journal*, vol. 60, no. 6, 2014.

[34] S. Spiliopoulos, A. M. Dimitriou, D. Guersoy, R. Koerfer, and G. Tenderich, "Expanding applicability of total artificial heart therapy: The 50-cc syncardia total artificial heart," *The Annals of thoracic surgery*, vol. 100, no. 3, pp. e55–7, 2015.

[35] U. Richez, H. De Castilla, C. L. Guerin, N. Gendron, G. Luraghi, M. Grimme, W. Wu, M. Taverna, P. Jansen, C. Latremouille, F. Migliavacca, G. Dubini, A. Capel, A. Carpentier, and D. M. Smadja, "Hemocompatibility and safety of the carmat total artifical heart hybrid membrane," *Heliyon*, vol. 5, no. 12, p. e02914, 2019.

[36] J. N. Schroder, S. L. McCartney, P. Jansen, R. Plichta, J. N. Katz, D. M. Smadja, K. C. Dewan, and C. A. Milano, "The first autoregulated total artificial heart implant in the united states," *Annals of Thoracic Surgery Short Reports*, vol. 1, no. 1, pp. 185–187, 2023.

[37] T. Gluck, D. L. Timms, A. Elgalad, A. Shafii, M. Freundt, R. Dowling, W. E. Cohn, and O. H. Frazier, "Abstract 16713: Pre-clinical 30-day survival results of the bivacor tah," *Circulation*, vol. 148, no. Suppl_1, pp. A16713–A16713, 2023.

[38] N. A. Greatrex, D. L. Timms, N. Kurita, E. W. Palmer, and T. Masuzawa, "Axial magnetic bearing development for the bivacor rotary bivad/tah," *IEEE Transactions on Biomedical Engineering*, vol. 57, no. 3, pp. 714–721, 2010.

[39] M. Cianchetti, C. Laschi, A. Menciassi, and P. Dario, "Biomedical applications of soft robotics," *Nature Reviews Materials*, vol. 3, no. 6, pp. 143–153, 2018.

[40] J. Fang, Y. Zhuang, K. Liu, Z. Chen, Z. Liu, T. Kong, J. Xu, and C. Qi, "A shift from efficiency to adaptability: Recent progress in biomimetic interactive soft robotics in wet environments," *Advanced Science*, vol. 9, no. 8, p. 2104347, 2022.

[41] B. Mazzolai, A. Mondini, E. Del Dottore, L. Margheri, F. Carpi, K. Suzumori, M. Cianchetti, T. Speck, S. K. Smoukov, I. Burgert, T. Keplinger, G. D. F. Siqueira, F. Vanneste, O. Goury, C. Duriez, T. Nanayakkara, B. Vanderborght, J. Brancart, S. Terryn, S. I. Rich, R. Liu, K. Fukuda, T. Someya, M. Calisti, C. Laschi, W. Sun, G. Wang, L. Wen, R. Baines, S. K. Patiballa, R. Kramer-Bottiglio, D. Rus, P. Fischer, F. C. Simmel, and A. Lendlein, "Roadmap on soft robotics: multifunctionality, adaptability and growth without borders," *Multifunctional Materials*, vol. 5, p. 032001, aug 2022.

[42] Y. Yim, Y. Noguchi, and F. Tanaka, "A wearable soft robot that can alleviate the pain and fear of the wearer," *Scientific Reports*, vol. 12, no. 1, p. 17003, 2022.

[43] Y. M. Zhou, C. J. Hohimer, H. T. Young, C. M. McCann, D. Pont-Esteban, U. S. Civici, Y. Jin, P. Murphy, D. Wagner, T. Cole, N. Phipps, H. Cho, F. Bertacchi, I. Pignataro, T. Proietti, and C. J. Walsh, "A portable inflatable soft wearable robot to assist the shoulder during industrial work," *Science Robotics*, vol. 9, no. 91, p. eadi2377, 2024.

[44] M. Runciman, A. Darzi, and G. P. Mylonas, "Soft robotics in minimally invasive surgery," *Soft Robotics*, vol. 6, no. 4, pp. 423–443, 2019.

[45] P. Polygerinos, Z. Wang, K. C. Galloway, R. J. Wood, and C. J. Walsh, "Soft robotic glove for combined assistance and at-home rehabilitation," *Robotics and Autonomous Systems*, vol. 73, no. NA, pp. 135–143, 2015.

[46] M. Pan, C. Yuan, X. Liang, T. Dong, T. Liu, J. Zhang, J. Zou, H. Yang, and C. Bowen, "Soft actuators and robotic devices for rehabilitation and assistance," *Advanced Intelligent Systems*, vol. 4, no. 4, p. 2100140, 2022.

[47] L. Hu, J. Bonnemain, M. Y. Saeed, M. Singh, D. Quevedo Moreno, N. V. Vasilyev, and E. T. Roche, "An implantable soft robotic ventilator augments inspiration in a pig model of respiratory insufficiency," *Nature Biomedical Engineering*, 2022.

[48] G. V. Letsou, C. M. Bolch, E. C. Hord, W. C. Altman, B. Leschinsky, and J. C. Criscione, "The corinnova implantable cardiac assist system for direct cardiac compression," *RCM*, vol. 23, no. 6, 2022.

[49] G. V. Letsou, C. M. Bolch, E. C. Hord, W. C. Altman, B. L. Youngblood, B. Leschinsky, and J. C. Criscione, "Mechanical cardiac support with an implantable direct cardiac compression device: Proof of concept," *The Annals of Thoracic Surgery*, vol. 114, no. 5, pp. 1944–1950, 2022.

[50] N. H. Cohrs, A. Petrou, M. Loepfe, M. Yliruka, C. M. Schumacher, A. X. Kohll, C. Starck, M. S. Daners, M. Meboldt, V. Falk, and W. J. Stark, "A soft total artificial heart-first concept evaluation on a hybrid mock circulation," *Artificial organs*, vol. 41, no. 10, pp. 948–958, 2017.

[51] A. X. Kohll, N. H. Cohrs, R. Walker, A. Petrou, M. Loepfe, M. Schmid Daners, V. Falk, M. Meboldt, and W. J. Stark, "Long-term performance of a pneumatically actuated soft pump manufactured by rubber compression molding," *Soft Robotics*, vol. 6, no. 2, pp. 206–213, 2019.

[52] L. G. Guex, L. S. Jones, A. X. Kohll, R. Walker, M. Meboldt, V. Falk, M. Schmid Daners, and W. J. Stark, "Increased longevity and pumping performance of an injection molded soft total artificial heart," *Soft Robotics*, vol. 8, no. 5, pp. 588–593, 2021.

[53] E. T. Roche, M. A. Horvath, I. Wamala, A. Alazmani, S. E. Song, W. Whyte, Z. Machaidze, C. J. Payne, J. C. Weaver, G. Fishbein, J. Kuebler, N. V. Vasilyev, D. J. Mooney, F. A. Pigula, and C. J. Walsh, "Soft robotic sleeve supports heart function," *Sci Transl Med*, vol. 9, no. 373, 2017.

[54] J. Davies, M. T. Thai, B. Sharma, T. T. Hoang, C. C. Nguyen, P. T. Phan, T. N. A. M. Vuong, A. Ji, K. Zhu, E. Nicotra, Y.-C. Toh, M. Stevens, C. Hayward, H.-P. Phan, N. H. Lovell, and T. N. Do, "Soft robotic artificial left ventricle simulator capable of reproducing myocardial biomechanics," *Science Robotics*, vol. 9, no. 94, p. eado4553, 2024.

[55] J. Davies, M. T. Thai, H. Low, P. T. Phan, T. T. Hoang, N. H. Lovell, and T. N. Do, "Bio-sharpe: Bioinspired soft and high aspect ratio pumping element for robotic and medical applications," *Soft Robotics*, vol. 10, no. 6, pp. 1055–1069, 2023.

[56] M. Metra and J. R. Teerlink, "Heart failure," *Lancet (London, England)*, vol. 390, no. 10106, pp. 1981–1995, 2017.

[57] P. A. Heidenreich, N. M. Albert, L. A. Allen, D. A. Bluemke, J. Butler, G. C. Fonarow, J. S. Ikonomidis, O. Khavjou, M. A. Konstam, T. M. Maddox, G. Nichol, M. Pham, I. L. Piña, and J. G. Trogdon, "Forecasting the impact of heart failure in the united states," *Circulation: Heart Failure*, vol. 6, no. 3, pp. 606–619, 2013.

[58] M. Colvin, J. M. Smith, N. Hadley, M. A. Skeans, K. Uccellini, R. Goff, J. Foutz, A. K. Israni, J. J. Snyder, and B. L. Kasiske, "Optn/srtr 2018 annual data report: Heart," *American journal of transplantation : official journal of the American Society of Transplantation and the American Society of Transplant Surgeons*, vol. 20, no. NA, pp. 340–426, 2020.

[59] E. J. Molina, P. Shah, M. S. Kiernan, W. K. Cornwell, H. Copeland, K. Takeda, F. G. Fernandez, V. Badhwar, R. H. Habib, J. P. Jacobs, D. Koehl, J. K. Kirklin, F. D. Pagani, and J. A. Cowger, "The society of thoracic surgeons intermacs 2020 annual report," *The Annals of thoracic surgery*, vol. 111, no. 3, pp. 778–792, 2021.

[60] J. J. Han, M. A. Acker, and P. Atluri, "Left ventricular assist devices," *Circulation*, vol. 138, no. 24, pp. 2841–2851, 2018.

[61] G. E. Gurvits and E. Fradkov, "Bleeding with the artificial heart: Gastrointestinal hemorrhage in cf-lvad patients," *World journal of gastroenterology*, vol. 23, no. 22, pp. 3945–3953, 2017.

[62] V. Galand, E. Flecher, V. Auffret, S. Boulé, A. Vincentelli, C. Dambrin, P. Mondoly, F. Sacher, K. Nubret, M. Kindo, T. Cardi, P. Gaudard, P. Rouvière, M. Michel, J.-B. Gourraud, P. Defaye, O. Chavanon, C. Verdonk, W. Ghodbane, E. Pelcé, V. Gariboldi, M. Pozzi, J.-F. Obadia, P.-Y. Litzler, F. Anselme, G. Babatasi, A. Belin, F. Garnier, M. Bielefeld, D. Hamon, C. Radu, B. Pierre, T. Bourguignon, R. Eschalier, N. D'Ostrevy, M.-C. Bories, E. Marijon, F. Vanhuyse, H. Blangy, J.-P. Verhoye, C. Leclercq, R. P. Martins, and A.-I. Investigators, "Predictors and clinical impact of late ventricular arrhythmias in patients with continuous-flow left ventricular assist devices," *JACC. Clinical electrophysiology*, vol. 4, no. 9, pp. 1166–1175, 2018.

[63] D. W. Ross, G. R. Stevens, R. Wanchoo, D. T. Majure, S. Jauhar, H. Fernandez, M. Merzkani, and K. D. Jhaveri, "Left ventricular assist devices and the kidney," *Clinical journal of the American Society of Nephrology : CJASN*, vol. 13, no. 2, pp. 348–355, 2017.

[64] N. Aissaoui, J. Jouan, M. Gourjault, B. Diebold, S. Ortuno, A. Hamdan, C. Latremouille, R. Pirracchio, and M. Morshuis, "Understanding left ventricular assist devices," *Blood purification*, vol. 46, no. 4, pp. 292–300, 2018.

[65] National Heart, Lung, and Blood institute, "What is total artificial heart?." `https://www.nhlbi.nih.gov/health/total-artificial-heart`, 2023. Accessed 10/8/2025.

[66] US National Library of Medicine, "Syncardia 70cc tah-t for destination therapy (dt) (ra-540)." `https://clinicaltrials.gov/study/NCT02232659`, 2021. Accessed 10/8/2025.

[67] T. Akutsu and W. J. Kolff, "Permanent substitutes for valves and hearts," *ASAIO Journal*, vol. 4, no. 1, 1958.

[68] C. S. Houston, T. Akutsu, and W. J. Kolff, "Pendulum type of artificial heart within the chest: Preliminary report," *American heart journal*, vol. 59, no. 5, pp. 723–730, 1960.

[69] S. W, T. Akutsu, N. A. Mirkovitch, B. Fd, and W. J. Kolff, "Air-driven artificial hearts inside the chest," *Transactions - American Society for Artificial Internal Organs*, vol. 7, no. NA, pp. 378–387, 1961.

[70] D. Liotta, T. Taliani, A. H. Giffoniello, F. S. Deheza, L. S, L. R, L. Tolocka, J. Panano, and E. Bianciotti, "Artificial heart in the chest: preliminary report," *Transactions - American Society for Artificial Internal Organs*, vol. 7, no. NA, pp. 318–322, 1961.

[71] A. K, H. M, I. S, S. Y, F. Y, and K. S, "Artificial heart incorporated in the chest," *Transactions - American Society for Artificial Internal Organs*, vol. 9, no. NA, pp. 292–298, 1963.

[72] W. S. Pierce, B. N. Gardiner, L. Morris, R. G. Burney, I. E. Leppik, and G. K. Danielson, "Total heart replacement by a single intrathoracic blood pump," *The Journal of surgical research*, vol. 5, no. 9, pp. 387–394, 1965.

[73] Y. Nosé, L. L. Tretbar, A. Sengupta, S. Topaz, W. J. Kolff, and D. B. Effler, "An artificial heart inside the chest," *The Journal of thoracic and cardiovascular surgery*, vol. 50, no. 6, pp. 792–799, 1965.

[74] W. E. Cohn, D. Timms, and O. H. Frazier, "Total artificial hearts: past, present, and future," *Nature reviews. Cardiology*, vol. 12, no. 10, pp. 609–617, 2015.

[75] W. J. Curran, "The first mechanical heart transplant: Informed consent and experimentation," *The New England journal of medicine*, vol. 291, no. 19, pp. 1015–1016, 1974.

[76] D. T. Morris and C. M. Couves, "Experiences with a sac-type artificial heart," *Canadian Medical Association journal*, vol. 105, no. 5, pp. 483–487, 1971.

[77] K.-G. Cs, K. R. Van Kampen, J. Kawai, N. Eastwood, W. J. Kolff, and R. K. Hughes, "Results of total artificial heart implantation in calves," *The Journal of thoracic and cardiovascular surgery*, vol. 62, no. 6, pp. 880–889, 1971.

[78] J. Kawai, P. Jl, F. Donovan, H. Ej, K. Rowley, and W. J. Kolff, "Implantation of a total artificial heart in calves under hypothermia with 10 day survival," *The Journal of thoracic and cardiovascular surgery*, vol. 64, no. 1, pp. 45–60, 1972.

[79] H. Wl, A. Jl, D. J, K. Tr, P. Ab, R. Kj, D. B. Olsen, and W. J. Kolff, "A retrospective study of nine calves surviving five months on the pneumatic total artificial heart," *Transactions - American Society for Artificial Internal Organs*, vol. 27, no. NA, pp. 71–76, 1981.

[80] F. H, F. Iwaya, D. B. Olsen, J. H. Lawson, and W. J. Kolff, "Surgical implantation of the jarvik-5 total artificial heart in a calf," *Transactions - American Society for Artificial Internal Organs*, vol. 25, no. 1, pp. 232–238, 1979.

[81] A. T, T. H, and T. H, "Total artificial hearts with built-in valves," *Transactions - American Society for Artificial Internal Organs*, vol. 16, no. NA, pp. 392–397, 1970.

[82] H. T, K. Y, G. Wh, N. T, J. V. Cockrell, and T. Akutsu, "One 25 day survivor with total artificial heart," *The Journal of thoracic and cardiovascular surgery*, vol. 69, no. 1, pp. 92–101, 1975.

[83] M. Nakazono, K. Koiso, T. Komai, T. Agishi, J. Urzua, R. J. Kiraly, H. Kembic, R. Surovy, C. Carse, and Y. Nosé, "A case report of 17 days survival with an implanted artificial heart in a calf," *Japanese heart journal*, vol. 15, no. 5, pp. 485–497, 1974.

[84] S. Kasai, I. Koshino, T. Washizu, G. Jacobs, N. Morinaga, R. J. Kiraly, and Y. Nosé, "Survival for 145 days with a total artificial heart," *The Journal of thoracic and cardiovascular surgery*, vol. 73, no. 4, pp. 637–646, 1977.

[85] J. H. Kennedy, M. E. De Bakey, W. W. Akers, J. N. Ross, W. O'Bannon, L. E. Baker, S. D. Greenberg, D. W. Wieting, C. W. Lewis, M. Adachi, C. P. Alfrey, W. J. Spargo, W. F. Walker, and F. Jm, "Development of an orthotopic cardiac prosthesis," *The Journal of thoracic and cardiovascular surgery*, vol. 65, no. 5, pp. 673–683, 1973.

[86] D. K. Backman, D. Fm, G. M. Sandquist, T. Kessler, and W. J. Kolff, "The design and evaluation of ventricles for the aec artificial heart nuclear power source," *Transactions - American Society for Artificial Internal Organs*, vol. 19, no. 1, pp. 542–552, 1973.

[87] L. Smith, K. Backman, G. Sandquist, W. J. Kolff, K. Schatten, and T. Kessler, "Development on the implantation of a total nuclear-powered artificial heart system," *Trans Am Soc Artif Intern Organs*, vol. 20 b, pp. 732–5, 1974.

[88] J. Urzua, O. Sudilovsky, T. Panke, R. J. Kiraly, and Y. Nosé, "Anatomic constraints for the implantation of an artificial heart," *The Journal of surgical research*, vol. 17, no. 4, pp. 262–268, 1974.

[89] D. A. Cooley, A. T, J. C. Norman, S. Ma, and F. Oh, "Total artificial heart in two-staged cardiac transplantation," *Cardiovascular diseases*, vol. 8, no. 3, pp. 305–319, 1981.

[90] D. A. Cooley, "The total artificial heart," *Nature medicine*, vol. 9, no. 1, pp. 108–111, 2003.

[91] P. A. Smith, W. E. Cohn, and O. H. Frazier, *Chapter 7 Total artificial hearts*, vol. NA, pp. 221–244. Elsevier, 2018.

[92] S. Emmanuel, P. Jansz, D. C. McGiffin, C. Kure, A. Watson, M. Connellan, E. Granger, A. Iyer, D. Timms, and C. S. Hayward, "Anatomical human fitting of the bivacor total artificial heart," *Artificial organs*, vol. 46, no. 1, pp. 50–56, 2021.

[93] K. Fukamachi, J. H. Karimov, G. Sunagawa, D. J. Horvath, N. Byram, B. D. Kuban, R. Dessoffy, S. Sale, L. A. R. Golding, and N. Moazami, "Generating pulsatility by pump speed modulation with continuous-flow total artificial heart in awake calves," *Journal of artificial organs : the official journal of the Japanese Society for Artificial Organs*, vol. 20, no. 4, pp. 381–385, 2017.

[94] Y. Abe, T. Isoyama, I. Saito, Y. Inoue, K. Ishii, M. Sato, S. Hara, T. Yurimoto, X. Li, H. Murakami, K. Ariyoshi, Y. Kawase, T. Ono, K. Fukazawa, and K. Ishihara, "Animal experiments of the helical flow total artificial heart," *Artificial organs*, vol. 39, no. 8, pp. 670–680, 2015.

[95] J. J. Glynn, H. K. Song, B. Hull, S. Withers, J. M. Gelow, J. O. Mudd, A. Starr, and R. K. Wampler, "The oregonheart total artificial heart: Design and performance on a mock circulatory loop," *Artificial organs*, vol. 41, no. 10, pp. 904–910, 2017.

[96] I. L. Pieper, S. J. Sonntag, B. Meyns, H. Hadi, and A. Najar, "Evaluation of the novel total artificial heart realheart in a pilot human fitting study," *Artificial organs*, vol. 44, no. 2, pp. 174–177, 2019.

[97] M. J. Slepian, Y. Alemu, G. Girdhar, J. S. Soares, R. G. Smith, S. Einav, and D. Bluestein, "The syncardia total artificial heart: in vivo, in vitro, and computational modeling studies," *J Biomech*, vol. 46, no. 2, pp. 266–75, 2013.

[98] J. Vak and P. Urbanek, "Constructional and functional characteristics of recent total artificial heart models tns brno vii, viii, and ix," *Artificial organs*, vol. 19, no. 6, pp. 535–543, 1995.

[99] P. K. Davis, W. E. Pae, and W. S. Pierce, "Toward an implantable artificial heart experimental and clinical experience at the pennsylvania state university," *Investigative radiology*, vol. 24, no. 1, pp. 81–87, 1989.

[100] C.-H. Hsu, "Fuzzy logic automatic control of the phoenix-7 total artificial heart," *Journal of artificial organs : the official journal of the Japanese Society for Artificial Organs*, vol. 7, no. 2, pp. 69–76, 2004.

[101] C.-H. Hsu, "In vivo and clinical study of phoenix-7 total artificial heart," *Biomedical Engineering: Applications, Basis and Communications*, vol. 13, no. 03, pp. 133–139, 2001.

[102] V. I. Shumakov, N. K. Zimin, A. A. Drobyshev, M. N. Petukhova, S. V. Agafonov, and G. P. Itkin, "Use of an ellipsoid artificial heart," *Artificial organs*, vol. 11, no. 1, pp. 16–19, 1987.

[103] V. I. Shumakov, E. Tl, G. P. Itkin, E. S. Shtengol'd, V. A. Drobyshev, A. A. Drobyshev, and L. Z. Khazen, "New design of an orthotopic fluorosiloxane rubber heart prosthesis," *Biomedical Engineering*, vol. 10, no. 4, pp. 223–224, 1976.

[104] Nawrat and Malota, "The analysis of driving mode influence on energy dissipation in pneumatic artificial heart chambers," *Artificial organs*, vol. 22, no. 10, pp. 898–904, 1998.

[105] R. A, A. Laczkovics, A. Prodinger, W. Trubel, U. Losert, and E. Wolner, "The new small viennese total artificial heart: experimental and first clinical experiences," *Artificial organs*, vol. 15, no. 2, pp. 129–135, 1991.

[106] A. Homma, Y. Taenaka, E. Tatsumi, Y. Takewa, T. Mizuno, K. Shioya, H. S. Lee, T. Tsukiya, Y. Kakuta, N. Katagiri, T. Nishinaka, and K. Koshiji, "Development of an electrohydraulic total artificial heart system: Improvement of pump unit," *Electronics and Communications in Japan*, vol. 93, no. 9, pp. 34–46, 2010.

[107] B. J. Ford, "A new generation of cardiology," *Air medical journal*, vol. 22, no. 4, pp. 26–30, 2003.

[108] R. D. Dowling, L. A. Gray, S. W. Etoch, H. Laks, D. Marelli, L. E. Samuels, J. W. Entwistle, C. Gs, G. J. Vlahakes, and O. H. Frazier, "The abiocor implantable replacement heart," *The Annals of thoracic surgery*, vol. 75, no. 6, pp. S93–9, 2003.

[109] US Food and Drug Administration, "Syncardia temporary cardio west total artificial heart (tah-t)." `https://www.accessdata.fda.gov/scripts/cdrh/cfdocs/cfpma/pma.cfm?ID=P030011`, 2004. Accessed 10/8/2025.

[110] SynCardia Marketing Department, "Over 2,100 patients implanted with the syncardia total artificial heart." `https://www.syncardia.com/download/2100-press-announcement-nov-20-2024_final.pdf`, 2024. Accessed 10/8/2025.

[111] US National Library of Medicine, "Carmat tah early feasibility study." `https://clinicaltrials.gov/study/NCT04117295`, 2022. Accessed 10/8/2025.

[112] B. G. Min, H. C. Kim, S. H. Lee, J. W. Kim, J. Kim, I. Y. Kim, S. W. Kim, P. D. Diegel, and D. B. Olsen, "A moving-actuator type electromechanical total artificial heart. i. linear type and mock circulation experiments," *IEEE transactions on bio-medical engineering*, vol. 37, no. 12, pp. 1186–1194, 1990.

[113] B.-G. Min, H. C. Kim, J.-W. Choi, G. H. Ryu, K. P. Seo, J. R. Rho, H. Ahn, S. W. Kim, P. D. Diegel, and D. B. Olsen, "A moving-actuator type electromechanical total artificial heart. ii. circular type and animal experiment," *IEEE transactions on bio-medical engineering*, vol. 37, no. 12, pp. 1195–1200, 1990.

[114] J. M. Ahn, D. W. Kang, H. C. Kim, and B. G. Min, "In vivo performance evaluation of a transcutaneous energy and information transmission system for the total artificial heart," *ASAIO journal (American Society for Artificial Internal Organs : 1992)*, vol. 39, no. 3, pp. M208–12, 1993.

[115] Y. Ohashi, A. de Andrade, and Y. Nosé, "Hemolysis in an electromechanical driven pulsatile total artificial heart," *Artificial organs*, vol. 27, no. 12, pp. 1089–1093, 2003.

[116] S. Takatani, T. Sakamoto, K. Ohuchi, M. Nakamura, T. Mizuno, and H. Arai, "One piece ultracompact totally implantable electromechanical total artificial heart for permanent use," *ASAIO journal (American Society for Artificial Internal Organs : 1992)*, vol. 48, no. 5, pp. 538–545, 2002.

[117] M. Kleinheyer, D. Timms, G. Tansley, F. Nestler, N. Greatrex, O. H. Frazier, and W. E. Cohn, "Rapid speed modulation of a rotary total artificial heart impeller," *Artificial organs*, vol. 40, no. 9, pp. 824–833, 2016.

[118] N. Greatrex, M. Kleinheyer, F. Nestler, and D. L. Timms, "The maglev heart," *IEEE Spectrum*, vol. 56, no. 09, pp. 22–29, 2019.

[119] A. Stepanenko and F. Kaufmann, "A novel total artificial heart: search for haemocompatibility," *Lancet (London, England)*, vol. 386, no. 10003, pp. 1517–1519, 2015.

[120] T. Miyamoto, D. J. Horvath, D. W. Horvath, B. D. Kuban, K. Fukamachi, and J. H. Karimov, "Analysis of cleveland clinic continuous-flow total artificial heart performance using the virtual mock loop: Comparison with an in vivo study," *Artificial organs*, vol. 44, no. 4, pp. 375–383, 2019.

[121] H. Irie, A. Massiello, R. J. Kiraly, C. Jf, R. Crouch, K. Fukamachi, G. Jacobs, H. Harasaki, L. R. Golding, and D. Thomas, "Initial in vivo tests of an electrohydraulic actuated total artificial heart," *ASAIO journal (American Society for Artificial Internal Organs : 1992)*, vol. 38, no. 3, pp. M497–500, 1992.

[122] K. Fukamachi, P. M. McCarthy, R. L. Vargo, A. Massiello, J. F. Chen, B. P. Byerman, R. Kunitomo, T. Matsuyoshi, Y. Okazaki, R. J. Kiraly, K. C. Butler, and H. Harasaki, "Anatomic fitting studies of a total artificial heart in heart transplant recipients: Critical dimensions and prediction of fit," *ASAIO journal (American Society for Artificial Internal Organs : 1992)*, vol. 42, no. 5, pp. 6–42, 1996.

[123] M. Sueshiro, S. Fukunaga, S. Hirai, T. Sueda, and Y. Matsuura, "Eccentric roller type total artificial heart designed for implantation," *Artificial organs*, vol. 22, no. 6, pp. 451–457, 1998.

[124] T. Isoyama, K. Imachi, Y. Abe, T. Chinzei, K. Imanishi, K. Mabuchi, H. Matsuura, and I. Fujimasa, "New version of flowtransformed pulsatile total artificial heart with no electrical switching valve," *Artificial organs*, vol. 19, no. 7, pp. 694–696, 1995.

[125] C. S. Fox, S. G. Chopski, N. M. Murad, P. E. Allaire, R. M. Mentzer, J. W. Rossano, F. A. Arabia, and A. L. Throckmorton, "Hybrid continuous-flow total artificial heart," *Artificial organs*, vol. 42, no. 5, pp. 500–509, 2018.

[126] K. X. Qian, W. M. Ru, P. Zeng, and H. Y. Yuan, "A novel impeller tah using magnetic bearings for load reduction," *Journal of medical engineering technology*, vol. 26, no. 5, pp. 214–216, 2002.

[127] M. Kobayashi, H. Wakiwaka, M. Watanabe, H. Mizuno, M. Karita, M. Maeda, Y. Matsuura, S. Fukunaga, and H. Yamada, "In vitro evaluation of linear motor-driven total artificial heart," *Artificial organs*, vol. 20, no. 12, pp. 1320–1324, 1996.

[128] H. Yamada, M. Yamaguchi, K. Kobayashi, Y. Matsuura, and H. Takano, "Development and test of a linear motor-driven total artificial heart," *IEEE Engineering in Medicine and Biology Magazine*, vol. 14, no. 1, pp. 84–90, 1995.

[129] S. Weber, K. Kamohara, R. S. Klatte, V. Luangphakdy, C. Flick, J. F. Chen, F. Casas, Y. Ootaki, M. Kopcak, M. Akiyama, G. B. Hirschman, P. A. Chapman, A. Donahue, W. Wetterau, C. Prisco, R. Mast, C. Sherman, K. Fukamachi, and W. A. Smith, "Magscrew tah: an update," *Asaio j*, vol. 51, no. 6, pp. xxxvi–xlvi, 2005.

[130] H. Gao, L. M. Smith, M. G. Krymkowski, R. J. Kohl, D. H. Schmidt, and C. W. Christensen, "In vitro assessment of the milwaukee heart and right to left balance," *ASAIO journal (American Society for Artificial Internal Organs : 1992)*, vol. 38, no. 3, pp. M722–5, 1992.

[131] P. Jurney, J. J. Glynn, I. V. Dykan, M. W. Hagen, S. Kaul, R. K. Wampler, M. T. Hinds, and G. D. Giraud, "Characterization of a pulsatile rotary total artificial heart," *Artificial organs*, vol. 45, no. 2, pp. 135–142, 2020.

[132] I. M. Sauer, F. J, A. Spiegelberg, and B. Es, "Ovalis tah: development and in vitro testing of a new electromechanical energy converter for a total artificial heart," *ASAIO journal (American Society for Artificial Internal Organs : 1992)*, vol. 46, no. 6, pp. 744–748, 2000.

[133] S. M. Mehta, W. J. Weiss, A. J. Snyder, G. A. Prophet, W. E. Pae, G. Rosenberg, and W. S. Pierce, "Testing of a 50 cc stroke volume completely implantable artificial heart: Expanding chronic mechanical circulatory support to women, adolescents, and small stature men," *ASAIO journal (American Society for Artificial Internal Organs : 1992)*, vol. 46, no. 6, pp. 779–782, 2000.

[134] Z. Szabó, J. Holm, A. Najar, G. Hellers, I. L. Pieper, and H. C. Ahn, "Scandinavian real heart (srh) 11 implantation as total artificial heart (tah)-experimental update," *Journal of Clinical Experimental Cardiology*, vol. 9, no. 3, pp. 1–4, 2018.

[135] S. J. Sonntag, B. Meyns, H. C. Ahn, F. Pahlm, G. Hellers, A. Najar, and I. L. Pieper, "Virtual implantations to transition from porcine to bovine animal models for a total artificial heart," *Artificial organs*, vol. 44, no. 4, pp. 384–393, 2019.

[136] B. Pelletier, S. Spiliopoulos, T. Finocchiaro, F. Graef, K. Kuipers, M. Laumen, D. Guersoy, U. Steinseifer, R. Koerfer, and G. Tenderich, "System overview of the fully implantable destination therapy–reinheart-total artificial heart," *Eur J Cardiothorac Surg*, vol. 47, no. 1, pp. 80–6, 2015.

[137] P. Tozzi, A. Maertens, J. Emery, S. Joseph, M. Kirsch, and F. Avellan, "An original valveless artificial heart providing pulsatile flow tested in mock circulatory loops," *The International Journal of Artificial Organs*, vol. 40, no. 12, pp. 683–689, 2017.

[138] Y. Abe, T. Isoyama, I. Saito, W. Shi, Y. Inoue, K. Ishii, H. Nakagawa, T. Ono, M. Ono, and K. Imachi, "Results of animal experiments with the fourth model of the undulation pump total artificial heart," *Artificial organs*, vol. 35, no. 8, pp. 781–790, 2011.

[139] D. Mihaylov, G. J. Verkerke, and G. Rakhorst, "Mechanical circulatory support systemsa review," *Technology and health care : official journal of the European Society for Engineering and Medicine*, vol. 8, no. 5, pp. 251–266, 2000.

[140] J. K. Kirklin, F. D. Pagani, R. L. Kormos, L. W. Stevenson, E. D. Blume, S. L. Myers, M. A. Miller, J. T. Baldwin, J. B. Young, and D. C. Naftel, "Eighth annual intermacs report: Special focus on framing the impact of adverse events," *The Journal of heart and lung transplantation : the official publication of the International Society for Heart Transplantation*, vol. 36, no. 10, pp. 1080–1086, 2017.

[141] E. Potapov, F. Kaufmann, M. Müller, J. Mulzer, and V. Falk, "Longest ongoing support (13 years) with magnetically levitated left ventricular assist device," *ASAIO journal (American Society for Artificial Internal Organs : 1992)*, vol. 66, no. 9, pp. e121–e122, 2020.

[142] A. H. Healy, S. H. McKellar, S. G. Drakos, A. Koliopoulou, J. Stehlik, and C. H. Selzman, "Physiologic effects of continuous-flow left ventricular assist devices," *The Journal of surgical research*, vol. 202, no. 2, pp. 363–371, 2016.

[143] A. Bhimaraj, C. Uribe, and E. E. Suarez, "Physiological impact of continuous flow on end-organ function: clinical implications in the current era of left ventricular assist devices," *Methodist DeBakey cardiovascular journal*, vol. 11, no. 1, pp. 12–17, 2015.

[144] J. Feng, W. E. Cohn, S. M. Parnis, N. R. Sodha, R. T. Clements, N. Sellke, O. H. Frazier, and F. W. Sellke, "New continuous-flow total artificial heart and vascular permeability," *The Journal of surgical research*, vol. 199, no. 2, pp. 296–305, 2015.

[145] G. Lebreton, C. Mastroianni, J. Amour, and P. Leprince, "Implantation of two hvads used as a total artificial heart: A new approach," *The Annals of thoracic surgery*, vol. 107, no. 3, pp. e165–e167, 2018.

[146] M. S. Mulvihill, J. T. Joseph, M. A. Daneshmand, C. B. Patel, C. A. Milano, and J. N. Schroder, "Usefulness of 2 centrifugal ventricular assist devices in a total artificial heart configuration: A preliminary report," *The Journal of heart and lung transplantation : the official publication of the International Society for Heart Transplantation*, vol. 36, no. 11, pp. 1266–1268, 2017.

[147] W. E. Cohn, K. M. Handy, S. M. Parnis, J. L. Conger, J. A. Winkler, and O. H. Frazier, "Eight-year experience with a continuous-flow total artificial heart in calves," *ASAIO journal (American Society for Artificial Internal Organs : 1992)*, vol. 60, no. 1, pp. 25–30, 2014.

[148] J. Pirk, J. Maly, O. Szarszoi, M. Urban, T. Kotulák, H. Riha, P. Neuzil, and I. Netuka, "Total artificial heart support with two continuous-flow ventricular assist devices in a patient with an infiltrating cardiac sarcoma," *ASAIO journal (American Society for Artificial Internal Organs : 1992)*, vol. 59, no. 2, pp. 178–180, 2013.

[149] O. H. Frazier and W. E. Cohn, "Continuous-flow total heart replacement device implanted in a 55-year-old man with end-stage heart failure and severe amyloidosis," *Texas Heart Institute journal*, vol. 39, no. 4, pp. 542–546, 2012.

[150] M. Strueber, J. D. Schmitto, I. Kutschka, and A. Haverich, "Placement of 2 implantable centrifugal pumps to serve as a total artificial heart after cardiectomy," *The Journal of thoracic and cardiovascular surgery*, vol. 143, no. 2, pp. 507–509, 2012.

[151] O. H. Frazier, W. E. Cohn, E. Tuzun, J. A. Winkler, and I. D. Gregoric, "Continuous-flow total artificial heart supports long-term survival of a calf," *Texas Heart Institute journal*, vol. 36, no. 6, pp. 568–574, 2009.

[152] A. C. W. Baldwin, C. J. Gemmato, W. E. Cohn, and O. H. Frazier, "Feasibility of long-term continuous flow total heart replacement in calves," *The International journal of artificial organs*, vol. 45, no. 1, pp. 039139882098785–51, 2021.

[153] M. A. Daneshmand, M. Bishawi, C. A. Milano, and J. N. Schroder, "The heartmate 6," *ASAIO journal (American Society for Artificial Internal Organs : 1992)*, vol. 66, no. 3, pp. e46–e49, 2020.

[154] D. L. Franklin, R. L. Van Citters, and R. F. Rushmer, "Balance between right and left ventricular output," *Circulation research*, vol. 10, no. 1, pp. 17–26, 1962.

[155] S. Ley, K.-F. Kreitner, I. Morgenstern, M. Thelen, and H.-U. Kauczor, "Bronchopulmonary shunts in patients with chronic thromboembolic pulmonary hypertension: Evaluation with helical ct and mr imaging," *AJR. American journal of roentgenology*, vol. 179, no. 5, pp. 1209–1215, 2002.

[156] E. M. Baile, H. Ling, J. R. Heyworth, J. C. Hogg, and P. D. Paré, "Bronchopulmonary anastomotic and noncoronary collateral blood flow in humans during cardiopulmonary bypass," *Chest*, vol. 87, no. 6, pp. 749–754, 1985.

[157] S. K. Bhunia and R. T. Kung, "Indirect bronchial shunt flow measurements in abiocor implantable replacement heart recipients," *Asaio j*, vol. 50, no. 3, pp. 211–4, 2004.

[158] F. Nestler, D. Timms, M. C. Stevens, A. P. Bradley, S. J. Wilson, M. Kleinheyer, N. H. Lovell, O. H. Frazier, and W. E. Cohn, "Investigation of the inherent left-right flow balancing of rotary total artificial hearts by means of a resistance box," *Artificial organs*, vol. 44, no. 6, pp. 584–593, 2020.

[159] C. Latremouille, A. Carpentier, P. Leprince, J.-C. Roussel, B. Cholley, E. Boissier, E. Epailly, A. Capel, P. Jansen, and D. M. Smadja, "A bioprosthetic total artificial heart for end-stage heart failure: Results from a pilot study," *The Journal of heart and lung transplantation : the official publication of the International Society for Heart Transplantation*, vol. 37, no. 1, pp. 33–37, 2017.

[160] J. R. Crosby, K. J. DeCook, P. L. Tran, R. G. Smith, D. F. Larson, Z. Khalpey, D. Burkhoff, and M. J. Slepian, "Physiological characterization of the syncardia total artificial heart in a mock circulation system," *ASAIO journal (American Society for Artificial Internal Organs : 1992)*, vol. 61, no. 3, pp. 274–281, 2015.

[161] M. Diedrich, S. Hildebrand, M. K. Lommel, T. Finocchiaro, E. Cuenca, H. De Ben, T. Schmitz-Rode, U. Steinseifer, and S. V. Jansen, "Experimental investigation of rightleft flow balance concepts for a total artificial heart," *Artificial organs*, vol. 45, no. 4, pp. 364–372, 2020.

[162] D. J. Horvath, N. Byram, J. H. Karimov, B. D. Kuban, G. Sunagawa, L. A. R. Golding, N. Moazami, and K. Fukamachi, "Mechanism of self-regulation and in vivo performance of the cleveland clinic continuous-flow total artificial heart," *Artificial organs*, vol. 41, no. 5, pp. 411–417, 2016.

[163] R. T. V. Kung, L. S. Yu, B. Ochs, S. M. Parnis, M. Mp, and O. H. Frazier, "Progress in the development of the abiomed total artificial heart," *ASAIO journal (American Society for Artificial Internal Organs : 1992)*, vol. 41, no. 3, pp. M245–8, 1995.

[164] H. Harasaki, K. Fukamachi, A. Massiello, J.-F. Chen, S. C. Himley, F. Fukumura, K. Muramoto, S. Niu, K. E. Wika, C. R. Davies, P. M. McCarthy, R. J. Kiraly, D. Thomas, T. C. Rintoul, J. Carriker, T. R. Maher, and K. C. Butler, "Progress in cleveland clinic-nimbus total artificial heart development," *ASAIO journal (American Society for Artificial Internal Organs : 1992)*, vol. 40, no. 3, pp. M494–8, 1994.

[165] H. C. Kim, P. Khanwilkar, G. B. Bearnson, and D. B. Olsen, "Development of a microcontroller-based automatic control system for the electrohydraulic total artificial heart," *IEEE transactions on bio-medical engineering*, vol. 44, no. 1, pp. 77–89, 1997.

[166] A. J. Snyder, G. Rosenberg, J. D. Reibson, J. H. Donachy, G. A. Prophet, J. D. Arenas, B. Daily, S. McGary, O. Kawaguchi, R. D. Quinn, and W. S. Pierce, "An electrically powered total artificial heart. over 1 year survival in the calf," *ASAIO journal (American Society for Artificial Internal Organs : 1992)*, vol. 38, no. 3, pp. M707–12, 1992.

[167] Y. Abe, T. Chinzei, T. Isoyama, T. Ono, S. Mochizuki, I. Saito, K. Iwasaki, M. Ishimaru, A. Baba, A. Kouno, T. Ozeki, T. Tohyama, and K. Imachi, "Third model of the undulation pump total artificial heart," *ASAIO journal (American Society for Artificial Internal Organs : 1992)*, vol. 49, no. 1, pp. 123–127, 2003.

[168] R. D. Dowling, S. W. Etoch, K. Stevens, A. R. T. Butterfield, S. E. Koenig, A. M. Y. Johnson, B. Chiang, and L. A. Gray, "Initial experience with the abiocor implantable replacement heart at the university of louisville," *ASAIO journal (American Society for Artificial Internal Organs : 1992)*, vol. 46, no. 5, pp. 579–581, 2000.

[169] C. Latremouille, D. Duveau, B. Cholley, L. Zilberstein, G. Belbis, M.-F. Boughenou, D. Méléard, P. Bruneval, C. Adam, A. Neuschwander, J.-C. Perlès, P. Jansen, and A. Carpentier, "Animal studies with the carmat bioprosthetic total artificial heart," *European journal of cardio-thoracic surgery : official journal of the European Association for Cardio-thoracic Surgery*, vol. 47, no. 5, pp. e172–8; discussion e178, 2015.

[170] J. Vak, C. J, U. E, D. M, P. Urbánek, G. P, N. A. Pavlícek, S. T, S. M, T. Úlehla, B. Hartmannová, N. A. Trbusek, J. H, O. otolová, E. otáková, W. P, S. Doleel, J. Filkuka, G. Z, B. Bednaík, and P. Svoboda, "A comparative study of a group of eight calves, surviving longer than 1 month with the total artificial heart," *Artificial organs*, vol. 7, no. 4, pp. 470–478, 1983.

[171] J. Vak, U. P, and M. Dostál, "The applicability of experimental experience with the total artificial heart to its clinical use," *The International journal of artificial organs*, vol. 15, no. 5, pp. 307–311, 1992.

[172] V. I. Shumakov, N. K. Zimin, E. Kazakov, A. I. Kormer, S. Vorontsov, E. Nikolaenko, K. Ia, and A. A. Drobyshev, "Clinical indications for the use of the "poisk-iom" total artificial heart: the experience of 13 implantations in humans," *Artificial organs*, vol. 15, no. 5, pp. 372–375, 1991.

[173] J. Wei, K. K. Cheng, D. Y. Tung, C. Y. Chang, W. M. Wan, and Y. C. Chuang, "Successful use of phoenix-7 total artificial heart," *Transplantation proceedings*, vol. 30, no. 7, pp. 3403–3404, 1998.

[174] W. Trubel, H. Schima, A. Rokitansky, M. R. Müller, U. Losert, and E. Wolner, "Clinical total artificial heart bridging: Viennese strategy and experiences," *Artificial organs*, vol. 13, no. 5, pp. 470–475, 1989.

[175] O. H. Frazier, R. D. Dowling, L. A. Gray, N. Shah, T. Pool, and I. D. Gregoric, "The total artificial heart: Where we stand," *Cardiology*, vol. 101, no. 1-3, pp. 117–121, 2004.

[176] S. M. Parnis, L.-S. Yu, B. Ochs, M. Mp, O. H. Frazier, and R. T. V. Kung, "Chronic in vivo evaluation of an electrohydraulic total artificial heart," *ASAIO journal (American Society for Artificial Internal Organs : 1992)*, vol. 40, no. 3, pp. M489–93, 1994.

[177] R. D. Dowling, S. W. Etoch, K. A. Stevens, A. C. Johnson, and L. A. Gray, "Current status of the abiocor implantable replacement heart," *The Annals of thoracic surgery*, vol. 71, no. 3, pp. S147–9; discussion S183, 2001.

[178] S. Takatani, Y. Orime, K. Tasai, Y. Ohara, K. Naito, K. Mizuguchi, K. Makinouchi, G. Damm, and J. Glueck, "Totally implantable total artificial heart and ventricular assist device with multipurpose miniature electromechanical energy system," *Artificial organs*, vol. 18, no. 1, pp. 80–92, 1994.

[179] S. Takatani, M. Shiono, T. Sasaki, Y. Orime, I. Sakuma, G. P. Noon, Y. Nosé, and M. E. DeBakey, "Left and right pump output control in one-piece electromechanical total artificial heart," *Artificial organs*, vol. 17, no. 3, pp. 176–184, 1993.

[180] W. E. Cohn, F. A. Arabia, D. L. Timms, N. Greatrex, M. Kleinheyer, F. Nestler, S. Diab, and O. H. Frazier, "Pulsatile outflow in cows supported long-term with the bivacor rotary tah," *The Journal of Heart and Lung Transplantation*, vol. 36, no. 4, pp. S14–NA, 2017.

[181] M. Dostál, J. Vask, J. Cerný, O. Sotolová, P. Guba, J. Vask, P. Urbánek, V. Pavlícek, A. Vask, J. Necas, and et al., "Hematological and biochemical studies in calves living over 100 days with the polymethylmethacrylate total artificial heart tns brno ii," *Int J Artif Organs*, vol. 9, no. 1, pp. 39–48, 1986.

[182] J. Vasku, J. Cerný, M. Dostál, P. Urbánek, J. Vask, P. Guba, J. Petrzilka, M. Smutný, O. Sotolová, and S. Dolezel, "Recent efforts in artificial heart research in czechoslovakia," *ASAIO transactions*, vol. 35, no. 4, pp. 805–811, 1989.

[183] D. M. Smadja, S. Susen, A. Rauch, B. Cholley, C. Latremouille, D. Duveau, L. Zilberstein, D. Méléard, M.-F. Boughenou, E. Van Belle, P. Gaussem, A. Capel, P. Jansen, and A. Carpentier, "The carmat bioprosthetic total artificial heart is associated with early hemostatic recovery and no acquired von willebrand syndrome in calves," *Journal of cardiothoracic and vascular anesthesia*, vol. 31, no. 5, pp. 1595–1602, 2017.

[184] J. H. Karimov, N. Moazami, M. Kobayashi, S. Sale, K. A. Such, N. Byram, G. Sunagawa, D. J. Horvath, S. Gao, B. D. Kuban, L. A. R. Golding, and K. Fukamachi, "First report of 90-day support of 2 calves with a continuous-flow total artificial heart," *The Journal of thoracic and cardiovascular surgery*, vol. 150, no. 3, pp. 687–693, 2015.

[185] Y. Taenaka, T. Masuzawa, T. F, H. Anai, K. Toda, H. Akagi, T. Nakatani, Y. Baba, F. K, and Y. Wakisaka, "Development and evaluation of components for a totally implantable artificial heart system," *ASAIO journal (American Society for Artificial Internal Organs : 1992)*, vol. 40, no. 3, pp. M314–8, 1994.

[186] Y. Taenaka, H. Sekii, E. Tatsumi, T. Nakatani, S. E, A. Yagura, H. Akagi, T. Masuzawa, M. Goto, and Y. Matsuo, "An electrohydraulic total artificial heart with a separately placed actuator," *ASAIO transactions*, vol. 36, no. 3, pp. M242–5, 1990.

[187] E. Tatsumi, P. D. Diegel, J. W. Holfert, D. Pa, C. Kr, A. C. Hansen, P. S. Khanwilkar, J. R. Rowles, and D. B. Olsen, "A blood pump with an interatrial shunt for use as an electrohydraulic total artificial heart," *ASAIO journal (American Society for Artificial Internal Organs : 1992)*, vol. 38, no. 3, pp. M425–30, 1992.

[188] E. Tatsumi, Y. Taenaka, A. Homma, T. Nishinaka, Y. Takewa, T. Tsukiya, H. Ohnishi, M. Oshikawa, Y. Shirakawa, Y. Kakuta, K. Shioya, N. Katagiri, T. Mizuno, T. Kamimura, H. Takano, K. Tsukahara, K. Tsuchimoto, H. Wakui, and H. Yamaguchi, "The national cardiovascular center electrohydraulic total artificial heart and ventricular assist device systems : Current status of development," *ASAIO journal (American Society for Artificial Internal Organs : 1992)*, vol. 49, no. 3, pp. 243–249, 2003.

[189] E. Tatsumi, Y. Taenaka, K. Uesho, A. Homma, T. Nishinaka, Y. Kakuta, T. Tsukiya, H. Takano, T. Masuzawa, M. Nakamura, K. Koshiji, Y. Fukui, K. Tsukahara, K. Tsuchimoto, and H. Wakui, "Current status of development and in vivo evaluation of the national cardiovascular center electrohydraulic total artificial heart system," *Journal of Artificial Organs*, vol. 3, no. 2, pp. 62–69, 2000.

[190] K. Doi, W. A. Smith, H. Harasaki, M. Takagaki, Y. Ochiai, M. W. Howard, S. Weber, B. P. Byerman, A. Massiello, N. Vitale, A. Donahue, G. B. Hirschman, and K. Fukamachi, "In vivo studies of the magscrew total artificial heart in calves," *ASAIO journal (American Society for Artificial Internal Organs : 1992)*, vol. 48, no. 3, pp. 222–225, 2002.

[191] H. Kuroda, G. Rosenberg, A. J. Snyder, W. J. Weiss, M. Rawhouser, G. A. Prophet, E. Stephenson, W. J. Pae, and W. S. Pierce, "Postoperative pulmonary complications in calves after implantation of an electric total artificial heart," *ASAIO journal (American Society for Artificial Internal Organs : 1992)*, vol. 44, no. 5, pp. M613–8, 1998.

[192] W. S. Pierce, G. Rosenberg, A. J. Snyder, W. E. Pae, J. H. Donachy, and J. A. Waldhausen, "An electric artificial heart for clinical use," *Annals of surgery*, vol. 212, no. 3, pp. 339–344, 1990.

[193] A. J. Snyder, G. Rosenberg, W. J. Weiss, S. Ford, R. A. Nazarian, H. Dl, J. A. Marlotte, O. Kawaguchi, G. A. Prophet, and J. S. Sapirstein, "In vivo testing of a completely implanted total artificial heart system," *ASAIO journal (American Society for Artificial Internal Organs : 1992)*, vol. 39, no. 3, pp. M177–84, 1993.

[194] L. J. Shaffer, J. H. Donachy, G. Rosenberg, P. Wm, D. L. Landis, G. A. Prophet, E. K. Olsen, J. A. Arrowood, and W. S. Pierce, "Total artificial heart implantation in calves with pump of an angled port design," *Transactions - American Society for Artificial Internal Organs*, vol. 25, no. 1, pp. 254–259, 1979.

[195] Y. Abe, T. Isoyama, I. Saito, S. Mochizuki, M. Ono, H. Nakagawa, N. Taniguchi, N. Mitsumune, A. Sugino, M. Mitsui, K. Takiura, T. Ono, A. Kouno, T. Chinzei, S. Takamoto, and K. Imachi, "Development of mechanical circulatory support devices at the university of tokyo," *Journal of artificial organs : the official journal of the Japanese Society for Artificial Organs*, vol. 10, no. 2, pp. 60–70, 2007.

[196] S. Mochizuki, Y. Abe, T. Chinzei, T. Isoyama, T. Ono, I. Saito, G. P, T. Karita, Y. P. Sun, A. Kouno, T. Suzuki, K. Baba, K. Mabuchi, and K. Imachi, "Results of animal experiments using an undulation pump total artificial heart: analysis of 10 day and 19

day survival," *ASAIO journal (American Society for Artificial Internal Organs : 1992)*, vol. 46, no. 4, pp. 500–504, 2000.

[197] C. Latrémouille, A. Carpentier, P. Leprince, J.-C. Roussel, B. Cholley, E. Boissier, E. Epailly, A. Capel, P. Jansen, and D. M. Smadja, "A bioprosthetic total artificial heart for end-stage heart failure: Results from a pilot study," *The Journal of Heart and Lung Transplantation*, vol. 37, no. 1, pp. 33–37, 2018.

[198] I. Netuka, Y. Pya, M. Bekbossynova, P. Ivak, M. Konarik, F. Gustafsson, D. M. Smadja, P. Jansen, and C. Latremouille, "Initial bridge to transplant experience with a bioprosthetic autoregulated artificial heart," *The Journal of heart and lung transplantation : the official publication of the International Society for Heart Transplantation*, vol. 39, no. 12, pp. 1491–1493, 2020.

[199] M. Carrier, J. Moriguchi, K. B. Shah, A. C. Anyanwu, C. Mahr, E. Skipper, M. Cossette, and P. E. Noly, "Outcomes after heart transplantation and total artificial heart implantation: A multicenter study," *J Heart Lung Transplant*, vol. 40, no. 3, pp. 220–228, 2021.

[200] M. Hulman, P. Artemiou, V. Hudec, I. Olejárová, and E. Goncalvesova, "Syncardia, total artificial heart, as a bridge to transplant," *Bratislavske lekarske listy*, vol. 120, no. 5, pp. 325–330, 2019.

[201] A. Nguyen, M. Pellerin, L. P. Perrault, M. White, A. Ducharme, N. Racine, and M. Carrier, "Experience with the syncardia total artificial heart in a canadian centre," *Canadian journal of surgery. Journal canadien de chirurgie*, vol. 60, no. 6, pp. 375–379, 2017.

[202] M. Kirsch, A. Nguyen, C. Mastroianni, M. Pozzi, P. Léger, M. Nicolescu, S. Varnous, A. Pavie, and P. Leprince, "Syncardia temporary total artificial heart as bridge to transplantation: Current results at la pitié hospital," *The Annals of thoracic surgery*, vol. 95, no. 5, pp. 1640–1646, 2013.

[203] J. G. Copeland, H. Copeland, M. Gustafson, N. Mineburg, D. Covington, R. G. Smith, and M. Friedman, "Experience with more than 100 total artificial heart implants," *The Journal of thoracic and cardiovascular surgery*, vol. 143, no. 3, pp. 727–734, 2012.

[204] J. C. Roussel, T. Senage, O. Baron, C. Perigaud, O. Al Habash, J. C. Rigal, M. Treilhaud, J. N. Trochu, P. Despins, and D. Duveau, "Cardiowest (jarvik) total artificial heart: a single-center experience with 42 patients," *The Annals of thoracic surgery*, vol. 87, no. 1, pp. 124–130, 2009.

[205] A. El-Banayosy, L. Arusoglu, M. Morshuis, L. Kizner, G. Tenderich, P. Sarnowski, H. Milting, and R. Koerfer, "Cardiowest total artificial heart: Bad oeynhausen experience," *The Annals of thoracic surgery*, vol. 80, no. 2, pp. 548–552, 2005.

[206] K. L. Thanavaro, D. G. Tang, V. Kasirajan, and K. B. Shah, "Clinical indications for implantation of the total artificial heart," *ASAIO journal (American Society for Artificial Internal Organs : 1992)*, vol. 60, no. 5, pp. 594–596, 2014.

[207] Carmat, Inc, "Carmat. carmat outlines commercial and development plan for its total artificial heart." https://www.carmatsa.com/carmat-content/uploads/2021/01/pr_carmat_conference_06-01-21.pdf, 2021. Accessed 10/8/2025.

[208] M. Alaeddine, M. Ploutz, F. A. Arabia, and D. A. Velez, "Implantation of total artificial heart in a 10-year-old after support with a temporary perventricular assist device," *The Journal of thoracic and cardiovascular surgery*, vol. 159, no. 3, pp. e227–e229, 2019.

[209] C. H. David, P. Lacoste, P. Nanjaiah, P. Bizouarn, T. Lepoivre, M. Michel, S. Pattier, C. Toquet, C. Périgaud, A. Mugniot, O. Al Habash, T. Petit, N. Groleau, B. Rozec, J. N. Trochu, J. C. Roussel, and T. Sénage, "A heart transplant after total artificial heart support: initial and long-term results," *Eur J Cardiothorac Surg*, vol. 58, no. 6, pp. 1175–1181, 2020.

[210] K. Unthan, F. Gräf, M. Laumen, T. Finocchiaro, C. Sommer, H. Lanmüller, and U. Steinseifer, "Design and evaluation of a fully implantable control unit for blood pumps," *BioMed research international*, vol. 2015, no. NA, pp. 257848–257848, 2015.

[211] E. Marieb and K. Hoehn, *Human Anatomy Physiology Global Edition*. Pearson Deutschland, 2018.

[212] R. K. Wampler, J. Glynn, S. Withers, B. Hull, M. S. Slaughter, A. Starr, and H. K. Song, "(124) - performance of a novel shuttling total artificial heart on a on a mock circulatory loop," *The Journal of Heart and Lung Transplantation*, vol. 36, no. 4, pp. S56–S57, 2017.

[213] L.-S. Yu, M. Finnegan, S. Vaughan, B. Ochs, S. M. Parnis, O. H. Frazier, and R. T. V. Kung, "A compact and noise free electrohydraulic total artificial heart," *ASAIO journal (American Society for Artificial Internal Organs : 1992)*, vol. 39, no. 3, pp. M386–91, 1993.

[214] G. Rosenberg, A. J. Snyder, W. J. Weiss, H. Kusagawa, M. Rawhouser, G. A. Prophet, S. M. Mehta, J. D. Reibson, and T. J. Cleary, "Dynamic in vitro and in vivo performance of a permanent total artificial heart," *Artificial organs*, vol. 22, no. 1, pp. 87–94, 1998.

[215] J. Kluin, H. Talacua, A. I. Smits, M. Y. Emmert, M. C. Brugmans, E. S. Fioretta, P. E. Dijkman, S. H. Söntjens, R. Duijvelshoff, S. Dekker, M. W. Janssen-van den Broek, V. Lintas, A. Vink, S. P. Hoerstrup, H. M. Janssen, P. Y. Dankers, F. P. Baaijens, and C. V. Bouten, "In situ heart valve tissue engineering using a bioresorbable elastomeric implant - from material design to 12 months follow-up in sheep," *Biomaterials*, vol. 125, pp. 101–117, 2017.

[216] P. Zilla, M. Deutsch, D. Bezuidenhout, N. H. Davies, and T. Pennel, "Progressive reinvention or destination lost? half a century of cardiovascular tissue engineering," *Frontiers in cardiovascular medicine*, vol. 7, no. NA, pp. 159–159, 2020.

[217] Z. Chen, J. Zhang, K. Kareem, D. Tran, R. G. Conway, K. Arias, B. P. Griffith, and Z. J. Wu, "Device-induced platelet dysfunction in mechanically assisted circulation increases the risks of thrombosis and bleeding," *Artif Organs*, vol. 43, no. 8, pp. 745–755, 2019.

[218] A. S. Zaiser, G. Fahrni, A. Hollinger, D. T. Knobel, Y. Bovey, N. Zellweger, A. Buser, D. Santer, H. Pargger, C. E. Gebhard, and M. Siegemund, "Adverse events of percutaneous microaxial left ventricular assist devicesa retrospective, single-centre cohort study," *Journal of clinical medicine*, vol. 10, no. 16, pp. 3710–NA, 2021.

[219] M. Arfaee, A. Vis, P. A. A. Bartels, L. C. van Laake, L. Lorenzon, D. M. Ibrahim, D. Zrinscak, A. I. P. M. Smits, A. Henseler, M. Cianchetti, P. Y. W. Dankers, C. V. C. Bouten, J. T. B. Overvelde, and J. Kluin, "A soft robotic total artificial hybrid heart," *Nature Communications*, vol. 16, no. 1, p. 5146, 2025.

[220] H. Banerjee, Z. T. H. Tse, and H. Ren, "Soft robotics with compliance and adaptation for biomedical applications and forthcoming challenges," *International Journal of Robotics and Automation*, vol. 33, no. 1, pp. NA–NA, 2018.

[221] Y. Yang, Y. Wu, C. Li, X. Yang, and W. Chen, "Flexible actuators for soft robotics," *Advanced Intelligent Systems*, vol. 2, no. 1, p. 1900077, 2020.

[222] M. Zhu, T. N. Do, E. Hawkes, and Y. Visell, "Fluidic fabric muscle sheets for wearable and soft robotics," *Soft Robotics*, vol. 7, no. 2, pp. 179–197, 2020.

[223] J. J. Huaroto, E. Suarez, H. I. Krebs, P. D. Marasco, and E. A. Vela, "A soft pneumatic actuator as a haptic wearable device for upper limb amputees: Toward a soft robotic liner," *IEEE Robotics and Automation Letters*, vol. 4, no. 1, pp. 17–24, 2019.

[224] D. Copaci, E. Cano, L. Moreno, and D. Blanco, "New design of a soft robotics wearable elbow exoskeleton based on shape memory alloy wire actuators," *Applied Bionics and Biomechanics*, vol. 2017, p. 1605101, 2017.

[225] A. A. Amiri Moghadam, S.-J. Jang, A. Caprio, J. Liu, H. S. Singh, J. K. Min, S. Dunham, and B. Mosadegh, "Using soft robotic technology to fabricate a proof-of-concept transcatheter tricuspid valve replacement (ttvr) device," *Advanced Materials Technologies*, vol. 4, no. 4, p. 1800610, 2019.

[226] M. Arfaee, A. Vis, and J. Kluin, "Future technologies in total artificial heart development: can a robot become as good as a donor heart?," *European heart journal*, vol. 43, no. 48, pp. 4970–4972, 2022.

[227] A. Pagoli, F. Chapelle, J.-A. Corrales-Ramon, Y. Mezouar, and Y. Lapusta, "Review of soft fluidic actuators: classification and materials modeling analysis," *Smart Materials and Structures*, vol. 31, no. 1, p. 013001, 2022.

[228] S. Li, J. Lin, H. Kang, Y. Cheng, and Y. Chen, "Bio-inspired origamic pouch motors with a high contraction ratio and enhanced force output," *Robotics and Autonomous Systems*, vol. 149, p. 103983, 2022.

[229] N. El-Atab, R. B. Mishra, F. Al-Modaf, L. Joharji, A. A. Alsharif, H. Alamoudi, M. Diaz, N. Qaiser, and M. M. Hussain, "Soft actuators for soft robotic applications: A review," *Advanced Intelligent Systems*, vol. 2, no. 10, pp. NA–NA, 2020.

[230] R. Niiyama, X. Sun, C. Sung, B. An, D. Rus, and S. Kim, "Pouch motors: Printable soft actuators integrated with computational design," *Soft Robotics*, vol. 2, no. 2, pp. 59–70, 2015.

[231] K. Narumi, H. Sato, K. Nakahara, Y. a. Seong, K. Morinaga, Y. Kakehi, R. Niiyama, and Y. Kawahara, "Liquid pouch motors: Printable planar actuators driven by liquid-to-gas phase change for shape-changing interfaces," *IEEE Robotics and Automation Letters*, vol. 5, no. 3, pp. 3915–3922, 2020.

[232] N. Oh, Y. J. Park, S. Lee, H. Lee, and H. Rodrigue, "Design of paired pouch motors for robotic applications," *Advanced Materials Technologies*, vol. 4, no. 1, p. 1800414, 2019.

[233] J. T. . Overvelde, D. M. . Dykstra, R. de Rooij, J. Weaver, and K. Bertoldi, "Tensile instability in a thick elastic body," *Physical Review Letters*, vol. 117, no. 9, p. 094301, 2016.

[234] H. Sugihardjo, T. Tavio, and Y. Lesmana, "Fe model of low grade rubber for modeling housings low-cost rubber base isolators," *Civil Engineering Journal*, vol. 4, no. 1, pp. 24–45, 2018.

[235] M. Vaduganathan, G. A. Mensah, J. V. Turco, V. Fuster, and G. A. Roth, "The global burden of cardiovascular diseases and risk," *Journal of the American College of Cardiology*, vol. 80, no. 25, pp. 2361–2371, 2022.

[236] A. Vis, M. Arfaee, H. Khambati, M. S. Slaughter, J. F. Gummert, J. T. B. Overvelde, and J. Kluin, "The ongoing quest for the first total artificial heart as destination therapy," *Nature Reviews Cardiology*, vol. 19, no. 12, pp. 813–828, 2022.

[237] A. Carpentier, C. Latrémouille, B. Cholley, D. M. Smadja, J.-C. Roussel, E. Boissier, J.-N. Trochu, J.-P. Gueffet, M. Treillot, P. Bizouarn, D. Méléard, M.-F. Boughenou, O. Ponzio, M. Grimmé, A. Capel, P. Jansen, A. Hagège, M. Desnos, J.-N. Fabiani, and D. Duveau, "First clinical use of a bioprosthetic total artificial heart: report of two cases," *The Lancet*, vol. 386, no. 10003, pp. 1556–1563, 2015.

[238] P. Capsi-Morales, C. Piazza, M. G. Catalano, G. Grioli, L. Schiavon, E. Fiaschi, and A. Bicchi, "Comparison between rigid and soft poly-articulated prosthetic hands in non-expert myo-electric users shows advantages of soft robotics," *Scientific Reports*, vol. 11, no. 1, p. 23952, 2021.

[239] H. K. Yap, J. H. Lim, F. Nasrallah, and C.-H. Yeow, "Design and preliminary feasibility study of a soft robotic glove for hand function assistance in stroke survivors," *Frontiers in Neuroscience*, vol. 11, 2017.

[240] L. Paternò and L. Lorenzon, "Soft robotics in wearable and implantable medical applications: Translational challenges and future outlooks," *Frontiers in Robotics and AI*, vol. 10, 2023.

[241] T. S. Hakky, R. Wang, and G. D. Henry, "The evolution of the inflatable penile prosthetic device and surgical innovations with anatomical considerations," *Current Urology Reports*, vol. 15, no. 6, p. 410, 2014.

[242] A. Weymann, J. Foroughi, R. Vardanyan, P. P. Punjabi, B. Schmack, S. Aloko, G. M. Spinks, C. H. Wang, A. Arjomandi Rad, and A. Ruhparwar, "Artificial muscles and soft robotic devices for treatment of end-stage heart failure," *Advanced Materials*, vol. 35, no. 19, p. 2207390, 2023.

[243] E. T. Roche, R. Wohlfarth, J. T. B. Overvelde, N. V. Vasilyev, F. A. Pigula, D. J. Mooney, K. Bertoldi, and C. J. Walsh, "A bioinspired soft actuated material," *Advanced Materials*, vol. 26, no. 8, pp. 1200–1206, 2014.

[244] M. A. Horvath, I. Wamala, E. Rytkin, E. Doyle, C. J. Payne, T. Thalhofer, I. Berra, A. Solovyeva, M. Saeed, S. Hendren, E. T. Roche, P. J. del Nido, C. J. Walsh, and N. V. Vasilyev, "An intracardiac soft robotic device for augmentation of blood ejection from the failing right ventricle," *Annals of Biomedical Engineering*, vol. 45, no. 9, pp. 2222–2233, 2017.

[245] C. J. Payne, I. Wamala, C. Abah, T. Thalhofer, M. Saeed, D. Bautista-Salinas, M. A. Horvath, N. V. Vasilyev, E. T. Roche, F. A. Pigula, and C. J. Walsh, "An implantable extracardiac soft robotic device for the failing heart: Mechanical coupling and synchronization," *Soft Robotics*, vol. 4, no. 3, pp. 241–250, 2017.

[246] C. J. Payne, I. Wamala, D. Bautista-Salinas, M. Saeed, D. Van Story, T. Thalhofer, M. A. Horvath, C. Abah, P. J. del Nido, C. J. Walsh, and N. V. Vasilyev, "Soft robotic ventricular assist device with septal bracing for therapy of heart failure," *Science Robotics*, vol. 2, no. 12, p. eaan6736, 2017.

[247] D. K. Molina and V. J. DiMaio, "Normal organ weights in men: part i-the heart," *Am J Forensic Med Pathol*, vol. 33, no. 4, pp. 362–7, 2012.

[248] A. G. Gheorghe, A. Fuchs, C. Jacobsen, K. F. Kofoed, R. Møgelvang, N. Lynnerup, and J. Banner, "Cardiac left ventricular myocardial tissue density, evaluated by computed tomography and autopsy," *BMC Med Imaging*, vol. 19, no. 1, p. 29, 2019.

[249] A. M. Maceira, S. K. Prasad, M. Khan, and D. J. Pennell, "Normalized left ventricular systolic and diastolic function by steady state free precession cardiovascular magnetic resonance," *J Cardiovasc Magn Reson*, vol. 8, no. 3, pp. 417–26, 2006.

[250] A. M. Maceira, S. K. Prasad, M. Khan, and D. J. Pennell, "Reference right ventricular systolic and diastolic function normalized to age, gender and body surface area from steady-state free precession cardiovascular magnetic resonance," *Eur Heart J*, vol. 27, no. 23, pp. 2879–88, 2006.

[251] M. Arfaee, J. Kluin, and J. T. B. Overvelde, "Modeling the behavior of elastic pouch motors," in *2023 IEEE International Conference on Soft Robotics (RoboSoft)*, pp. 1–6, 2023.

[252] X. Wang, S. K. Mitchell, E. H. Rumley, P. Rothemund, and C. Keplinger, "High-strain peano-hasel actuators," *Advanced Functional Materials*, vol. 30, no. 7, p. 1908821, 2020.

[253] D. Sidebotham and I. J. Le Grice, "Physiology and pathophysiology," *Cardiothoracic critical care*, pp. 3–27, 2007.

[254] M. Ragosta and J. L. W. Kennedy, *Chapter 2 - Normal Waveforms, Artifacts, and Pitfalls*, pp. 17–55. Elsevier, 2018.

[255] G. Liljestrand, E. Lysholm, G. Nylin, and C. G. Zachrisson, "The normal heart volume in man," *American Heart Journal*, vol. 17, no. 4, pp. 406–415, 1939.

[256] D. Bamira and M. H. Picard, "Imaging: Echocardiology–assessment of cardiac structure and function." https://api.semanticscholar.org/CorpusID:80169033, 2018. Accessed 10/8/2025.

[257] C. Institute of Medicine Committee on Social Security Cardiovascular Disability. Washington (DC): National Academies Press (US) Copyright 2010 by the National Academy of Sciences. All rights reserved., 2010.

[258] A. Corsini, L. Cercenelli, M. Zecchi, E. Marcelli, and I. Corazza, *Chapter 30 - Basic Hemodynamic Parameters*, pp. 463–474. Academic Press, 2022.

[259] E. M. Lau, L. Godinas, O. Sitbon, D. Montani, L. Savale, X. Jaïs, F. Lador, S. Gunther, D. S. Celermajer, G. Simonneau, M. Humbert, D. Chemla, and P. Herve, "Resting pulmonary artery pressure of 21-24mmhg predicts abnormal exercise haemodynamics," *Eur Respir J*, vol. 47, no. 5, pp. 1436–44, 2016.

[260] N. L. Bragazzi, W. Zhong, J. Shu, A. Abu Much, D. Lotan, A. Grupper, A. Younis, and H. Dai, "Burden of heart failure and underlying causes in 195 countries and territories from 1990 to 2017," *European Journal of Preventive Cardiology*, vol. 28, no. 15, pp. 1682–1690, 2021.

[261] R. Tatum, A. Briasoulis, V. Tchantchaleishvili, and H. T. Massey, "Evaluation of donor heart for transplantation," *Heart Fail Rev*, vol. 27, no. 5, pp. 1819–1827, 2022.

[262] C. W. Tsao, A. W. Aday, Z. I. Almarzooq, A. Alonso, A. Z. Beaton, M. S. Bittencourt, A. K. Boehme, A. E. Buxton, A. P. Carson, Y. Commodore-Mensah, M. S. Elkind, K. R. Evenson, C. Eze-Nliam, J. F. Ferguson, G. Generoso, J. E. Ho, R. Kalani, S. S. Khan, B. M. Kissela, K. L. Knutson, D. A. Levine, T. T. Lewis, J. Liu, M. S. Loop, J. Ma, M. E. Mussolino, S. D. Navaneethan, A. M. Perak, R. Poudel, M. Rezk-Hanna, G. A. Roth, E. B. Schroeder, S. H. Shah, E. L. Thacker, L. B. VanWagner, S. S. Virani, J. H. Voecks, N.-Y. Wang, K. Yaffe, and S. S. Martin, "Heart disease and stroke statistics2022 update: A report from the american heart association," *Circulation*, vol. 145, no. 8, pp. e153–e639, 2022.

[263] E. Dal Sasso, A. Bagno, S. T. G. Scuri, G. Gerosa, and L. Iop, "The biocompatibility challenges in the total artificial heart evolution," *Annu Rev Biomed Eng*, vol. 21, pp. 85–110, 2019.

[264] G. Gerosa, S. Scuri, L. Iop, and G. Torregrossa, "Present and future perspectives on total artificial hearts," *Ann Cardiothorac Surg*, vol. 3, no. 6, pp. 595–602, 2014.

[265] N. Moazami, W. P. Dembitsky, R. Adamson, R. J. Steffen, E. G. Soltesz, R. C. Starling, and K. Fukamachi, "Does pulsatility matter in the era of continuous-flow blood pumps?," *J Heart Lung Transplant*, vol. 34, no. 8, pp. 999–1004, 2015.

[266] A. Cheng, C. A. Williamitis, and M. S. Slaughter, "Comparison of continuous-flow and pulsatile-flow left ventricular assist devices: is there an advantage to pulsatility?," *Annals of Cardiothoracic Surgery*, vol. 3, no. 6, pp. 573–581, 2014.

[267] J. Zhang, J. Sheng, C. T. ONeill, C. J. Walsh, R. J. Wood, J. H. Ryu, J. P. Desai, and M. C. Yip, "Robotic artificial muscles: Current progress and future perspectives," *IEEE Transactions on Robotics*, vol. 35, no. 3, pp. 761–781, 2019.

[268] S. Saleh, O. J. Liakopoulos, and G. D. Buckberg, "The septal motor of biventricular function," *Eur J Cardiothorac Surg*, vol. 29 Suppl 1, pp. S126–38, 2006.

[269] J. King and D. R. Lowery, *Physiology, Cardiac Output*. Treasure Island (FL): StatPearls Publishing Copyright I' 2025, StatPearls Publishing LLC., 2025.

[270] K. R. Kumar, R. E. Kirsch, and C. P. Hornik, *13 - Cardiovascular Physiology for Intensivists*, pp. 111–133.e5. Philadelphia: Elsevier, 2019.

[271] M. Willemet, P. Chowienczyk, and J. Alastruey, "A database of virtual healthy subjects to assess the accuracy of foot-to-foot pulse wave velocities for estimation of aortic stiffness," *Am J Physiol Heart Circ Physiol*, vol. 309, no. 4, pp. H663–75, 2015.

[272] T. Wehrum, P. Hagenlocher, T. Lodemann, W. Vach, I. Dragonu, A. Hennemuth, C. von Zur Mühlen, J. Stuplich, B. T. Ngo, and A. Harloff, "Age dependence of pulmonary artery blood flow measured by 4d flow cardiovascular magnetic resonance: results of a population-based study," *J Cardiovasc Magn Reson*, vol. 18, no. 1, p. 31, 2016.

[273] G. Savarese and L. H. Lund, "Global public health burden of heart failure," *Cardiac Failure Review 2017;3(1):711.*, 2017.

[274] M. A. Mamas, M. Sperrin, M. C. Watson, A. Coutts, K. Wilde, C. Burton, U. T. Kadam, C. S. Kwok, A. B. Clark, P. Murchie, I. Buchan, P. C. Hannaford, and P. K. Myint, "Do patients have worse outcomes in heart failure than in cancer? a primary care-based cohort study with 10-year follow-up in scotland," *Eur J Heart Fail*, vol. 19, no. 9, pp. 1095–1104, 2017.

[275] S. Hildebrand, M. Diedrich, M. Brockhaus, T. Finocchiaro, E. Cuenca, H. De Ben, U. Steinseifer, T. Schmitz-Rode, and S. V. Jansen, "Controlling the flow balance: In vitro characterization of a pulsatile total artificial heart in preload and afterload sensitivity," *Artif Organs*, vol. 46, no. 1, pp. 71–82, 2022.

[276] M. Pahuja and D. Burkhoff, "Right ventricular afterload sensitivity has been on my mind," *Circ Heart Fail*, vol. 12, no. 9, p. e006345, 2019.

[277] Q. Ze, S. Wu, J. Nishikawa, J. Dai, Y. Sun, S. Leanza, C. Zemelka, L. S. Novelino, G. H. Paulino, and R. R. Zhao, "Soft robotic origami crawler," *Science Advances*, vol. 8, no. 13, p. eabm7834, 2022.

[278] J. Ou, M. Skouras, N. Vlavianos, F. Heibeck, C.-Y. Cheng, J. Peters, and H. Ishii, "aeromorph - heat-sealing inflatable shape-change materials for interaction design," p. 121132, Association for Computing Machinery, 2016.

[279] L. Pocivavsek, S. H. Ye, J. Pugar, E. Tzeng, E. Cerda, S. Velankar, and W. R. Wagner, "Active wrinkles to drive self-cleaning: A strategy for anti-thrombotic surfaces for vascular grafts," *Biomaterials*, vol. 192, pp. 226–234, 2019.

[280] O. J. Gülcher, A. Vis, M. Peirlinck, and J. Kluin, "Balancing the ventricular outputs of pulsatile total artificial hearts," *Artif Organs*, vol. 47, no. 12, pp. 1809–1817, 2023.

[281] P. Y. Dankers, M. C. Harmsen, L. A. Brouwer, M. J. van Luyn, and E. W. Meijer, "A modular and supramolecular approach to bioactive scaffolds for tissue engineering," *Nat Mater*, vol. 4, no. 7, pp. 568–74, 2005.

[282] V. Bonito, A. I. P. M. Smits, O. J. G. M. Goor, B. D. Ippel, A. Driessen-Mol, T. J. A. G. Münker, A. W. Bosman, T. Mes, P. Y. W. Dankers, and C. V. C. Bouten, "Modulation of macrophage phenotype and protein secretion via heparin-il-4 functionalized supramolecular elastomers," *Acta Biomaterialia*, vol. 71, pp. 247–260, 2018.

[283] T. Mes, A. Serrero, H. S. Bauer, M. A. J. Cox, A. W. Bosman, P. Y. W. Dankers, and E. W. Meijer, "Supramolecular polymer materials bring restorative heart valve therapy to patients," *Materials Today*, vol. 52, pp. 175–187, 2022.

[284] D. L. Morales, C. Herrington, E. A. Bacha, V. O. Morell, Z. Prodán, T. Mroczek, S. Sivalingam, M. Cox, G. Bennink, and F. M. Asch, "A novel restorative pulmonary valve conduit: Early outcomes of two clinical trials," *Frontiers in Cardiovascular Medicine*, vol. 7, 2021.

[285] H. Talacua, S. H. M. Söntjens, S. H. Thakkar, A. M. A. Brizard, L. A. van Herwerden, A. Vink, G. C. van Almen, P. Y. W. Dankers, C. V. C. Bouten, R. P. J. Budde, H. M. Janssen, and J. Kluin, "Imaging the in vivo degradation of tissue engineering implants by use of supramolecular radiopaque biomaterials," *Macromolecular Bioscience*, vol. 20, no. 7, p. 2000024, 2020.

[286] X. Gu, Y. Matsumura, Y. Tang, S. Roy, R. Hoff, B. Wang, and W. R. Wagner, "Sustained viral gene delivery from a micro-fibrous, elastomeric cardiac patch to the ischemic rat heart," *Biomaterials*, vol. 133, pp. 132–143, 2017.

[287] T. B. Wissing, V. Bonito, C. V. C. Bouten, and A. I. P. M. Smits, "Biomaterial-driven in situ cardiovascular tissue engineeringa multi-disciplinary perspective," *npj Regenerative Medicine*, vol. 2, no. 1, p. 18, 2017.

[288] H. Izawa, N. Okuda, T. Yonemura, K. Kuroda, K. Ochi, S. Ifuku, M. Morimoto, H. Saimoto, M. Noda, K. Azuma, Y. Okamoto, and N. Ito, "Application of bio-based wrinkled surfaces as cell culture scaffolds," *Colloids and Interfaces*, vol. 2, no. 2, p. 15, 2018.

[289] M. G. J. Schmitz, D. M. Ibrahim, P. A. A. Bartels, S. A. E. Twisk, A. I. P. M. Smits, C. V. C. Bouten, and P. Y. W. Dankers, "Heparin-guided binding of vascular endothelial growth factor to supramolecular biomaterial surfaces," *Journal of Polymer Science*, vol. n/a, no. n/a, 2023.

[290] K. Barszcz, O. Szalu-Jordanow, M. Czopowicz, M. Mickiewicz, A. Moroz, J. Kaba, M. Polguj, G. Wysiadecki, R. Haadaj, and H. Purzyc-Orwaszer, "Topography of coronary arteries and their ramifications in the goat," *Biologia*, vol. 74, no. 6, pp. 683–689, 2019.

[291] Y. Gumusalan, D. Ozbag, H. Ozden, B. G. Saruhan, and A. Demirant, "The comparative investigation of left ventricle papillary muscle arteries in different species," *Saudi Med J*, vol. 27, no. 6, pp. 826–32, 2006.

[292] M. Li, Y.-S. Wang, T. Elwell-Cuddy, R. E. Baynes, L. A. Tell, J. L. Davis, F. P. Maunsell, J. E. Riviere, and Z. Lin, "Physiological parameter values for physiologically based pharmacokinetic models in food-producing animals. part iii: Sheep and goat," *Journal of Veterinary Pharmacology and Therapeutics*, vol. 44, no. 4, pp. 456–477, 2021.

[293] E. Wisse, A. J. H. Spiering, E. N. M. van Leeuwen, R. A. E. Renken, P. Y. W. Dankers, L. A. Brouwer, M. J. A. van Luyn, M. C. Harmsen, N. A. J. M. Sommerdijk, and E. W. Meijer, "Molecular recognition in poly(-caprolactone)-based thermoplastic elastomers," *Biomacromolecules*, vol. 7, no. 12, pp. 3385–3395, 2006.

[294] S. Yousefi, H. Borna, A. Rohani Shirvan, C. Wen, and A. Nouri, "Surface modification of mechanical heart valves: A review," *European Polymer Journal*, vol. 205, p. 112726, 2024.

[295] S. Loerakker, G. Argento, C. W. J. Oomens, and F. P. T. Baaijens, "Effects of valve geometry and tissue anisotropy on the radial stretch and coaptation area of tissue-engineered heart valves," *Journal of Biomechanics*, vol. 46, no. 11, pp. 1792–1800, 2013.

[296] M. J. Webber, E. A. Appel, E. W. Meijer, and R. Langer, "Supramolecular biomaterials," *Nat Mater*, vol. 15, no. 1, pp. 13–26, 2016.

[297] P. Y. W. Dankers and E. W. Meijer, "Supramolecular biomaterials. a modular approach towards tissue engineering," *Bulletin of the Chemical Society of Japan*, vol. 80, no. 11, pp. 2047–2073, 2007.

[298] E. L. Chaikof, H. Matthew, J. Kohn, A. G. Mikos, G. D. Prestwich, and C. M. Yip, "Biomaterials and scaffolds in reparative medicine," *Ann N Y Acad Sci*, vol. 961, pp. 96–105, 2002.

[299] Y. Hong, S. H. Ye, A. Nieponice, L. Soletti, D. A. Vorp, and W. R. Wagner, "A small diameter, fibrous vascular conduit generated from a poly(ester urethane)urea and phospholipid polymer blend," *Biomaterials*, vol. 30, no. 13, pp. 2457–67, 2009.

[300] A. M. Seifalian, H. J. Salacinski, A. Tiwari, A. Edwards, S. Bowald, and G. Hamilton, "In vivo biostability of a poly(carbonate-urea)urethane graft," *Biomaterials*, vol. 24, no. 14, pp. 2549–57, 2003.

[301] H. Talacua, A. I. Smits, D. E. Muylaert, J. W. van Rijswijk, A. Vink, M. C. Verhaar, A. Driessen-Mol, L. A. van Herwerden, C. V. Bouten, J. Kluin, and F. P. Baaijens, "In situ tissue engineering of functional small-diameter blood vessels by host circulating cells only," *Tissue Engineering Part A*, vol. 21, no. 19-20, pp. 2583–2594, 2015.

[302] D. L. Rabenstein, "Heparin and heparan sulfate: structure and function," *Natural Product Reports*, vol. 19, no. 3, pp. 312–331, 2002.

[303] H. A. Behanna, K. Rajangam, and S. I. Stupp, "Modulation of fluorescence through coassembly of molecules in organic nanostructures," *Journal of the American Chemical Society*, vol. 129, no. 2, pp. 321–327, 2007. doi: 10.1021/ja062415b.

[304] Y. Ding, Z. Yang, C. W. C. Bi, M. Yang, S. L. Xu, X. Lu, N. Huang, P. Huang, and Y. Leng, "Directing vascular cell selectivity and hemocompatibility on patterned platforms featuring variable topographic geometry and size," *ACS Applied Materials Interfaces*, vol. 6, no. 15, pp. 12062–12070, 2014. doi: 10.1021/am502692k.

[305] M. T. Koobatian, S. Row, J. Smith, R. J., C. Koenigsknecht, S. T. Andreadis, and D. D. Swartz, "Successful endothelialization and remodeling of a cell-free small-diameter arterial graft in a large animal model," *Biomaterials*, vol. 76, pp. 344–58, 2016.

[306] B. Jiang, R. Suen, J. A. Wertheim, and G. A. Ameer, "Targeting heparin to collagen within extracellular matrix significantly reduces thrombogenicity and improves endothelialization of decellularized tissues," *Biomacromolecules*, vol. 17, no. 12, pp. 3940–3948, 2016. doi: 10.1021/acs.biomac.6b01330.

[307] Y. Wei, Y. Wu, R. Zhao, K. Zhang, A. C. Midgley, D. Kong, Z. Li, and Q. Zhao, "Msc-derived sevs enhance patency and inhibit calcification of synthetic vascular grafts by immunomodulation in a rat model of hyperlipidemia," *Biomaterials*, vol. 204, pp. 13–24, 2019.

[308] Y.-T. Hu, X.-D. Pan, J. Zheng, W.-G. Ma, and L.-Z. Sun, "Inăvitro and inăvivo evaluation of a small-caliber coaxial electrospun vascular graft loaded with heparin and vegf," *International Journal of Surgery*, vol. 44, pp. 244–249, 2017.

[309] R. Duijvelshoff, N. C. A. Van Engeland, K. M. R. Gabriels, S. H. M. Söntjens, A. I. P. M. Smits, P. Y. W. Dankers, and C. V. C. Bouten, "Host response and neo-tissue development during resorption of a fast degrading supramolecular electrospun arterial scaffold," *Bioengineering*, vol. 5, no. 3, p. 61, 2018.

[310] X. Yang, Q. Wang, A. Zhang, X. Shao, T. Liu, B. Tang, and G. Fang, "Strategies for sustained release of heparin: A review," *Carbohydrate Polymers*, vol. 294, p. 119793, 2022.

[311] P. D. Stein and H. N. Sabbah, "Measured turbulence and its effect on thrombus formation," *Circ Res*, vol. 35, no. 4, pp. 608–14, 1974.

[312] E. Falk, "Coronary thrombosis: pathogenesis and clinical manifestations," *Am J Cardiol*, vol. 68, no. 7, pp. 28b–35b, 1991.

[313] E. C. Filipe, M. Santos, J. Hung, B. S. L. Lee, N. Yang, A. H. P. Chan, M. K. C. Ng, J. Rnjak-Kovacina, and S. G. Wise, "Rapid endothelialization of off-the-shelf small diameter silk vascular grafts," *JACC: Basic to Translational Science*, vol. 3, no. 1, pp. 38–53, 2018.

List of Publications

Included in the thesis

- A. Vis, **M. Arfaee**, H. Khambati, M. S. Slaughter, J. F. Gummert, J. T. B. Overvelde, J. Kluin, *The ongoing quest for the first total artificial heart as destination therapy.* nature reviews cardiology, 19(12):813-828 (2022).
  (Chapter 2)

- **M. Arfaee**, J. Kluin, J.T.B. Overvelde, *Modeling the behavior of elastic pouch motors.* 2023 IEEE International Conference on Soft Robotics (RoboSoft), Singapore, 2769-4534 (2023).
  (Chapter 3)

- **M .Arfaee**, L. C. van Laake, S. Zou, C. Bording, J. Kluin, J. T. B. Overvelde, *Toward developing a compact total artificial heart using a soft robotic fluidic transmission system.* Science Advances. 11,eadv4854 (2025).
  (Chapter 4)

- **M. Arfaee***, A. Vis*, P.A.A. Bartels, L.C.V. Laake5, L. Lorenzon, D.M. Ibrahim, D. Zrinscak, A.I.P.M. Smits, A. Henseler8, M. Cianchetti, P.Y.W. Dankers, C.V.C. Bouten, J.T.B. Overvelde, J. Kluin, *A soft robotic total artificial hybrid heart.* nature Communications 16, 5146 (2025). (* contributed equally)
  (Chapter 5)

Not included in the thesis

- **M. Arfaee**, A. Vis, J. Kluin, *Future technologies in total artificial heart development: can a robot become as good as a donor heart?*, European Heart Journal, Volume 43, Issue 48, Pages 49704972 (2022).

- P. C. Vaquero, A. Rozenbaum, M. Rocchi, **M. Arfaee**, P. Gründeman, J. Kluin, *Bioartificial Hearts, Assist Devices, and Myocardium: New Developments.* Transplantation (2025).

Portfolio

General Courses	**Year**	**Workload (ECTs)**
The AMC world of science	2019	0.7
Endnote	2019	0.1
Introduction to Python	2019	0.7
Data analysis in MATLAB	2020	0.7
Scientific writing in English for publication	2020	1.5
Pitching Masterclass	2024	0.7
Entrepreneurship Awakening	2024	0.1
TTT Team up workshop	2024	0.3
Academic spin-offs	2024	0.4
Lectures		
Artificial Heart Valves, AMOLF, Amsterdam	2024	1
(Inter)national conferences/presentations/Meetings		
Hybrid Heart consortium meetings	2018-2023	1
Hybrid Heart EU meetings	2018-2023	1
Emtec company visit, Achen, Germany	2019	0.5
AMOLF group presentations, Amsterdam	2019-2024	1
Journées Robotique Souple 2019, Lille, France	2019	0.5
ICTAM 2021	2021	1
SES 2021 (Poster presentation)	2021	0.5
APS 2022 (Poster presentation)	2022	0.5
Modern Mechanics at AMOLF (Oral presentation)	2022	0.5
Cardiac Surgery meeting in AMC (Oral presentation)	2022	0.5
Lab visit SSSA, Pisa, Italy	2022	0.5
EE labels company (visiting)	2022	0.5
Techtextile, Frankfurt, Germany	2022	0.5
Robosoft 2023, Singapore	2023	0.5
Dutch Soft robotic Symposium 2023, Enschede	2023	0.5
Lab visit ETH, Zurich, Switzerland	2023	1
EuroELSO 2024, Krakov, Poland (Invited speaker)	2024	1
Holland Hybrid Heart webinar	2024	1
Dutch Soft robotic Symposium 2024, Eindhovan	2024	0.5
27th Gdansk Cardiac Surgery Meeting (Invited speaker)	2025	1
Robosoft 2025, Lausanne, Switzerland	2025	1
ISHLT Cardiothoracic Surgery Professional Community Webinar	2025	0.5

Publications/Patents	**Year**	**Workload (ECTs)**
Future technologies in total artificial heart development: can a robot become as good as a donor heart? (EHJ)	2022	0.5
The ongoing quest for the first total artificial heart as destination therapy (nature review cardiology)	2022	1
Modeling the behavior of elastic pouch motors (Robosoft 2023)	2023	1
An implantable artificial heart (WO2024023749A1)	2023	1
A soft robotic total artificial Hybrid Heart (nature communications)	2025	1
Toward developing a compact total artificial heart using a soft robotic fluidic transmission system (Science Advances)	2025	1
Bioartificial Hearts, Assist Devices, and Myocardium: New Developments (Transplantation)	2025	0.5
Supervising		
Charlotte Bording, Bachelor student	2023	1
Maxime van Creij, Bachelor student	2024	0.5
Bas Geerlings, Bachelor student	2024	0.5
Bruce Jacobs, Bachelor student	2024	0.5
Anthony Verweij, Bachelor student	2024	0.5

Acknowledgements

There are countless people who made this journey possible, and I am sure I will forget to mention someone. For that, I apologize in advance. Please know that even if your name doesn't appear here, your support, advice, or even a simple smile along the way meant more than you can imagine.

First and mostly, I thank my supervisor Prof. Jolanda Kluin for your unwavering support and guidance throughout my PhD journey. You gave me the freedom to explore my ideas while always being there with thoughtful advice and encouragement. Beyond the academic path, I truly cherish the personal bond and trust we built over the years. I will always remember the warmth of the Christmas dinners at your home before the pandemic, where I had the chance to meet your family and feel genuinely welcomed. During the difficult moments I faced in my personal life during the past years, your understanding and kindness meant a great deal to me. I am also grateful that our collaboration continues within the Holland Hybrid Heart project, where we share a common goal and the excitement of moving this vision forward together.

Dear Dr. Bas Overvelde, I would like to sincerely thank you for giving me the opportunity to work in your group at AMOLF and for welcoming me as part of the Soft Robotic Matter group. I feel truly fortunate to have spent my PhD years in such an inspiring environment, where I not only gained invaluable experience as an engineer but also shared countless amazing memories with the group. I am especially grateful for all the fun and memorable outings we had together, which created a strong sense of belonging and made my time at AMOLF even more enjoyable. I deeply appreciate your guidance and support throughout my journey, which helped me grow both scientifically and personally. Among the many experiences and memories, I will always treasure our trip to Singapore for Robosoft 2023. In the challenging period of my PhD, when I felt lost as many PhDs do, our conversation by "Marina Bay" gave me hope and peace, and renewed motivation to continue.

Dear Prof. Ed van Bavel, during the first year of my PhD, you kindly helped us set up our mock circulatory loop in your lab. Thank you for your generous support, valuable guidance, and, of course, for allowing us to use part of your lab space to carry out our work.

Next "thank you" flies to Iran, to my amazing parents, Esfandiar and Azar, and my lovely sister, Mahsa. I am endlessly grateful for your unconditional support and belief in me throughout my life. To my father, who has taught me so much since childhood; working by your side at home truly made me into an engineer. I even mentioned in my motivation letter for this PhD how those early experiences, fixing and building things together with you, sparked my passion for technical work and shaped my path. To my mother, whose love and care have always been a source of strength; I could never forget your sacrifices. I still remember the day in my second year of school when I missed the school bus, and despite being pregnant, you took me by public transport to make sure I would not miss my

classes. Such moments remain in my heart as a reminder of your devotion and selflessness. Without your encouragement and love, this achievement would never have been possible. Dear Mahsa, I have been away from home for my studies since I was 18, and it has always saddened me that I missed seeing you grow up. Yet, I am so proud of the person you have become and of the way you are pursuing your own dreams. You have always been a source of love, energy, and passion for me. A truly memorable period of my PhD was your visit to the Netherlands, when we shared unforgettable trips to Paris and Switzerland, including our time in the beautiful Heidi village. Those moments remain among the happiest memories of these years.

To Bita, my girlfriend. Over the past few years, you have stood by my side during the most demanding phases of my PhD, especially while I was struggling to publish my last two papers, the main works of my thesis. Those were tremendously difficult times, filled with stress, uncertainty, and countless setbacks, yet your presence made them bearable and, ultimately, possible to overcome. I clearly remember the days when I came home exhausted and frustrated after experiments failed, carrying all the weight of doubt and pressure. You listened patiently to my endless stories, calmed my nerves, and always gave me hope to keep going. Your belief in me, even in the moments when I doubted myself most, gave me the strength to persevere. Without your love, patience, and unwavering support, this journey would have been infinitely harder. For all the encouragement, kindness, and warmth you brought into my life, I am deeply grateful.

To my paranymphs, Luuk and Mojtaba. First of all, thank you for all your efforts and for being such amazing paranymphs, colleague, and friends.

Dear Luuk, it was a true pleasure working with you on the Hybrid Heart project. I learned so much from you, not only scientifically, but also in how to approach problems thoughtfully. I am grateful for the genuine interest you showed, even in the less important things I was doing during my first year as I was trying to find my way. I have always admired the passion with which you can speak about every topic, like a walking encyclopedia. And, of course, apologies again for mistaking you as a supervisor on my very first day!

Dear Mojtaba, thank you for being exactly who you are! We shared so many moments together that I hardly know where to start. You were the perfect buddy in every sense; my gym buddy, volleyball buddy, FIFA buddy, guitar-and-singing buddy, party buddy, and many other buddies. Our friendship made this journey unforgettable. Unfortunately, we could not add postdoc buddy to the list as you saved yourself just in time. And sorry for being so hard on you in volleyball!

Dear Annemijn and Husain, together we slowly built the Hybrid Heart lab at AMC, navigating many failures and leakages, but also celebrating the joyful moments each time a prototype worked flawlessly and we could finally collect the data we needed. Annemijn, thank you for helping me on the very first day of my PhD, when we traveled to Eindhoven for an experiment. I was so new to the country and had no idea how to manage things, and your support meant a lot to me. I still fondly remember having coffee with you at Canvas that day, enjoying the beautiful view of the city. Husain, thank you for all your help in the lab and for the many advancements you brought to the project. I also greatly enjoyed

the lighter moments we shared, like your suggestion to try that delicious steak in Florence, which made the trip even more memorable.

Dear Sulayman, I have always admired you, not only for your impressive achievements, but even more for your kindness and humility. I'm very happy to have had the opportunity to work with you on the project involving 4D-MRI imaging of the wire-driven heart. Thank you for arranging this study and for your effective collaboration.

Dear Niels, thank you for your endless patience every time I managed to break a 3D printer, which, unfortunately, happened more than once. I am convinced that no project in the group would have gone as smoothly without your skills and dedication. It was always a pleasure working alongside you on different projects, where I learned a lot and enjoyed our collaboration.

Dear Giorgio, I still remember your group presentation on the very first day I visited AMOLF where it was my very first encounter with soft robotics, and it left a lasting impression. Thank you for that great introduction to the field.

Dear Agustin, thank you for bringing the sharing is caring tradition to our lunch breaks with tortillas, beans, and hummus. I truly missed it after you and Luuk left AMOLF. I also often think back to your words about taking the PhD journey lightly–that I did not have to finish it if it ever became too much pressure. That perspective always gave me a sense of peace and reassurance.

Dear Charlotte, thank you for bringing your creativity and enthusiasm into the LIMO heart project. The techniques you developed for its fabrication were truly key in accelerating the progress, and your contributions made a significant difference to the project's success.

Dear Shibo, working with you on the LIMO Heart project was such an amazing and smooth experience for me. I am truly grateful for your openness and willingness to help with anything that came up in the lab. And of course, thank you for buying me seaweed from the Chinese supermarket, a kindness that I will always remember fondly.

Next, my gratitude goes to our amazing AMOLF crew, who made the group such a pleasant and inspiring place to work in. I learned so much from each of you and carry wonderful memories from our time together. Thank you all from the bottom of my heart! Dear Jelle, thanks for improving the fluidics setup and HH application, and developing the MATLAB script to analyze fluidics data. It made my PhD life so much easier. Dear Bob, I am always impressed by the information you bring to the table in the conversations. Thanks for sharing your knowledge with us! Dear Lio, I really enjoyed the interactive group presentation with those paintings, very funny to see the results! I always admire the way industrial design students work, and learn a lot from it. Dear Sumit, thanks for breaking the killing silence whenever coming to the lab by your famous "Hello Bro, what's up?!". Dear Elif, I wish you a great success in your PhD. Sorry that our help was not helpful in winning Paul and Sergio in chess. Dear Clyde, thank you for preparing the best offices so that we could do great science. Indeed, great science comes after a great working space. Dear Stijn, I'm very happy that we are now working together on the Holland Hybrid Heart project. Having you

on board to take charge of controlling our future soft robotic heart gives me great confidence. I truly believe it's now in the best possible hands! Dear Petra, thank you for making our work at AMOLF visible to the world. Your efforts in sharing and communicating our research have played a vital role in showing others the creativity and impact of what people do at AMOLF. Jack and Dhawal, thank you for your enthusiasm in bringing everyone together through the AMOLF football team–what a fantastic initiative! And Dhawal, I will never forget your emotional support during the Mahsa Amini protests in Iran. It meant a lot to me–thank you, my friend. Dear Parisa, I still remember Christmas 2022, when I was feeling low and didn't want to join the Christmas party for personal reasons. You convinced me to go, and I'm so glad you did. I ended up enjoying the day, and it truly lifted my spirits. Thank you for your kindness, support, and for reminding me how much a little warmth and friendship can mean.

Dear Alberto, you are one of the most spontaneous and lively men-in-science I have ever met. Thanks for teaching me how we should dream-and-do in science. Keep shining, man!

Dear Mannus, it was always a challenge for me to fully grasp the complex topics you worked on, but thanks to your clear and engaging presentations, I eventually did!

Dear Sergio, thank you for bringing the cafternoon tradition to the group. I'm still sad I missed all the boat gatherings, but I hope we can someday catch up on your boat over a couple of beers.

Dear Paul, thank you first of all for developing the great "Springables",and more importantly, taking your time to show me how to work with it. It is very cool, man!

Dear Katrien, you were always so kind and thoughtful whenever there were a problem in the lab, offering helpful and constructive suggestions. I also appreciate your help arranging the vacuum-forming machine at TU/e.

Dear Nienke, I am very happy that you have taken over the LIMO Heart project. I wish you great success in your PhD and I'm excited to see you bring the heart to the next level.

This project was initiated within the Hybrid Heart consortium, a collaboration between several universities and companies, including TU/e, AMOLF, AMC, SSSA in Italy, and EVOS in Germany. I would like to express my gratitude to everyone involved in this project for their valuable contributions and support in making this research possible. It was a true pleasure working with all of you and being part of such an inspiring and collaborative effort.

This work is now being continued by our wonderful team at Erasmus MC, as part of the Holland Hybrid Heart consortium. I would like to thank Patricia for taking over the so-called wire-driven heart project and advancing it toward the chronic animal trials stage.

Dear Paul, thank you for bringing your vast suitcase of experience into our consortium. I'm constantly learning from you and truly appreciate your insights and support.

Dear Martin, we are very fortunate to have you as the project manager of the Holland Hybrid Heart project and the Erasmus MC team. The way you care for both the people and the project is truly inspiring and motivating. Thank you for all your efforts, and also for the great BBQ at your place, especially the Denver steak!

Dear Kirsten, Celeste, and Oskar, my wonderful office mates, I'm so glad that we are continuing the project together and bringing it one step further. It's a real pleasure to work with you as a team, and I'm learning so much from each of you. Thank you for making the EE office such a pleasant and enjoyable place to work. Kirsten, thank you for organizing the engineering brainstorm meetings. I truly believe these kinds of discussions are exactly what our team needs, and you manage them exceptionally well. Celeste, thank you for bringing so much energy and enthusiasm into the office. It truly came to life after you joined us! Oskar, I've always admired your creativity and passion for the project. You bring great ideas and dedication to everything you do. I wish you a wonderful journey throughout your PhD!

The next thank you, and a big one, goes to my FIFA friends–a bunch of doctors who love playing FIFA (and many other things!) together. I was incredibly lucky to meet you all just a few months after arriving in the Netherlands, and since then, we've shared countless unforgettable moments, laughter, and memories.
Dear Reza, Reza, Reza, thank you for inviting me to the Amstehran Football Club, where I met most of the FIFA crew for the first time. That truly marked the beginning of a great friendship.

Dear Mehran, we've had so many fun moments together that it's hard to choose which one to mention first, but the highlight must still be our trip to Poland, with all the unexpected accidents along the way! Thank you also for playing the tar in the Corona Alphabet track–such a beautiful piece of work!

Dear Hossein, thank you for cooking your special *ghorme sabzi* and hosting so many amazing parties. Your home will always shine in my memories as a place of warmth, laughter, and great company.

Dear Keyvan, thank you for your constant encouragement and advice about the PhD journey, especially your honest reflections about how frustrating it can be at times. Our talks always gave me relief and perspective.

Dear Hadi, thank you for organizing sushi nights and for that great trip to Belgium. I still don't know why we decided to watch that movie at the Amsterdam Eye, but it certainly added to the memories!

Dear Masoud, I was so lucky to have you as both a friend and a neighbor. I'll never forget having *kale pacheh* at your place while Sobh ast Saghia played on TV. those breakfasts brought back the same feelings and vibes as being with my own family. And thank you again for cooking kale pacheh after our long walk-and-talk in the snow at Flevopark–truly unforgettable moments.

Dear Erfan, I will never forget your kindness during all those times you came to my place to teach us Dutch. My Dutch may not have improved much, but our friendship certainly did! Thank you also for taking us to Kebabci restaurant, another great memory to add to the list.

Dear Bita and Jonathan, a huge part of my PhD memories belongs to the wonderful moments spent in your warm and welcoming home, enjoying great food (especially your delicious *ash*) and the heartfelt conversations that always made me feel at ease.

The next thank you goes to my party-freak friends; Don, Ashkan, Omid, Maryam, Majid, Elnaz, Hosein, Darya, Amir, Shohreh, Arash, Pegah, Nina, with whom I shared so many unforgettable moments, not only at parties, but in real life as well. Thank you all for calling me doctor long before I actually became one!

Dear Mohammad (Don), let's plan another one of those legendary road trips, with a stop every 100 km. I truly miss those days!

Dear Arash, accompanying you to the robotics lab and later working there together somehow changed my life for the better. Thank you, man!

Dear Amir, first of all, thank you for taking such great photos at my ceremony. And secondly, thanks for letting me drive your car for about two years, I really wish you soon get your driving license and drive your Honda. Maybe then have another road trip together?!

Dear Shohreh, one of the best parts of our parties was always the moment you'd jump on the couch and start singing. Thank you for those performances, for cooking that amazing *Nasi goreng* for me, and for patiently listening to all my sad and boring stories every time.

Dear Omid, our parties always rocked thanks to your music! You were the best DJ. And I'm still glad to have a crazy dance partner for Gangnam Style.

Dear Maryam, my friendship with you and Omid started on that unforgettable night when you showed up at my door unannounced, almost at midnight! It was such an awkward yet funny moment, and it became the start of a wonderful friendship. Thank you also for that delicious lentil-meat soup!

Dear Majid (dadachi), thank you for hosting so many great parties at your place, and of course for treating us to *dizi* and *kale pacheh*.

Dear Hosein, I will never forget your help when I was buying my first house in the Netherlands. No words can express how grateful I am. I was also very lucky to have you as a neighbor.

Dear Ashkan, sorry again for not joining the canoeing weekend–cycling all the way there was just too much for me! But later we made up for it with all the bouldering sessions, and I'm grateful to you for teaching me how to climb.

And so this long, wild, wonderful journey finally reaches its end. What started as an idea

slowly grew into pages of experiments, mistakes, discoveries, and way too many cups of coffee. To all the people who filled these years with laughter, warmth, and food, you made the science worth doing. If you've started reading here at the acknowledgements (which I suspect you did), I forgive you, but I still encourage you to browse a few chapters; I promise there are some nice pictures and maybe even a few sentences that make sense.

About the author

Maziar Arfaee was born on September 23rd 1993, in Shiraz, Iran, where he completed his secondary education at Imam Reza High School. He pursued his academic studies in biomedical engineering at Amirkabir University of Technology (Tehran Polytechnic), earning a Bachelors degree (2011-2015) in Biomedical Engineering Biomechanics, followed by a Masters degree (2015-2018) in Biomedical Engineering - Sports Engineering. His Masters thesis focused on the design and implementation of a 5-DoF wearable robot for hand rehabilitation, combining his academic training with a strong passion for practical and hands-on problem solving.

Throughout his studies, he consistently gravitated toward work that blended theory with application. As the head of the mechanical design of the Parsian Robotic Team, he found an ideal outlet for his passion for hands-on design and fabrication. He participated in several international RoboCup competitions in Germany, China, and Japan, gaining deep experience in system integration, mechanical prototyping, and real-world testing. These early experiences were pivotal in developing his love for robotics, iterative design, and interdisciplinary innovation.

Professionally, he worked as a mechanical designer in multiple settings where he could directly engage in the building and refining of hardware systems. At Aysun Lighting, he was responsible for product design and the development of a production line, turning concepts into manufacturable systems. He later contributed to the creation of medical measurement devices, including wrist and back dynamometers and a dynamic balance assessment system, continuing to explore practical engineering solutions in the biomedical space.

In December 2018, he moved to the Netherlands to join the Hybrid Heart project, a collaborative research initiative focused on developing the first soft robotic total artificial hybrid heart. He is currently based at Erasmus Medical Center (Erasmus MC) in Rotterdam, where he serves as the technical lead for the Holland Hybrid Heart projectthe continuation of this pioneering effort.

His doctoral research draws on this extensive hands-on background, integrating soft robotics, mechanical engineering, and biomedical engineering to push the boundaries of artificial heart design. With a commitment to turning ideas into working systems, his work envisions a future where implantable soft robotic hearts are not only mechanically efficient but also biologically integrated and life-changing for patients with end-stage heart failure.